

AD-A056 535

ILLINOIS UNIV AT URBANA-CHAMPAIGN COORDINATED SCIENCE LAB F/G 7/4
CHEMISORPTION ON PERFECT SURFACES AND STRUCTURAL DEFECTS.(U)

OCT 77 R LIU

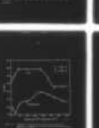
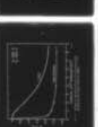
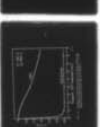
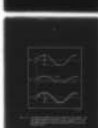
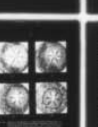
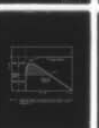
DAAB07-72-C-0259

UNCLASSIFIED

R-790

NL

1 OF 4
AD
A056 535



AD A056535

REPORT R-790 OCTOBER, 1977

UILU-ENG 77-2237

CSL COORDINATED SCIENCE LABORATORY

LEVEL II

12

**CHEMISORPTION ON
PERFECT SURFACES
AND STRUCTURAL DEFECTS**

SHICHEN LIU



This document has been approved
for public release and sale; its
distribution is unlimited.

UNIVERSITY OF ILLINOIS - URBANA, ILLINOIS

78 07 18 037

UNCLASSIFIED

LEVEL II

SECURITY CLASSIFICATION OF THIS PAGE (When Data Entered)

REPORT DOCUMENTATION PAGE		READ INSTRUCTIONS BEFORE COMPLETING FORM
1. REPORT NUMBER	2. GOVT ACCESSION NO.	3. RECIPIENT'S CATALOG NUMBER
4. TITLE (and Subtitle) CHEMISORPTION ON PERFECT SURFACES AND STRUCTURAL DEFECTS.		5. TYPE OF REPORT & PERIOD COVERED Technical Report.
7. AUTHOR(s) Ruichen Liu		6. PERFORMING ORG. REPORT NUMBER R-790, JULU-ENG-77-2237
9. PERFORMING ORGANIZATION NAME AND ADDRESS Coordinated Science Laboratory University of Illinois at Urbana-Champaign Urbana, Illinois 61801		8. CONTRACT OR GRANT NUMBER(s) DMR-76-82088; DAAB-07-72-C-0259.
11. CONTROLLING OFFICE NAME AND ADDRESS Joint Services Electronics Program		10. PROGRAM ELEMENT, PROJECT, TASK AREA & WORK-UNIT NUMBERS NSF-DMR-76-82088
14. MONITORING AGENCY NAME & ADDRESS (if different from Controlling Office) 12346p.		12. REPORT DATE October 1977
		13. NUMBER OF PAGES 335
		15. SECURITY CLASS. (of this report) UNCLASSIFIED
		15a. DECLASSIFICATION/DOWNGRADING SCHEDULE
16. DISTRIBUTION STATEMENT (of this Report) Approved for public release; distribution unlimited		
17. DISTRIBUTION STATEMENT (of the abstract entered in Block 20, if different from Report)		
18. SUPPLEMENTARY NOTES		
19. KEY WORDS (Continue on reverse side if necessary and identify by block number) Surfaces Defects Solids Surface Reactions		
20. ABSTRACT (Continue on reverse side if necessary and identify by block number) Chemisorption of nitrogen and hydrogen on densely packed planes of tungsten, molybdenum, iridium, and rhenium has been studied by probe-hole field emission microscopy. Adsorption on perfect planes, as well as on planes containing structural defects, has been investigated. The results can be interpreted by the promotion of chemisorption at structural defects on smooth surfaces. A model, which can account for our results as well as observations on macroscopic surfaces, is presented.		

DDC
 123456
 JUL 19 1978
 123456
 F

UILU-ENG 77-2237

CHEMISORPTION ON PERFECT SURFACES
AND STRUCTURAL DEFECTS

by

Ruichen Liu

* Carried out under NSF Grant DMR-76-82088 from the National Science Foundation.

† Supported in part by the Joint Services Electronics Program (U.S. Army, U.S. Navy and U.S. Air Force) under Contract DAAB-07-72-C-0259.

Reproduction in whole or in part is permitted for any purpose of the United States Government.

Approved for public release. Distribution unlimited.

CHEMISORPTION ON PERFECT SURFACES
AND STRUCTURAL DEFECTS

BY

RUICHEN LIU

B.S., National Tsinghua University, 1968
M.S., Ohio State University, 1972

THESIS

Submitted in partial fulfillment of the requirements
for the degree of Doctor of Philosophy in Metallurgical Engineering
in the Graduate College of the
University of Illinois at Urbana-Champaign, 1977

Thesis Adviser: Professor Gert Ehrlich

Urbana, Illinois

ACCESSION for	
NTIS	White Section <input checked="" type="checkbox"/>
DDC	Buff Section <input type="checkbox"/>
UNANNOUNCED	<input type="checkbox"/>
JUSTIFICATION	
BY	
DISTRIBUTION/AVAILABILITY CODES	
SPECIAL	
A	

CHEMISORPTION ON PERFECT SURFACES
AND STRUCTURAL DEFECTS

Ruichen Liu, Ph.D.
Coordinated Science Laboratory and
Department of Metallurgical Engineering
University of Illinois at Urbana-Champaign, 1977

Chemisorption of nitrogen and hydrogen on densely packed planes of tungsten, molybdenum, iridium, and rhenium has been studied by probe-hole field emission microscopy. Adsorption on perfect planes, as well as on planes containing structural defects, has been investigated. The results can be interpreted by the promotion of chemisorption at structural defects on smooth surfaces. A model, which can account for our results as well as observations on macroscopic surfaces, is presented.

For the adsorption of nitrogen on W(110) surface, two different adsorption states are found. At a surface temperature T_s below 150 K, adsorption is characterized by a large drop of the emission current. At surface temperatures above 150 K, adsorption on the (110) depends strongly on the surface temperature. The change in the (110) work function is small, ranging from 0.04 eV at 150 K to 0.07 eV at 550 K.

Adsorption of hydrogen on Ir(111) at 80 K results in two distinct states. An initial increase of 0.3 eV in the work function is observed, followed by a long plateau in which no additional adsorption is detected. Further exposure produces a work function drop of 0.4 eV. Both states are unstable at 400 K.

At 80 K, hydrogen does not adsorb immediately on the Re(0001) plane. Rather, adsorption on this surface starts only after other surfaces on the emitter are saturated with hydrogen. A drop in the work function by 0.4 eV accompanies adsorption. At 300 K, adsorption of hydrogen becomes rapid. Nitrogen is found not to chemisorb on the (0001) plane at $T_s = 300$ K. Chemisorption on the (0001) plane can be brought about by heating the surface to

550 K during exposure, or after exposure. In both cases, the work function is increased by 0.04-0.08 eV.

Adsorption of both hydrogen and nitrogen on the Mo(110) plane is found to be different from its iso-electronic partner, W(110). The rate of adsorption on Mo(110) is much faster than that on W(110). The work function also changes quite differently. For the adsorption of hydrogen, the Mo(110) work function first decreases, then increases to 0.1 eV above the clean value. For nitrogen, the Mo(110) work function is increased by 0.2 eV, while the change on the W(110) is < 0.1 eV.

The mechanism that leads to adsorption on W(110) and Re(0001) planes has been investigated by sequential adsorption studies, and by studying surfaces with structural defects. In sequentially adsorbing nitrogen and hydrogen (deuterium), adsorption on flat surfaces is found dependent on the conditions of their surrounding areas. Direct processes on the flat surface are therefore excluded. Studies on surfaces with structural defects further reveal that adsorption on the flat surface is catalyzed by defects. Adsorption on structural defects is found at least one order of magnitude faster than that on flat W(110) surfaces. A quantitative analysis for the promotion of chemisorption by defects, based on experiments on surfaces with different defect concentrations, is presented.

This systematic investigation reveals that chemisorption of diatomic gases on metal surfaces is highly complicated. It is affected by surface perfection, the crystal structure, as well as by the detailed electronic structure of the substrate. More extensive studies are necessary to distinguish the relative dominance of these factors.

ACKNOWLEDGEMENT

I would like to thank my advisor, Professor Gert Ehrlich, for his guidance and personal concern. I would also like to thank Mr. William Lawrence, for his expert glass blowing under frequently difficult conditions, the machine shop, the drafting room, and the photographic shop for their technical support. Special thanks are due to Rob Chambers, Dave Reed, and Dick Polizzotti, for their helpful discussions and suggestions. Finally, I would like to thank Mrs. Phyllis Young and Mrs. Trudy Williams for their excellent job in preparing the final manuscript.

TABLE OF CONTENTS

CHAPTER	Page
I. INTRODUCTION.....	1
II. EXPERIMENTAL TECHNIQUES.....	5
2.1 Field emission and field ion microscopy.....	5
2.2 Experimental arrangement.....	13
2.3 Gas handling and sample preparation.....	17
2.4 Surface cleaning.....	23
2.5 Surface characterization.....	25
2.5a Surface characterization by FIM.....	26
2.5b Surface characterization by FEM.....	31
2.6 Detection of adsorption.....	35
2.6a Techniques of detection.....	35
2.6b Perturbation of adsorbate during observation.....	40
III. ADSORPTION ON TUNGSTEN.....	49
3.1 Introduction.....	49
3.2 Nitrogen on tungsten (110).....	55
3.2a Adsorption at $T_s \geq 150$ K.....	55
3.2b Adsorption at $T_s < 150$ K.....	65
3.3 Sequential adsorption of nitrogen and hydrogen.....	68
IV. ADSORPTION ON IRIDIUM.....	72
4.1 Introduction.....	72
4.2 Experimental results.....	75
4.2a Adsorption on the emitter as a whole.....	77
4.2b Adsorption on the (111) plane.....	82
4.3 Discussion.....	83

CHAPTER	Page
V. ADSORPTION ON RHENIUM.....	86
5.1 Hydrogen on rhenium.....	86
5.1a Adsorption studies.....	86
5.1b Changes in the emission pattern.....	94
5.1c Desorption measurements.....	96
5.1d Re-adsorption studies.....	99
5.2 Nitrogen on rhenium.....	101
5.2a Adsorption at $T_s \leq 80$ K.....	101
5.2b Adsorption at $T_s \geq 300$ K.....	104
5.3 Sequential adsorption of nitrogen and deuterium.....	110
5.4 Adsorption near the edge of the (0001) plane.....	115
5.5 Discussion.....	119
VI. ADSORPTION ON MOLYBDENUM.....	123
6.1 Introduction.....	123
6.2 Hydrogen on molybdenum.....	127
6.2a Adsorption on field evaporated emitters.....	127
6.2b Adsorption on thermally annealed emitters.....	134
6.2c Discussion.....	137
6.3 Nitrogen on molybdenum.....	141
6.3a Adsorption on field evaporated emitters.....	141
6.3b Adsorption on thermally annealed emitters.....	147
6.3c Discussion.....	149
VII. THE ROLE OF STRUCTURAL DEFECTS IN CHEMISORPTION.....	153
7.1 Surface topography.....	154
7.1a Determination of surface structures.....	154
7.1b Estimating the cluster size.....	159

CHAPTER		Page
VII.	7.2 Adsorption on clusters.....	162
	7.2a Small clusters.....	162
	7.2b Intermediate clusters.....	169
	i. Work function changes.....	170
	ii. Studies at $T_s < 80$ K.....	176
	7.2c Large clusters.....	179
	7.3 Adsorption studies using scanning techniques.....	184
	7.3a Adsorption on clusters.....	185
	7.3b Adsorption on a flat (110) plane.....	191
	7.4 Summary.....	197
VIII.	DISCUSSION.....	199
	8.1 The promotion of chemisorption by defects.....	199
	8.1a A summary of experimental findings.....	199
	8.1b Models for defect promoted chemisorption.....	201
	i. Polizzotti's model.....	201
	ii. The rate limiting process for chemisorption on tungsten (110).....	202
	iii. A modified model.....	205
	iv. Extension to macroscopic surfaces.....	207
	8.1c Chemisorption on field emitters.....	217
	i. Perfect (110) planes.....	218
	ii. Surfaces with clusters.....	221
	iii. The rate of dissociation on plane edges.....	225
	iv. The rate of chemisorption on flat (110) planes as promoted by plane edges.....	229
	8.1d The variation of sticking coefficient with surface geometry.....	231
	i. Sticking coefficient on cluster edges.....	231
	ii. Sticking coefficient on surfaces with different size clusters on top.....	234
	8.1e Direct dissociation on the tungsten (110) plane.....	235
	8.1f Diffusion on the (110) plane.....	239
	8.1g Summary.....	240
	8.2 Chemisorption of hydrogen on Re(0001).....	241
	8.2a Mechanism of chemisorption.....	241
	8.2b Rate of chemisorption.....	243

CHAPTER	Page
VIII. 8.3 Chemisorption of hydrogen on Ir(111).....	245
8.4 Chemisorption of nitrogen on W(110).....	247
8.5 Chemisorption of nitrogen on Re(0001).....	250
8.6 Chemisorption on Mo(110).....	253
8.7 Summary.....	254
APPENDIX	
A. TECHNIQUES OF SAMPLE PREPARATION.....	256
B. SIMULATION OF PROBE HOLE SCANS.....	269
C. EFFECTS OF EDGES ON SINGLE PLANE WORK FUNCTION.....	291
D. SIMULATION OF WORK FUNCTION CHANGES.....	300
E. COMPUTER PROGRAMS.....	318
REFERENCES AND FOOTNOTES.....	326
VITA.....	335

CHAPTER I

INTRODUCTION

The presence of gas on metal surfaces affects reactions in many important industrial processes, such as sintering, corrosion, catalysis, sputtering, etc. Studies of the interaction of molecular gases with metal surfaces therefore become a prerequisite to a fundamental understanding of these processes. Considerable effort has been spent to establish the correlation between the morphology of surfaces and their reactivity toward gases, but several important questions still remain unanswered. 1.) Although there is now ample evidence indicating that the interaction of gas with metal surfaces is strongly affected by the structure of the surface [1,2], the real role of structural defects on surface reactions is not yet established. 2.) The bulk crystal structure of the substrate is known to have a significant effect upon the rate of reaction on the surface [3], but the extent of this effect is little understood. 3.) The role of the electronic properties of the substrate upon bonding also remains largely unknown. These factors, together with the chemical nature of the substrate, and that of the gas, are the dominant effects on the rate of chemical reactions on a surface. An understanding of the relative importance of these factors would provide a useful guide in predicting the reactivity for particular systems, and is the aim of this thesis.

Of many possible reactions worth investigating, we have chosen to study the interaction of two diatomic gases, hydrogen and nitrogen, with metal surfaces. The interaction of diatomic gases with metal surfaces is important not only because these are the most commonly encountered con-

taminants, but also because the chemisorption of these simple gases is likely to be an essential step in many surface reactions. An understanding of the mechanism leading to dissociative chemisorption of these gases is likely to lead to a better understanding of more complex interactions as well.

Recent studies [3] have shown that the ability of hydrogen and nitrogen to adsorb on crystallographically smooth surfaces of tungsten is extremely limited. However, on the closest packed planes of rhodium, an fcc metal, the chemisorption of hydrogen does not show any peculiarity as compared to rougher surfaces. Obviously the surface structure of the substrate is not the only factor that dictates the rate of chemisorption. Even with these, the simplest molecular gases, the physical parameters that affect chemisorption on a surface are not clearly known. A systematic investigation is therefore very desirable.

Structural defects have been suspected as active sites which promote the chemisorption on that surface. In the past efforts to assess the importance of such defects have largely concentrated on surfaces of macroscopic dimensions. However, for these samples experimental parameters determining the surface reactivity are difficult to control and conflicting results have often been reported [4-6]. Furthermore, whether the observed difference between a relatively smooth surface and a surface with a high density of defects is caused by an actual defect-promoted adsorption or by adsorption on the defects alone is hard to distinguish. To solve these problems, a technique which can control the experimental parameters unequivocally, and provides better spatial resolution of surface features is necessary.

In this study, the rate of chemisorption of nitrogen and hydrogen is systematically investigated on substrates of various surface structure, bulk crystal structure, and of different electronic and chemical properties. Tungsten, rhenium, and iridium are chosen as representatives of bcc, hcp, and fcc metals in order to learn the effects of the bulk structure on chemisorption. The interaction of hydrogen and nitrogen with molybdenum has been studied to compare with its isoelectronic partner, tungsten. On the closest packed plane, the (110), of tungsten, chemisorption has been examined as a function of surface geometry by carefully controlling the defect density on that surface. The choice of these materials is also inspired by practical interests in addition to historical reasons: iridium is an important precious metal catalyst; the structural selectivity in the interaction of gases with iridium is of intrinsic interest. Rhenium has recently become a major candidate for the dual-purpose catalyst used in automobile emission controls [7].

For systems showing a very low rate of chemisorption, we have investigated the possible mechanisms responsible for limiting the rate of interaction. We have also determined the exposure and temperature necessary to bring about interaction on these surfaces. For surfaces showing rapid chemisorption at room temperature, attempts have been made to determine the conditions under which the chemisorption can be prevented, although these attempts have not always been successful. These results will be presented in Chaps. III-VI, with a review of the available experimental data on the particular system preceding our results. The experimental technique we have chosen to unequivocally control surface conditions, as

well as the experimental procedures, will be discussed in the next chapter. The effects of structural defects on chemisorption observed by this technique will be presented in Chap. VII, and a quantitative treatment of surface kinetics involved will be discussed in Chap. VIII.

CHAPTER II

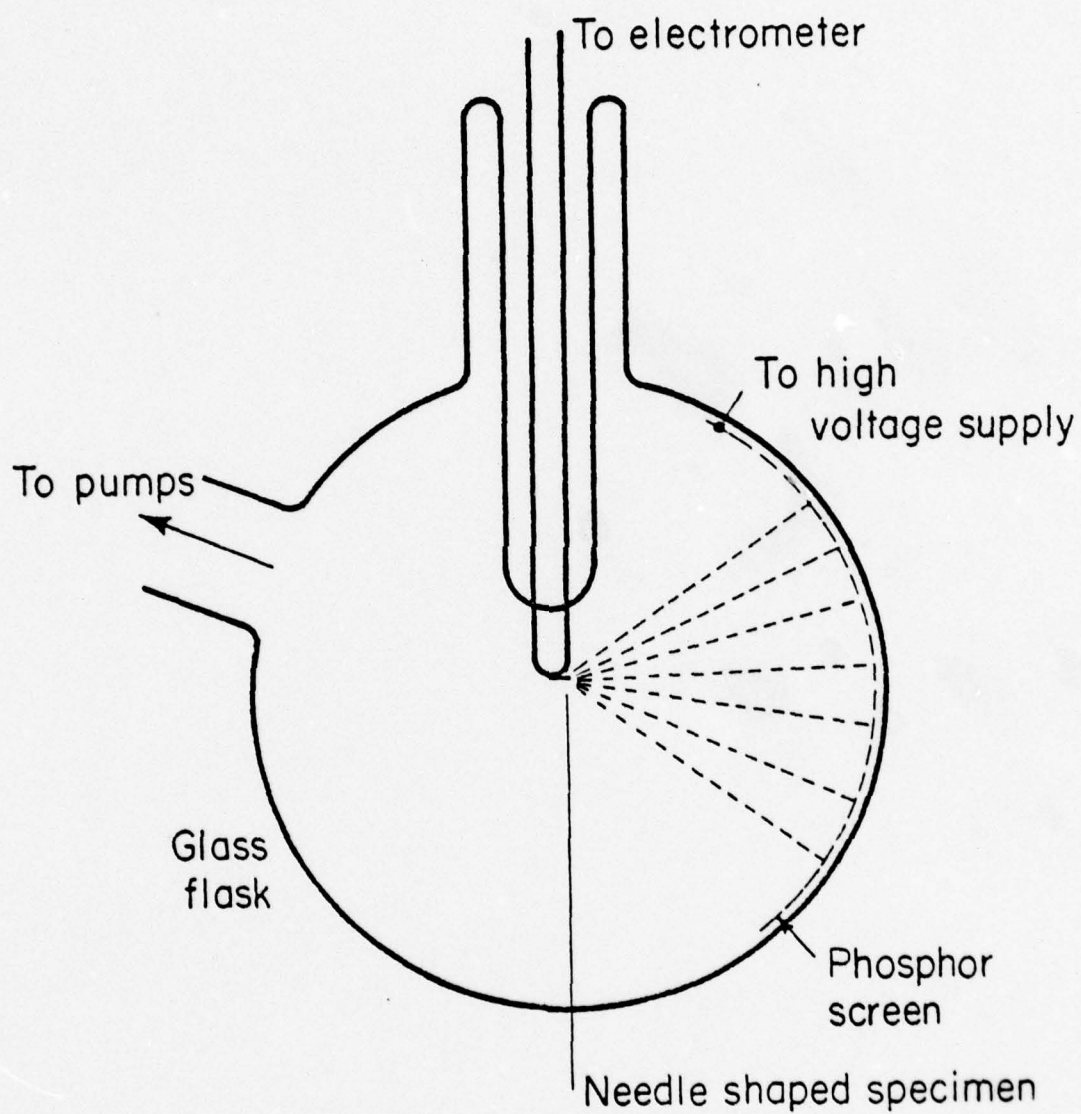
EXPERIMENTAL TECHNIQUES

The techniques available for monitoring the chemisorption of gases on metal surfaces can be divided into two general categories, depending upon whether they employ macroscopic or microscopic samples. The principal difficulties common to all macroscopic methods are the inability to characterize the surfaces as free of structural defects and, to a lesser extent, the inability to determine the degree of cleanliness of the surface. The combined use of field ion microscopy and probe hole field emission microscopy avoids these difficulties by employing atomically perfect microscopic samples, while at the same time providing excellent control of the surface conditions. This is the method we have chosen to carry out our experimental program.

2.1. Field emission and field ion microscopy

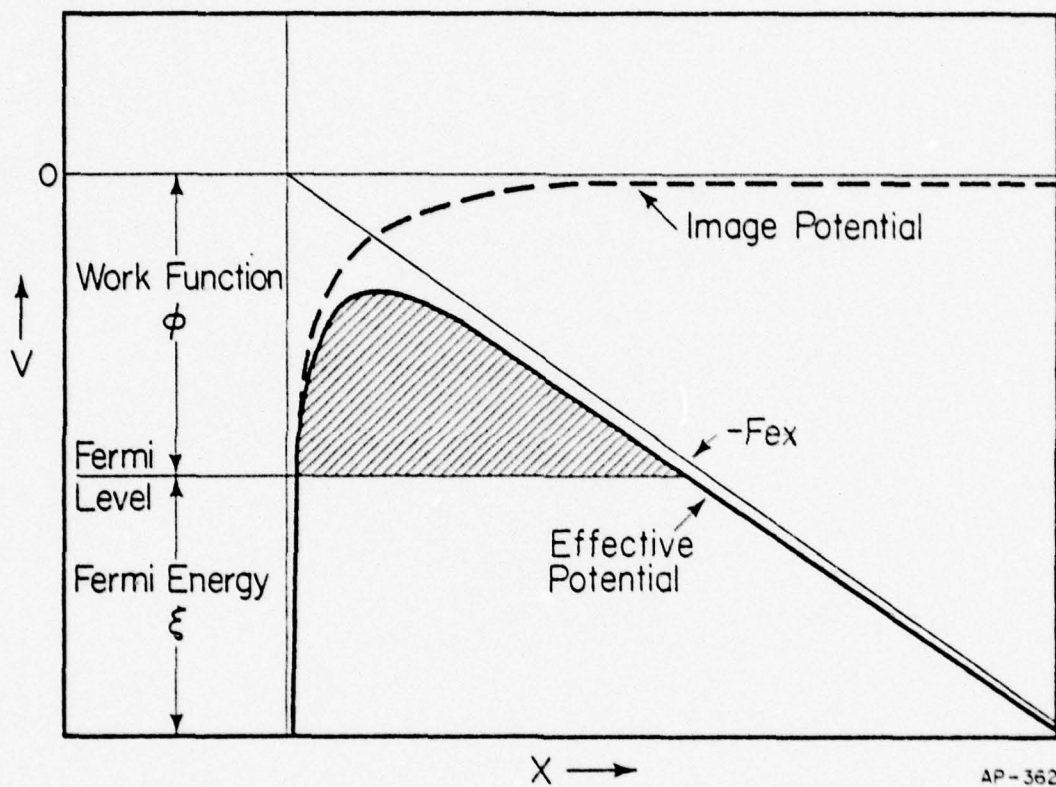
The essentials of a field emission microscope [8-10] are shown in Fig. 2.1. A sharply pointed emitter is held at a negative potential relative to the fluorescent screen and walls of the vacuum envelope. In the presence of the external electric field, the surface potential barrier of the metal becomes distorted, as shown in Fig. 2.2. When the field is sufficiently high, the penetration of the barrier by electrons tunneling at energies close to the Fermi level becomes significant. The electrons tunneling from the metal surface are accelerated to the fluorescent screen and there produce an image of the emitting surface area.

The current density of electrons tunneling from a metal surface has been calculated by Fowler and Nordheim [11,12] on the assumption of a free electron metal at 0 K. This model assumes a planar surface, whose surface potential barrier $V(x)$ is given by the sum of the electron image potential



AP-936

Fig. 2.1. Schematic diagram of field emission microscope.



AP-362

Fig. 2.2. Potential diagram for electrons at the surface of a metal under the action of an applied electric field. (From Reference 3.)

and the potential of the external field. Expressing the current density J in A/cm^2 , the electric field F in V/cm and the work function ϕ in eV , one obtains the expression for the current density of emitted electrons

$$J(F) = 1.54 \times 10^{-6} \frac{F^2}{\phi t^2(y)} \exp\left[-6.83 \times 10^7 \frac{\phi^{3/2}}{F} v(y)\right], \quad (2.1)$$

where $y = \sqrt{e^3 F/\phi}$, and $v(y)$ and $t(y)$ are special elliptical functions whose values have been tabulated [13].

In real experiments, the current-voltage characteristics of an emitter are measured. In terms of these Eq. (2.1) becomes

$$I = 1.54 \times 10^{-6} \frac{\beta^2 V^2 A}{\phi t^2(y)} \exp\left[-6.83 \times 10^7 \frac{\phi^{3/2}}{\beta V} v(y)\right], \quad (2.2)$$

where A is the emitting area, and β a geometrical factor which relates the emitting voltage to the electric field through $F = \beta V$. Since ϕ , β , and A are independent of the emitter voltage, the curve obtained by plotting $\ln(I/V^2)$ versus $1/V$ (a Fowler-Nordheim or F-N plot) is a straight line with slope m proportional to $\phi^{3/2}$. From Eq. (2.2),

$$m = -2.97 \times 10^7 \frac{\phi^{3/2}}{\beta} s(y),$$

where $s(y) = v(y) - 1/2 y \left(\frac{dv(y)}{dy}\right)$. The tabulated values of $s(y)$ [13] are generally close to unity for typical experimental conditions and vary only slowly with the applied field.

In order to study the emission characteristics of a single crystal plane on the emitter, a small hole is made in the screen. The image of the emitting area whose current-voltage characteristic is to be determined is positioned over the probe hole and the current passing through the hole is measured as a function of the applied voltage. By using the value of ϕ determined from macroscopic samples as the average work function of the emitter, the geometrical factor β can be calculated from Eq. (2.3), once the slope of the Fowler-Nordheim plot for the total emission from a clean sample is known. The work function of the single crystal plane can then be calculated using this β and the slope of the Fowler-Nordheim plot of the single crystal plane. The work function thus obtained is uncompensated for the local variation of field (variation of β) and is consistently higher than the real work function of the single plane. This drawback may be amended by considering the geometry of the emitter [14,15] or by measuring the total energy distribution [16,17,18] from the plane. In our study only changes in the work function are of interest. No attempt is made to account for local variations in the field, and all values of ϕ reported here are not compensated for local variations in β .

A field ion microscope [14,15] is obtained when the polarity of the applied field in a field emission microscope is reversed and some imaging gas introduced. If the field at the surface is high enough ($2-5 \times 10^8$ V/cm), field ionization occurs when gas atoms impinge on the surface: an electron of the gas atom tunnels into the metal, leaving behind a positively charged

ion. In Fig. 2.3a the metal atoms of the sample are represented by the array of solid circles, the imaging gas atoms by broken circles. The conduction electrons of the metal are bound by the work function ϕ below the vacuum level. The equipotential of the metal surface is modified by the local roughness of the surface and is shown by the solid line in Fig. 2.3a. Field ionization does not occur directly on the surface, but several angstroms above it. The potential seen by an electron of a gas atom is shown in Fig. 2.3b. A gas atom that sits directly on the surface cannot lose an electron to the conduction band because the ionization potential, I , of the electron of the gas atom is greater than the work function of the metal: all the electron states at this energy in the metal are already occupied. If, however, the gas atom is at (or beyond) a critical distance R_c above the surface, where the gas electron energy is equal to (or above) the Fermi level, tunneling can occur. This critical distance is given approximately by $R_c = (I - \phi)/F$ and has a typical value of 4 Å. The equipotential at the critical distance, shown by the dashed line in Fig. 2.3a, will not vary nearly as much as the metal equipotential at the surface. However, the ionization probability, largely determined by the overlap between wave functions of initial and final states [20], is still much higher over protruding surface atoms. Once the electron has tunneled into the metal, the remaining positive ion accelerates along the electric field lines until it strikes the fluorescent screen, creating an image spot. Since field ionization occurs primarily over protruding surface atoms, the complete field ion image is actually a projection of the loci of points on the surface that protrude significantly above the metal equipotential [14].

Field Ionization of Helium

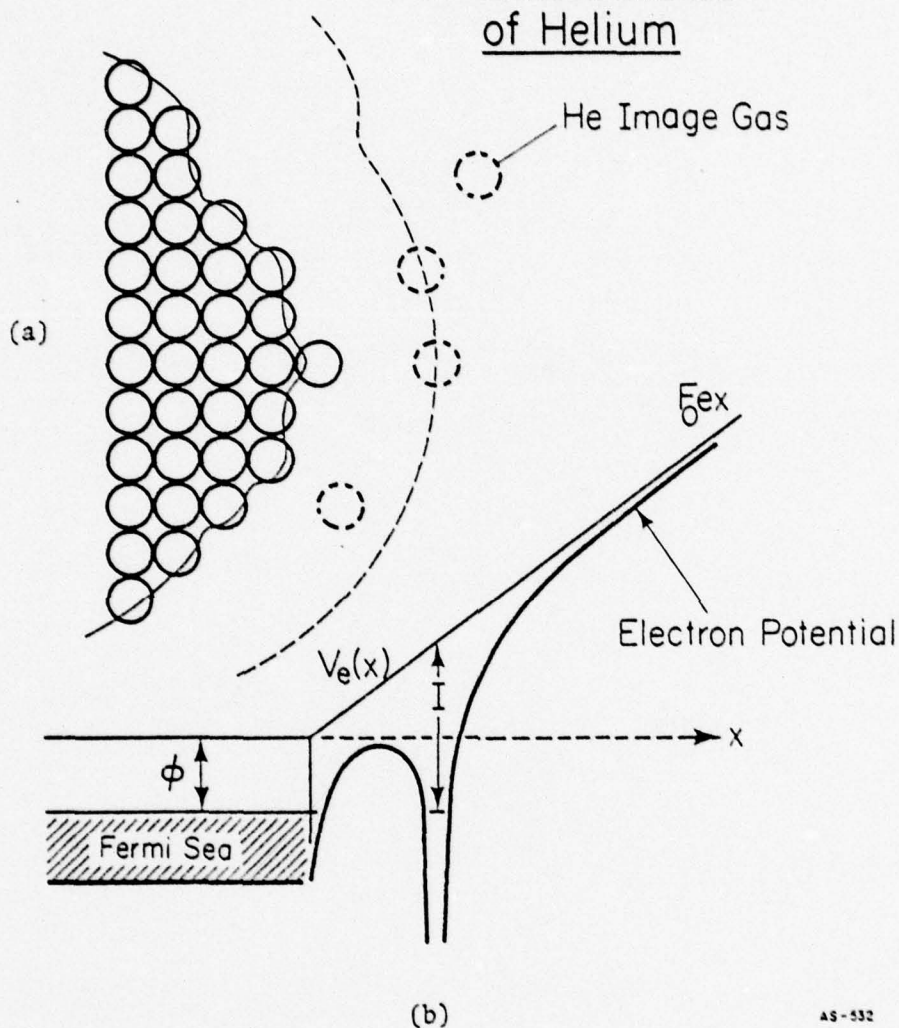


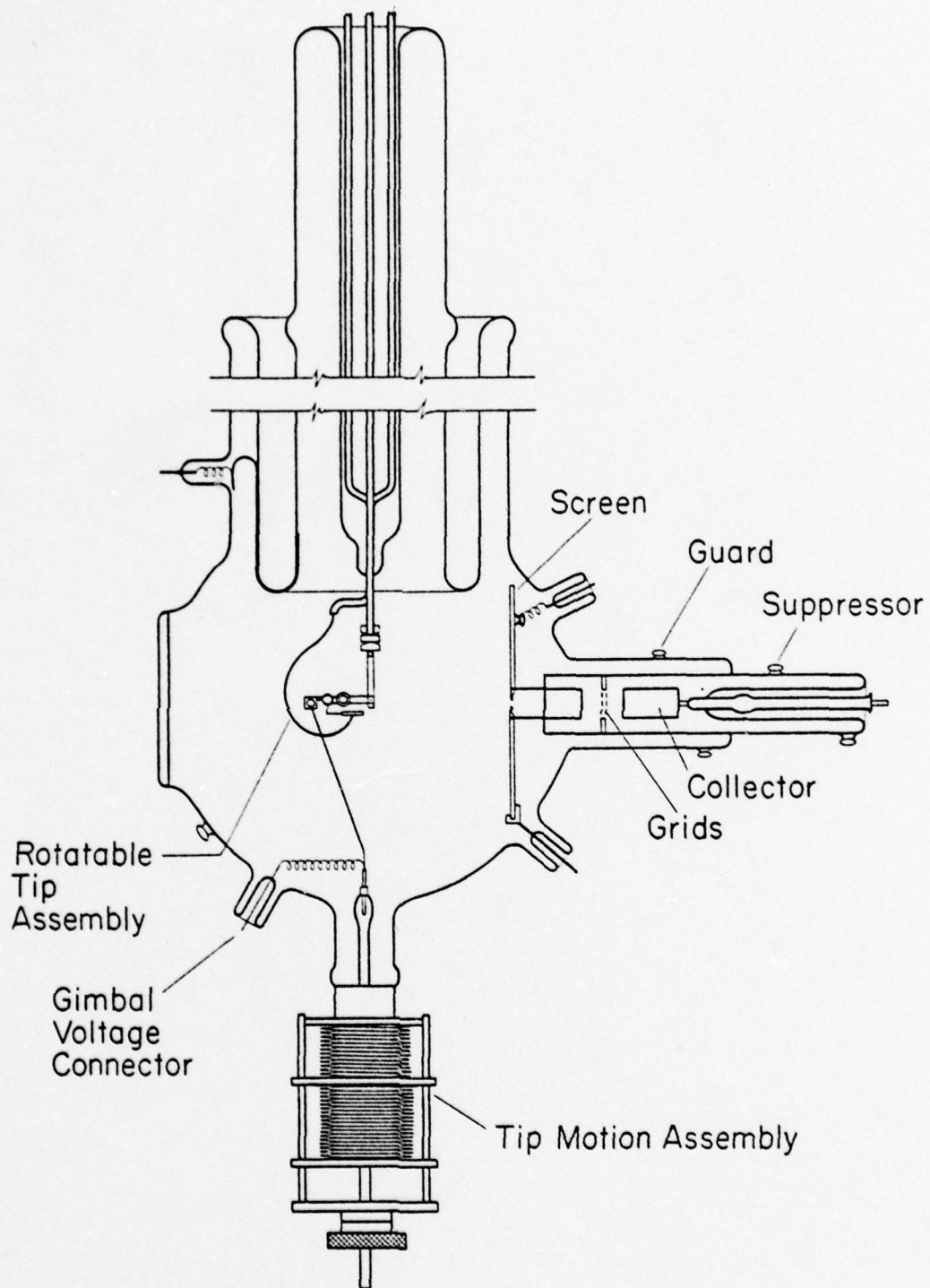
Fig. 2.3. One-dimensional model for field ionization at a metal surface. The solid circles represent the atoms of a metal. The equipotential of the metal is terminated at the surface and is re-represented by the irregular solid line. The image gas (the dashed circles) can ionize in a high electric field at or beyond the critical distance, R_c , represented by the dashed line. The potential energy of an electron of a gas atom (whose nucleus is located at R_c) is shown as a function of electron distance, z , from the surface. (From Reference 19.)

The magnification of either the field emission or the field ion microscope is determined by geometry as well as by electron trajectories. It is given roughly by the ratio of the distance between emitter and screen to the radius of curvature of the field emitter. The magnification is typically 10^5 to 10^6 , and can be made arbitrarily large by using sharper emitters and longer screen-to-emitter distances. However, the crucial parameter in a microscope is not its magnification but its resolution. The significant factors that limit resolution are the tangential motion of the electron or imaging gas at the surface, and, for the field ion microscope alone, the size of the imaging site itself. These have been treated in detail by Müller [15] and by Good [21]. For the field ion microscope, the contribution from the tangential motion of the imaging gas can be reduced by cryogenic cooling. A resolution as low as 2 \AA can be reached in this way, and resolutions of 3 to 4 \AA are routinely achieved in most field ion microscopes. For the field emission microscope, the field emitted electrons have large kinetic energies, controlled by the Fermi energy, regardless of the temperature of the surface. The resolution of the field emission microscope is thus restricted to $\gtrsim 20 \text{ \AA}$, insufficient to reveal the location of individual atoms. In this study, the detailed structure of the surface is examined by field ion microscopy. Field emission microscopy is used to characterize the surface to a less quantitative degree, and to study the interaction with gas, which can be accomplished with considerably less perturbation than possible by the former technique.

2.2. Experimental arrangement

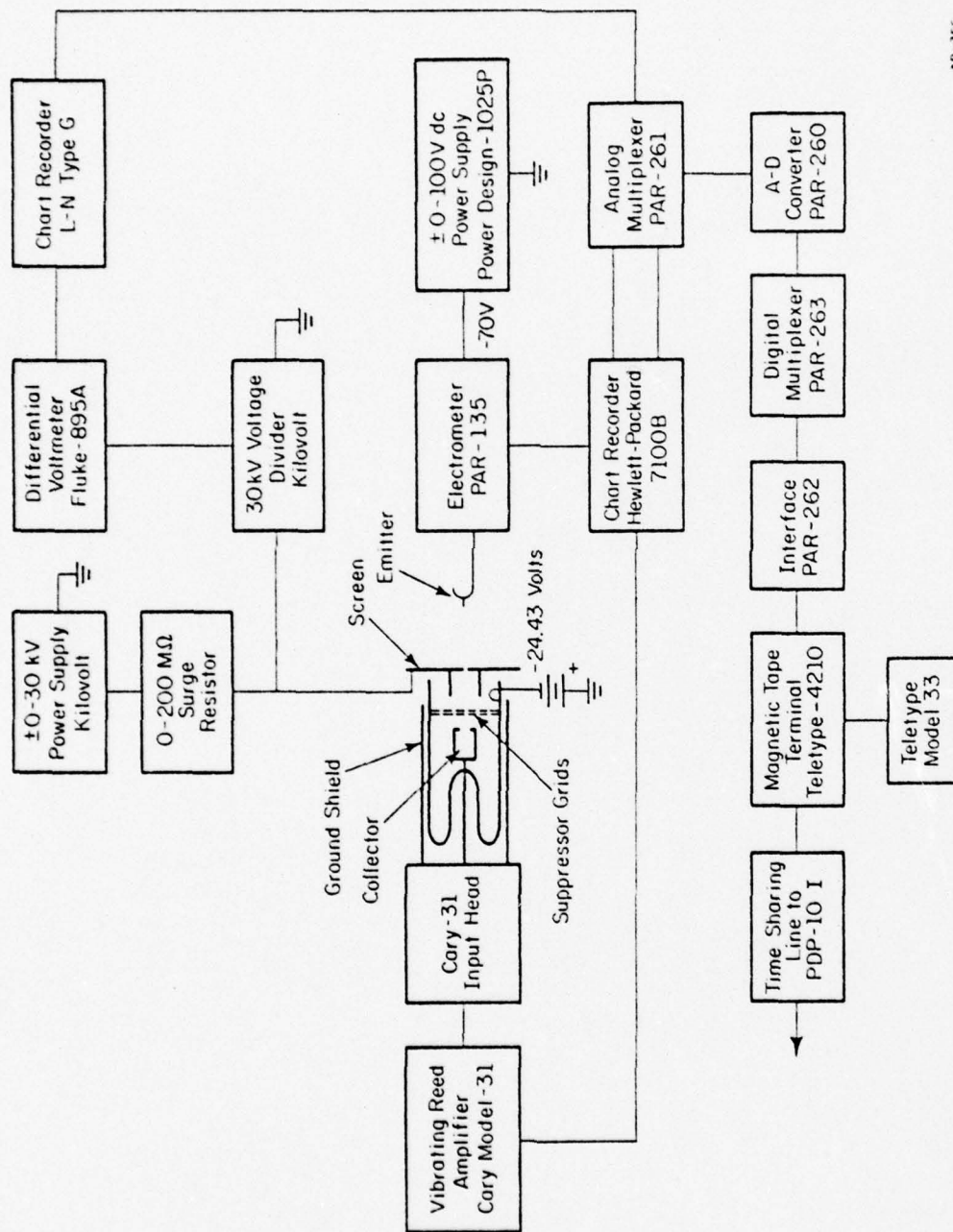
The probe hole field emission microscope used in this study is shown in Fig. 2.4. The construction and operation of the microscope have been described in detail by Polizzotti in his thesis [3]. The essential features of the microscope are a probe hole, which allows measurements on single crystal planes, and a mechanical motion assembly which allows the adjustment of the emitter position with virtually no distortion in the emission image. The electronic arrangement of the experiments is outlined in Fig. 2.5. The electrons passing through the probe hole are collected by a guarded Faraday cup and measured by a Gary 31 vibrating reed electrometer. The current passing through the probe hole, as well as the total emission current, are recorded as a function of the screen-to-emitter voltage. Fowler-Nordheim plots are then constructed, and work functions are calculated according to Eq. (2.3). The work function for a single crystal plane obtained in this way is not corrected for the local variation of electric field and is higher than the real work function. However, in studying the interaction of a surface with gas, only the change in the work function is of interest. The changes in the work function are not seriously affected by the local field; no effort is therefore made to correct for such errors.

The gases to be studied are admitted to the microscope through a 5.3 cm long, 0.003 in. diameter capillary from a separately pumped gas handling system, shown schematically in Fig. 2.6. The vacuum in both the microscope and the gas handling system is achieved using 40 l/sec three-stage all



AS-116

Fig. 2.4. Schematic diagram of the probe hole field emission microscope used in the single plane adsorption studies. (From Reference 3.)



AP-356

Fig. 2.5. Block diagram showing the arrangement of the electronics and the bias voltages used in the single plane measurements. (From Reference 3.)



Fig. 2.6. Schematic diagram of gas handling system. V_1, V_2, V_3, V_4, V_5 --Granville-Phillips type C valves; BAG--Bayard-Alpert Ionization gauge; P_1, P_2, P_3 --Pirani gauges; Pd--Palladium thimble; G_1 and G_2 --nickel getters in Dewars; C--capillary; V_6 --glass vacuum seal-off. (From Reference 3.)

glass mercury diffusion pumps, with liquid nitrogen cooled traps on both the high and low pressure sides. The entire system, from the top of the diffusion pumps to the breakoff seals of the gas bottles, is bakable to 420 C; pressures $< 1 \times 10^{-10}$ Torr are routinely achieved following two or three bake-outs, employing standard ultra-high vacuum techniques.

2.3. Gas handling and sample preparation

A schematic diagram of the gas handling system has already been shown in Fig. 2.6. All gases used in this study are Airco assayed reagent grade; typical lot analyses of the hydrogen, deuterium, and nitrogen used are shown in Tables 1-3. Reactive impurities in the nitrogen gas were removed by allowing the gas to equilibrate over freshly evaporated nickel films, following the suggestion of Ehrlich and Hudda [22]. Final purification of the hydrogen is achieved by passing the gas through a palladium thimble [23] located above the hydrogen reservoir. After the palladium thimble is thoroughly outgassed by r-f heating in vacuum, the glass seal-off at the gas bottle side of the thimble is sealed and the hydrogen gas bottle opened. The thimble allows a low rate of hydrogen flow initially even at room temperature. When a pressure increase in the system is detected by the Bayard-Alpert ionization gauge, the Granville-Phillips type C valve closest to the thimble, V_5 , is closed, and the hydrogen pressure builds up behind this valve.

Table 1

Mass spectrometer analysis^{a,b} for Airco
hydrogen gas, cylinder No. W-93825-B^c

Impurity	Concentration ppm, atomic	Impurity	Concentration ppm, atomic
He	2.0	CO ₂	< 1.0
N ₂	1.0	Hydrocarbons	< 1.0
O ₂	0.5		

- a. Threshold for most impurities = 2.0 ppm.
b. Only detectable impurities listed.
c. Breakseal Nos. 40710001-40710060.

Table 2

Mass spectrometer analysis^{a,b} for Airco
deuterium gas, cylinder No. RSG 12-3981^c

Impurity	Concentration %, atomic	Impurity	Concentration %, atomic
H ₂	< 0.2	O ₂	0.001
HD	0.5	Ar	0.0004
N ₂	< 0.0004	CO ₂	0.0004

- a. Sample scanned from mass 2 through mass 100.
b. Threshold for most impurities < 0.0004%.
c. Breakseal Nos. 40215003-40215011.

Table 3
Mass spectrometer analysis^a for Airco
nitrogen gas, cylinder No. 81111A^b

Impurity	Concentration ppm, atomic	Impurity	Concentration ppm, atomic
H ₂	< 1.0	O ₂	0.3
Ne	< 1.0	CO + CO ₂	0.4
Ar	2.3	Hydrocarbons	< 0.5

a. Only detected impurities listed.

b. Breakseal Nos. 50129001-50129046.

The nitrogen exposure is estimated from calibration curves, which are obtained before actual experiments, by directly measuring the pressure in the microscope using a Bayard-Alpert ionization gauge. During an experiment, a fixed pressure is kept behind the capillary (monitored by a Pirani gauge) and the time of exposure is measured. The actual exposure is then estimated from the appropriate calibration curve. Hydrogen cannot be measured accurately by ionization gauges since it interacts strongly with the hot filaments. The exposure to hydrogen is therefore estimated from calibration curves for nitrogen, compensated for the different rate of passing through the capillary. Details of these calibrations have been discussed by Polizzotti [3]. Typical calibration curves for nitrogen are shown in Fig. 2.7.

All field emitters studied here are prepared from zone refined single crystal wires supplied by the Field Electron and Ion Source Co. at McMinnville, Oregon. Chemical analyses of these wires are given in Tables 4 through 6. After a section of wire is mounted on the 10 mil

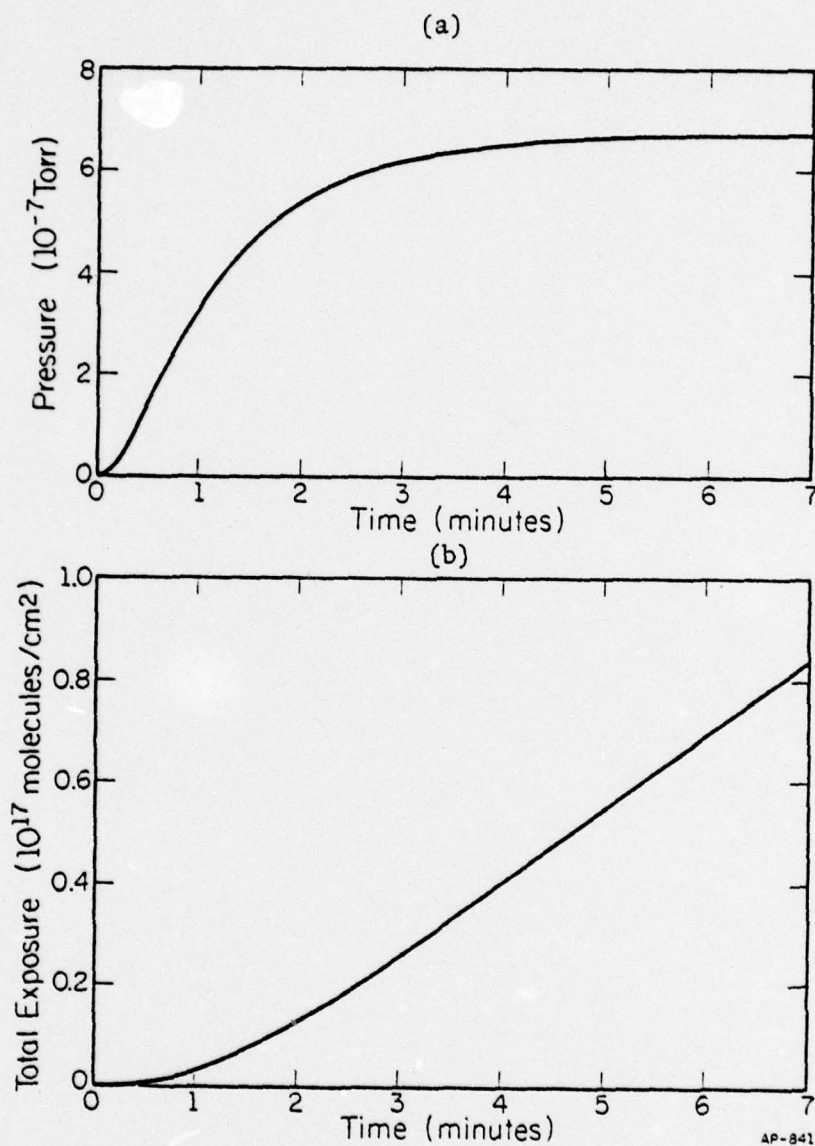


Fig. 2.7. Typical calibration curves for nitrogen exposure: (a) the variation of pressure in the microscope with time; pressure behind the capillary $= 50 \times 10^{-3}$ Torr; (b) corresponding total exposure estimated by assuming ideal gas law.

Table 4

Spark mass spectrometer analysis^a of
3 pass electron-beam zone refined tungsten single crystal

Element	Concentration ppm, wt.	Element	Concentration ppm, wt.
H	NR ^(b)	K	0.12
Li	< 0.01	Ca	0.63
Be	< 0.02	Ti	0.02
B	< 0.02	V	0.02
C	5.9	Cr	0.09
N	25	Mn	0.04
O	73	Fe	0.18
F	0.01	Co	0.02
Na	0.56	Ni	0.24
Mg	0.79	Cu	0.05
Al	0.16	Zn	0.05
Si	1.85	Zr	0.07
P	< 0.10	Mo	0.53
S	0.24	Bi	< 0.01
Cl	0.93		

a. All elements not reported < 0.1 ppm.

b. NR = not reported.

Table 5

Spark mass spectrometer analysis^a of 3 pass electron-
beam zone refined iridium single crystal wire

Element	Concentration ppm, wt.	Element	Concentration ppm, wt.
H	NR ^(b)	Fe	0.05
C	NR	Co	0.03
N	NR	Cu	0.06
O	NR	Zn	0.05
Al	0.47	Zr	1.6
P	0.01	Nb	0.05
Si	3.8	Mo	68
S	0.26	Ru	19
Cl	0.16	W	NR
K	0.04	Ta	0.38
Ca	0.05	Os	0.78
Ti	1.7	Pt	18
Cr	0.10	Pb	0.06
Mn	0.02	Th	10

a. All elements no listed < 0.1 ppm.

b. NR = not reported.

Table 6

Spark mass spectrometer analysis^a for 3 pass electron-beam zone refined molybdenum single crystal

Element	Concentration ppm, wt.	Element	Concentration ppm, wt.
H	NR ^(b)	V	< 0.03
C	NR	Cr	0.79
N	NR	Mn	0.01
O	NR	Fe	0.04
F	0.02	Co	0.12
Na	< 0.01	Ni	0.71
Mg	0.73	Cu	< 0.03
Al	0.40	Zn	< 0.03
Si	8.6	Zr	< 0.04
P	0.04	Nb	0.08
S	0.3	Ag	0.20
Cl	0.60	Cd	< 0.50
K	0.008	Ta	0.25
Ca	0.01	W	94
Ti	NR	Pb	3.0

a. All elements not listed < 0.1 ppm.

b. NR = not reported.

tungsten support loop, the whole loop and the zone refined wire are first electropolished in a suitable solution to remove asperities and possible contaminants introduced by spot welding. The end of the wire is then etched electrochemically in an appropriate polishing solution. Details of the emitter preparation are given in Appendix A for five metals: tungsten, molybdenum, rhenium, iridium, and platinum. The final sample preparation is done in vacuum, either by field evaporation or heating, as will be discussed next.

2.4. Surface cleaning

One advantage of field emission and field ion microscopy is the ability to clean the substrate to an unequivocal degree. This is accomplished by field evaporation [15]: when a high enough positive electric field is applied to the surface, the surface atoms ionize and accelerate away from the emitter, in much the same way as the field ionization of gas atoms. The physical principles underlying field evaporation are not yet completely understood, but the technique provides an ideal way to clean a surface. Field evaporation of several surface layers of a metal emitter produces a clean and geometrically smooth surface. The cleanliness is unequivocally assured, since the surface impurity concentration now is no higher than that of the bulk.

Throughout this study, cleaning the surface by field evaporation was attempted whenever practical. However, for single plane studies, the change in emission characteristics caused by adsorption must be distinguished from effects due to adsorption at the plane edges. An emitter cleaned by field evaporation usually contains single crystal planes no larger than 100 \AA in diameter. Contributions from strongly emitting plane edges can be eliminated only through carefully adjusting experimental parameters to maximize the plane size. The apparent work function change due to events at the plane edges is treated in detail in Appendix C, and will be further discussed in chapter VII.

When the contribution of the plane edges cannot be eliminated effectively by maximizing the size of the plane formed by field evaporation, the emitter is cleaned by heating to high temperatures. Thermal desorption of surface contaminants is a well-known method of cleaning

metal surfaces, and is used universally for cleaning macroscopic samples. The major objections to this technique are that the annealed surface is left rough on the atomic scale, and that the degree of surface cleanliness is not as unequivocal as for surfaces cleaned by field evaporation. In this study, these difficulties are resolved by monitoring the topographic structure of the single crystal plane by scanning across the surface [24], and by qualitatively checking data from thermally annealed emitters against comparable data from field evaporated emitters. The characterization of surface topography by probe-hole scanning will be discussed in detail in the next section and in Appendix B.

The mere achievement of an initially clean surface by either field evaporation or thermal annealing is not enough to guarantee that the surface remains free of further contamination in the course of an experiment. Contaminants may come in from the gas phase, or from diffusion through the bulk or over the surface of the sample. It is imperative to eliminate all of these sources in order to assure reliable experimental results. By following standard ultra-high vacuum procedures, the residual gas pressure in both the microscope and the gas handling system is reduced to $< 1 \times 10^{-10}$ Torr after two or three bake-outs. This low pressure effectively eliminates any significant contamination from the gas phase during the time span (~ 60 min) of one experiment. For a field evaporated emitter, only the tiny end cap is removed by field stripping; care must therefore be taken to reduce the diffusion of contaminants from the emitter shank to the emitting area. This is done by first flash heating the whole emitter and the 10 mil tungsten support loop to red heat, in order to desorb the loosely bound

contaminants without excessively blunting the emitter; the sample is then cleaned by field evaporation. Repeating this procedure five or six times proves effective in removing the diffusible contaminants. For thermally annealed emitters, mobile contaminants pose no threat since the whole emitter and shank are cleaned by thermal desorption. The only necessary precaution then is to outgas the sample and the 10 mil tungsten support loop thoroughly, so that no significant contamination is introduced by outgassing of the sample and sample support. For all experiments with thermally shaped emitters reported in this study, the sample and sample support loop have been completely outgassed, so that even on heating to white heat the pressure in the microscope remains $< 2 \times 10^{-10}$ Torr.

The real degree of contamination can be tested only by observation. Therefore, all experiments reported here are accompanied by blank runs in which the emitter is cleaned in the same fashion as in real experiments and the emission characteristics are recorded every 15 to 20 min. Real experiments are not started until the contamination level drops to a level at which the change in the emission current at constant voltage is less than 5% per hour.

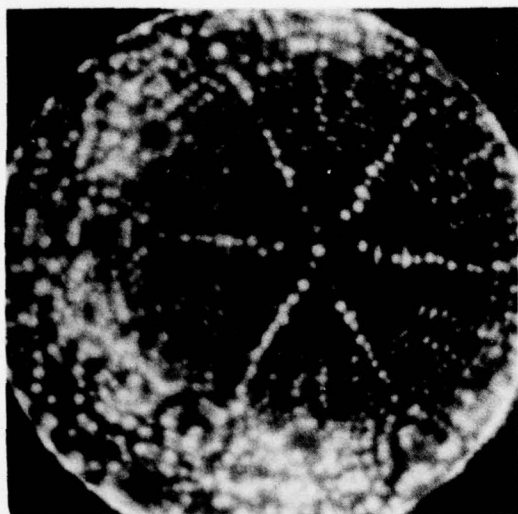
2.5. Surface characterization

The ability to resolve surface features in atomic detail makes field ion microscopy the best technique today for revealing the atomic arrangement of a surface. Field emission microscopy, by comparison, is about 10 times poorer in resolution. However, it is imperative to

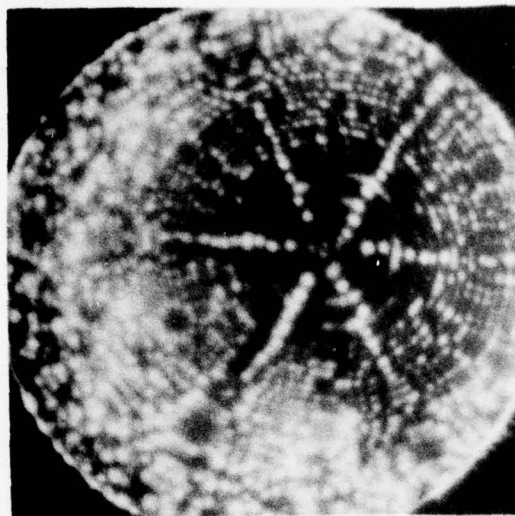
characterize a surface using field emission for one important reason: field ion microscopy gives no direct chemical information about the surface. Besides, the electron showers produced by the field ionization of imaging gas severely perturbs adsorbed gases [25-27]. Field emission microscopy, which uses no imaging gas, provides high sensitivity for gas detection and low disturbance of the adsorbate, hence provides non-destructive characterization of the adsorbate layers.

2.5a. Surface characterization by FIM

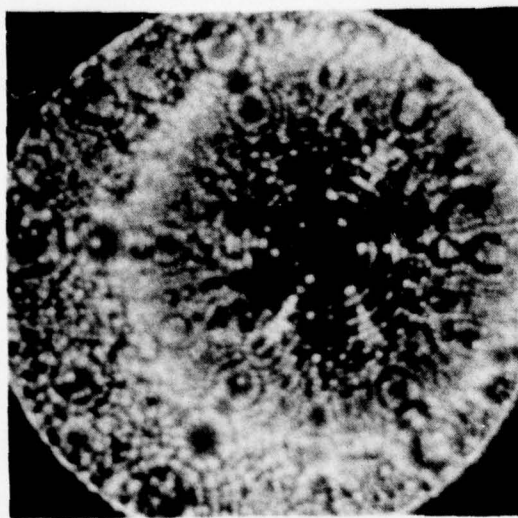
It is clear from the above discussion that the ideal way to characterize a surface and to study a chemical reaction on it is to combine a field ion and field emission microscope into one. However, the field emission microscope shown in Fig. 2.4 cannot be used effectively as a field ion microscope -- it lacks an image intensifier. A separate field ion microscope, which can accommodate exactly the same tungsten support loop as used by the field emission microscope, was therefore built. The emitter and support loop to be used in field emission studies is first characterized in the field ion microscope. The emitter is formed, and field stripped at 10 to 15 kV. The conditions that yield the desired endform are then studied. This is best illustrated by the field evaporation of a (0001) oriented rhenium emitter. As shown in Fig. 2.8a,b, field evaporation of (0001)Re below 150 K leaves some atoms in the center of the (0001) plane. To achieve a smooth (0001) plane, the emitter has to be held at temperatures higher than 150 K. In Fig. 2.8c is shown such a smooth (0001) plane, obtained by field evaporation at 200 K.



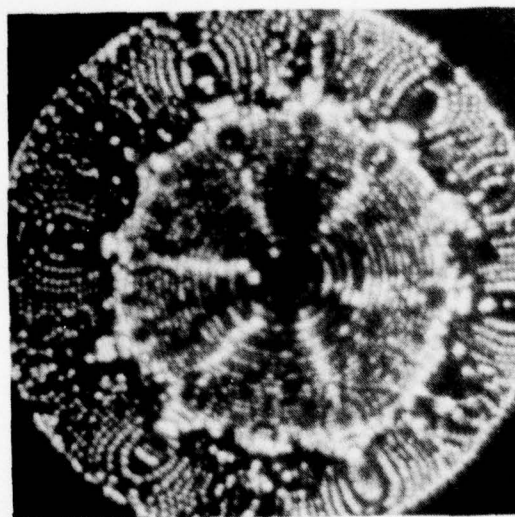
(a)



(b)



(c)



(d)

Fig. 2.8. Field ion micrographs of a $[0001]$ -oriented rhenium emitter, subject to field evaporation under different conditions. (a) Field evaporated at 80 K (10.5 kV). (b) Field evaporated at 80 K again to expose the next layer. (c) Same tip field evaporated at 200 K (9.7 kV). (d) Field evaporated at 300 K (9.0 kV).

However, at temperatures higher than 300 K, plastic deformation due to field stresses starts to show up about 20 degrees from the tip apex, as is evident in Fig. 2.8d. Thus by examining the surface in a field ion microscope the conditions leading to the desired emitter endform can be decided easily.

in the field ion microscope one can also learn how to control surface topography. In Fig. 2.9 is shown a sequence of field ion micrographs recording the evaporation at 200 K of two successive layers of the Re(0001) plane. Starting from a perfectly smooth (0001) plane (2.9a), the atoms in this plane gradually evaporate (Fig. 2.9b,c) and finally leave a small island at the center of the next layer (2.9d); stripping down the next layer creates the same situation (2.9e,f,g) but, in addition, also reveals the ABAB stacking sequence of the h.c.p. structure as evidenced by the reversal in the direction of the small triangular island. These field ion micrographs show clearly that the surface topography can be controlled on a fine scale by controlled field evaporation: one can choose to create a perfectly smooth surface (2.9a) or a defective surface (2.9d). This makes it possible to study the contribution of surface defects to chemisorption in a direct way, as will be discussed in more detail in Chapter VII.

Field ion micrographs of thermally cleaned emitter are generally difficult to obtain, since the excessive blunting of the emitter during heating makes imaging at less than 30 kV impossible. Unlike field evaporation, thermal treatment leaves rough steps on the surface, as is evident in Fig. 2.10a, which shows a thermally annealed (0001)Re emitter.

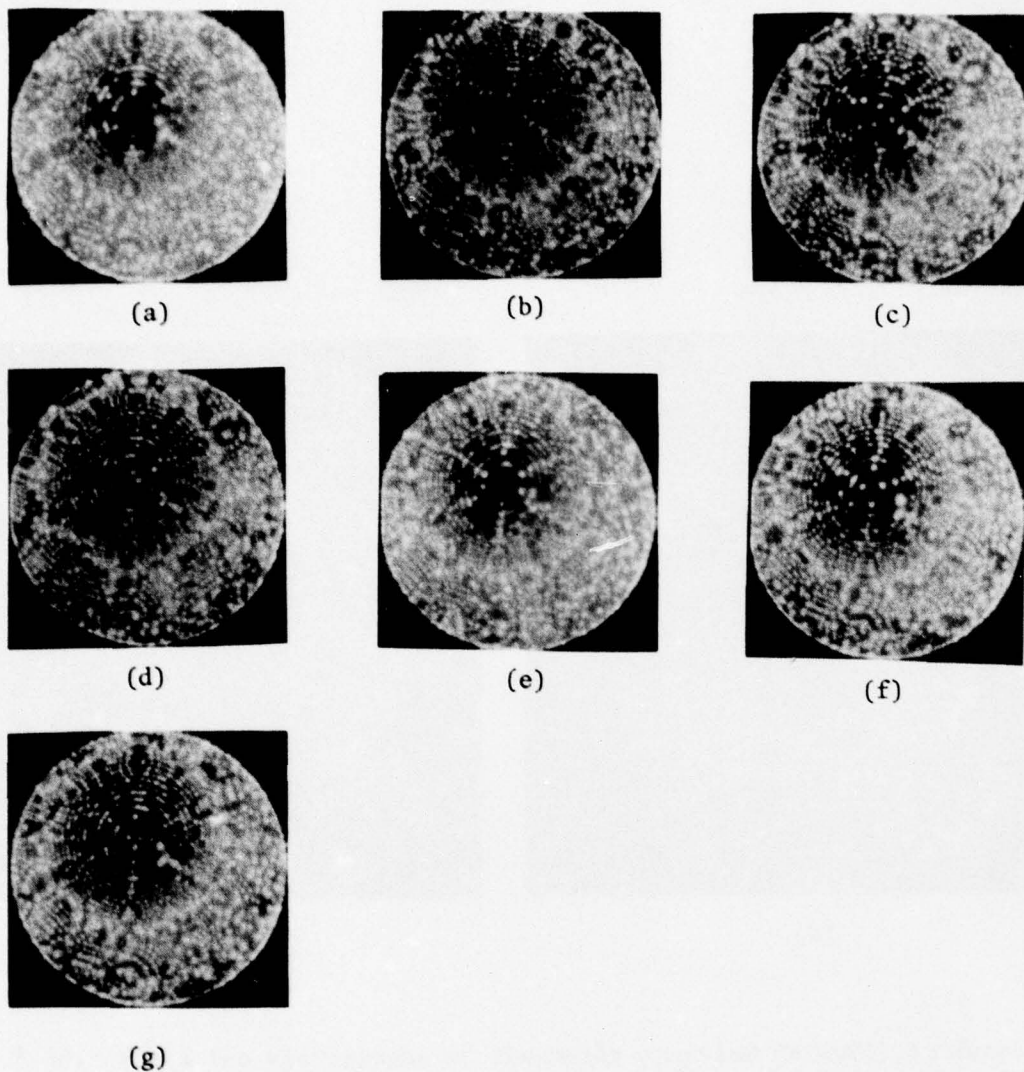


Fig. 2.9. Field ion micrographs showing the controlled field evaporation of a Re(0001) surface: (a) a perfect (0001) plane; (b) (0001) plane shrinks after evaporation; (c) further evaporation of the same layer reduces the (0001) plane to triangular shape; (d) a small triangle containing a few atoms is obtained upon further evaporation; (e) the first layer of the (0001) plane is completely evaporated, revealing the second layer; (f) the second layer also becomes triangular, but the direction of the cluster is reversed compared to the first layer; (g) further evaporation reduces the size of the triangle. All micrographs are obtained by field evaporation at 200 K and imaged at 80 K with imaging voltage ~ 10.5 kV.

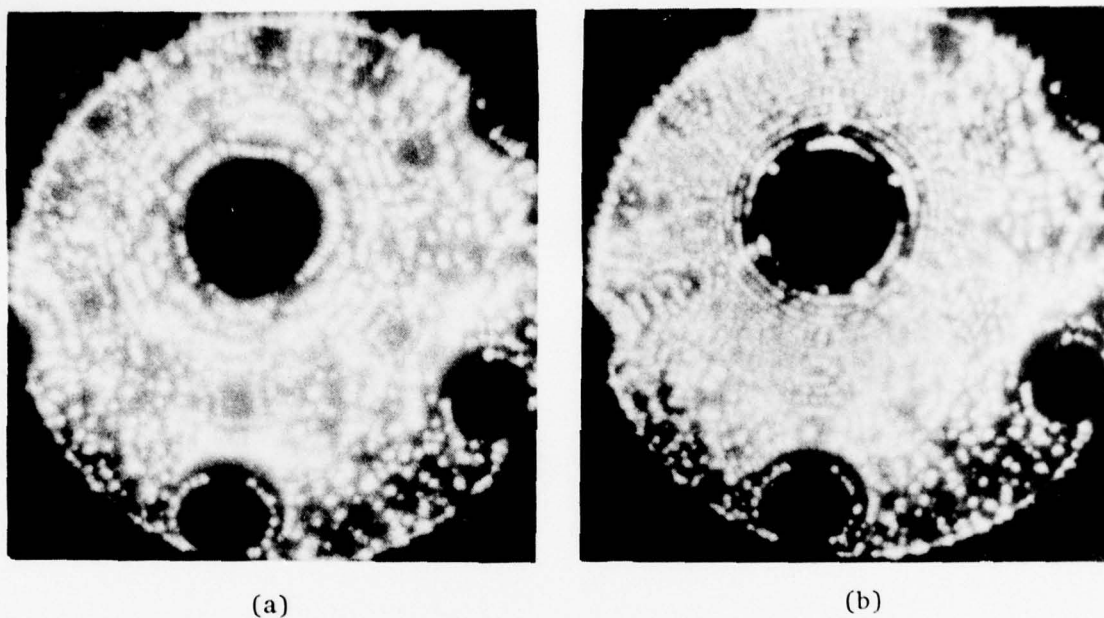


Fig. 2.10. Field ion micrographs of thermally annealed Re(0001) surfaces;
(a) after the sample is heated to ~ 1500 C for two minutes;
(b) after the tip is partially cleaned by field evaporation.
Imaged at 80 K with imaging voltage ~ 15 kV.

In Fig. 2.10b this surface is partially field evaporated by raising the voltage, to illustrate the degree of roughness of the thermally formed surface as compared to field evaporated surfaces. However, in both cases the (0001) plane, which we are primarily interested in, is large and smooth. This was later confirmed by field emission techniques, which are described next.

2.5b. Surface characterization by FEM

Surface characterization by field emission is performed by scanning across the single crystal plane and recording the probe hole current [3, 24]. This is shown in Fig. 2.11. For a medium sized plane, the collector current shows a minimum when the probe hole is placed at the geometrical center of the plane. When moving away from the center, the probe hole current reveals a maximum, followed by a minimum on either side of the plane center, as illustrated in Fig. 2.11a. The maxima of the collector current presumably correspond to electron emission from the edges of the plane. If, after these measurements, the field evaporation voltage is increased slightly, allowing evaporation to proceed further, the scan diagram changes as shown in Fig. 2.11b: instead of a minimum, a maximum appears at the geometrical center, indicating that a small cluster of atoms is left at the center of a flat surface. When moving away from the center, the probe hole current shows only one minimum at each side, indicating that the immediate vicinity of the cluster is flat. When the evaporation is allowed to proceed further still, by

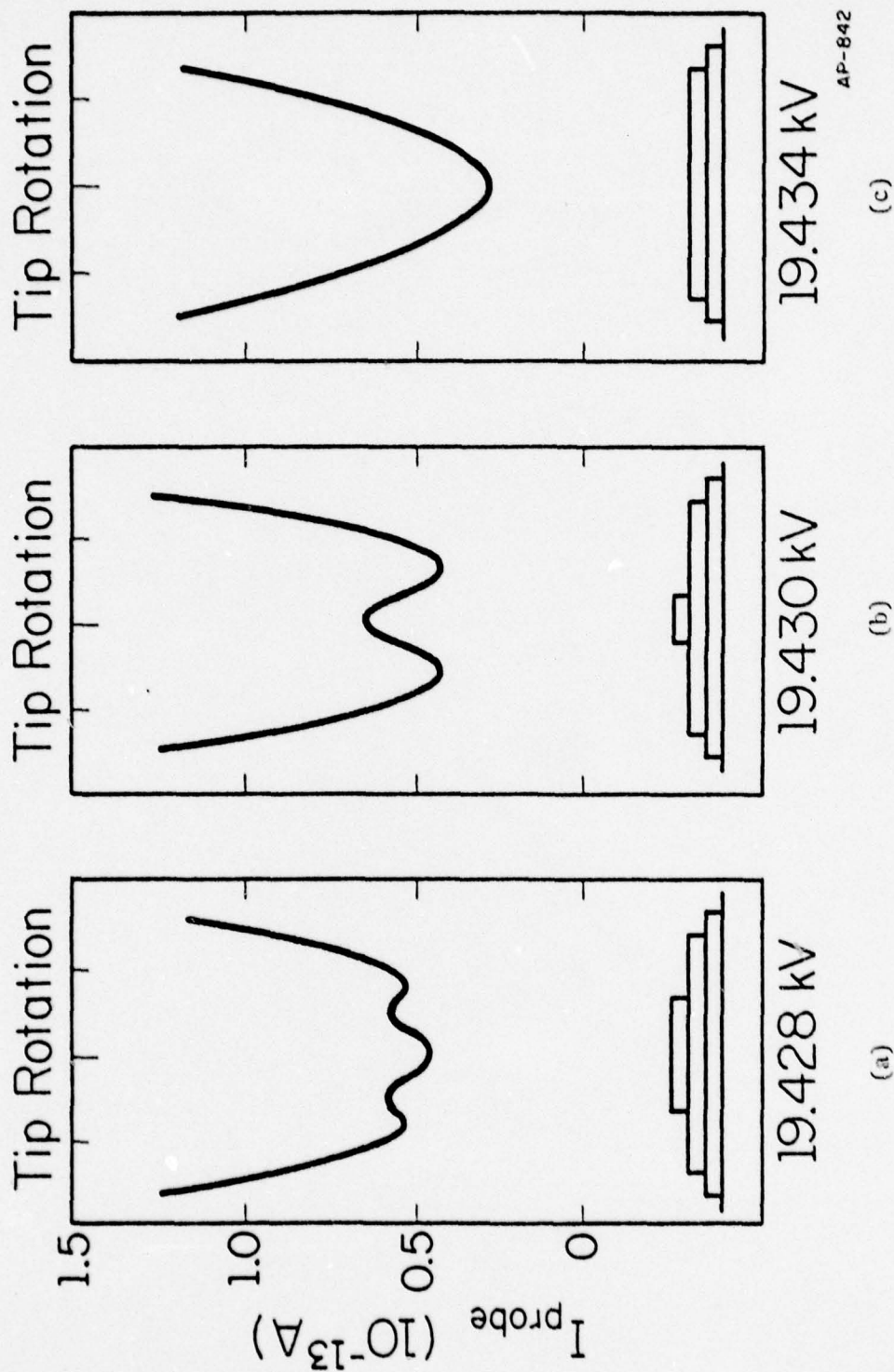


Fig. 2.11. Variation of scan diagrams with field evaporation voltage for a W(110) plane. Total emission current = 3×10^{-8} A at 1,514 V and 80 K.

raising the voltage again, a large, flat plane is achieved, as suggested by Fig. 2.11c: a single minimum corresponding to the geometric center of the emission pattern is the only feature to appear in the scan diagram. Qualitatively, the three scanning diagrams in Fig. 2.11 should correspond to situations shown in c, e, and f of Fig. 2.9, where the detailed surface topography is documented by field ion micrographs.

The value of the probe hole current at the geometrical center also shows a periodic behavior when the evaporation voltage is increased. As shown in Fig. 2.12, the probe hole current increases steadily with increasing stripping voltage. It finally reaches a maximum, then suddenly drops to a very low value when the desorption voltage is further raised. Scanning at the maximum and minimum probe currents yields the diagram shown in b and c of Fig. 2.11, respectively. The sudden drop in the probe hole current obviously is associated with the evaporation of the small cluster from the smooth plane. From this close correspondence between the sequence of scanning diagrams and the probe currents it is clear that the essential features on a surface can be revealed by the scanning technique.

The correspondence between the surface features and the scanning diagrams is further illustrated by a computer simulation of the surface scans. The details of the simulation constitute Appendix B. In this simulation the surface topography is defined by the radius r_0 of the central plane. The electron emission from different areas of the emitter surface is governed by the work function and the local variation of electric field, which are estimated in a semi-quantitative manner. After

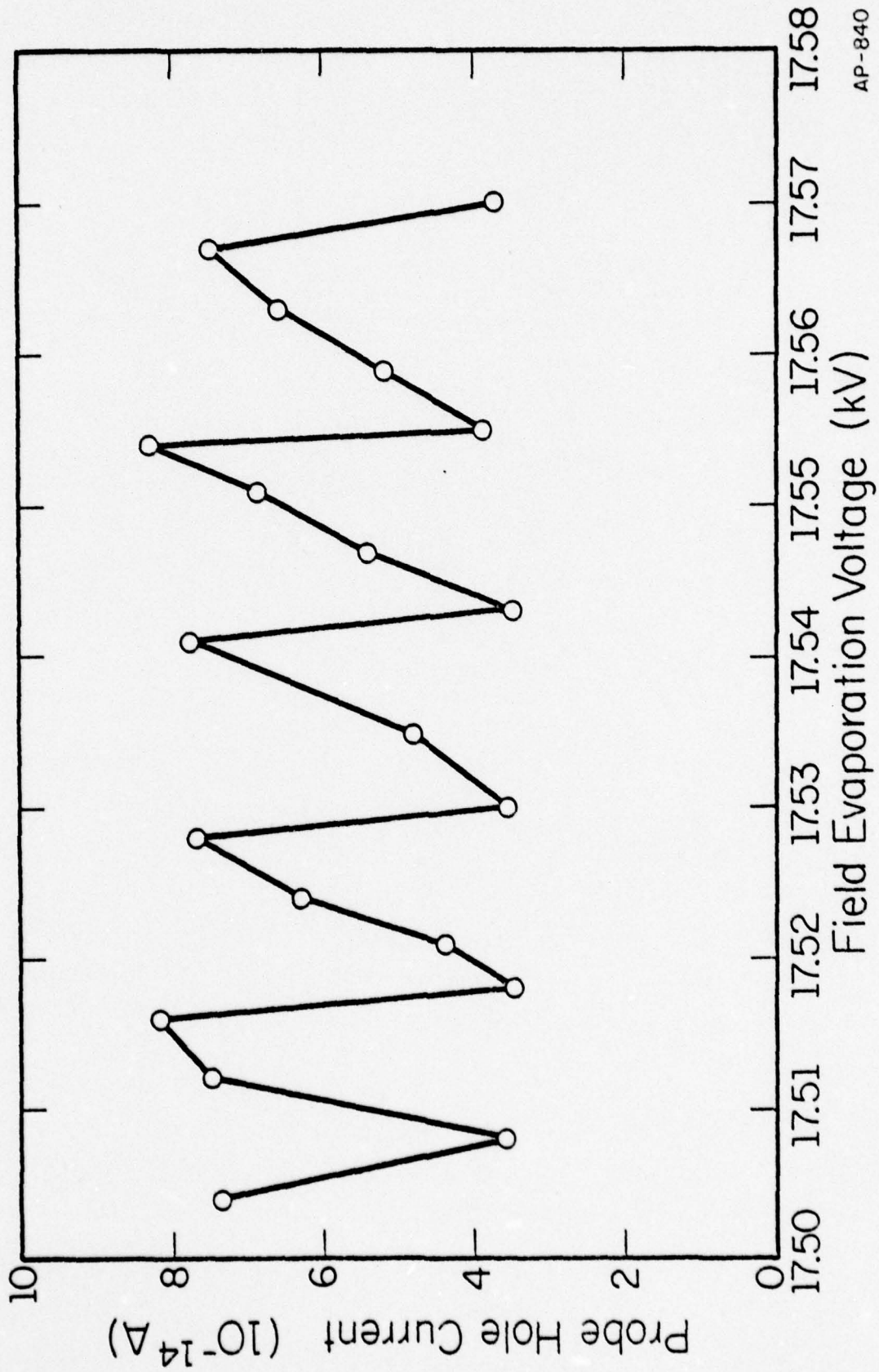


Fig. 2.12. Variation of probe hole current with field evaporation voltage for a W(110) plane.

the position (x_0, y_0) of the probe hole relative to the emitter apex is assigned, the probe hole current is calculated by considering the electron trajectories and the total energy distribution [28,29] of the emitted electrons, following the outline given by Plummer and Gadzuk [30]. These simulations are shown in Fig. 2.13 for $r_0 = 45, 35, 25, 18, 10$, and 5 \AA . They agree remarkably well with the real scanning diagrams: for a large plane, $r_0 = 45 \text{ \AA}$, only one broad minimum appears; for a smaller plane, e.g., $r_0 = 35$, kinks appear; for an even smaller plane, $r_0 = 25$, two satellites similar to those in Fig. 2.11a appear. These satellites gradually merge together when the plane becomes smaller ($r_0 = 18$ and 10). Finally, when only a cluster of atoms is left at the center of a large plane ($r_0 = 5 \text{ \AA}$), a single prominent maximum appears in the current, similar to the experimental findings in Fig. 2.11b.

Characterizing the surface by first examining the surface topography in the field ion microscope and then by the scanning technique just before an experiment proves to be highly effective and accurate. This procedure was routinely employed for all experiments reported here. The scanning technique also provides a unique way of determining the surface topography of a thermally cleaned emitter, for which field ion microscopy is quite often impractical.

2.6. Detection of adsorption

2.6a. Techniques of detection

Field ion microscopy is not suited for studying adsorption on surfaces; it is insensitive to surface chemical constitution and the strong electric field and the imaging gas disturb the surface. In field emission microscopy,

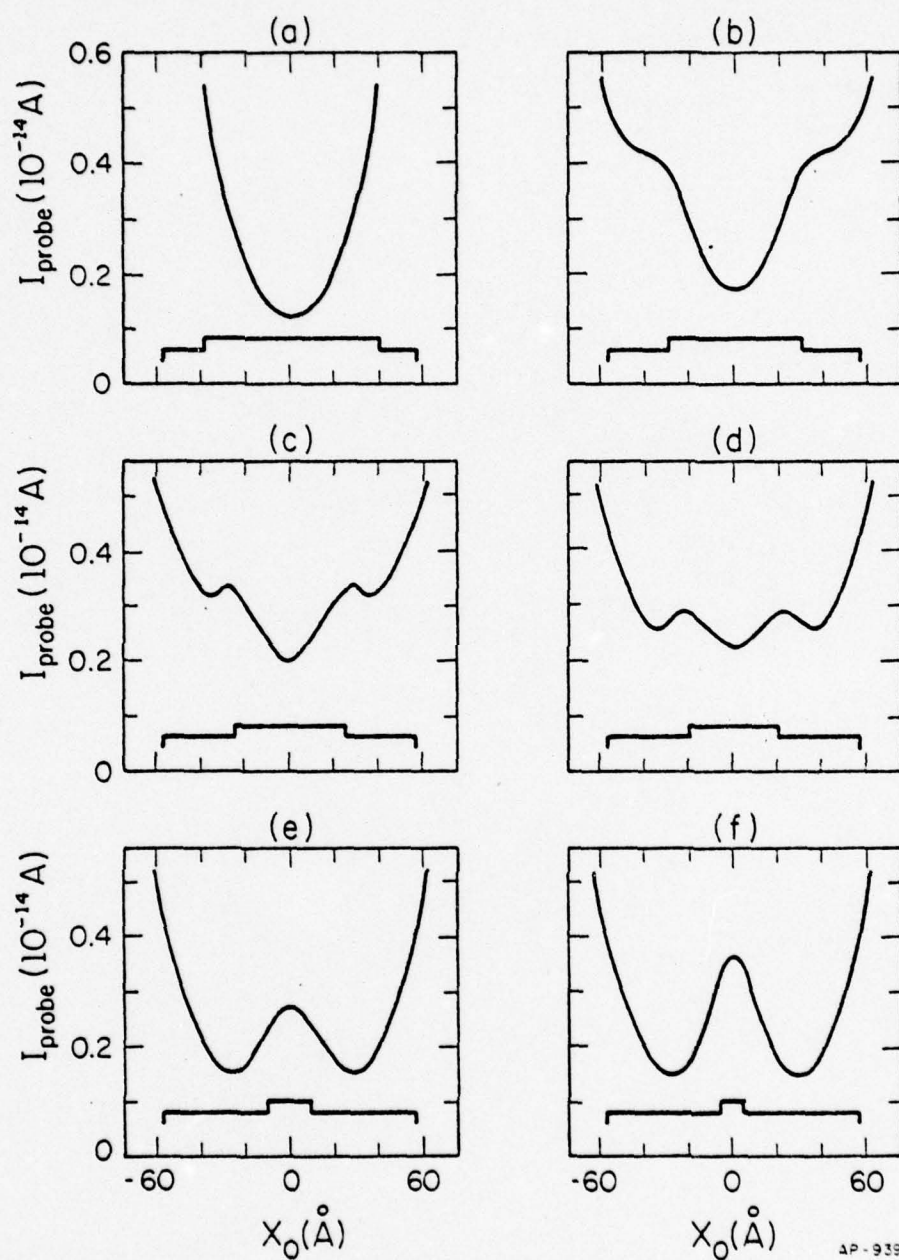


Fig. 2.13. Computer simulated scan diagrams. The size of the central plane (or cluster) $r_0 =$ (a) 40; (b) 30; (c) 25; (d) 20; (e) 10 and (f) 5 \AA .

the image is formed by electrons emitted from the sample surface rather than by an imaging gas, and the electric field employed is 10 times weaker than the ionization field. Field emission microscopy is also very sensitive to the surface coverage: the emission characteristics are affected by even minute amounts of contaminants. This technique is therefore very convenient for adsorption studies on single crystal planes.

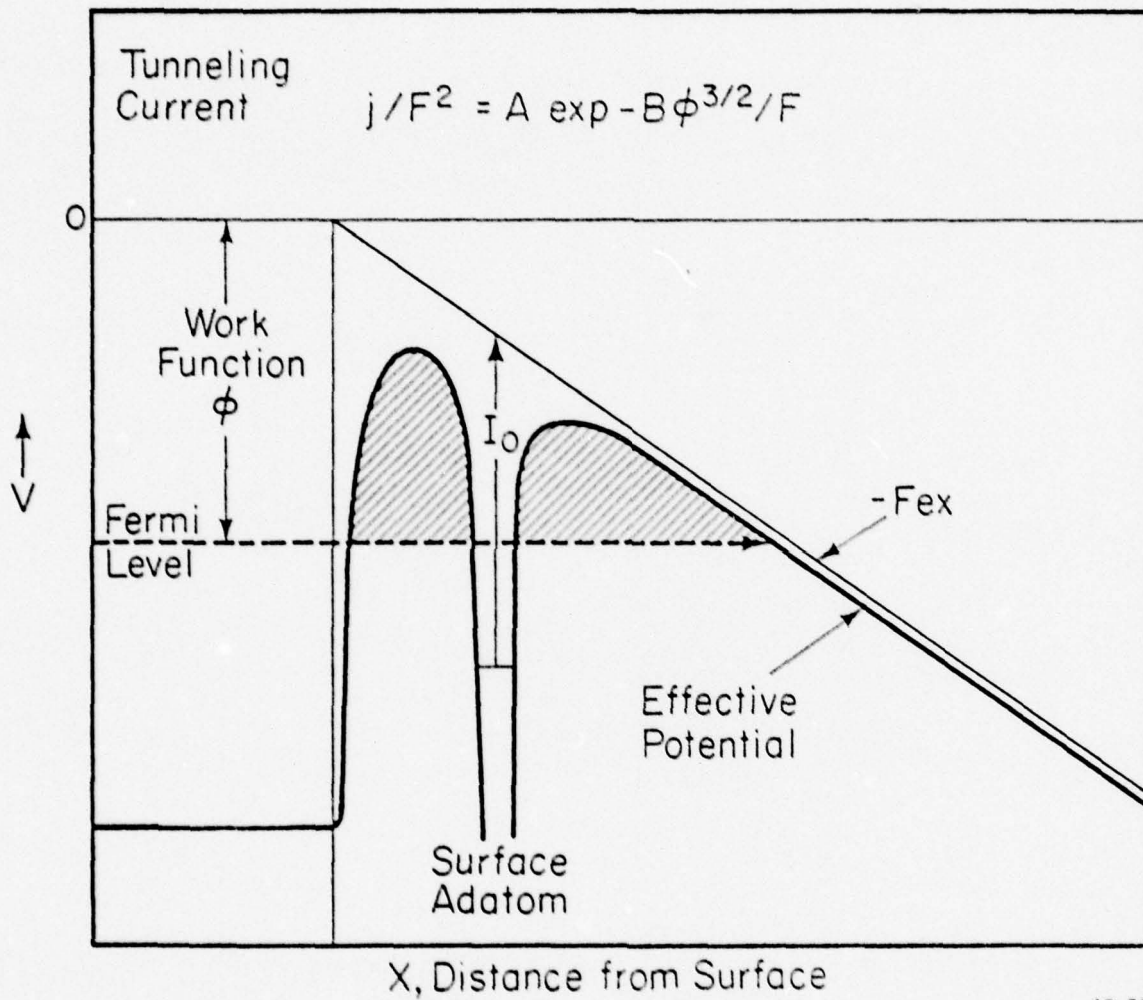
The course of adsorption can be followed by monitoring the work function change on exposure to gas. When adsorption occurs, each individual adatom acts like an area with different emitting properties. Addition of n adatoms per cm^2 , each adatom having an effective dipole moment M , will alter the work function by $\Delta\phi = -1.25 \times 10^{-15} \pi nM$, where M is expressed in Debye units. For a typical monolayer coverage of the surface, this gives a change in the work function of 0.2 - 1.0 eV. The standard error for work function measurements on a single plane is only slightly higher than for average work function measurements, and ranges from 0.01 to 0.04 eV. This makes it possible to detect $\sim 1/10$ monolayer of adsorbate for most systems.

The adsorption of gases on a metal surface usually changes not only the work function of the surface but also the pre-exponential factor of the F-N plot. Unlike the work function change, which is accounted for by charge transfer from or to the adatoms, producing dipole moments, the variation of the pre-exponential factor cannot always be understood on the basis of the simple Fowler-Nordheim theory. This variation has been attributed to the polarization of adsorbate by the applied field [31], depolarization effects in the adsorbed layer [32], modification of the

image potential [33], and, most recently and most successfully, to a change in the quantum-mechanical tunneling probability due to the potential well of the adatoms [34]. This last effect is shown in Fig. 2.14: the presence of adsorbed gas on the surface introduces a potential well in the surface potential barrier. The electron tunneling process is complicated by resonances within the potential well. However, even when resonance tunneling is important, no significant error is introduced in obtaining work functions from Fowler-Nordheim plots. This agrees with the results of earlier calculations that the slope of the Fowler-Nordheim plot is insensitive to the detailed barrier shape [35,36].

Since the variation in the pre-exponential factor is dominated by many complicated factors, it is impossible at present to quantitatively relate the experimentally detected variations to physical changes. This does not prevent the use of pre-exponential variations to detect adsorption empirically, but restricts the obtainable information to more qualitative factors, endowed with much larger errors [3].

For most situations, monitoring the work function change of a surface is enough to follow the course of adsorption. Occasionally, however, adsorption is accompanied by little or no significant work function change. For such systems, the emission currents at constant voltage are interpolated from the Fowler-Nordheim plots and are compared with that of the clean surface. This method is much more sensitive than work function measurements. It also avoids the introduction of large errors inherent in the ordinary method of determining the pre-exponential factor. The Fowler-Nordheim equation (Eq. (2.2)) may



AP-363

Fig. 2.14. Potential diagram for electrons at the surface of a metal in the presence of a surface adatom and an applied electric field. (From Reference 3.)

be written in a simplified form as

$$\frac{I}{V^2} = A \exp\left(-\frac{B\phi^{3/2}}{V}\right),$$

where A is commonly referred to as the pre-exponential factor. When the change in the work function $\Delta\phi$, is small, one obtains directly from this relation

$$\ln(I/I_0) \approx \ln(A/A_0), V = \text{constant}.$$

Therefore under suitable conditions ($\Delta\phi \approx 0$, $V = \text{constant}$), the change in the pre-exponential factor may be represented by the change in the emission current at constant voltage.

2.6b. Perturbation of adsorbates during observation

A rather large electric field has to be applied to the surface during field emission experiments. This may potentially disturb the gas adsorbed on the surface. In this section we shall examine the cause and the extent of the perturbation.

The dipole moment M (in Debye units) induced on an adatom of polarizability $\alpha(\text{\AA}^3)$ is given by $M = \alpha F/3$, where F is the external electric field in V/ \AA . Assuming the surface polarizability is the same as the gas phase, for an external field F in the range of 0.3 V/ \AA the induced dipole moment causes a work function change in the order of 0.2 eV for a full monolayer of a typical adsorbed gas. This value is comparable to the work function change arising from charge transfer on adsorption. However, even in the case of such a field dependent work function, the slope of

the F-N plot gives a good approximation to the work function in zero field [31]. Comparing the saturation work function changes for typical adsorbate obtained by field emission with values obtained by other low field techniques confirms that these polarization effects do not significantly alter the work function changes determined by field emission.

Desorption of the adsorbate by the electric field is a significant difficulty in field ion microscopy. For field emission, not only is the field far weaker than required to desorb adatoms, but also the polarity is reversed. Ionization is discouraged rather than encouraged. Disturbance of adsorbates by desorption in field emission seems highly unlikely and has not been reported.

The only real threat the electric field may impose on the adsorbate is through field-induced diffusion. The applied electric field may cause the polarized adatoms to diffuse on the surface. In this case, Fick's law of diffusion cannot be applied directly. Let the effective charge of the polarized adatom be q . The driving force for diffusion now consists not only of a chemical contribution, arising from the gradient in the chemical potential μ , but also includes a term from the gradient in the electric potential. On a planar surface, the mass flux \vec{J} may be expressed by the phenomenological equation of diffusion [37]

$$\vec{J} = -K(\vec{\nabla} \mu + q\vec{\nabla} V), \quad (2.4)$$

where V is the electric potential function, q the effective charge, and K a coefficient related to the mobility B through $K = BC$, where C is the

surface concentration of adsorbate. The gradient operator is understood to be in two dimensions, assuming that diffusion is isotropic on the surface. From Eq. (2.4) it is easily seen that with a strong enough tangential electric field, diffusion of the adsorbate may occur in the absence of, even against, a concentration gradient.

Since metals are good conductors, we are accustomed to think of a metal surface as an equipotential, for which the tangential electric field on the surface is zero [38]. However, a tangential electric field may exist immediately above the surface, due to the local variation of the work function. This is clear from the following consideration: a field emitter consists of many planes each having a work function characteristic of its crystallographic orientation. The work function is defined as the electrochemical potential inside a metal, $\bar{\mu}$, plus the difference in electrostatic potentials inside and outside the metal. Consider, for example, two neighboring regions on a field emitter with work functions ϕ_1 and ϕ_2 . From the above definition we can write:

$$\phi_1 = -e(V_1 - V_0) + \bar{\mu} = -e(V_1 - V_0) + E_f$$

and

$$\phi_2 = -e(V_2 - V_0) + \bar{\mu} = -e(V_2 - V_0) + E_f,$$

where V_1 , V_2 are the electrostatic potential outside these regions, V_0 the potential inside the metal, and E_f the Fermi energy. It is clear that $\phi_1 - \phi_2 = -e(V_1 - V_2)$, since E_f is independent of surface orientation.

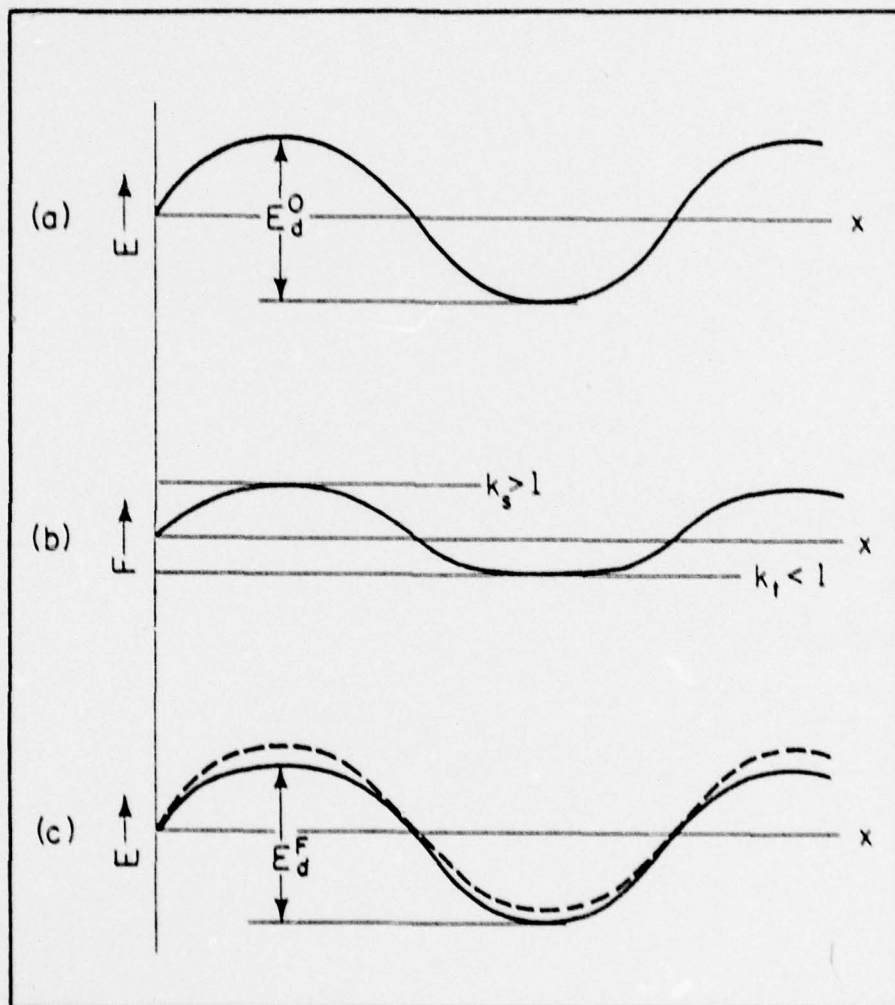
Therefore, the electrostatic potentials above these two neighboring regions differ by $\frac{1}{e}(\phi_2 - \phi_1)$, and $\nabla_t V$ is non-zero, where ∇_t is the gradient operator along the tangential directions of the surface. Thus an electric field tangential to the surface, which can act as the driving force for surface diffusion, can be produced.

If we ignore the concentration gradient, the diffusion flux J_t along the tangential field may be written, from Eq. (2.4), as:

$$J_t = -Kq\nabla_t V = KqF_t = BCqF_t, \quad (2.5)$$

where F_t is the tangential electric field seen by the adatoms. A detailed account of surface diffusion using the above equation is difficult, however, as the tangential electric field, as well as the mobility B , are not known accurately. Therefore we only attempt an order of magnitude estimate.

The mobility B is related to the diffusion coefficient D through Einstein's relation: $D/B = kT$. The diffusion coefficient D is also affected by the electric field on the surface. This is caused by the lowering of the activation energy due to the electric field. The surface potential energy seen by an adatom may be depicted by a periodic train of saddles and troughs, as in Fig. 2.15a. The electric field on the surface follows roughly the same periodicity of the surface potential, as depicted in Fig. 2.15b. The field at the saddle and at the trough can be expressed by two dimensionless factors k_s and k_t through $F_{\text{saddle}} = k_s F$ and $F_{\text{trough}} = k_t F$, respectively. The surface potential energy is affected through two interaction terms: the permanent dipole interaction, $\vec{\mu} \cdot \vec{F}$; and



AP-787

Fig. 2.15. (a) Potential diagram for atomic diffusion on a surface. The activation energy for diffusion is E_d^0 . (b) The variation of the applied electric field with surface roughness. (c) The activation energy for diffusion as affected by the external electric field.

the induced dipole interaction, $1/2 \alpha F^2$, where $\vec{\mu}$ is the permanent dipole moment and α the polarizability of the adatoms. The effect of the external field on the surface potential energy is depicted in Fig. 2.15c. The activation energy for diffusion in the presence of an electric field is just the difference of potential energies at the new saddle and trough. Explicitly, this may be written as [39]

$$\begin{aligned} E_d^F &= E_d^0 + (k_s - k_t) \vec{\mu} \cdot \vec{F} - (k_s^2 - k_t^2) \cdot 1/2 \alpha F^2 \\ &= E_d^0 + (k_s - k_t) \cdot (\vec{\mu} \cdot \vec{F} - \alpha F^2), \end{aligned} \quad (2.6)$$

where E_d^0 and E_d^F are the activation energies without and with the electric field. It is seen from Eq. (2.5) that the activation energy for diffusion is modified by the external electric field to an extent depending largely on the sign and magnitude of the surface charge transfer, as well as the polarizability of the adatoms.

A quantum mechanical calculation of the effective dipole moment $\vec{\mu}$ and the polarizability α for chemisorbed adatoms is done by Bennett [40]. Using a rather simplified model, he estimated that the variation in activation energy ranges from 1 to 20%, depending strongly on chemisorption bond, at typical fields used for field emission. Experimental investigations by Swanson et al. [41] on field induced diffusion of cesium adatoms on tungsten show that the change of activation energy fits well with Eq. (2.6). In their experiments, the change in the activation varies from 1% for one diffusion mode to $\sim 30\%$ for another mode.

In an earlier study, similar results were obtained by Gomer et al. [42] on the diffusion of barium on tungsten. Note that these observations are all on metal adatoms. For non-metal adatoms one would expect a much smaller variation in the activation energies for diffusion, since the polarizability α is much smaller [43].

From the above discussion we get some idea about the change in the diffusion coefficient, and hence the mobility B , due to the electric field on the surface. Now we may estimate the matter flux caused by the tangential field F_t from Eq. (2.5). The tangential field F_t should not be confused with the electric field on the surface, F . The tangential field F_t is caused by the local variation of the electric field F , as well as the variation in the work function, as we have mentioned earlier. Therefore the magnitude of the tangential field is at least one order lower than the electric field on the surface. If we assign $F_t = (1/10)F$, $C = 0.1$ monolayer $= 10^{13}$ atoms/cm², and $q = 0.05$ electron charge (this corresponds typically to a $\Delta\phi$ of 0.5 eV for a full monolayer [44]), Eq. (2.5) becomes

$$\begin{aligned} J_t &= 1.5 \times 10^{18} B (\text{in cm}^2/\text{sec/eV}) \quad (\text{atoms/cm/sec}) \\ &= 2.4 \times 10^6 B (\text{in cm}^2/\text{sec/erg}) \quad (\text{atoms/cm/sec}). \end{aligned} \quad (2.7)$$

As an example we shall estimate the diffusion flux J_t for the nitrogen-W(110) system. The diffusion of β -nitrogen on W(110) has recently been measured by an Auger technique [45]. The diffusion coefficient D may be expressed as $D = D_0 \exp(-E_d/kT)$, with $D_0 \sim 10^{-2}$ cm²/sec and $E_d \sim 21$ kcal/mole. At 300 K, $D \sim 3 \times 10^{-17}$ cm²/sec. Suppose E_d is not

affected by the applied field, then $D^F = D$, and $B = D^F/kT = 1.2 \times 10^{-15}$ ($\text{cm}^2/\text{sec}/\text{eV}$). Substituting this value into Eq. (2.6), we get the diffusion flux $J_t \sim 2 \times 10^3$ atoms/cm/sec = 2×10^{-5} atoms/Å/sec = 0.002 atoms/100Å/sec. This corresponds to the passing of one adatom per 500 seconds across a boundary 100 Å in length. In the typical time of ~ 100 seconds required for a F-N measurement, essentially no adatoms is gained or lost by a typical (110) plane.

If the activation energy for diffusion E_d is lowered by the external field by 10%, then $D^F/D \sim 20$ at 300 K. We get $B \sim 2.4 \times 10^{-14}$ ($\text{cm}^2/\text{sec}/\text{eV}$). From Eq. (2.6) we get $J \sim 4 \times 10^{-4}$ atoms/Å/sec = 0.04 atoms/100Å/sec. In a 100 second interval, roughly four atoms are now gained or lost by a (110) plane. This is a significant fraction of the adatoms originally on the (110) plane. Therefore, under adverse conditions, the external electric field may have some effects on the adsorbate. But in general these effects should be small, since the polarizability of gas atoms is small and a change of the activation energy by more than 10% is unlikely [43].

The above analysis only provides a qualitative description of how the external electric field might possibly affect the adsorbate. It is obvious that quantitative predictions cannot be made without detailed information on surface dipole moments, polarizabilities, and field distributions. In all experiments reported here, the lowest possible field is used, and Fowler-Nordheim measurements are done in as short a time as possible. If flickering of the field emission current, which is related directly to surface diffusion [46-48], occurs, the surface temperature is lowered to reduce the diffusion rate. This is a very

effective way to stop diffusion on the surface. Take the example of nitrogen on the W(110) surface; on lowering the surface temperature from 300 K to 200 K, the diffusion flux is lowered by 3 to 4 orders of magnitude. As will be seen later in this thesis, in our experiments, lowering the surface temperature does not significantly alter the chemisorption behavior (unless new adsorption states are formed). From this we conclude that in these experiments field-induced diffusion does not play an important role.

CHAPTER III

ADSORPTION ON TUNGSTEN

3.1. Introduction

Despite the large volume of experimental data, our understanding of the interactions between the simplest molecular gases and densely packed planes of metals is still in a confused state. Data on the chemisorption behavior of diatomic gases with these surfaces are often conflicting, and little is known of the mechanism limiting the rate of interaction with these surfaces, or of the influences of imperfections. The principal difficulty seems to be the lack of unequivocal control of surface conditions--contamination and imperfections on the surface may have caused the often conflicting observations. These problems may be solved by studying small crystals using field emission. By employing this technique we hope to understand kinetic processes on the surface under unequivocal conditions of cleanliness and perfection.

The adsorption of nitrogen on polycrystalline tungsten has been studied thoroughly by flash desorption [49-55] and by field emission [22,56-60]. Three binding states, namely α , β , and γ , with binding energies ~ 20 kcal/mole, 155 kcal/g-atom, and 10 kcal/mole, respectively, have been observed. The β and γ nitrogen have been identified as atomic and molecular, respectively, by isotope exchange studies [54].

On the densely packed (110) plane, nitrogen also adsorbs readily at temperatures below ~ 150 K. A change of -0.15 eV in the work function is reported by Delchar and Ehrlich [61] and more recently by Yates et al. [62]. By studying the isotope exchange on the (110), Yates et al.

also concluded that the nitrogen adsorbed at low temperature is not dissociated, and does not convert to atomically chemisorbed form when heated rapidly from 123 K. Compared to the rate on other surfaces the non-dissociative adsorption of nitrogen at low temperature seems not affected profoundly by the surface structure.

For adsorption at room temperature, the early work by Delchar and Ehrlich [61], using the contact potential method, revealed that the work function of the (110) plane does not change even when exposed to large amounts of nitrogen. Similar results were later on observed by van Oostrom, using probe-hole field emission microscopy [63]. In contrast to these results, Hopkins and Usami [64], using a contact potential method, reported an increase of 0.18 eV on the (110) plane of tungsten at 300 K. More recently, Polizzotti [3] in his thesis also reported observations of the interaction of nitrogen with the W(110) plane. He again found that the work function of the (110) remains unchanged when exposed to nitrogen. However, he observed that above an exposure of $\sim 5 \times 10^{16}$ molecules/cm², the pre-exponential factor in the F-N plots decreases almost linearly with the amount of exposure. Unfortunately, the data on the pre-exponential factors show large statistical errors and the threshold for chemisorption is not well-established.

LEED studies [65] of the interaction of nitrogen with W(110) reveal no changes in the LEED patterns, while changes in patterns have been observed on other low index planes of tungsten when exposed to nitrogen [66,67]. Caution must be exercised, however, in interpreting

this result as evidence for the absence of adsorption on the (110) plane. Changes in LEED patterns on adsorption occur only if the adsorbate forms a surface structure different from that of the substrate. Lack of any changes in the LEED patterns has been reported by the same authors [65] for low index planes of many other refractory metals when exposed to nitrogen and hydrogen.

Combining contact potential and flash desorption techniques, Madey and Yates [68] observed an increase of 0.03 eV in the (110) work function at 300 K after being exposed to $> 7.7 \times 10^{16}$ molecules/cm² of nitrogen. An initial sticking coefficient of < 0.001 and a saturation surface concentration of $\sim 1.5 \times 10^{14}$ atoms/cm² are reported. More recently, flash desorption studies by Tamm and Schmidt [69] yielded results comparable to those by Madey and Yates. Tamm and Schmidt report an initial sticking coefficient of ≤ 0.004 and a desorption energy of 75 kcal/mole.

Attempts to directly observe the presence of nitrogen on the (110) plane of tungsten at 300 K using field ion microscopy have not been very successful. Evidence has been reported both in support and against nitrogen adsorption on the (110) [70,71]. These results are subject to some doubts, however, as the field ionization of the imaging gas may perturb the adsorbate seriously.

It is clear from the above discussion that whether or not nitrogen adsorption occurs on the perfect (110) plane of tungsten at 300°K is still unsolved. Even if nitrogen does adsorb on the (110) surface, the sticking coefficient on this plane seems unusually low compared to other surfaces of tungsten. This leads to the question whether the discrepancies in the

observations discussed above are caused by the different degrees of perfection in the surfaces studied. If the sticking coefficient on the (110) is two or more orders of magnitude lower than on rougher surfaces, even minute concentrations of defects on the (110) plane could accelerate chemisorption on this surface significantly. Further studies under more carefully controlled conditions are obviously necessary to understand the interaction of nitrogen with this densely packed surface.

The adsorption of hydrogen on the (110) plane of tungsten has been investigated by many different techniques and has been reviewed by Polizzotti [3]. Although there are large variations in the values of the surface potential change reported for hydrogen adsorption, there is general agreement on the rate of chemisorption on the (110) plane. The sticking coefficient on the (110) ranges from 0.07 to 10^{-3} , as compared to a typical value of ~ 0.2 for other crystal planes. This unusually low sticking coefficient on the W(110) is reminiscent of the behavior of nitrogen on this plane, and is a clear indication that the structure of a surface can profoundly affect chemical processes on the surface.

To positively establish this structural effect, Polizzotti thoroughly and carefully studied the adsorption of hydrogen on the (110) plane of tungsten, from 38 to 300 K, using field emission microscopy. On both thermally annealed and field evaporated emitters, he found that the rate of adsorption depends strongly on the temperature of the surface. At 80 K, adsorption on the (110) plane does not occur immediately upon exposure to hydrogen; there is a prolonged delay on the (110) plane,

while other surfaces on the emitter are reacting with hydrogen. The (110) plane starts to show adsorption only after the rest of the emitter surface is completely saturated by hydrogen. When the temperature of the surface is raised, the length of the initial delay also diminishes. At 300 K, the initial hesitation disappears and adsorption on the (110) plane proceeds at about the same pace as on the rest of the emitter surface.

To explain the initial delay in adsorption on the (110) plane, as well as the strong dependence of adsorption on the surface temperature, Polizzotti proposed the following mechanism for adsorption on the (110) surface. He assumes that direct dissociation of hydrogen into atoms on the (110) plane is very slow, so that its contribution to the observed changes can be ignored. Also, the gas can adsorb on the edges of the (110) plane as a precursor to dissociation. He then attributes the chemisorption that occurs on the (110) after some initial delay to an activation barrier that prevents adatoms, formed from this precursor by dissociation at the edges of the plane, from leaving the edges. Since the rate limiting step is a thermally activated process, this naturally explains the observed temperature dependence.

Polizzotti's model is simple and is potentially powerful. However, more work is required to unequivocally establish, and to refine (or modify) this mechanism. Polizzotti himself made the first move toward this goal. By lowering the surface temperature to 38 K, he found a new state of hydrogen, probably molecular as judged from its temperature stability, formed on the (110) plane. By raising the temperature of the surface, the hydrogen adsorbed in this form gradually desorbed, and a

clean (110) surface was restored at about 63 K. That the loosely bound hydrogen desorbed rather than converted into tightly bound atomic hydrogen during warming up is a clear indication that the (110) surface is quite inert in dissociating hydrogen into atoms. This gives strong support to his assumptions.

After the loosely bound hydrogen was desorbed from the (110) plane, he re-exposed the whole surface at 80 K to a relatively small amount of hydrogen ($\sim 5 \times 10^{16}$ molecules/cm²). Instead of a delay, he then observed an immediate change of the work function of the (110) plane. That is, by saturating the other areas on the emitter first, the (110) plane can be brought to saturation by a small amount of hydrogen, even at low temperature. This gives further strong support to his model: the reaction observed on the (110) plane indeed depends on the state of adsorption of other areas.

The apparently activated process that causes chemisorption on the (110) plane of tungsten inspires many interesting questions. Apart from the obvious question of seeking the reason for this unusual behavior, it is also interesting to know the generality of such behavior. Should we expect to see similar effects on all densely packed planes of other materials? Is this restricted to hydrogen, or is it general for diatomic gases? It is partly to answer such questions that this study was conducted.

3.2. Adsorption of nitrogen on W(110)

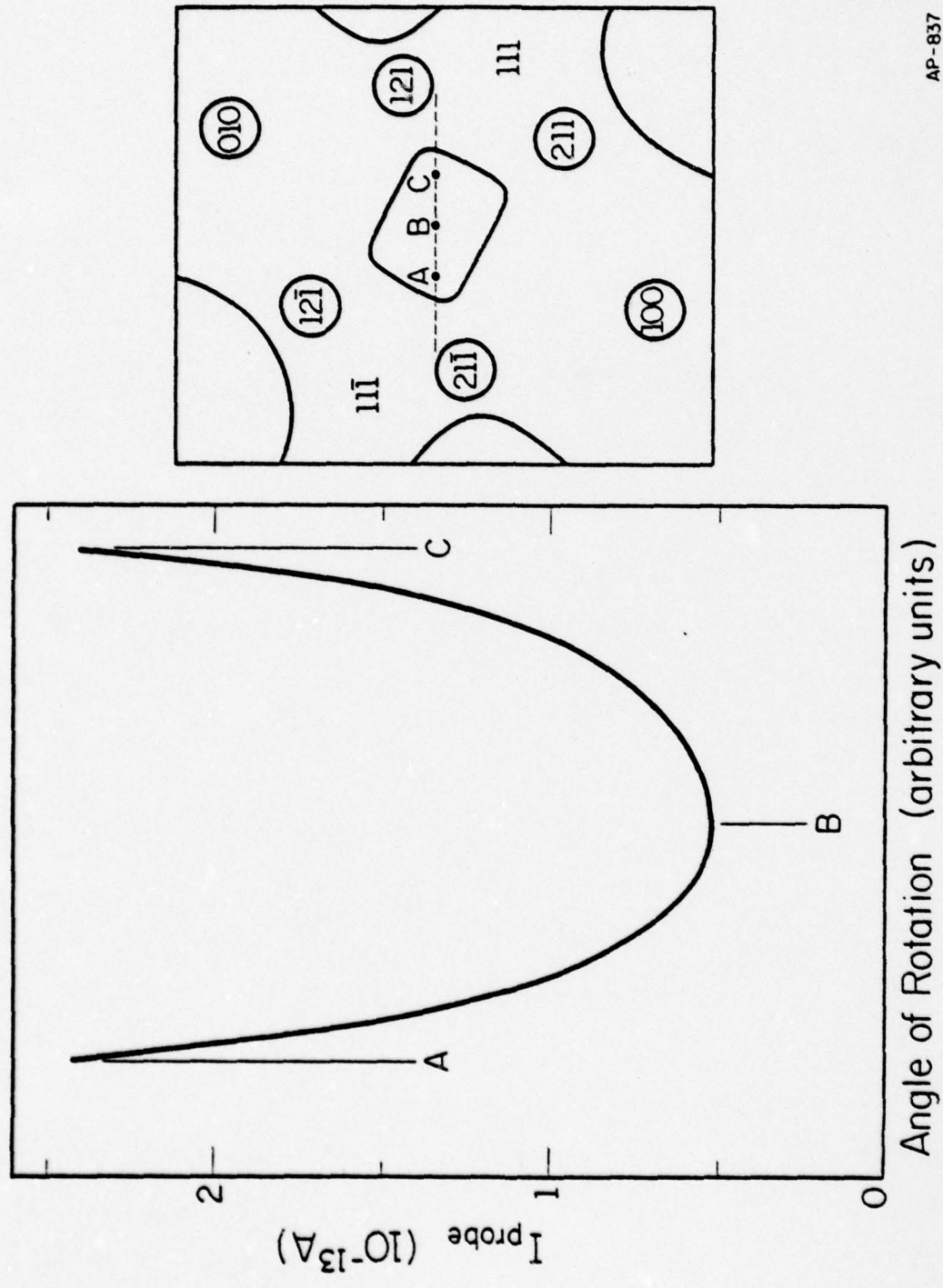
The first extension beyond previous work is obviously to investigate the interaction of tungsten with other gases. Nitrogen is a good candidate because its chemisorption behavior resembles hydrogen in many aspects. Furthermore, the contradictory results on the chemisorption of nitrogen on the (110) plane of tungsten previously noted may be resolved only by studying this surface under more carefully controlled conditions.

3.2a. Adsorption at $T_s \geq 150$ K

We have studied the adsorption of nitrogen on the W(110) plane for surface temperatures T_s ranging from 80 to 550 K. At temperatures below ~ 150 K, nitrogen may adsorb as molecules in the γ -state. Here we shall first discuss experiments for which γ -nitrogen does not contribute significantly. For the (110) plane of tungsten, even when the emitter is field evaporated to > 20 kV, adsorption at the plane edges still contribute significantly. A change of $\gtrsim 20\%$ in the probe hole current has been estimated due to adsorption on the plane edges alone (Appendix C). It shall become clear later in this chapter that the change in the emission current is the only experimental observable which gives a clear indication of chemisorption of nitrogen on the W(110) surface, and a 20% change in the emission current due to edges is too significant an effect to be ignored. Thermally cleaned emitters with much larger (110) planes are therefore used in these nitrogen experiments in order to avoid the edge effects.

The emitter is repeatedly heated and flashed to ~ 2500 K until the emission pattern becomes smooth. The emitter is judged clean when further heating does not change the value of the probe-hole current. Field ion microscopy has already shown that the (110) plane of thermally annealed emitters is smooth [72]. In our experiments, the smoothness of the (110) plane is further assured by the scanning technique, described in Chap. II. The results of a typical scan of the (110) plane are shown in Fig. 3.1, together with the approximate path of scanning on a field emission image. It is clear from this scan diagram that this thermally annealed (110) plane is large and flat.

On adsorbing nitrogen on such a surface at temperatures between 150 and 550 K, the change in the (110) work function is found to be small. Despite a clear diminution in the emission current, the work function of the (110) plane increases only slightly, and is roughly independent of temperature. The change in the work function at saturation, as measured from the slope of the F-N plots, is very small ranging from 0.05 ± 0.03 eV at 150 K to 0.08 ± 0.04 eV at 550 K. Changes in work function therefore cannot be used as an effective indicator for chemisorption. Polizzotti approached this problem by extrapolating the Fowler-Nordheim plots to infinite field to get the pre-exponential factor [Eq. (2.3)]. Large statistical errors are introduced by this extrapolation process, and it is not possible to discern a clear threshold for chemisorption in this way. A simple solution to this problem has been discussed in Chap. II: the course of chemisorption can be followed by simply monitoring the change

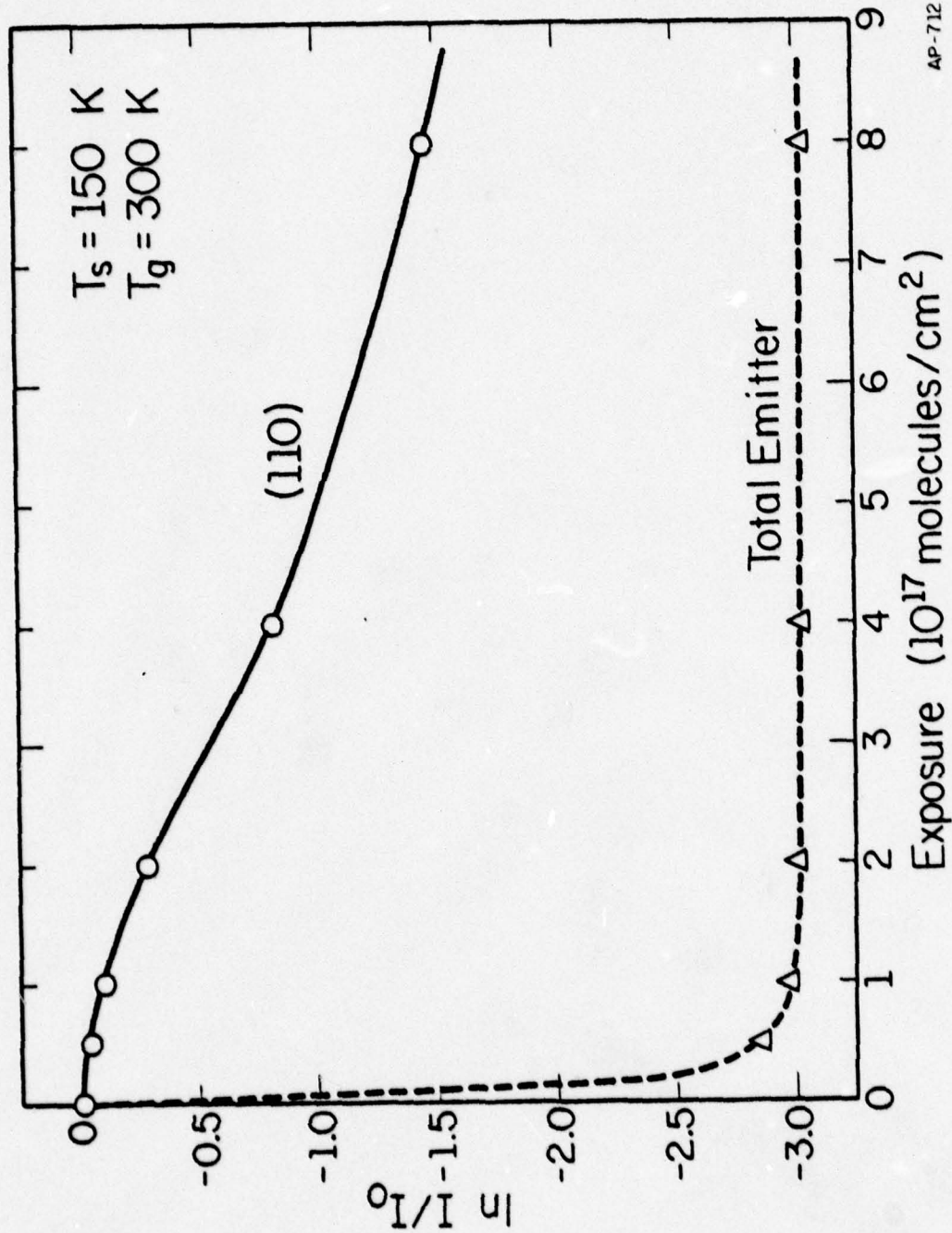


AP-837

Fig. 3.1. A typical scan diagram for a thermally cleaned W(110) plane. Total emission current is 2.4×10^{-7} A at 5,615 V. Figure on right shows approximately the path of scanning.

in the emission current. The logarithmic change in the emission current at constant voltage, relative to a clean surface, is interpolated from the F-N plots, and plotted as a function of exposure to gas. As has been discussed previously in Chap. II, the logarithmic ratio for the emission current, $\ln(I/I_0)$, is approximately the same as the logarithmic ratio for the pre-exponential factors, $\ln(A/A_0)$, provided the change in the (110) work function is small [Eq. (2.4)]. It is thus clear that in this particular case the change in the pre-exponential factor of the F-N plots can be monitored, at least approximately, with reasonable accuracy.

The adsorption of nitrogen on the (110) plane of tungsten at 150, 200, 300, and 550 K is indicated in Figs. 3.2, 3.3, 3.4, and 3.5, respectively. In these figures, the logarithmic ratio $\ln(I/I_0)$ is plotted against exposure to nitrogen. When the surface is at 150 K, exposure to nitrogen brings about adsorption on the (110) plane slowly, as is evident in Fig. 3.2. There is no obvious hesitation before adsorption on the (110) plane occurs, but the rate on the (110) is much slower than on the total emitter. The initial sticking coefficient on the (110) cannot be estimated accurately, since the change in the emission current does not provide a quantitative relation to the surface coverage. A rough estimate may be obtained if an approximately linear relationship between the change in the emission current and surface coverage is assumed. An estimate based on this assumption gives an initial sticking coefficient on the order of 5×10^{-4} on the (110) plane, compared to ~ 0.5 for the total emitter. The adsorption on the (110) plane keeps its slow pace even after the rest of the emitter is completely saturated by



AP-712

Fig. 3.2. Variation of logarithmic ratios for the total emission and the emission from the (110) plane with exposure to nitrogen. Thermally annealed tungsten emitter at $T_s = 150 \text{ K}$.

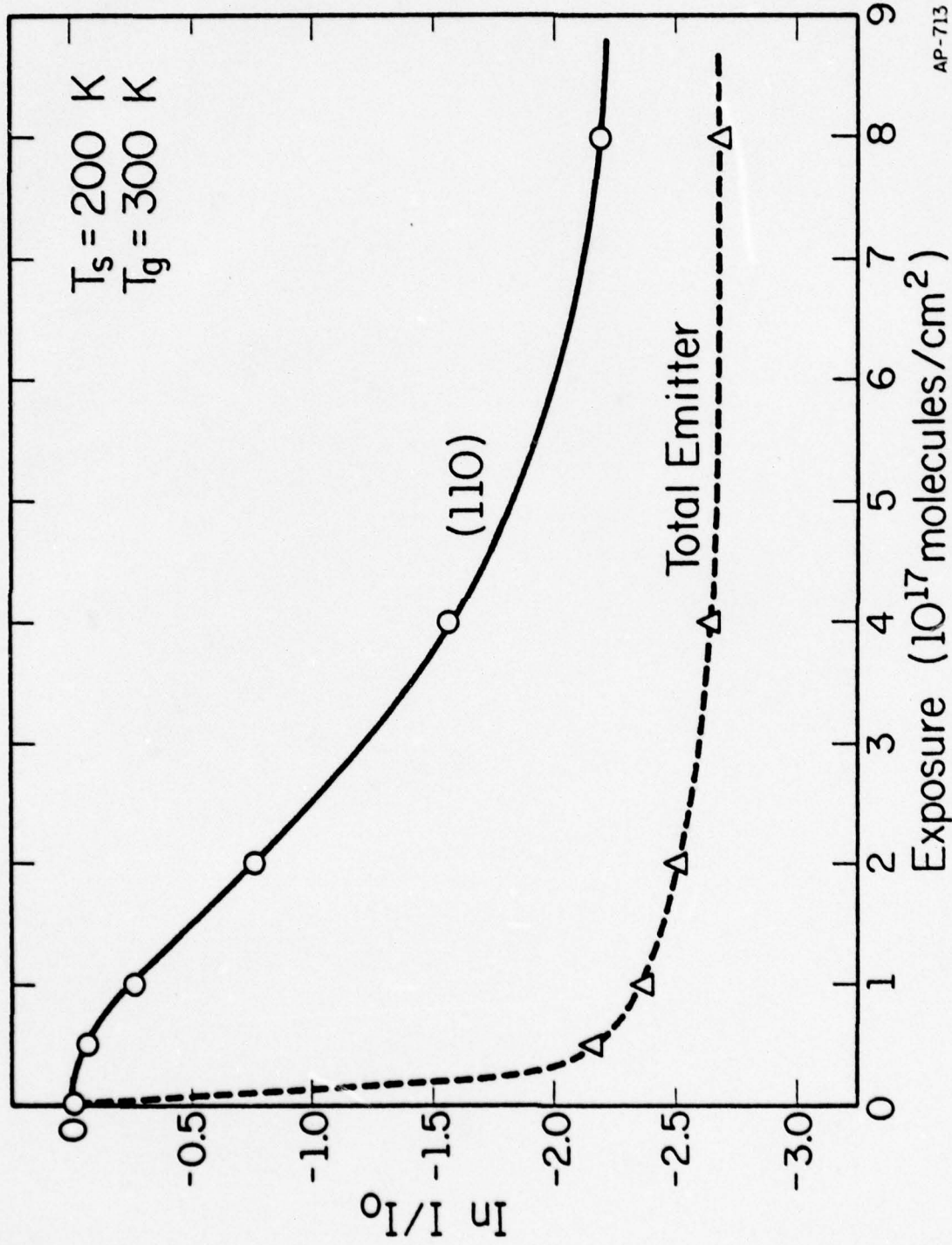


Fig. 3.3. Variation of logarithmic ratios for the total emission and the emission from the (110) plane with exposure to nitrogen. Thermally annealed tungsten emitter at $T_s = 200 \text{ K}$.

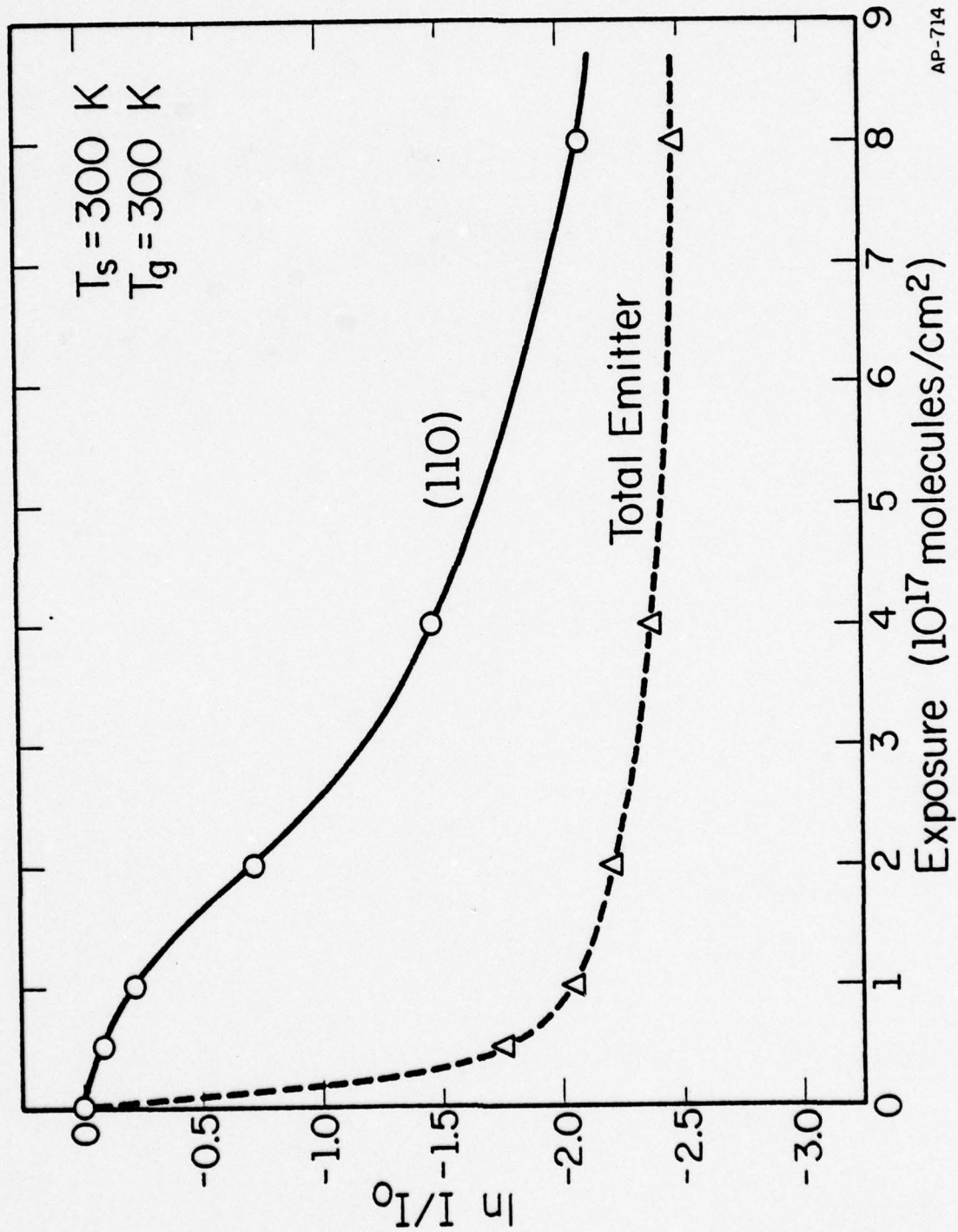


Fig. 3.4. Variation of logarithmic ratios for the total emission and the emission from the (110) plane with exposure to nitrogen. Thermally annealed tungsten emitter at $T_s = 300 \text{ K}$.

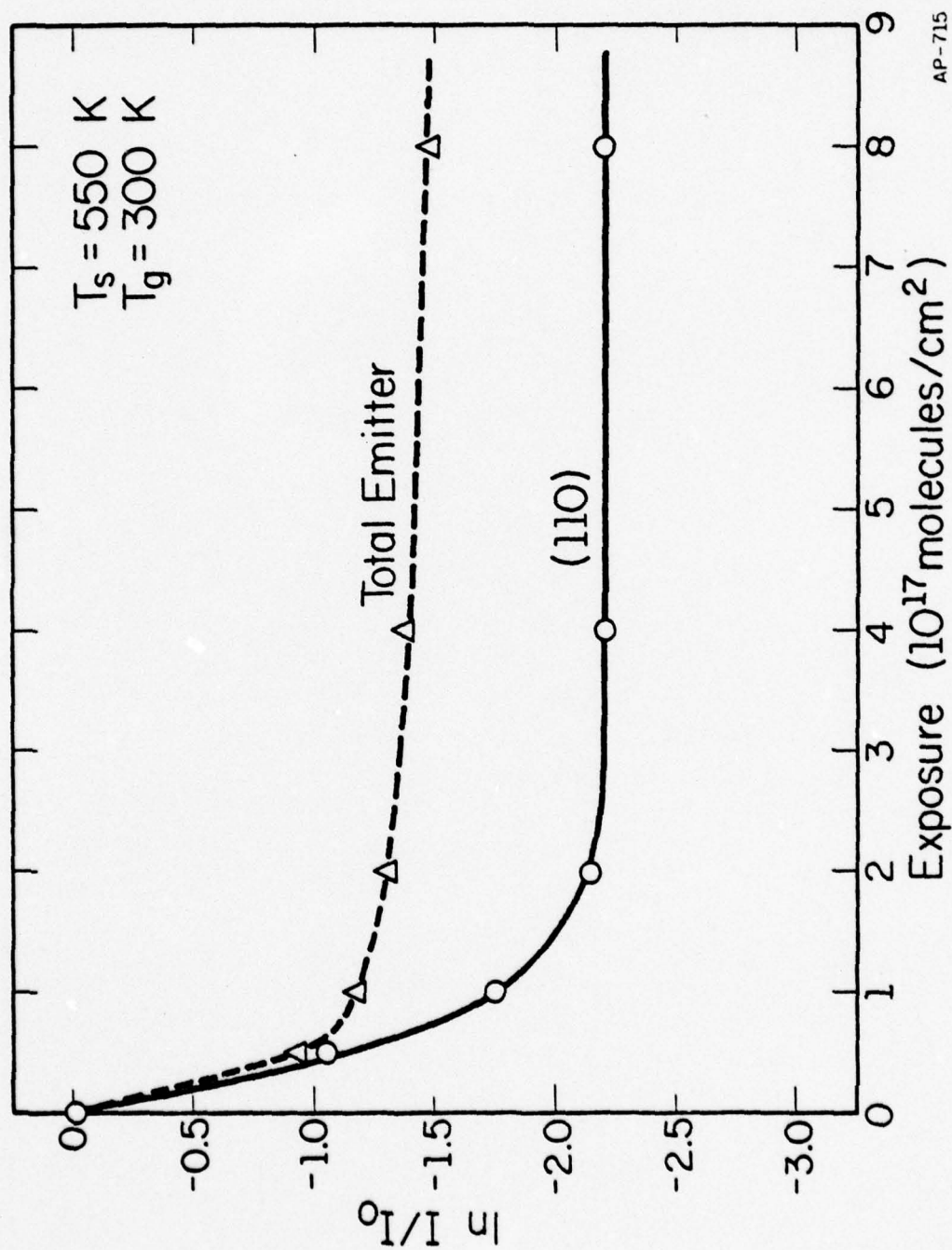


Fig. 3.5. Variation of logarithmic ratios for the total emission and the emission from the (110) plane with exposure to nitrogen. Thermally annealed tungsten emitter at $T_s \sim 550 \text{ K}$.

nitrogen. This is different from the interaction of hydrogen observed by Polizzotti [3]. There the filling in of the (110) plane is accelerated after the total emitter is saturated by hydrogen. Complete saturation of the (110) plane with nitrogen is not reached at the highest exposure, $\sim 8 \times 10^{17}$ molecules/cm², in the experiment shown in Fig. 3.2. Thus at 150 K, the adsorption of nitrogen on the (110) plane of tungsten is seen to be slow but quite continuous.

When the temperature of the surface is brought up higher, the rate of chemisorption on the total emitter decreases, but that on the (110) plane becomes more rapid. These trends are evident in Figs. 3.4 and 3.5. At 200 K it takes roughly twice as much nitrogen to saturate the total emitter as at 150 K. The chemisorption on the (110) plane, on the contrary, becomes almost twice as fast as at 150 K. The (110) plane seems to chemisorb nitrogen slowly and steadily, except that now the sticking coefficient, roughly estimated by the same method, is about 10^{-3} , compared to $\sim 5 \times 10^{-4}$ at 150 K. There appears to be no hesitation in nitrogen adsorption on the (110) plane. The (110) plane nearly reaches saturation at a total exposure of 8×10^{17} molecules/cm².

Adsorption of nitrogen at 300 K is not much different from that at 200 K. The rate of saturation for the total emitter is slightly slower than at 200 K, but the rate on the (110) plane is similar to that at 200 K. The general features of adsorption at 300 K and at 200 K are the same. Our observations at 300 K are within the experimental errors of Polizzotti's results. However, our results do not suffer from the large

errors common in the past, caused by extrapolating the F-N plots. It is evident from Fig. 3.4 that no threshold exists near 5×10^{16} molecules/cm² exposure, as was suspected by Polizzotti. In fact, even at 150 K, some changes in emission current are apparent at low exposures. These changes are definitely not caused by electron emission from the plane edges: thermally annealed emitters with large (110) planes have been used in all these experiments.

By increasing the surface temperature to about 550 K, rapid adsorption of nitrogen can be brought about on the (110) plane of tungsten. This is evident from Fig. 3.5. At 550 K, the rate of filling of the (110) plane is nearly as fast as for the total emitter. At this temperature, the rate of saturation of the total emitter is similar to the rate at 300 K. However, the current change at saturation at 550 K is only $\sim 50\%$ of the change at 300 K (Figs. 3.4, 3.5). This is in reasonable agreement with the observations of Ehrlich et al. [22]. On a tungsten emitter they found that the change in emitter current at 560 K is only $\sim 45\%$ of the change at 300 K. The difference has been attributed to the formation of α -nitrogen below 400 K. More interesting are the rapid changes on the (110) plane when the surface at 550 K is exposed to nitrogen. The change in the work function is about the same as that at lower temperatures, < 0.1 eV. The logarithmic ratio of the current from the (110) also reaches about the same value at saturation as that at 300 K. Both of these indicate that the species adsorbed on the (110) plane are similar to β -nitrogen formed at 300 K.

The drastic change in the chemisorption rate between 300 and 550 K can only be explained by some activated process--it is not caused by the formation of different entities on the surface. At 550 K, it is likely, from previous observations [22], that the diffusion of nitrogen adatoms is appreciable; equilibration of adatoms on different crystallographic planes of the emitter may be established through surface redistribution of adsorbed nitrogen atoms. If this occurs, then the concentration of adsorbed atoms on a particular plane is not dominated by the sticking coefficient of that plane, but rather by the rate of surface migration of adatoms. Our results can be rationalized following this thought: at 550 K, the (110) plane is filled in rapidly by nitrogen atoms dissociated on rougher surfaces of the emitter through an equilibration process. The rate of adsorption on the (110) plane therefore reflects the rate of surface redistribution of adatoms rather than the real sticking coefficient on the (110) itself. At lower temperatures, the nitrogen adatoms are essentially immobile and the rate of adsorption on the (110) plane reflects largely the real rate of dissociation on that plane.

3.2b. Adsorption at $T_s < 150$ K

When the emitter is cooled to 80 K and exposed to nitrogen at 300 K, γ -nitrogen forms on the (110) plane as well as on rougher surfaces of the emitter. In this experiment, the surface is exposed to a single dose ($\sim 6 \times 10^{16}$ molecules/cm²) of nitrogen. The exposure is only a rough estimate based on the pressure in the system; the rapid condensation of nitrogen on the cold finger at this temperature makes exact measurement of the exposure difficult. Some flickering of the probe hole current

was observed, resulting in a larger than average error in the work function. The work function thus measured indicates an increase of 0.15 ± 0.08 eV. The adsorption on the (110) plane is more clearly shown by a pronounced diminution in the emission current. When nitrogen is adsorbed on the (110) plane, the emission current decreases by $\sim 98.7\%$, or to a value only $\sim 1.3\%$ that of the clean surface. This large diminution in emission current cannot be accounted for by the change in the work function -- that can only contribute a drop of $< 30\%$. The larger decrease in the emission current therefore must be caused by the change in the tunneling process for field emitted electrons (Chap. II).

Yates et al. [62], using flash desorption and isotope exchange techniques, found that nitrogen adsorbed on the (110) plane at this low temperature is not dissociated, and has a binding energy ~ 6 kcal/mole. By warming up the surface, we found that the thermal stability of the adsorbed nitrogen is consistent with their results. On heating the emitter slowly from 80 to 300 K, γ -nitrogen desorbs from the (110) surface. This is indicated by a decrease in the (110) work function amounting to ~ 0.08 eV, and by a rise in the (110) emission current by a factor of 20. However, the emission characteristics of the (110) plane do not resume the values for a clean surface. After warming to 300 K, the emission from the (110) plane is only 26% that of a clean surface, indicating that a substantial amount of γ -nitrogen has converted into tightly bound β -nitrogen. An accurate estimate for the percentage of conversion is not possible, owing to the qualitative nature of the change in the emission current relative to surface coverage.

Yates et al. [62] observed no conversion from γ - to β -nitrogen on the (110) plane during rapid heating from 123 K. This does not necessarily conflict with our results. It is possible that heating the sample more rapidly and to higher temperature would increase the rate of desorption and hence decrease the chance of conversion. Assuming a simple activated process for both evaporation and dissociation on the (110) surface, the rate of evaporation compared to that of dissociation is given by $\frac{\nu_1}{\nu_c} \exp((-V_1+V_c)/kT)$, where V_1 , V_c are the activation energies for evaporation and for dissociation, and ν_1 , ν_c are the corresponding attempt frequencies. If the activation energy V_c for dissociation is smaller than the activation energy V_1 , then $\exp((-V_1+V_c)/kT)$ would increase sharply with increasing temperature. Therefore desorption becomes increasingly more favorable than dissociation on the (110) plane at higher temperatures. Our work function results are also different from those of Yates et al. and of Delchar and Ehrlich [61]; both reported a decrease in the work function. This difference is probably caused by the higher concentration of molecular nitrogen at 80 K in our experiments. Experiments by Yates et al. and Delchar and Ehrlich were done at above 100 K. At these higher temperatures the concentration of γ -nitrogen on the surface should be much smaller.

The (110) plane therefore does have some power to dissociate nitrogen, although inert to the dissociation of hydrogen. However, the rate of dissociation is some one thousand times smaller than on the rougher surfaces. Judging from our observations, the efficiency of adsorption on the (110) plane is increased several hundred fold if we bring the surface to a temperature at which diffusion occurs, rather than if we solely rely on direct dissociation on the surface.

3.3. Sequential adsorption of nitrogen and hydrogen

We can make use of the peculiarities of nitrogen adsorption established above to learn more about the mechanism of hydrogen adsorption on the W(110). From his experiments, Polizzotti concluded that hydrogen does not dissociate directly on the (110) surface of tungsten, as we have discussed earlier in this chapter. He then deduced from these experiments that chemisorption on the (110) plane is eventually brought about by surface migration from steps and rougher surfaces surrounding the (110) plane. Whether this is true or not can be tested by studying sequential adsorptions. If direct dissociation on the (110) plane really occurs, then blocking the rougher surfaces surrounding the (110) plane by some immobile adsorbate should not have any effect on the rate on (110). If conversely, chemisorption on the (110) plane is brought about by some indirect mechanism, then filling the region surrounding the (110) with other gases should alter the rate on the (110) plane appreciably.

In our studies the emitter is first cooled to 150 K and then exposed to a total of 2×10^{17} molecules/cm² of nitrogen. At this temperature the total emitter is saturated by nitrogen at a much faster rate than the (110) plane. In fact, at an exposure of 2×10^{17} molecules/cm², the total emitter is completely saturated by nitrogen, yet the (110) plane just barely starts to show chemisorption. A rough estimate, based on assuming a linear relationship between surface coverage and the logarithmic difference in emission current, $\ln(I/I_0)$, gives a coverage of $\sim 13\%$ relative to saturation on the (110) plane.

After the residual gas is pumped out and the pressure in the microscope lowered to 10^{-10} Torr, the emitter is cooled down further to 80 K, and the emission rechecked to ensure that no γ -nitrogen has formed during cooling. The emitter is then exposed to hydrogen gas. Contrary to the adsorption of hydrogen on a clean (110) plane at low temperature, adsorption on the (110) now becomes rapid, as is evident from the disappearance of the hesitation at low exposures, as shown in Fig. 3.6. The work function of the (110) plane changes immediately after the emitter is exposed to hydrogen. Chemisorption on the (110), as reflected by the work function changes, is more rapid and generally less abrupt compared to chemisorption on a clean (110) plane. The work function at saturation is ~ 0.35 eV below that of the clean (110) plane, not much different from the adsorption on a clean surface.

The sequential adsorption experiments provide positive evidence that the chemisorption of hydrogen on the W(110) plane depends on the state of coverage of the adjacent, rougher surfaces. The difference in the initial rate of chemisorption on the (110) plane for a clean and a nitrogen covered emitter excludes the possibility that chemisorption on the (110) plane is caused by direct sticking and dissociation of hydrogen. Direct dissociation processes should not depend on the state of coverage of other areas. The difference also cannot be explained by a difference in the accommodation of molecular hydrogen on the surface alone -- Polizzotti has already shown that molecularly adsorbed hydrogen can exist on the (110) plane at low temperatures. It must be the inability to dissociate hydrogen molecules that is responsible for the inertness of the (110) plane toward hydrogen adsorption.

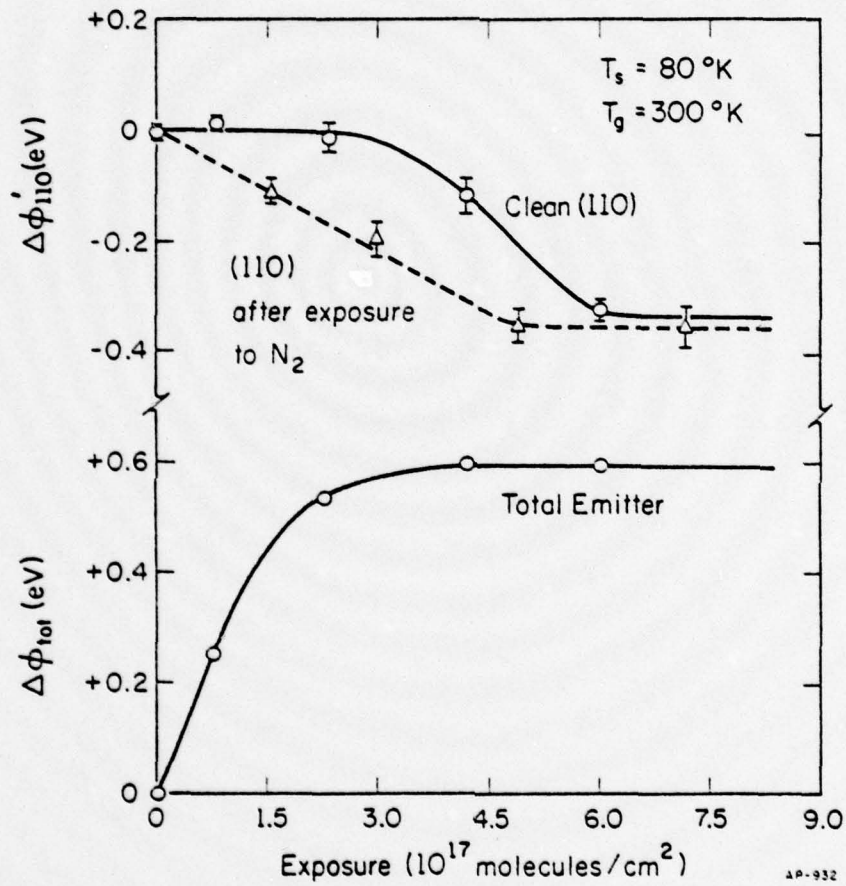


Fig. 3.6. Variation of work function for clean and nitrogen covered emitters with exposure to hydrogen. The clean (110) and the total emitter data shown are from an emitter cleaned by field evaporation.

The saturation of the (110) plane in our sequential adsorption experiment must depend on the supply from the rougher surfaces surrounding it, since direct dissociation cannot account for our results. This supply must be provided through a diffusion mechanism. It has been reported by several authors [73-75] that after a tungsten surface is saturated by nitrogen, strong chemisorption of hydrogen cannot occur. However, below 100 K, loosely bound hydrogen on nitrogen covered surfaces has been reported [72]. The migration rate of this loosely bound hydrogen is likely to be high even at 80 K. The (110) plane might trap this hydrogen effectively.

The sequential adsorption experiment confirms that direct dissociation of hydrogen on the (110) plane cannot account for the observed results. The filling in of the (110) plane must be related to the surrounding rougher surfaces. In other words, the observed chemisorption on the flat (110) plane is catalyzed by the defects surrounding it. To achieve a better understanding of the mechanism we need to know more about the role of defects during chemisorption. This will be discussed in greater detail in Chapter VII.

CHAPTER IV

ADSORPTION ON IRIDIUM

4.1. Introduction

The experiments described in Chapter III have shown that for both hydrogen and nitrogen the adsorption on tungsten depends strongly on the crystallographic structure of the surface: direct chemisorption on the most densely packed plane, the (110), is an unusually slow process. Our next effort is to investigate the generality of this structural specificity during chemisorption. The fcc metals afford a natural choice, not only because they offer a different type of crystal structure, but also because among them are the catalytically active platinum-group metals.

Nitrogen is only weakly adsorbed on the group VIII metals [22,76-79]. The adsorption of nitrogen on rhodium has been studied by Ehrlich et al. [78]. Using field emission technique, they found that nitrogen adsorbs weakly on rhodium, showing little dependence on surface structures at temperatures below 112 K; at a higher temperature, 135 K, considerable dependence on the surface structure was found. In both cases, the binding energy for nitrogen is low, on the order of 11 kcal/mole, and complete desorption occurs at $T \leq 180$ K. Similar behavior was noted in the adsorption of nitrogen in iridium by Nieuwenhuys et al. [79], also using field emission. In this study, three weakly bound states of nitrogen were reported on different regions of the surface, with desorption energies ranging from 7-11 kcal/mole on the (110), to ~ 14 kcal/mole on rough surfaces. The rate of adsorption on iridium does not depend drastically upon the surface structure.

The chemisorption of hydrogen on densely packed planes of heavier fcc metals is still in dispute. On the Pt(111) plane, Somorjai et al. [4] found no catalytic conversion of H_2 and D_2 into HD between 300-1300 K, using a chopped molecular beam technique. Lu and Rye [5,80], using flash desorption, however, found a sticking coefficient of 0.016 for H_2 on the Pt(111) at 125 K. Recently, Christmann et al. [81], using LEED, ELS, thermal desorption, and contact potential techniques, reported a rather high sticking coefficient (0.1) on Pt(111) at 150 K. Earlier studies on the adsorption of hydrogen on the (111) surface of platinum generally indicate dissociative chemisorption [82]; these have been adequately reviewed by Christmann et al. [81].

Not only is the rate of chemisorption on the Pt(111) in dispute, the dependence of hydrogen chemisorption upon the surface structure is also unsettled. Somorjai et al. [4] reported that on a stepped Pt(s)-[9(111) \times (111)] surface (or Pt(997) surface) catalytic conversion of H_2 and D_2 to HD is greatly enhanced by the steps. Lu and Rye [5,80], however, reported that the rate of isotope exchange on Pt(997) is only five times higher than on the (111). Recently Christmann et al. [6] found that the stepped Pt(997) surface has an initial sticking coefficient four times higher than the (111), and that the isotope exchange on the (997) is enhanced by an order of magnitude. Although the general trends within these experiments agree, there is considerable difference in the degree of enhancement by the surface steps. Furthermore, in a field

emission study by Nieuwenhuys [83], the rate of hydrogen adsorption on the smooth (111) plane was found similar to that on rougher surfaces. He actually found a much lower rate for adsorption on regions near the (110) plane. His results on microscopic crystals appear quite different from those on macroscopic surfaces.

The lack of agreement between results on macroscopic crystals could be caused by differences in surface conditions. Techniques employing macroscopic crystals lack unequivocal controls over the details of surface structure: experimental results can vary depending upon the cleanliness of the surface and defects on the surface. Some discrepancies might also be caused by inadequate analysis of experimental data. In a chopped beam experiment, the kinetic process occurring on a surface may not be faithfully revealed. As pointed out by Wachs and Madix [84], in such an experiment on stepped surfaces only the reactions on steps are probably measured, since the reaction via other kinetic processes lags behind, and hence desorption products from these processes may be out-of-phase with the incoming beam. It is thus clear that experiments under more controllable conditions are necessary to unequivocally establish the chemisorption behavior on fcc metals.

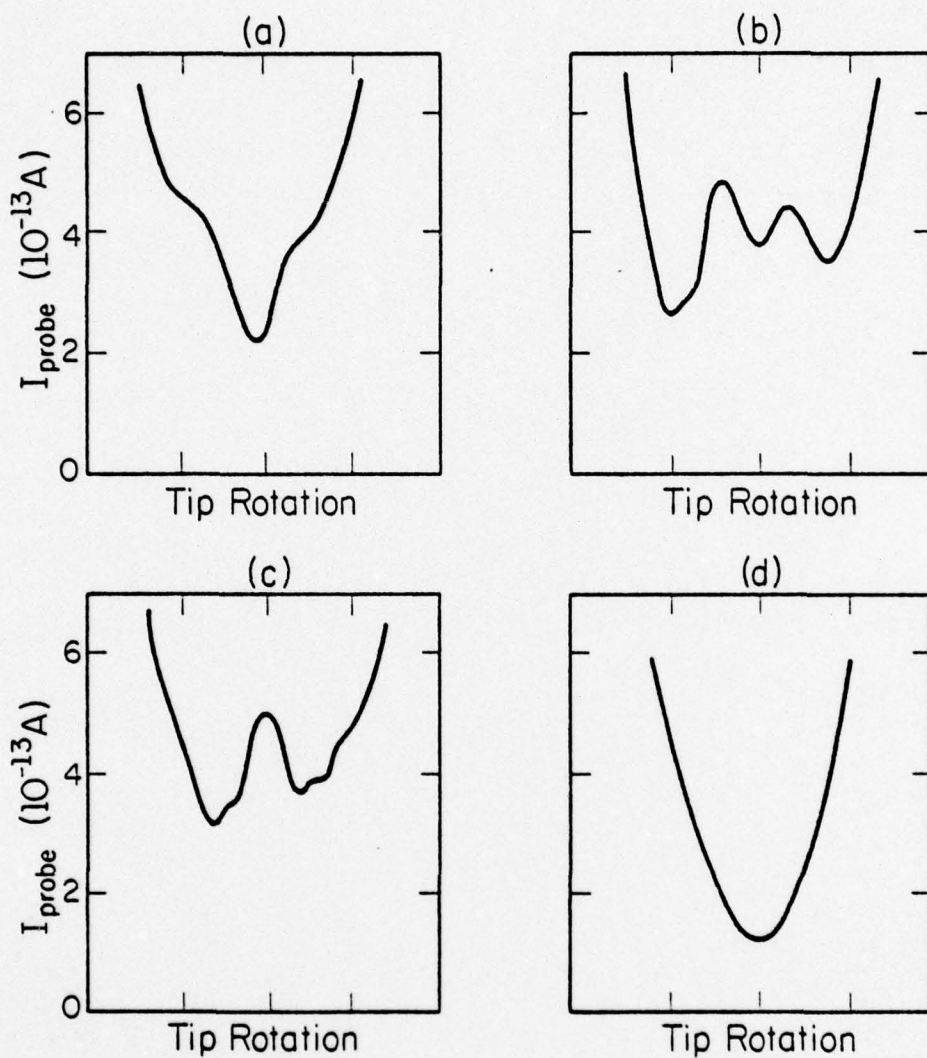
Concomitant with Somorjai's studies on H_2 - D_2 exchange on platinum, Polizzotti [3], using field emission techniques, already studied structural effects in the chemisorption of hydrogen on rhodium, another platinum-group metal with the fcc structure. At temperatures

ranging from 80 to 298 K, he found that the rates of chemisorption on three major low index planes, the (111), (100), and (110), are at least as fast as those on the rough surfaces of the rhodium emitter. No apparent temperature dependence, nor structural effects, were observed.

In Polizzotti's experiments the surface was unequivocally cleaned by field evaporation and was structurally well-characterized. However, the lack of structural specificities on rhodium surfaces should not be generalized to other fcc metals without caution. Although rhodium is one of the platinum metals, it belongs to the 5th period in the periodic table. As we shall see later in chapter VI, the generalization of chemisorption behavior from one period to another is not advisable. To test the extent of structural effects in chemisorption within the 6th period, we decided to study adsorption on iridium, which is also a member of the platinum group and is located directly below rhodium in the periodic table.

4.2. Experimental results

We have studied adsorption of hydrogen on iridium at 40 and at 80 K. In these experiments the emitter is cleaned by vacuum field evaporation and the surface is then characterized by the scanning technique described in chapter II. Typical scan diagrams, showing different stages of evaporation of the (111) plane, are shown in Fig. 4.1. Data reported here were collected only after the emitter had been field evaporated to more than 20 kV, so that the contribution from plane edges is negligible. At the maximum stripping voltage, 26 kV, the diameter of the (111) plane is $\sim 75 \text{ \AA}$, as estimated from the applied voltage and the evaporation field for iridium (5.0 V/\AA) by the method described in appendix C. The



AP-838

Fig. 4.1. Scan diagrams for an Ir(111) plane. Field evaporation voltage at 80 K= (a) 22.201 kV; (b) 22.210 kV; (c) 22.214 kV; and (d) 22.217 kV. Total emission current = 2×10^{-8} A at 2,060 V.

contribution from the plane edges for iridium is generally small. The average work function for the emitter is high (5.0 eV), and therefore emission from the edges is not as important as that of tungsten. Our estimate of the edge contribution is $\lesssim 0.02$ eV, hardly significant considering the accuracy of F-N measurements.

4.2a. Adsorption on the emitter as a whole

In Fig. 4.2, work functions of the (111) plane and the emitter as a whole are plotted as functions of the exposure to hydrogen. A value of 5.0 eV is assigned to the average work function for the total emitter, following the survey by Nieuwenhuys et al. [79]. The clean (111) work function thus obtained without correction for local fields is 5.7 eV, slightly lower than the value of 5.79 eV obtained both by Nieuwenhuys, and by Zandberg and Tontegode [85], and the value of 5.76 ± 0.04 eV reported by Strayer et al. [86].

When the surface is at 80 K, exposing the emitter to hydrogen induces immediate adsorption on both the (111) plane and the emitter as a whole, as is evident in Figs. 4.2 and 4.3. On the total emitter, the work function as obtained from F-N measurements follows a rather complicated course. It increases by only 0.02 eV immediately after exposure to $\sim 4 \times 10^{16}$ molecules/cm² of hydrogen. The work function then drops 0.10 eV below the clean value after exposure to 8×10^{16} molecules/cm² of hydrogen. The work function rises again to a stable value 0.17 eV above that of the clean surface at a total exposure of $\sim 3 \times 10^{17}$ molecules/cm². Up to this point the pre-exponential factor of the total emitter has been decreasing. The logarithm of the ratio of the pre-exponential factor relative to a clean surface $\ln(A/A_0)$, reaches a

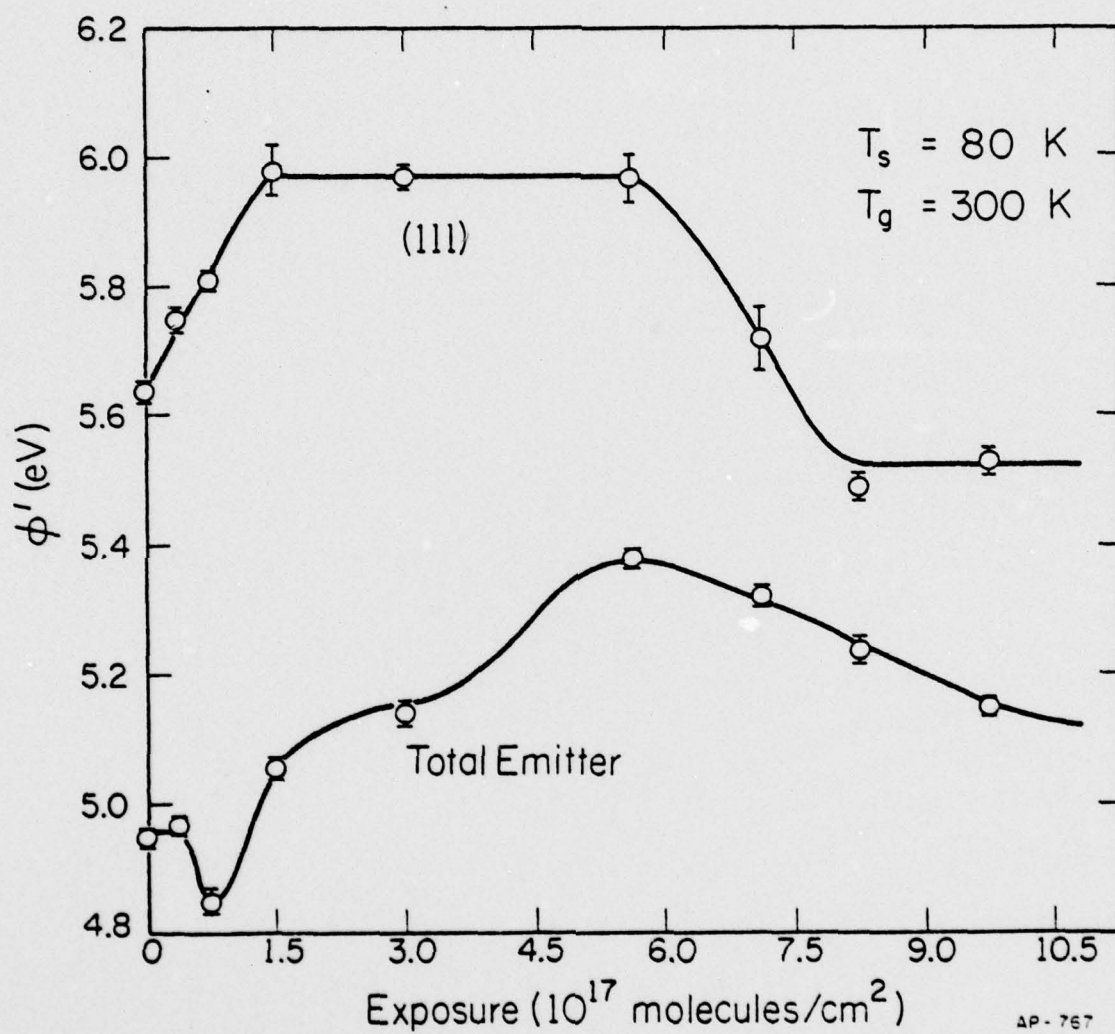


Fig. 4.2. Variation of the total and (111) work function with exposure to hydrogen for a vacuum field evaporated iridium emitter at $T_s = 80 \text{ K}$.

minimum of -1.4 at an exposure of $\sim 3 \times 10^{17}$ molecules/cm², as shown in Fig. 4.3. Beyond this point, when the emitter is further exposed to hydrogen, the work function rises again to 0.43 eV above the clean surface. Accompanying this increase in the total emitter work function is a large increase in the pre-exponential factor by $\ln(A/A_0) \approx 1.75$, at an exposure of $\sim 4 \times 10^{17}$ molecules/cm², as shown in Fig. 4.3. Further additions of hydrogen decrease both the work function and the pre-exponential factor gradually. This trend was not stopped at the highest exposure reached, 1×10^{18} molecules/cm².

The decrease in the work function at low exposures and the increase in the pre-exponential factor at $\sim 4 \times 10^{17}$ molecules/cm² of exposure are quite reproducible. The complicated change on the total emitter may be understood by considering the many rough and flat areas which make up a field emitter. The contribution to the total emission current from each small area depends on its own work function and local electric field. For an iridium emitter, the dominant emitting area changes with exposure to hydrogen. For a clean iridium emitter, the regions near the {012} planes are dominant, as shown in Fig. 4.4a,b. After being exposed to 1.6×10^{17} molecules/cm² of hydrogen, the emission pattern changes drastically. As shown in Fig. 4.4c, the emission becomes less uniform, and only relatively small areas near the {321} planes are bright. At exposures above 4×10^{17} molecules/cm², emission becomes more uniform again and most of the emitter surface is bright, as shown in Fig. 4.4d. The complicated changes in the work function and in the pre-exponential factor therefore reflect different adsorption events on different regions of the surface, rather than the formation of many adsorption states on one surface.

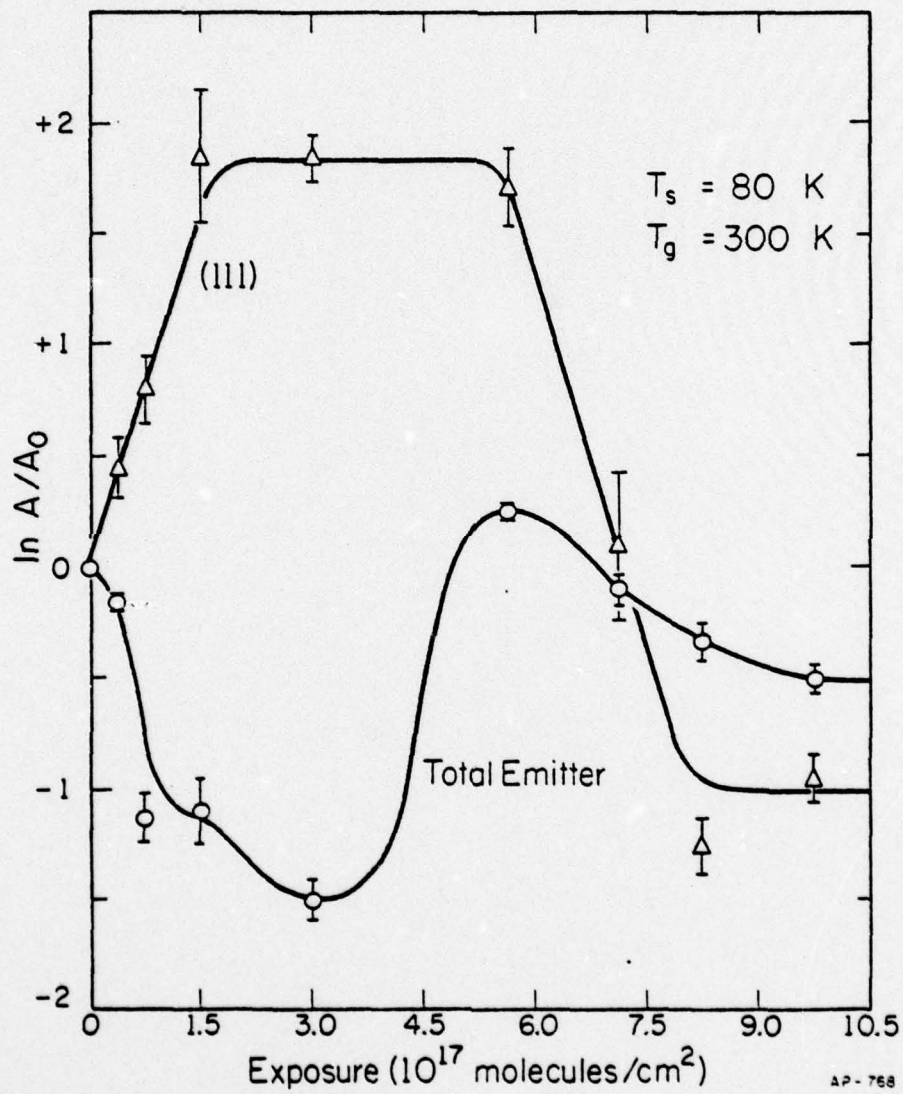
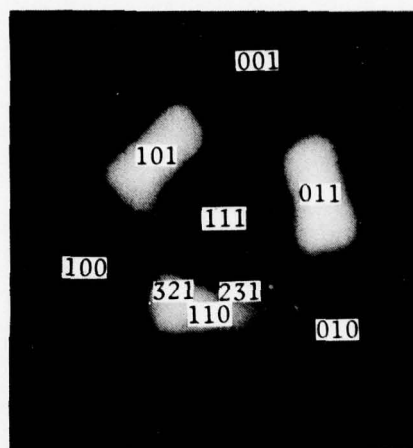


Fig. 4.3. Variation of the F-N pre-exponential factors with exposure to hydrogen for the iridium emitter in Fig. 4.2.



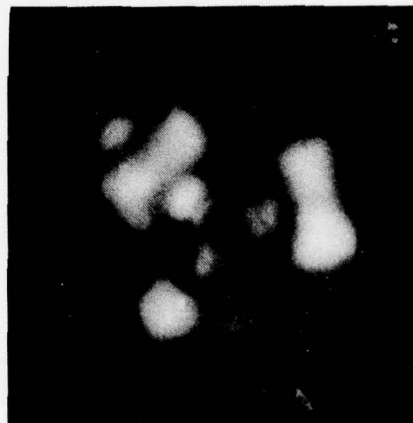
(a)



(b)



(c)



(d)

Fig. 4.4. Field emission patterns for a (111) oriented iridium emitter. (a) Clean emitter. (b) Clean, with major planes labelled. (c) After exposure to 1.6×10^{17} molecules/cm² of hydrogen. (d) After exposure to $> 4 \times 10^{17}$ molecules/cm² of hydrogen.

4.2b. Adsorption on the (111) plane

On the (111) plane the changes are less complicated than on the total emitter. As is evident in Fig. 4.2, the work function of the (111) increases steadily with hydrogen exposure, and reaches a value 0.32 eV above that of the clean surface at an exposure of 1.6×10^{17} molecules/cm². Thereafter it remains stable, until the exposure reaches $\sim 6 \times 10^{17}$ molecules/cm²; then the work function drops sharply by 0.45 eV, reaching a saturation value 0.12 eV below that of the clean (111) plane. The changes in the pre-exponential factor of the (111) plane are parallel to the work function changes, as evident from Fig. 4.3. Initially the pre-exponential factor rises steadily to $\ln(A/A_0) \approx 1.75$, then drops sharply at an exposure of 6×10^{17} molecules/cm², reaching a value $\ln(A/A_0) \approx -1.05$. As is clear in Figs. 4.2 and 4.3, there is no hesitation before adsorption occurs on the (111) plane, the closest packed plane of fcc metals. There appears to be no structural specificities parallel to the hydrogen-W(110) system on this plane.

Exposing the emitter to hydrogen when the surface is cooled to 40 K also does not bring about appreciable changes in the chemisorption behavior. On the (111) plane, just as elsewhere, adsorption occurs immediately upon exposure to hydrogen, and brings the work function to 0.3 eV above the value for the clean surface. At $\sim 6 \times 10^{17}$ molecules/cm² a second state occurs, featuring a decrease in both the work function and the pre-exponential factor. The emission characteristics for the total emitter do not deviate appreciably from those at 80°K.

The hydrogen adsorbed on the (111) plane at both 40 and 80 K can be desorbed by heating the emitter to ~ 400 K for a few minutes. The (111) plane then almost resumes the work function and pre-exponential factor typical of the clean surface. The total emitter, however, is not cleaned by warming to 400 K. The desorption temperature for the total emitter is not known, since heating above 400 K usually results in contamination for surfaces cleaned by field evaporation.

4.3. Discussion

There is yet no comparable study of the chemisorption of hydrogen on the Ir(111). Our results, however, are in reasonable accord with results on the Pt(111) plane. Two atomic states were found by Christmann et al. [81]; both desorb at less than 400 K. This is quite similar to our observations on the Ir(111), where two states are clearly distinguished and complete desorption occurs at 400 K. The sticking coefficient, 0.005, on Ir(111), estimated approximately from Fig. 4.2, is about 3 times lower than that obtained by Lu and Rye [5] and is about 20 times lower than that by Christmann on the Pt(111) plane. This might be a reflection of the difference between iridium and platinum. It is more likely a reflection of the difference in surface conditions. On a macroscopic sample, surface defects cannot be eliminated, while in our experiments surface perfection is documented by field evaporation and by the scanning technique. Our work function change on the Ir(111) plane is

also different from the changes on the Pt(111) reported by Christmann et al. [81] (-0.35 eV), and by Nieuwenhuys [83] (-0.61 eV) for hydrogen adsorption. This is probably caused by the difference in the chemical nature of the substrate. As we shall see later in chapter VI, chemisorption behavior can be different even for isoelectronic materials.

Our results on the total emitter are also consistent with the early flash desorption work of Mimeault and Hansen [87]. At 100 K, they found two distinct binding states of hydrogen on polycrystalline iridium, with desorption energies of ~ 24 kcal/mole. Arthur and Hansen [88], using field emission technique, also observed the formation of two binding states of hydrogen on the total emitter at 77 K. The change in the work function at saturation was 0.25 eV above the value for a clean surface, comparable to our results.

From the complicated changes in the field emission pattern of the iridium emitters, it is obvious that the adsorption of hydrogen depends on the crystallographic structure of the surface. Using a field desorption microscope, Panitz [89] has also found that hydrogen selectively adsorbs on the vicinity of the iridium {321} planes--the same area which shows the strongest emission after our iridium emitter has been exposed to 1.6×10^{17} molecules/cm² of hydrogen.

The general adsorption behavior of hydrogen on iridium is not appreciably different from that on platinum and rhodium. For these fcc metals the chemisorption of hydrogen varies with surface structure, as indicated by different isosteric heats of adsorption and changes in work functions, as well as the difference in the rate of adsorption. However,

astounding structural specificities similar to those on the W(110) plane are not found, at least for iridium and rhodium. For these two metals experiments have been carried out in this laboratory under unequivocally controlled conditions. The rate of chemisorption on the (111) plane, the closest packed plane of fcc metals, has been shown no slower than on the rougher surfaces.

AD-A056 535

ILLINOIS UNIV AT URBANA-CHAMPAIGN COORDINATED SCIENCE LAB F/G 7/4
CHEMISORPTION ON PERFECT SURFACES AND STRUCTURAL DEFECTS. (U)

OCT 77 R LIU

DAAB07-72-C-0259

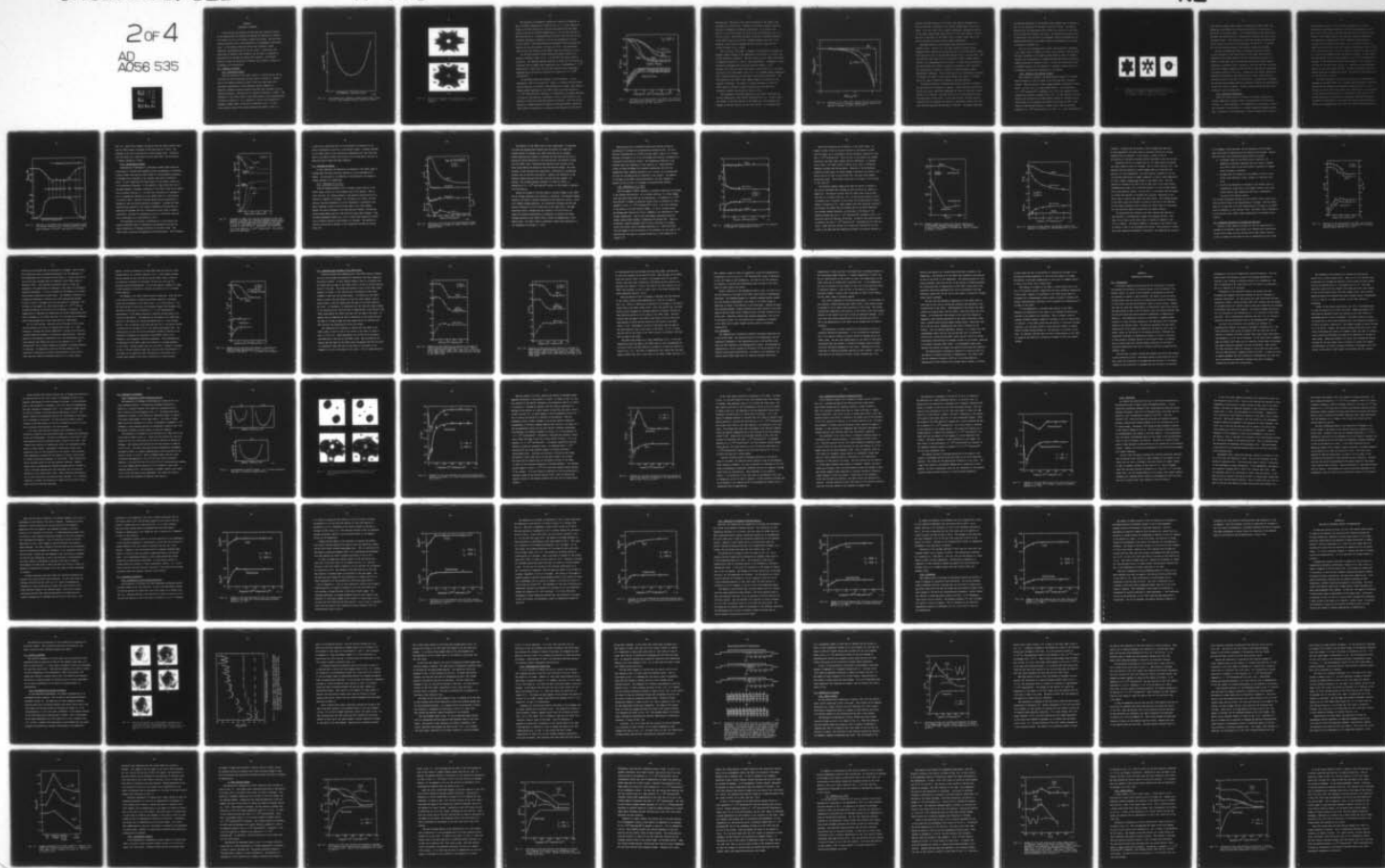
UNCLASSIFIED

R-790

NL

2 of 4

AD
A056 535



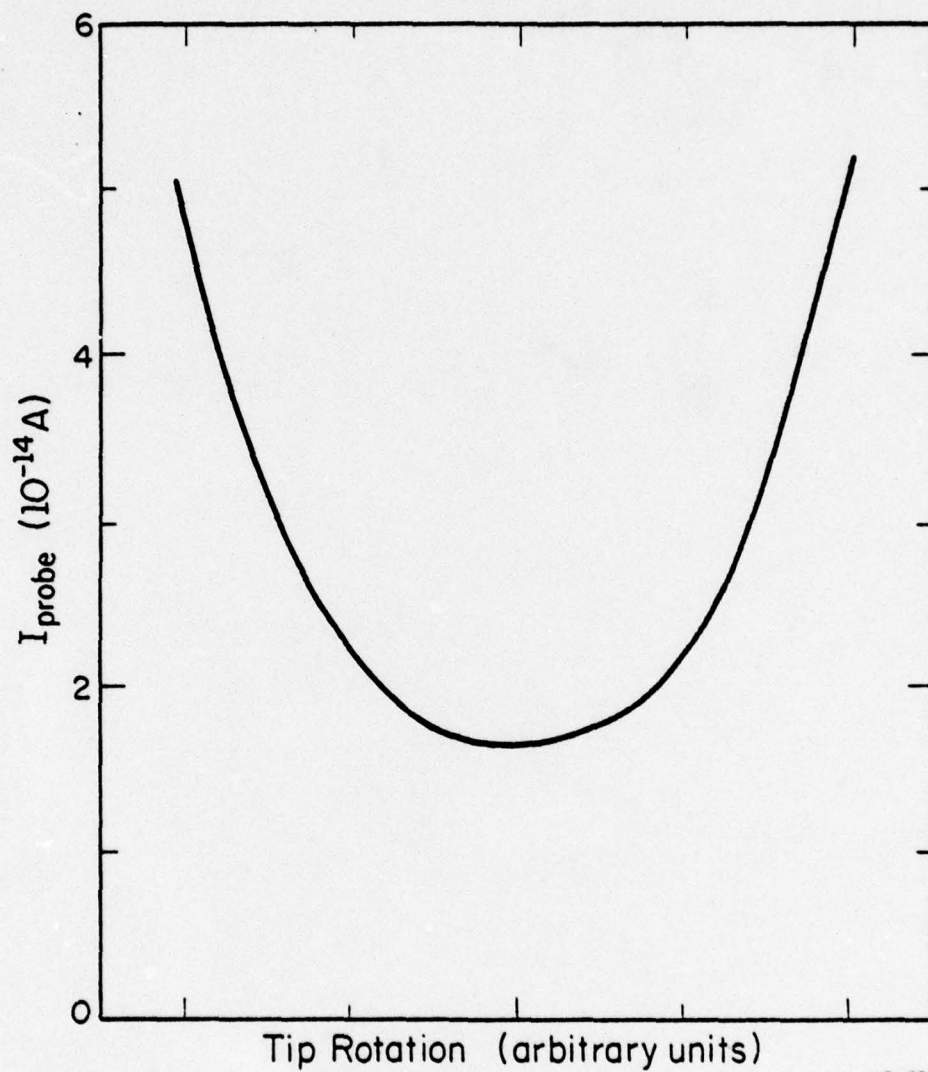
CHAPTER V

ADSORPTION ON RHENIUM

In the previous two chapters we have seen that structural effects in the chemisorption of nitrogen and hydrogen are important on tungsten, a bcc metal, but not on fcc metals, rhodium and iridium. The only type of metal structure that is left unexplored is the hexagonal close packed (hcp). Of the heavier transition metals only ruthenium, osmium, technetium, and rhenium occur in the hcp lattice. Among these, the metallurgy of rhenium is most advanced, and the metal is available as high purity wire suitable for making field emitters. We therefore decided to study the adsorption of hydrogen and nitrogen on rhenium, as an example of an hcp material.

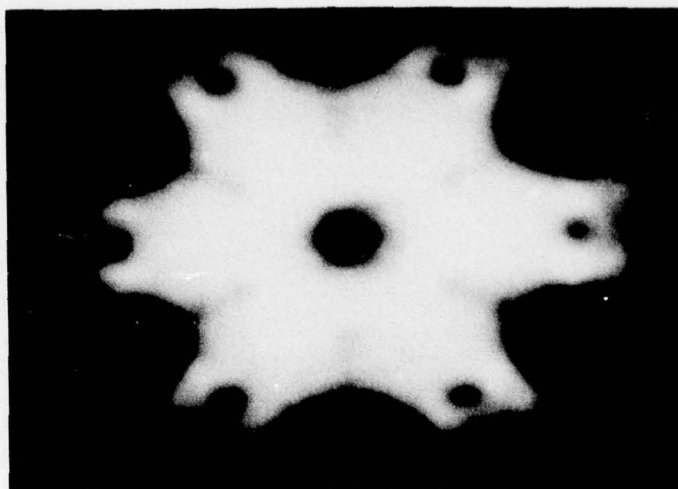
5.1. Hydrogen on rhenium5.1a. Adsorption studies

That the perfection of the (0001) plane of a rhenium emitter can be controlled by field evaporation has been shown in chapter II. However, even at the maximum stripping voltage (30 kV) the plane edges still contribute significantly to the probe-hole current (Appendix C). Therefore, thermally annealed emitters have been used throughout for the rhenium experiments. The emitters are cleaned by heating to $\sim 2500^{\circ}\text{C}$. The smoothness of the (0001) plane is then characterized by the scanning method discussed in chapter II. As a reference, a typical scan diagram for a thermally cleaned (0001) Re emitter is displayed in Fig. 5.1, and a field emission pattern with planes appropriately labeled in Fig. 5.2.

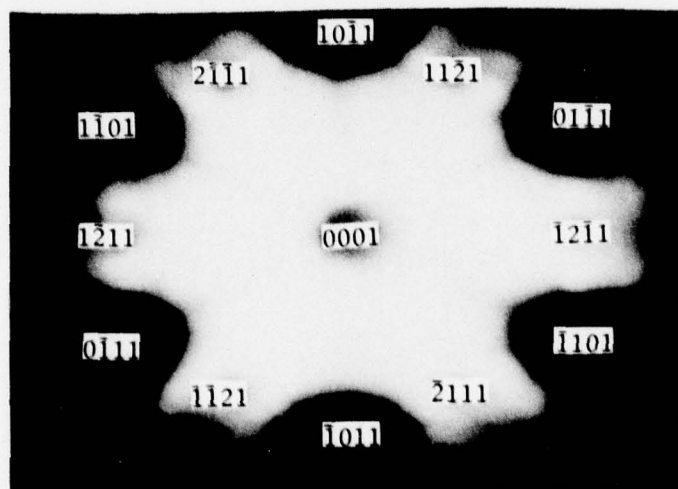


AP-836

Fig. 5.1. Scan diagram for a thermally cleaned rhenium (0001) plane at 80 K. Total emission current = $5 \times 10^{-7} \text{ A}$ at 8,900 V.



(a)



(b)

Fig. 5.2. Field emission patterns for a rhenium emitter cleaned by annealing at ~ 2500 C. (a) Clean; (b) major planes labelled.

The adsorption of hydrogen on rhenium as a function of exposure to gas at different temperatures is shown in Fig. 5.3. In this figure the change in the work function for both the total emitter and the (0001) plane are plotted for surface temperatures $T_s = 50, 80, 200, \text{ and } 300 \text{ K}$. The work function ϕ' is estimated from the slope of the F-N plots by the procedures described in chapter II, and is not compensated for local electric fields. Following Zandberg and Tontegode [90] the average work function for the total emitter is taken as 4.93 eV. The uncorrected value for the work function of the (0001) plane thus obtained is 6.4 eV.

For the total emitter the work function increases steadily with exposure, reaching a value $\sim 0.30 - 0.36 \text{ eV}$ above the clean surface at saturation. The hydrogen exposure necessary to bring the total emitter to saturation varies slightly with temperature, but is approximately $3 \times 10^{17} \text{ molecules/cm}^2$. Beyond this point the work function stays essentially unchanged and no new state is observed up to exposure of $1.5 \times 10^{18} \text{ molecules/cm}^2$.

On the (0001) plane the situation is quite different. At low temperatures, that is at 50 and 80 K, there is an induction period before the work function of the (0001) plane undergoes any change. Work function changes become significant on the (0001) plane only after exposure to $\sim 3 \times 10^{17} \text{ molecules/cm}^2$ of hydrogen, or approximately the amount necessary to bring the total emitter to saturation. This is quite similar to the behavior of the W(110) plane when exposed to hydrogen. After the initial hesitation, further exposure of rhenium to hydrogen gradually brings the (0001) plane to saturation, as indicated by the diminution of the (0001)

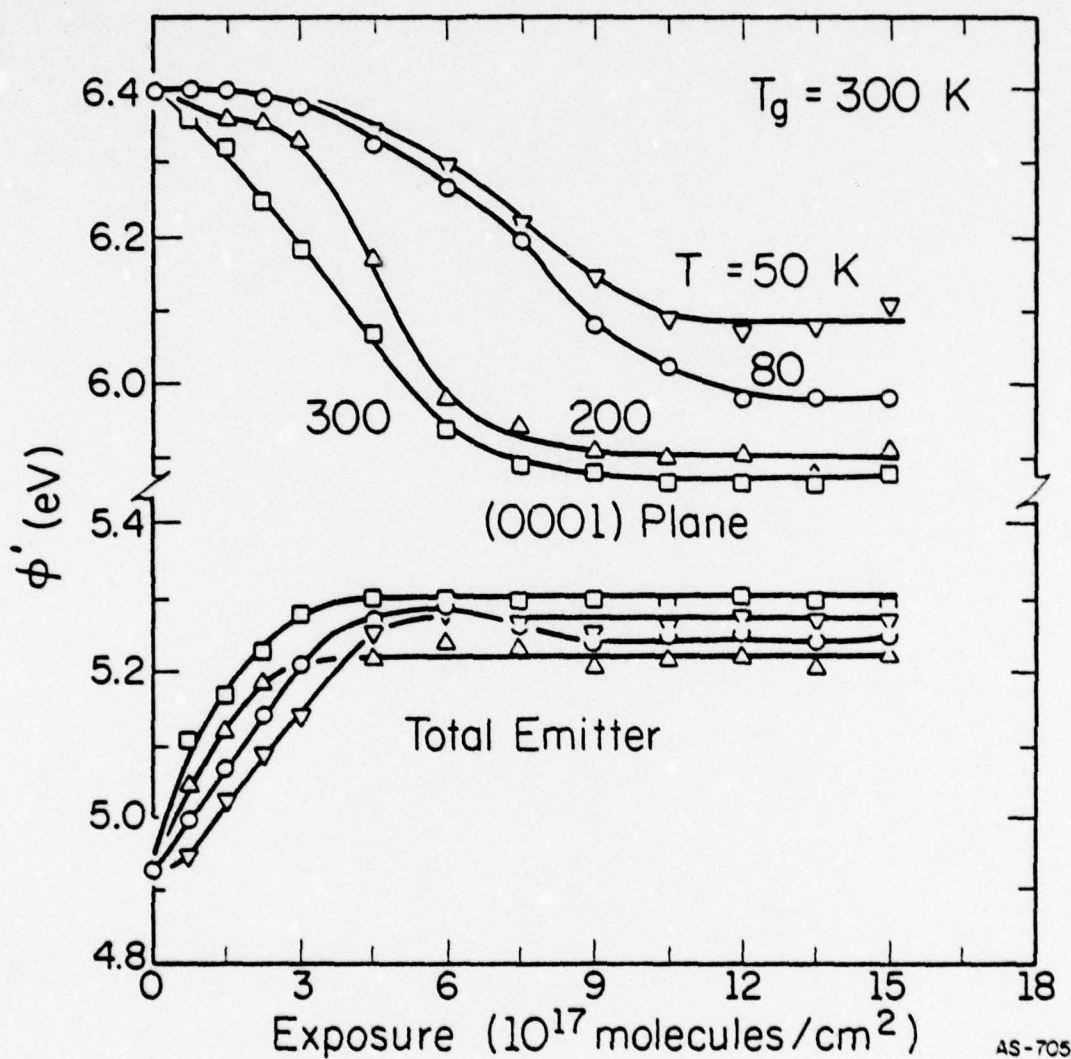


Fig. 5.3. Variation of the total emission and (0001) work functions with exposure to hydrogen for a thermally cleaned rhenium emitter at $T_s = 50, 80, 200, \text{ and } 300$ K.

work function. The rate of work function decrease of the (0001) plane is similar at 50 and at 80 K. However, the saturation value of the work function is different at different temperatures, as is evident from Fig. 5.3; it is 0.32 eV below the value of the clean surface at 50 K, but 0.42 eV at 80 K. The initial sticking coefficient of hydrogen adsorption on the (0001) plane at 50 and 80 K, roughly estimated from Fig. 5.3 by assuming a linear relation between the work function change and the surface coverage, is $s_0 \sim 0.0003$.

Just as on the (110) plane of tungsten, the adsorption of hydrogen on Re(0001) depends strongly on the temperature of the surface. At 200 K, the initial hesitation disappears. The work function of the (0001) plane shows an immediate decrease by ~ 0.05 eV, quite reproducibly. Thereafter it stays essentially unchanged until the total exposure reaches 3×10^{17} molecules/cm²; then the (0001) work function drops sharply to 0.5 eV below the value of the clean surface (Fig. 5.3). At a somewhat higher temperature, 300 K, hydrogen adsorption on the (0001) plane becomes even faster. The work function of the (0001) plane changes roughly in proportion to the exposure to hydrogen. The amount of hydrogen necessary to bring the (0001) plane to saturation, and the value of the work function at saturation, however, are similar to those at 200 K.

The dependence of hydrogen adsorption on the (0001) plane upon the surface temperature is more clearly revealed by Fig. 5.4. In this figure the changes in the work function of the (0001) are plotted against the changes in the work function for the total emitter. It is evident that

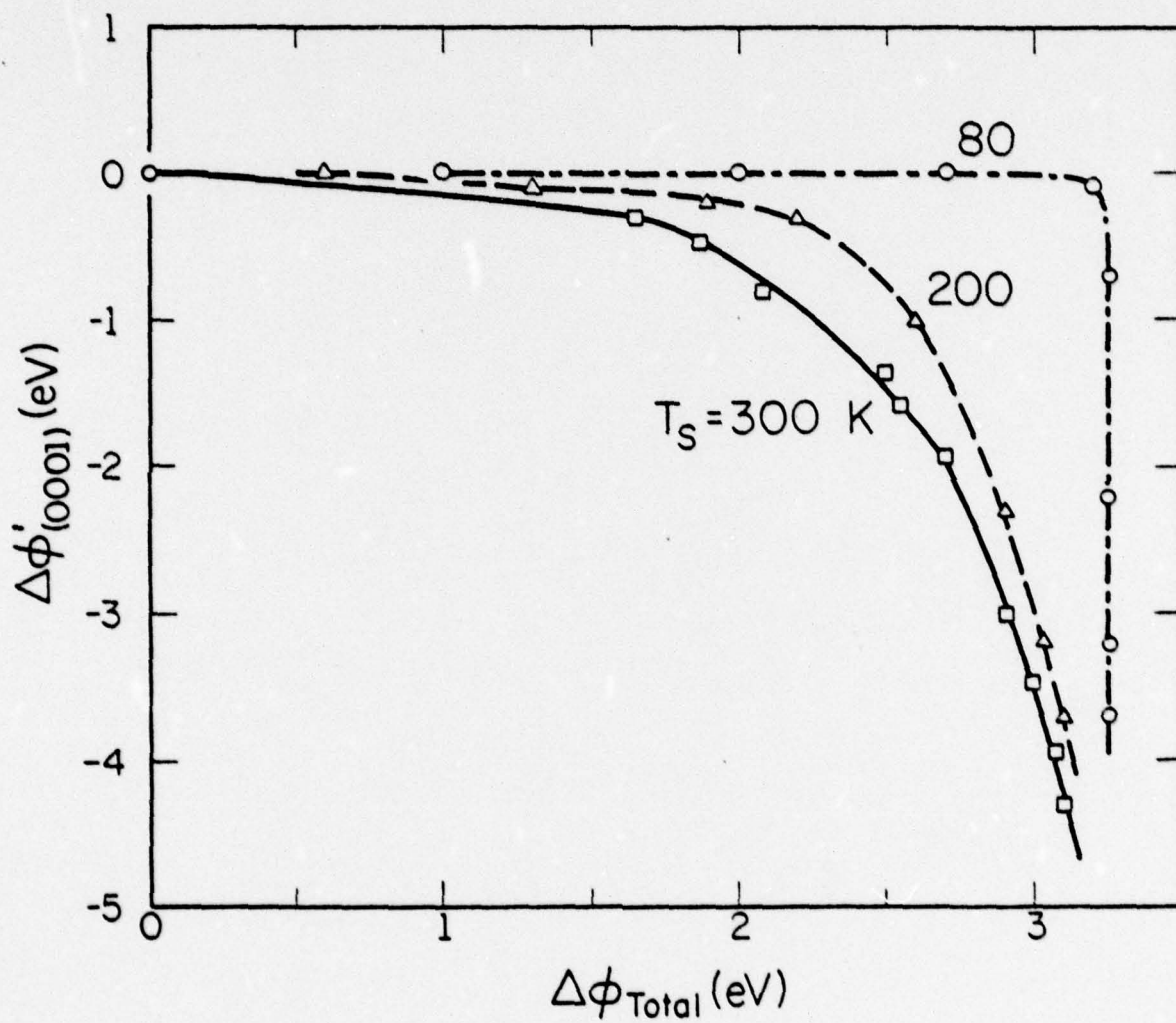


Fig. 5.4. Variation of the (0001) work function with the total emitter work function for a thermally annealed rhenium emitter when exposed to hydrogen at $T_s = 80, 200$ and 300 K.

at 80 K, the work function of the (0001) plane remains unchanged until the total emitter is saturated; only then do changes begin on the (0001) plane. It is also clear that at higher temperatures, hydrogen adsorption on the (0001) plane becomes rapid relative to the total emitter. However, the rate of adsorption on the (0001) plane is always slower than on the rest of the emitter surface, even at higher temperatures.

Hydrogen adsorbed on the rhenium surface between 80 and 300 K is probably atomic. Gasser et al. [91] have observed complete isotope exchange between hydrogen and deuterium at 300 K on polycrystalline rhenium. Flash desorption work on the hydrogen-rhenium system is not available. The only LEED and Auger study [92] on a macroscopic (0001) oriented rhenium crystal is in disagreement with our results. In that study no adsorption was detected when the surface is exposed to hydrogen at 300 K and above. This discrepancy is probably a reflection of the difference between experimental techniques. The low cross section for scattering of electrons by hydrogen [93] makes it questionable whether the presence of hydrogen can in all cases be detected by changes in the LEED patterns.

The general behavior of hydrogen adsorption on rhenium is analogous to the adsorption of hydrogen on tungsten. Clear structural specificities as well as a strong temperature dependence are found on the densely packed planes of both systems. Even the direction of the work function changes are reminiscent of each other. On the total emitter, the work function increases for both tungsten and rhenium; on the densely packed plane, the work functions decrease when hydrogen is adsorbed. The general mechanism

for hydrogen adsorption on the Re(0001) plane probably also is similar to that for the adsorption of hydrogen on the W(110) plane. The initial hesitation at low temperatures would reflect the inability of the (0001) plane to dissociate hydrogen into atoms. The gradually accelerated rate of adsorption at 200 and 300 K is presumably caused by the migration of hydrogen dissociated on the rougher surfaces surrounding the flat plane, as discussed in chapter III.

Just as in the hydrogen-W(110) system, the mechanism of adsorption on the (0001) plane of rhenium is likely to be different at 80 and 300 K. The rapid adsorption on the densely packed planes at 300 K is probably caused by the redistribution of chemisorbed hydrogen which is relatively tightly bound and is immobile at 80 K. At 80 K the close-packed plane is probably filled in by the diffusion of a mobile, loosely bound layer of hydrogen, existing only temporarily on the surface.

5.1b. Changes in the emission pattern

When exposed to hydrogen, the field emission pattern of a rhenium emitter changes in a way not found in any other gas-metal systems we studied. The peculiarity of these changes deserves a discussion in some detail. In Fig. 5.5a is a clean rhenium pattern. After exposure to $\sim 3 \times 10^{17}$ molecules/cm² of hydrogen at $T_s = 80$ K, the emission pattern appears quite uniform, as shown in Fig. 5.5b. At this exposure, the work function for the emitter as a whole almost reaches its saturation value. When exposed to more hydrogen, the region surrounding the (0001) plane starts to dominate the emission; a bright ring is seen at exposures between $4.5-6 \times 10^{17}$ molecules/cm², as in Fig. 5.5c. This strong emission

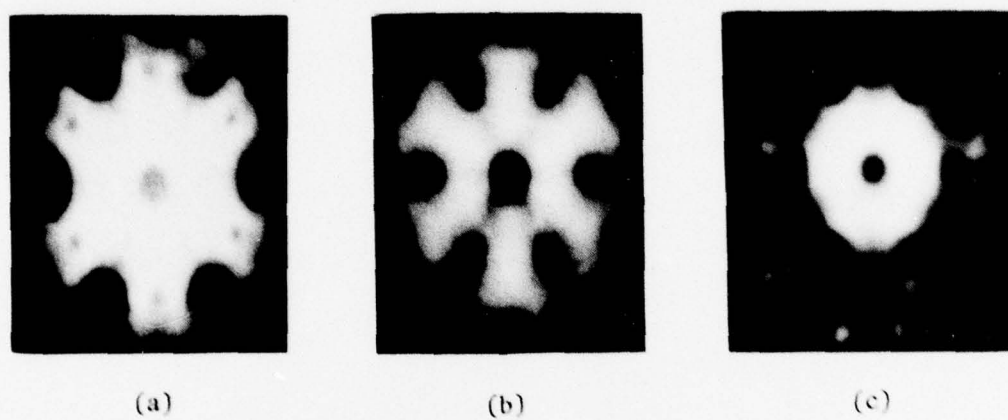


Fig. 5.5. Changes in the field emission pattern upon exposure to hydrogen for a thermally annealed rhenium emitter at $T = 80$ K. (a) Clean; (b) exposed to 3×10^{17} molecules/cm² of hydrogen; (c) exposed to 6×10^{17} molecules/cm² of hydrogen.

comes from the rough terraced region surrounding the (0001) plane. The appearing of the bright ring coincides approximately with the onset of adsorption on the (0001) plane. As the chemisorption on the (0001) plane proceeds, the pattern persists, although more structures now show up near the (0001) region. The strong emission from the terraces surrounding the (0001) plane occurs only at low temperatures (50 and 80 K). At 200 and 300 K no such bizarre changes in the emission pattern was observed.

The most intriguing discovery in studying the emission patterns is the coincidence of the chemisorption on the (0001) plane with the appearing of the bright emission from the rough terraces outside of it. There is little doubt that the strong emission from the (0001) terraces represents a different state of adsorption. The fact that this state does not exist at higher temperatures (200 and 300 K) indicates the instability of hydrogen adsorbed in this form. Judging from this thermal instability, hydrogen thus adsorbed on the surface must be loosely bound, and has a desorption energy in the order of 10 kcal/mole. In many ways it resembles the loosely bound hydrogen Polizzotti proposed to explain the chemisorption on the (110) plane of tungsten. However, without further evidence such a conclusion cannot be unequivocal.

5.1c. Desorption measurements

After the rhenium surface is covered by hydrogen, increasing the surface temperature eventually leads to the desorption of the adsorbed hydrogen. In these experiments, the temperature of the emitter is controlled by passing a pre-calibrated d.c. current through the tungsten support loop. Calibration of the temperature is done by measuring the resistance

of the support loop at $T < 900$ K, and by a pyrometer at $T > 900$ K. Desorption of the hydrogen adsorbed on the (0001) plane starts at 400 K and a clean (0001) plane is restored when the emitter is heated to 900 K. However, if the (0001) plane is not completely covered by hydrogen at low temperature, increasing the surface temperature brings about an increase in the coverage of the (0001). This is evident from Fig. 5.6, where both the work function and the change in the emission current of the (0001) plane are plotted, first as a function of exposure to gas, and then as a function of temperature when the emitter is heated. In this experiment the emitter at 80 K is first exposed to 6.75×10^{17} molecules/cm² of hydrogen, so that the (0001) plane is half-saturated. This treatment is indicated by the solid lines in Fig. 5.6. After the residual hydrogen is pumped out and a good vacuum restored, the emission characteristics are checked again and no changes were found. The emitter is then heated step by step from 80 K to 1100 K.

The initial heating to 110 and 200 K increases the concentration of hydrogen on the (0001) plane, as is evident from the decrease of the work function and the increase in the emission current in Fig. 5.6. Even without any supply from the gas phase, the redistribution of the adsorbate on the surface appears sufficient to saturate the (0001) plane at 200 K. Further heating up to 400 K does not bring about additional changes in the emission characteristics; the (0001) work function and the emission current stay unchanged from 200 to 400 K, as shown by the dashed lines in

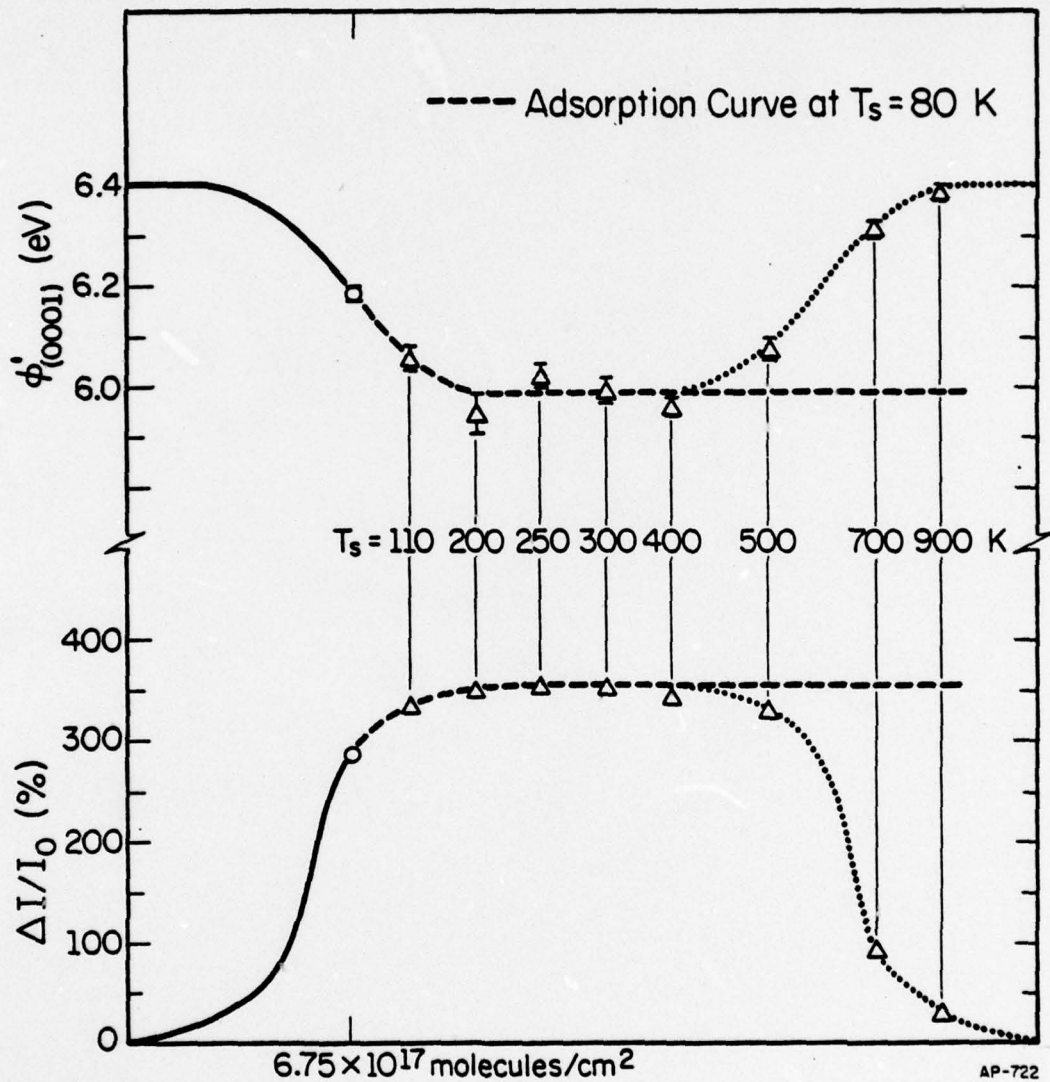


Fig. 5.6. Variation of the (0001) work function and emission current with surface temperature for a thermally annealed rhenium emitter exposed to 6.75×10^{17} molecules/cm² of hydrogen.

Fig. 5.6. Above 400 K, however, desorption from the (0001) surface starts and the (0001) plane is restored to the clean state at ~ 900 K. The hydrogen on the rest of the emitter is more strongly bound. Desorption from the emitter as a whole does not occur below 900 K, and the emitter is largely cleaned at ~ 1100 K.

5.1d. Re-adsorption studies

Re-adsorption of hydrogen on a previously cleaned (0001) plane was investigated to provide more information about the mechanism of adsorption. We have already seen that the (0001) plane of a rhenium emitter saturated by hydrogen can be restored to its original clean state by heating to 900 K. At this temperature the other regions of the emitter surface are still populated by hydrogen. If the emitter is then cooled down to 80 K and again exposed to hydrogen, adsorption on the (0001) plane occurs rapidly. This is evident from Fig. 5.7, in which the re-adsorption of hydrogen at 80 K is compared with adsorption on the (0001) plane of a clean emitter at 80 and at 300 K. The most striking feature during re-adsorption of hydrogen is that the initial hesitation disappears. Although the (0001) plane has been restored to its original cleanliness during heating, by redosing with hydrogen the rate of adsorption on this plane is greatly accelerated. The rate of re-adsorption at 80 K is even faster than the rate of adsorption on a clean surface at 300 K.

The difference in the rates of adsorption on a clean emitter and during re-exposure cannot be explained by any mechanism involving the direct dissociation of hydrogen molecules on the (0001) plane. The (0001) plane is clean at the beginning of both experiments. The differences

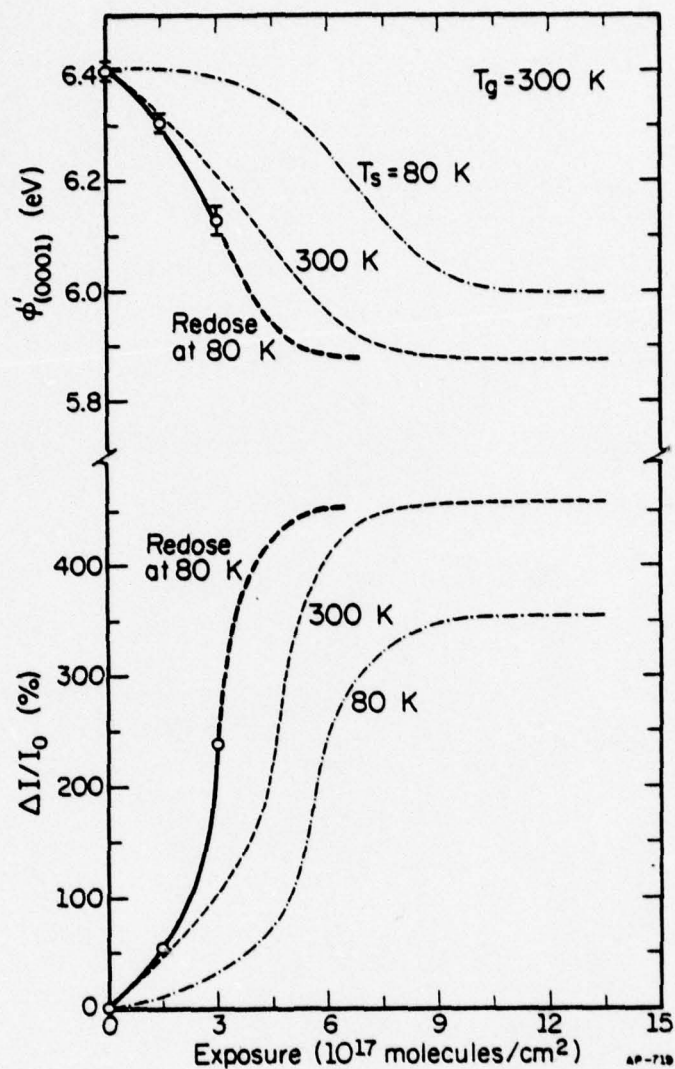


Fig. 5.7. Variation of (0001) work function and emission current with exposure to hydrogen for a thermally annealed rhenium emitter which is previously saturated with hydrogen and then heated to 1,100 K. Thin dashed curves show adsorption on clean surfaces at $T_s = 80$ and 300 K. Experiments are carried only up to total exposures of 3×10^{17} molecules/cm². Heavy dashed curves are speculative.

in the rate of adsorption have to be attributed to differences in the state of adsorption on the rest of the emitter surface. Hydrogen adsorbed on the (0001) plane in the re-adsorption experiments must come from other areas on the emitter rather than directly from the gas phase: the rate of adsorption should remain the same otherwise.

5.2. Nitrogen on rhenium

As just indicated, the adsorption of hydrogen on the (0001) plane of rhenium shows the same structural specificity as the hydrogen-W(110) system. Our next goal is to establish if the adsorption of nitrogen on rhenium proceeds in a similar way.

5.2a. Adsorption at $T_s \leq 80$ K

With the rhenium surface at 80 K, nitrogen adsorbs rapidly on the (0001) plane, as well as on the rougher areas of the emitter. This is clear from Fig. 5.8, showing changes in the emission characteristics as a function of exposure to nitrogen. For the emitter as a whole, the work function initially decreases by 0.15 eV; thereafter, it gradually rises again, reaching a value of 0.05 eV below that of the clean surface. Despite the initial decrease in the work function, however, the emission current drops sharply and after the first few doses stays constant. From the Fowler-Nordheim relation, Eq. (2.2), we would have expected an initial rise in emission current by 40% instead of a decrease. The emission is obviously controlled by changes in the transmission through the surface layer [34].

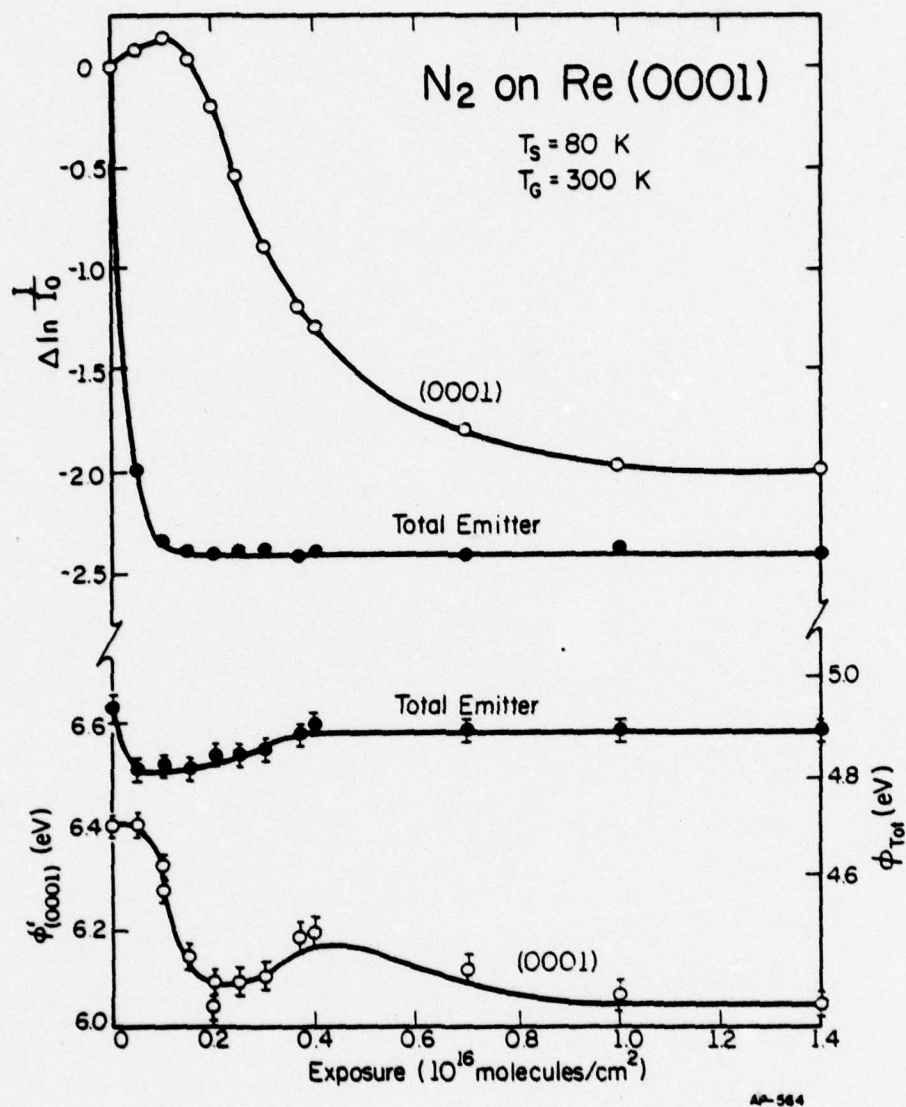


Fig. 5.8. Variation of work function and field emission current with exposure to nitrogen for (0001)-oriented rhenium emitter at 80 K.

The behavior of the (0001) plane is more complicated. At exposures for which the average work function from the emitter as a whole has already reached its minimum, the (0001) plane has not yet changed. Further additions are required to decrease the work function by 0.35 eV. During the initial hesitation of the work function, the emission current from the (0001) rises, indicating that adsorption has occurred on the basal plane despite the absence of any work function change. The later decrease in work function also brings about a diminution of the emission current, just as for the total emitter. However, the diminution in the emission current persists even after the work function reaches its minimum. The nitrogen exposure necessary to bring the (0001) to saturation is $4-5 \times 10^{15}$ molecules/cm², similar to that needed to saturate the total emitter.

Beyond the minimum in the work function, further changes on the (0001) due to nitrogen adsorption are difficult to determine. The emission becomes unstable, and there is intense flickering of the probe-hole current. After still higher nitrogen exposures, the fluctuations disappear and the work function stabilizes at 0.37 eV below that of the clean value. The same saturation value is reached with the surface at 50 K as at 80 K; in these less detailed observations no instability in emission was found. Nitrogen adsorbed on the (0001) plane at these low temperatures is only weakly bound. The (0001) plane is completely cleared after adsorption at low temperature by heating to ~ 150 K.

These results are in reasonable accord with previous studies on the behavior of nitrogen on polycrystalline rhenium [94,95]. In field emission investigations of a [10 $\bar{1}$ 1]-oriented sample, Klein et al. already observed a decrease of 0.4 eV in the average work function, accompanied by a decrease in the emission current. The temperature stability of the adsorbed layer was comparable to that found by us. Flash desorption studies by Yates and Madey [95] revealed sometime ago that this low temperature layer, commonly referred to as a γ -state, is not dissociated and that the nitrogen exists as molecules on the surface. The behavior of nitrogen on the (0001) plane established in our work conforms in general outline to that of γ -nitrogen on polycrystalline rhenium.

5.2b. Adsorption at $T_s \geq 300$ K

With the sample at 300 K, exposure to nitrogen brings about an increase in the average work function. As is evident from Fig. 5.9, these changes occur much more slowly than at low temperatures. An exposure of 5×10^{18} molecules/cm² is needed to bring the surface close to saturation at 300 K, compared to only $\sim 4 \times 10^{15}$ molecules/cm² at 80 K. Also quite different is the nature of the work function change. At 300 K, nitrogen raises the average work function by 0.25 eV, compared to the diminution at lower surface temperatures. This is also the behavior previously noted for several single-crystal planes of rhenium by van Oostrom [96]. There is, furthermore, general agreement that at 300 K, adsorption of nitrogen occurs only slowly, with a sticking coefficient of ~ 0.002 [95,97,98]. From the change in the work function at low exposures (on the order of 10^{17} molecules/cm²) we derive a sticking coefficient at room temperature of roughly 10^{-3} .

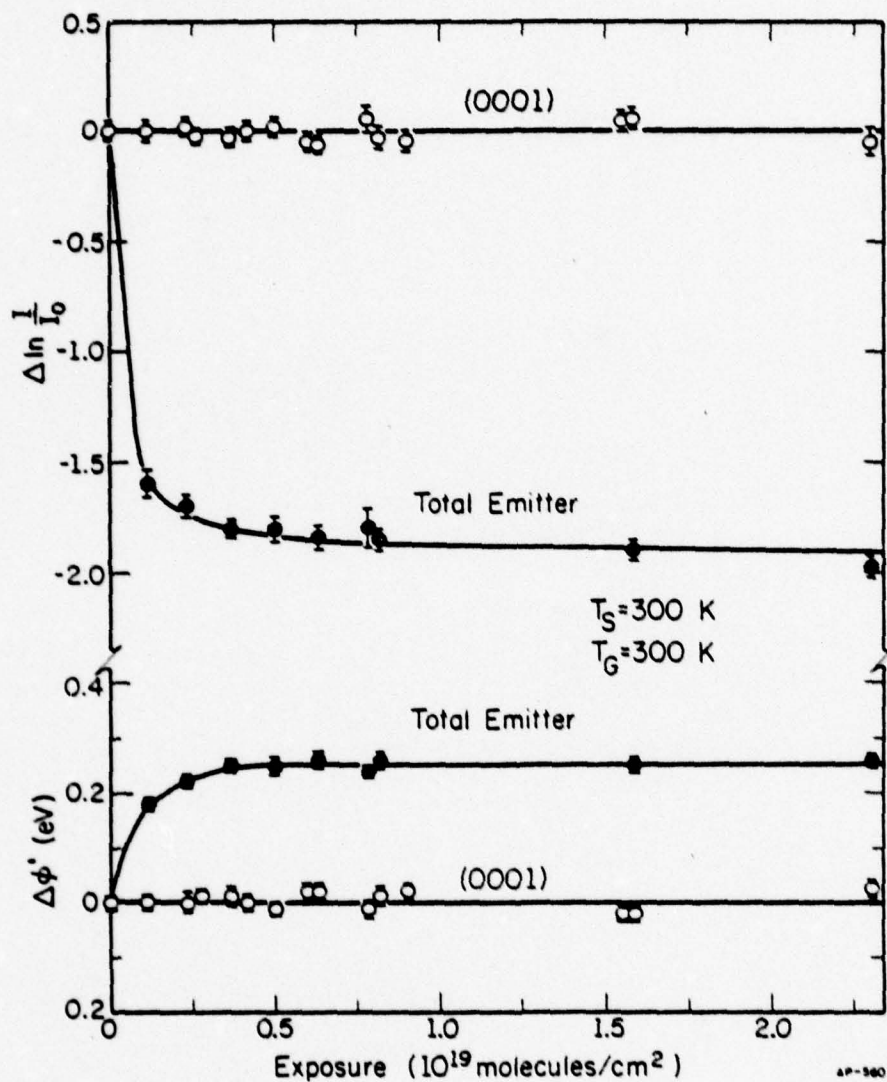


Fig. 5.9. Changes in work function and emission current with exposure to nitrogen for rhenium emitter at 300 K.

Much more interesting is the behavior of the (0001) plane. No change is found, either in the work function or the emission current from this plane, up to the highest nitrogen exposures, amounting to more than 3×10^{19} molecules/cm². While the rest of the emitter has reached saturation, the basal plane remains entirely unaffected. We conclude that at 300 K, the (0001) plane of rhenium is not able to efficiently chemisorb nitrogen from the gas phase. Compared to the surrounding, atomically rough planes, for which changes in emission are evident in our work as well as in that of van Oostrom [96], the basal plane appears essentially inert. The sticking coefficient of nitrogen on this surface is less than 10^{-5} .

The situation changes dramatically when the emitter is heated to 550 K after saturation with nitrogen at 300 K and after all ambient is pumped out. The emission current from the (0001) plane drops by more than 30%, as is evident from Fig. 5.10. On heating the surface to 550 K, no pressure rise is observed in the system; the average emission current, however, increases by 17%. These changes arise from processes confined to the surface--the supply from the residual gas can be shown inadequate. The nitrogen exposure necessary to bring about a 30% change in the emission current must be $> 1 \times 10^{17}$ molecules/cm², according to Fig. 5.11. During the period of heating, the residual nitrogen in the system provides an exposure less than 1×10^{15} molecules/cm². Contamination also does not enter. Blank runs were carried out in which the clean emitter was subjected to the same time and temperature schedule, but without exposure to

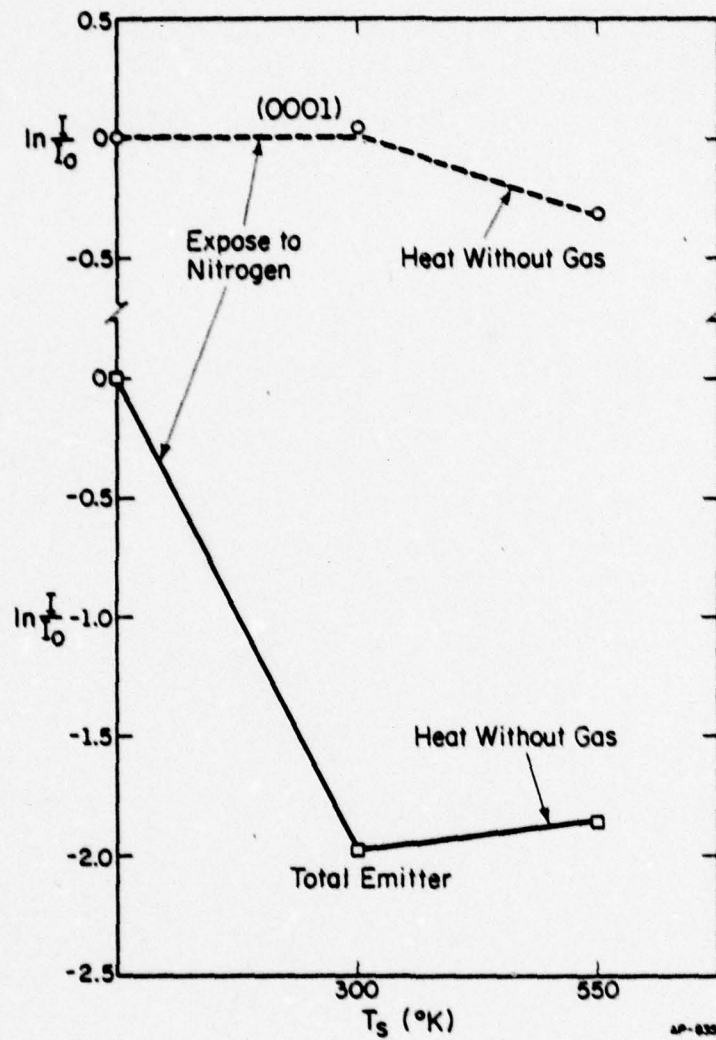


Fig. 5.10. Changes in emission current with surface temperature T for a thermally annealed rhenium emitter. The emitter^s at 300 K is first exposed to nitrogen gas, then it is heated in vacuum to ~ 550 K.

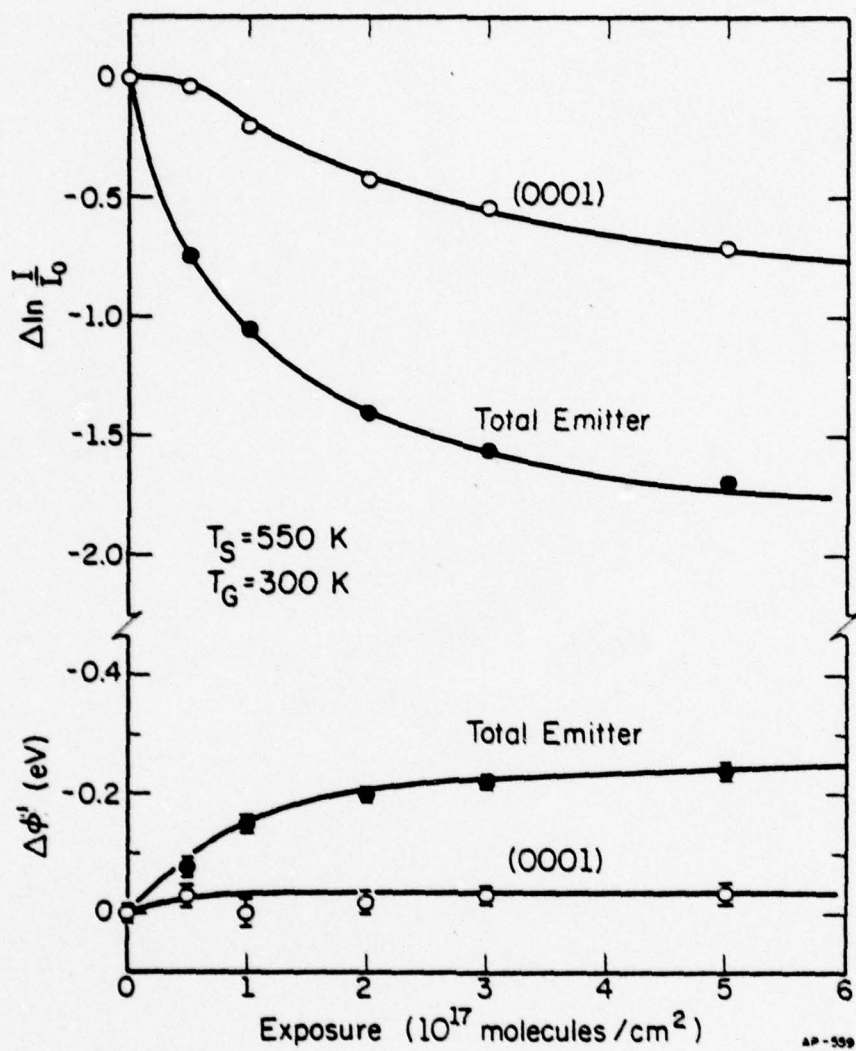


Fig. 5.11. Variation of work function and emission current with exposure to nitrogen for a rhenium emitter at $T_s \sim 550$ K.

nitrogen. In these runs the emission current changed less than 0.5%. At high temperatures the basal plane is evidently filled with nitrogen supplied from the remainder of the surface, similar to the redistribution of hydrogen on rhenium surfaces discussed in the last section.

Adsorption can also be brought about on the (0001) plane by exposing the clean surface at 550 K to nitrogen. This is clear from Fig. 5.11. The emission from the surface as a whole changes much as it does when the emitter is at room temperature. The work function increases by 0.25 eV; the sticking coefficient is roughly comparable to that at room temperature. At 550 K, however, changes are evident on the (0001) plane. The work function at saturation is 0.08 ± 0.03 eV above that of the clean surface. Accompanying the small rise in the work function is a much clearer diminution of the emission current. Even at 550 K, it is evident from the change in current with exposure to nitrogen that initially, adsorption on the basal plane of rhenium lags behind the other planes. The nitrogen adsorbed on the (0001) plane also differs in stability from that on the remainder of the surface--heating to 900 K restores the (0001) plane to cleanliness, but only partially desorbs nitrogen from the rougher surfaces.

For polycrystalline surfaces it has been reported that rhenium is more resistant to contamination by gases than tungsten [99,100]. This trend is also found on the (0001) plane of rhenium as compared to the (110) of tungsten. The general behavior of nitrogen on the Re(0001) plane is similar to that in the nitrogen-W(110) system. The reluctance to adsorb, the strong temperature dependence of adsorption, the magnitude and direction

of the changes in work functions, and the existence of low and high temperature forms of adsorption are all shared by both systems. However, there are three clear differences between these two systems:

- a. γ -nitrogen formed on the (0001) plane of rhenium at low temperature evaporates completely when the surface is warmed up to 300 K, while on the W(110) partial conversion to tightly bound β -nitrogen is observed;
- b. Nitrogen does not chemisorb on the Re(0001) at 300 K; on the W(110) plane adsorption occurs, though at a relatively slow rate;
- c. At 550 K the adsorption of nitrogen on the Re(0001) plane is substantially slower than on the rougher surfaces, but on the W(110) plane at that temperature the rate is comparable to the rest of the emitter surface.

All of these differences indicate that the Re(0001) plane is more inert than the W(110) plane in the chemisorption of nitrogen. From our experiments it is clear that the direct chemisorption of nitrogen on the (0001) plane of rhenium is a very unlikely event. The (0001) plane of rhenium is by far the most inert surface toward chemisorption of nitrogen we have studied.

5.3. Sequential adsorption of nitrogen and deuterium

Earlier in this chapter we pointed out that the chemisorption of hydrogen on the Re(0001) plane cannot occur through direct dissociation of gas on this plane, but must instead involve some indirect process. If this is indeed the case then the rate of chemisorption on this plane

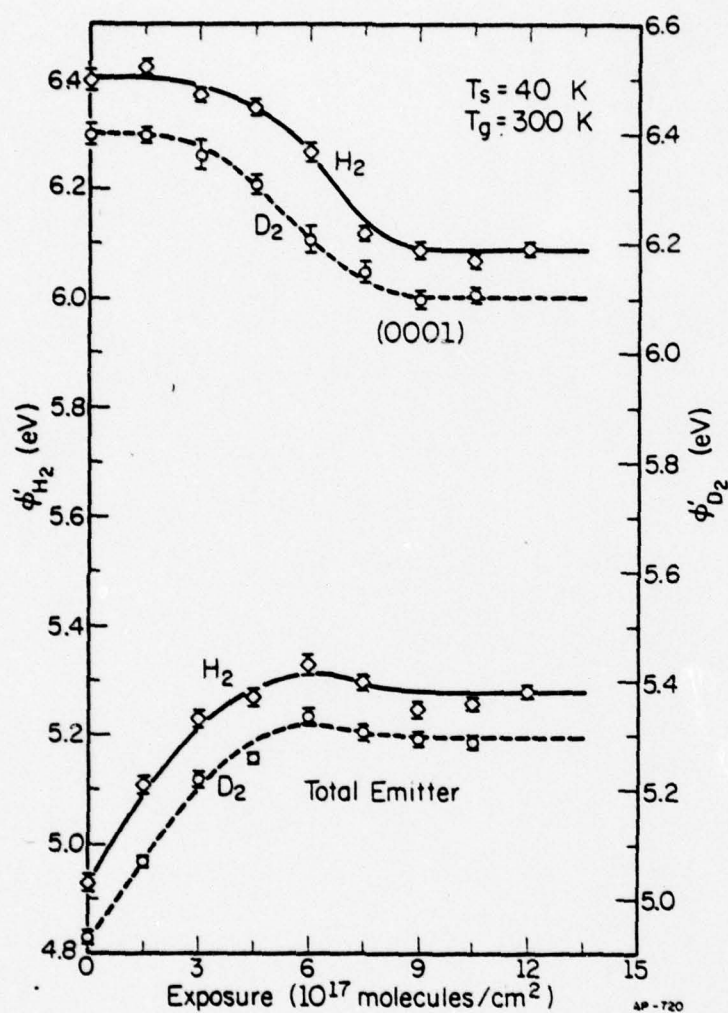


Fig. 5.12. Variation of the total emission and (0001) work function with exposure to hydrogen and to deuterium for a thermally annealed rhenium emitter at $T_s = 40 \text{ K}$.

should also be affected when its environment is changed. Such an effect has already been noted in redosing experiments, but the importance of the surroundings can be checked even more directly. We have seen in the last section that nitrogen does not chemisorb on the (0001) plane of rhenium at 300 K. This provides an excellent chance to study the mechanism of the chemisorption of hydrogen on this plane in a sequential adsorption experiment -- we can now change the environment of the (0001) plane without affecting the plane itself. The sequential adsorption of nitrogen and deuterium is carried out by first exposing the rhenium emitter at 300 K to nitrogen until the total emitter is saturated. The nitrogen is then pumped out; when a good vacuum ($< 2 \times 10^{-10}$ Torr) is restored the emitter is cooled to 80 K and exposed to deuterium. The chemisorption of deuterium on rhenium does not differ significantly from that of hydrogen, as is evident from Fig. 5.12, and the use of deuterium rather than hydrogen has no other than historical significance.

For the total emitter, saturation with β -nitrogen at 300 K raises the work function by 0.25 eV, as already shown in Fig. 5.9. After saturation, lowering the surface temperature in vacuum to 80 K does not introduce measurable changes in the emission characteristics. When the emitter is then exposed to deuterium at 80 K, the work function of the total emitter rises sharply by 0.22 eV at an exposure of $\sim 1 \times 10^{17}$ molecules/cm², and no further changes are observed on continued exposure to deuterium. The magnitude of the work function change for the adsorption of deuterium on nitrogen covered rhenium is only slightly lower than that caused by deuterium adsorption on a clean surface.

However, the rate of adsorption is much higher than the rate on a clean rhenium surface, as is evident from Fig. 5.13. In this figure the work function change for the total emitter and the (0001) plane is plotted as a function of exposure to deuterium, for both the clean and the nitrogen covered rhenium emitter. On the clean emitter, roughly 2-3 times as much deuterium is required to saturate the surface as for a nitrogen covered emitter.

The changes on the (0001) plane are more interesting. After the rest of the emitter surface is covered by nitrogen, exposure to deuterium causes rapid adsorption on the (0001) plane. As is clear from Fig. 5.13, the work function of the (0001) now decreases linearly with exposure, and the plane is saturated at an exposure of $\sim 3 \times 10^{17}$ molecules/cm², approximately 1/3 the amount necessary to saturate the same plane on an initially clean emitter. The magnitude of the change in the (0001) work function is the same as for deuterium chemisorption on a clean rhenium emitter. This is expected, since even when the rest of the emitter surface is saturated with nitrogen at 300 K, the (0001) plane remains bare. The striking point is that the initial hesitation ordinarily observed in the adsorption of hydrogen and deuterium on the Re(0001) plane at 80 K vanishes in this sequential adsorption experiment. The accelerated rate of adsorption on the (0001) cannot be attributed to nitrogen adsorbed on this plane. We have already seen that the (0001) is immune to nitrogen at 300 K. We must therefore reach the conclusion that the adsorption on the (0001) is not caused by direct dissociation on this plane--such a process cannot depend on the state of adsorption of other surfaces.

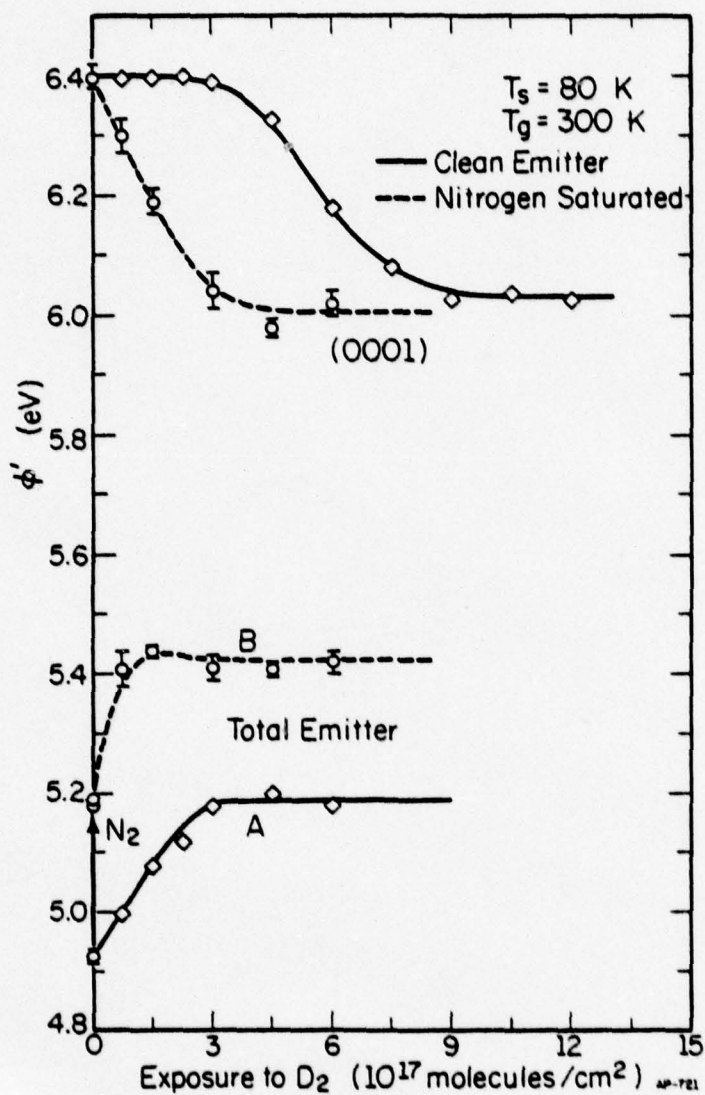


Fig. 5.13. Changes in work functions with exposure to deuterium for (0001)-oriented rhenium emitters at $T = 80 \text{ K}$. A: an originally clean emitter. B: a nitrogen covered emitter.

5.4. Adsorption near the edge of the (0001) plane

We have concluded that chemisorption on the (0001) plane of rhenium can occur only through the migration of adsorbates from other regions of the emitter surface. If this actually happens, then it is possible that the region near the edge of the (0001) plane is filled in earlier than the center of the plane. The actual distribution of gas on the (0001) plane depends, of course, on the relative rate of diffusion on this plane compared to that over the outside region. If diffusion on the (0001) plane is slower than the diffusion of gas from other regions, then we should expect to see the regions near the edge of the plane covered by gas first. If conversely, the migration over the steps and rough surfaces is the limiting factor, then the rate of chemisorption at the center of the (0001) plane should not differ from that near the edge of the plane. It appears that by comparing the rate of adsorption at the center and near the edge of a plane we might get some insight about the limiting step that restricts the chemisorption on the flat planes.

The chemisorption of hydrogen on regions near the edges of the (0001) plane, as well as that at the center of the plane, is shown in Figs. 5.14 and 5.15. These experiments are carried out by adjusting the probe hole to one side of the (0001) plane. The work function for regions near the edges of the (0001) plane, determined from the F-N plots, is considerably lower than that at the center of the plane (5.9 eV compared to 6.4 eV at the center of the plane). This is caused partially

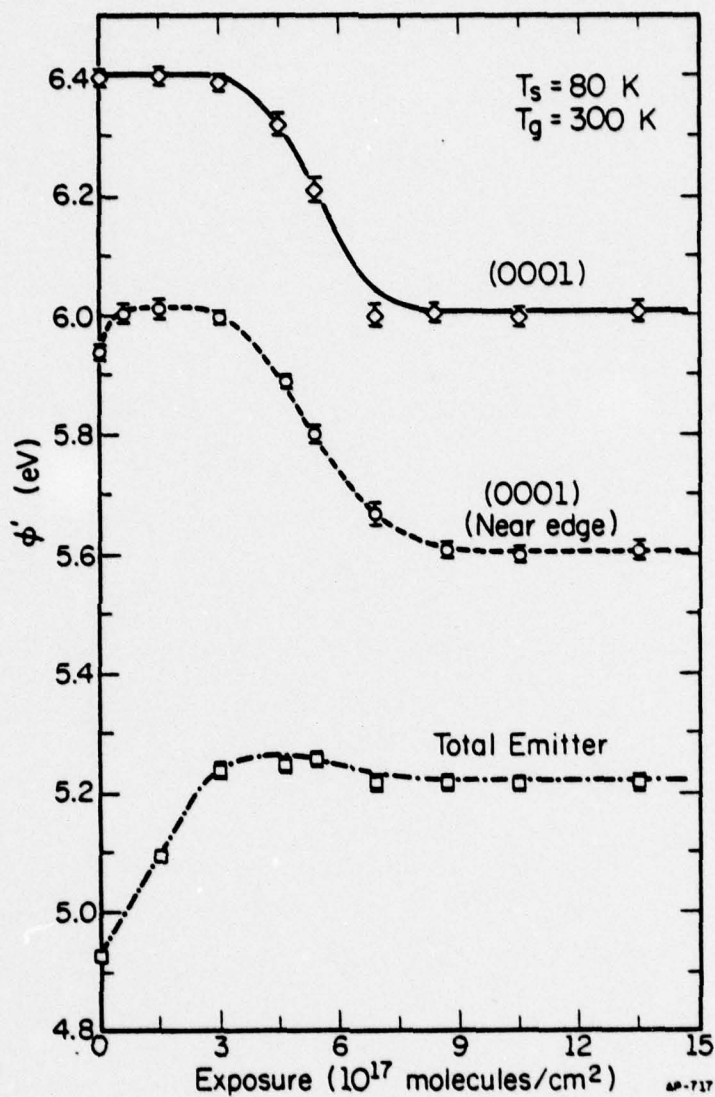


Fig. 5.14. Variation in work function with exposure to hydrogen for (0001)-oriented rhenium emitters at $T = 80 \text{ K}$. Lower curve: total emitter; upper curve: probe hole at the center of the (0001) plane; middle curve: probe hole near the edge of the (0001) plane.

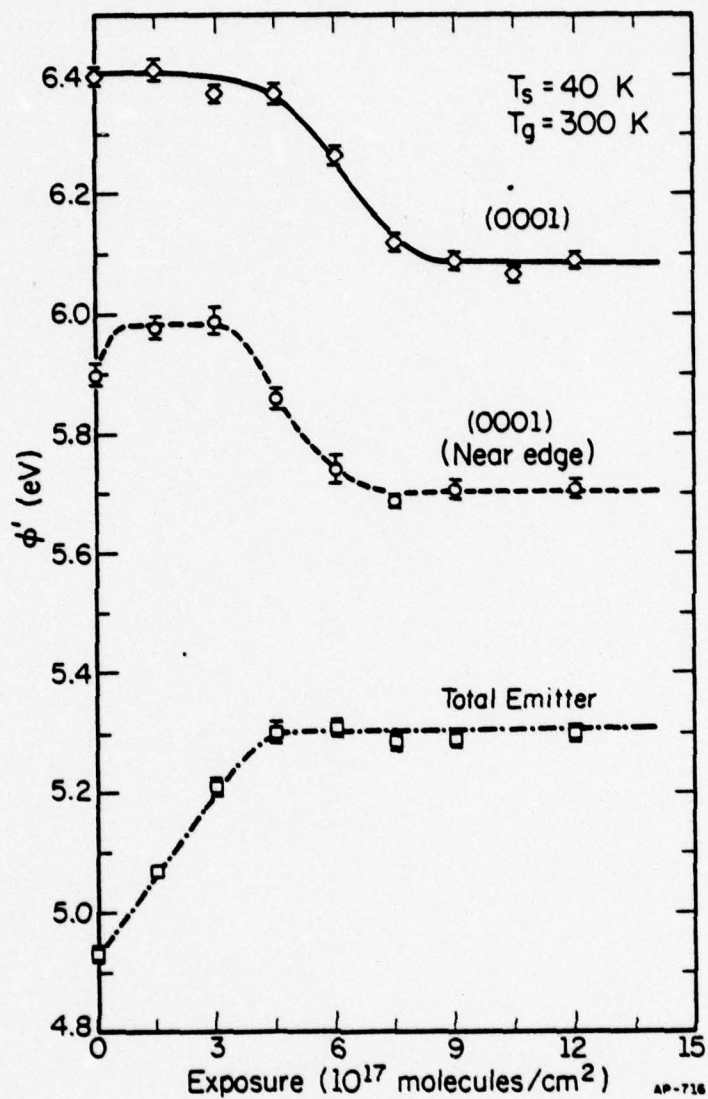


Fig. 5.15. Variation in work function with exposure to hydrogen for (0001)-oriented rhenium emitters at $T = 40 \text{ K}$. Lower curve: total emitter; upper curve: probe hole^s at the center of the (0001) plane; middle curve: probe hole near the edge of the (0001) plane.

by contributions from the strongly emitting plane edges, and partially by the local variation of the electric field. Near the edge of the (0001) plane the electric field is closer to the average field for the whole emitter, and errors thus introduced in evaluating the work function are therefore also smaller. In fact, the value of the work function for the (0001) thus obtained, 5.9 eV, is quite close to the value obtained from field evaporated emitters, 5.8 eV.

When the emitter at 80 K is exposed to hydrogen, the work function at the probed location rises immediately by ~ 0.06 eV, as shown in Fig. 5.14. This is a reflection of adsorption on the edges of the (0001), rather than on the (0001) plane itself. After the initial rise, the work function stays unchanged on continued exposure to hydrogen, showing the same induction period as at the center of the (0001) plane. The work function near the edge of the (0001) plane starts to drop at about the same exposure at which the work function at the center of the plane starts to drop. Furthermore, the rate of saturation near the edge of the plane parallels that at the center of the plane. At 80 K it seems that the rate at the center of the (0001) plane is no different from that near the edge of the plane.

The same trend prevails at a lower temperature, 40 K. At 40 K the chemisorption near the edge of the (0001) plane is also distinguished by an initial rise in the work function, followed by an induction period, as shown in Fig. 5.15. The onset of chemisorption for regions near the edge appears earlier than that at the center of the plane, judged from Fig. 5.15.

This, however, cannot be taken as unequivocal, since the reproducibility of exposure at 40 K is only 0.5×10^{17} molecules/cm², owing to adsorption on the cold finger at this temperature. Our data at 40 K are therefore not adequate to conclude that chemisorption near the edge of the (0001) plane is faster than at the center.

Another difficulty in the experiments shown in Figs. 5.14 and 5.15 is that the position of the edge of the (0001) plane cannot be unambiguously determined. The scanning diagram of a thermally annealed emitter reveals only one minimum corresponding to the center of the (0001) plane; no indication is given to the position of the plane edges. Lacking the guide from scanning diagrams, visually adjusting the probe relative to the field emission pattern cannot yield information about the exact position of the probed area. Therefore, without more detailed experiments, such as will be discussed in Chap. VII, the relative rate of migration of hydrogen on the (0001) and on nearby rougher surfaces cannot be determined unequivocally.

5.5. Discussion

The chemisorption of hydrogen on Re(0001) essentially parallels that on the W(110) plane. The induction period at low temperatures, and the temperature dependence of the chemisorption rate on the Re(0001) plane have also been observed in the hydrogen-W(110) system. The mechanism for chemisorption on W(110) proposed by Polizzotti [3] can be applied to the Re(0001) plane without modifications. According to this mechanism, the densely packed (0001) plane does not chemisorb hydrogen effectively;

chemisorption on this plane must be brought about by hydrogen adsorbed on the surrounding rougher surfaces. At higher temperatures (≥ 200 K) the rate of redistribution on the surface is rapid, and chemisorption on the (0001) plane can be brought about reasonably fast. At low temperatures the rate of diffusion on the surface is slow, and a long induction period is therefore observed. After the rest of the emitter is completely saturated, however, a mobile form of hydrogen can exist on the surface, and the (0001) plane is saturated rapidly.

This view is supported by the heating experiments. In the absence of gas, heating a rhenium emitter whose (0001) plane is only barely-covered by hydrogen to 200 K causes rapid saturation of this plane. The process causing this change must occur entirely on the surface, since the residual pressure in the system is too low to cause any measurable changes. It is thus clear that surface redistribution of the adsorbate can occur at 200 K, and chemisorption on the (0001) can be brought about by surface diffusion.

This mechanism is further supported by re-adsorption, as well as sequential adsorption measurements. In the re-adsorption experiments, most of the emitter surface is already covered by hydrogen except the (0001) plane. The fact that chemisorption on the (0001) is drastically accelerated when this surface is redosed by hydrogen clearly excludes any direct adsorption mechanism on this plane. Chemisorption on this plane must be induced by hydrogen adsorbed on other surfaces. Since all other areas on the surface are already covered, hydrogen must first

adsorb on the emitter in a loosely bound form which is mobile at low temperature. The filling in of the (0001) then proceeds in the same way as that on the W(110) at low temperature. The induction period is eliminated naturally, since now the rest of the emitter is already saturated. The accelerated rate of chemisorption on the (0001) plane found in the sequential adsorption experiments must also be explained by the same mechanism, except that now the rest of the surface is covered by nitrogen rather than by hydrogen.

The fact that the desorption temperature for the (0001) plane is lower than for the rest of the emitter indicates that hydrogen is less strongly bound on the (0001). Thermodynamically this favors the chemisorption on surfaces other than the (0001), since that lowers the total energy. If contributions from entropy in the total free energy are negligible, then hydrogen chemisorbed on the (0001) would tend to move away to surfaces which provide higher binding energy. Kinetically this may or may not occur, depending upon the rate of diffusion on the surface. From our heating experiments, however, it is evident that this thermodynamic effect does not play an important role: by heating an emitter with a barely-covered (0001) plane from 80 to 200 K in vacuum, considerable redistribution of hydrogen occurred on the surface, resulting in an almost saturated (0001) plane. If thermodynamic effects were dominant this should not happen; the opposite should have been observed.

The chemisorption of nitrogen on rhenium is a clear-cut proof for the effects of surface structures on chemisorption. The (0001) plane does not chemisorb nitrogen at 300 K up to very high exposures. Chemisorption on this surface can be brought about, however, by heating

to 550 K after the rest of the emitter is saturated by nitrogen, or by raising the surface temperature to 550 K and then expose to nitrogen. The behavior of nitrogen chemisorption on this plane is somewhat similar to that on the W(110), but is much slower.

The binding of nitrogen on the (0001) is again weaker than on the rest of the emitter surface, judging from the lower desorption temperature on this plane. However, the inertness of the (0001) plane cannot be accounted for by thermodynamic effects--there is plenty of evidence that surface redistribution by heating to 550 K increases the concentration of nitrogen on the (0001).

At low temperatures, γ -nitrogen forms readily on the (0001). Therefore the adsorption on this plane is not prevented by difficulties involved in the formation of precursors. This is evident, since by warming a Re(0001) surface covered by γ -nitrogen to 300 K a clean surface is restored. If the (0001) plane had some ability to dissociate nitrogen molecules, the γ -nitrogen should at least partially convert to tightly bound β -nitrogen during warming up. The precursor is plentiful in this case. We therefore conclude that the lack of chemisorption on the (0001) is caused by the inability to dissociate nitrogen on this close packed surface.

CHAPTER VI

ADSORPTION ON MOLYBDENUM

6.1. Introduction

In previous chapters we have discussed the interaction of nitrogen and hydrogen with surfaces of transition metals in the 6th period of the periodic table. As a part of our systematic investigation we now turn our attention to metals in the 5th period. For metals in the 5th period, we might expect that the variation in chemisorption caused by differences in the surface structure should parallel those in the 6th period. However, this does not imply that chemisorption on these metals would follow exactly the same pattern as that in the 6th period, since the bonding electrons from the 4d and 5d bands may cause significant differences in chemisorption behaviors. Such differences can best be elucidated by comparing chemisorption on a pair of metals belonging to the same group, but to different periods in the periodic table. The physical parameters that may affect chemisorption on the surface are essentially the same for such a pair of metals, except for the nature of the bonding electrons. Therefore any significant difference in chemisorption behavior is solely a reflection of their being in different periods of the periodic table. By studying pairs of metals under well defined surface conditions, we can hope to establish unequivocally the order of catalytic activity on going down the periodic table.

One such pair of metals, rhodium and iridium, has already been studied in this laboratory [3,101]. Both metals belong to group VIIIb and are fcc. While there are differences in the magnitude and direction of the charge transfer in the interaction of hydrogen with the two metals, no essential

differences in the rate of chemisorption have been observed. The close packed planes of both metals interact with hydrogen immediately on exposure to gas, showing no induction periods at low temperature. The rate of chemisorption for these metals does not reflect a strong effect due to 4d compared to 5d electrons.

Differences in the adsorption behavior for another such pair, molybdenum and tungsten, have been observed by several techniques in different laboratories. For these metals the (100) planes have been most extensively studied. Dooley and Haas [102] first reported that the changes in the LEED pattern of a Mo(100) surface during the interaction with hydrogen are different from those for tungsten. The observed changes indicating a $C(4 \times 2)$ structure at low coverage and a (1×1) structure at high coverage [103]. This is substantially different from the $C(2 \times 2)$ structure observed by Estrup and Anderson [104] on the hydrogen-W(100) system.

Not only is the structure of the adsorbed gas different for molybdenum and tungsten, the bonding of hydrogen is different also. The flash desorption study by Han and Schmidt [105] has shown that the adsorption of hydrogen on Mo(100) produces three atomic states with desorption energies at 16, 20, and 27 kcal/mole. On the (100) plane of tungsten, Tamm and Schmidt [106] found only two atomically bound states for hydrogen, with higher desorption energies at 26 and 32 kcal/mole. More recently the three adsorption states for hydrogen on the Mo(100) have been associated with LEED patterns by Huang and Estrup [107-109]. It seems now there is general agreement that the interaction of hydrogen with the (100) surface of molybdenum is appreciably different from that of tungsten, although the two metals are isoelectronic.

The findings on the interaction of nitrogen with the Mo(100) surface are in a more confused state. Hayek et al. [110] reported that no adsorption of nitrogen was observed on this surface and that nitrogen can only be adsorbed after it is activated into N or N^+ . The flash desorption study of Han and Schmidt [105] shows one atomic state similar to that on the W(100) surface, but more strongly bound. More recently, Huang and Estrup [107] reported two atomic nitrogen states, corresponding to (1 x 1) and C(2 x 2) LEED structures, on the (100) surface of molybdenum.

Studies of the closest packed plane, the (110), of molybdenum have not been as extensive as for the (100) plane. Mahnig and Schmidt [111] have reported adsorption states for hydrogen on the (110) surface of molybdenum similar to those on tungsten. Two atomic states, β_1 and β_2 , are identified in their flash desorption work, with desorption energies of 28 and 34 kcal/mole, respectively. The binding strength is nearly the same as on the W(110). However, the initial sticking coefficient on the (110) plane of molybdenum was found to be somewhat larger than that for tungsten. A more substantial difference was found in the adsorption of nitrogen on these planes. Mahnig and Schmidt [111] report that although the binding strength for the only atomic state of nitrogen is similar for tungsten and molybdenum, the initial sticking coefficient of nitrogen on the (110) surface is more than 20 times larger for molybdenum than for tungsten.

Dooley and Haas [65] earlier reported that no changes were observed on the LEED patterns for the (110) surface of molybdenum, as well as for tungsten, when exposed to either hydrogen or nitrogen. A field emission study of the adsorption of hydrogen on the (110) plane of molybdenum has also been reported by Chrzanowski [112]. On a thermally flashed emitter he finds an increase of the work function amounting to 0.48 eV. The general trends of the adsorption parallel his observations on the adsorption of hydrogen on the W(110). For that system he found an initial increase of the work function by 0.83 eV, followed by a drop of 1.13 eV, and a saturation value similar to the clean surface.

It is clear from the above discussion that differences in the adsorption of gases on the close packed planes of tungsten and molybdenum are not well-established. The study of adsorption on the Mo(110) is far from complete and the few reported results contradict each other. This confused state reflects an insufficient control over experimental parameters in these studies. Experiments on macroscopic samples lack unequivocal proof for the cleanliness of the surface. More seriously, these experiments are marred by the presence of defects, which cannot be removed by existing techniques, on the surface. These difficulties may be overcome readily by the field emission technique. However, proper steps for preparing and cleaning the sample must be followed in order to establish unequivocally the cleanliness and the structural perfection of the surface under study. These conditions unfortunately are not met by the only field emission study reported. It is therefore important to examine the interaction of gases with the Mo(110) surface under strictly controlled conditions.

6.2. Hydrogen on molybdenum

6.2a. Adsorption on field evaporated emitters

The adsorption of hydrogen on molybdenum was studied at 80 K on a field evaporated emitter. Following the procedures described in chapter II, a perfectly smooth (110) plane can be achieved at 80 K: this is shown by the scan diagram in Fig. 6.1. The emitter was field evaporated in vacuum to 18 kV before any experiments began, to ensure a (110) plane large enough to avoid edge effects. The effect of plane edges on the work function is < 0.06 eV, as estimated in Appendix C. For reference, a field emission pattern for molybdenum is shown in Fig. 6.2a. The general features are quite similar to those for tungsten.

The adsorption of hydrogen on both the emitter as a whole and on the (110) plane is shown in Fig. 6.3. There the work function for the total emitter and for the (110) plane are plotted as functions of exposure to hydrogen. The average work function for the total emitter is taken as 4.20 eV [113]. The clean (110) work function determined by the method described in Chap. II, without compensating for local variations of the electric field, is 5.32 eV. This is somewhat higher than the values obtained by photoemission, 4.95 ± 0.02 eV [114], and by thermionic emission, 5.0 ± 0.05 [115] and 5.10 ± 0.05 eV [116] from macroscopic samples. It is also higher than the value of 5.15 eV obtained in other field emission studies [117]. The difference is probably caused by the larger size of the (110) plane in our experiments; this lowers the electric field locally and increases the apparent work function.

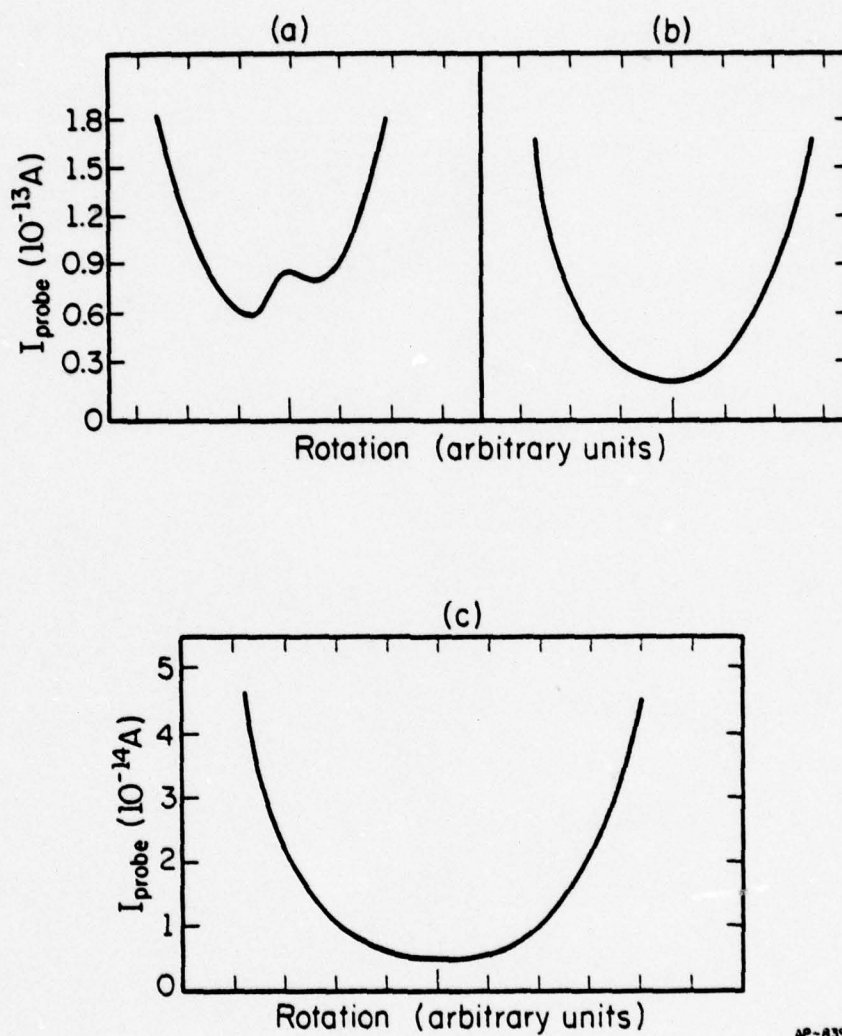
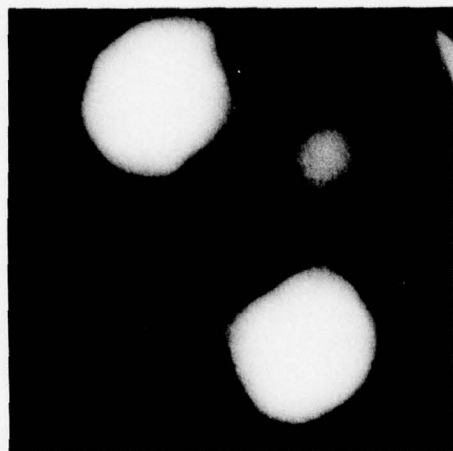
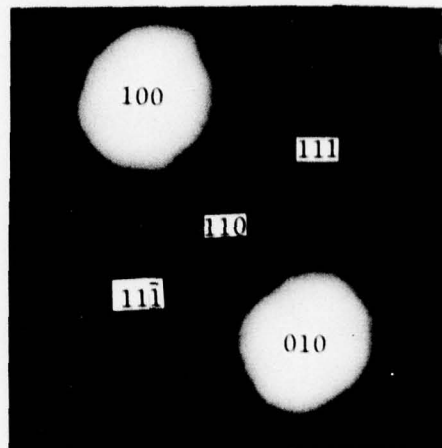


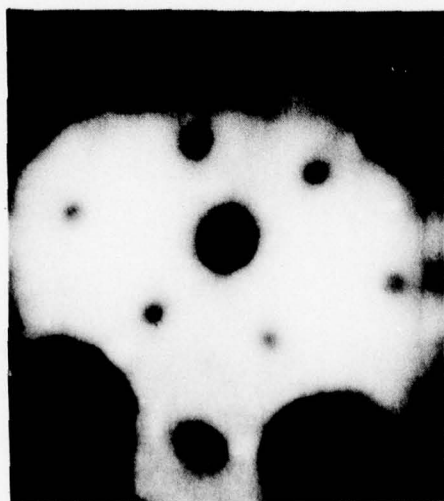
Fig. 6.1. Scan diagrams for Mo(110) planes. (a), (b) Field evaporated emitters; (c) thermally annealed emitter.



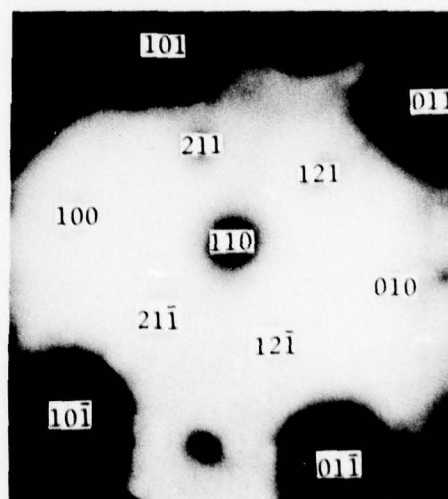
(a)



(b)



(c)



(d)

Fig. 6.2. Field emission patterns for molybdenum emitters. (a), (b) Field evaporated emitters; (c), (d) thermally annealed emitters.

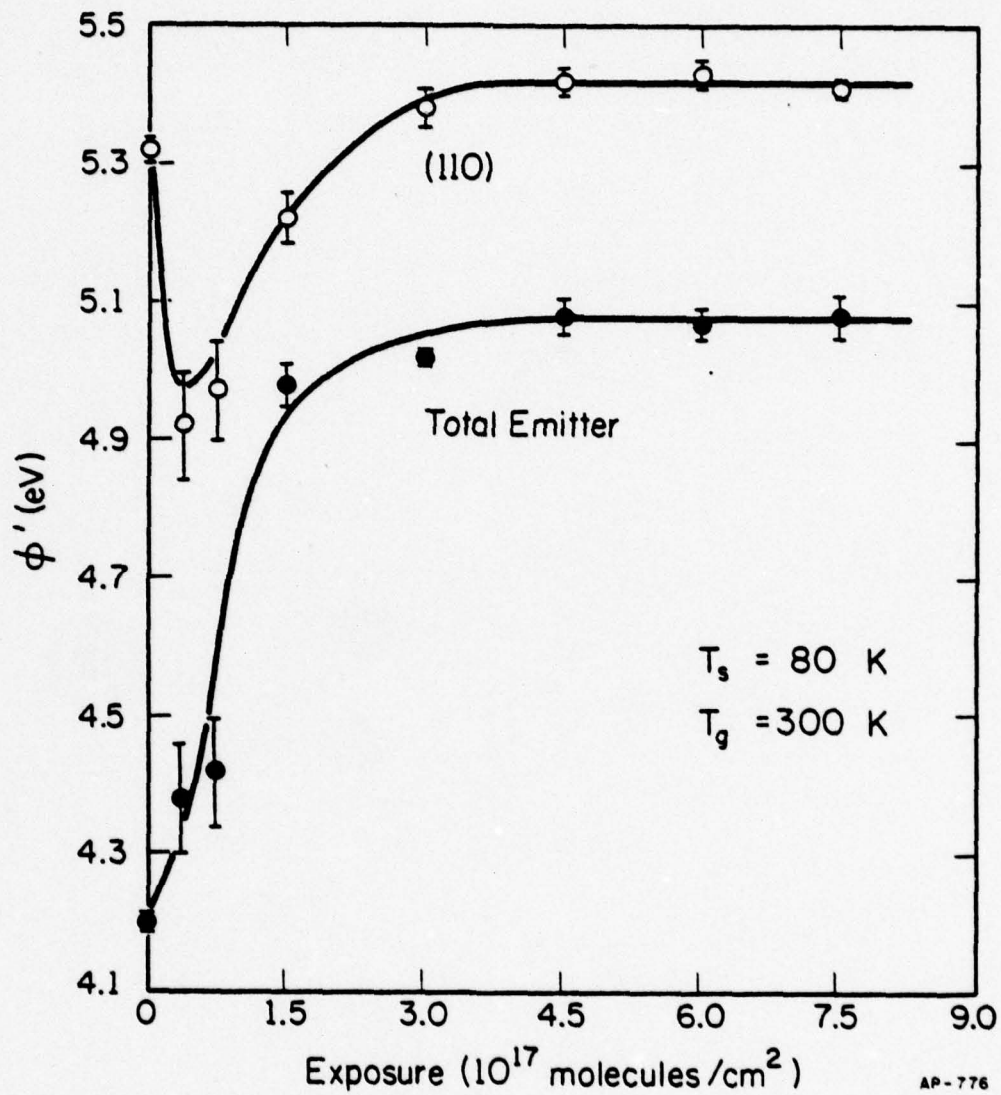


Fig. 6.3. Variation of the total emission and (110) work function with exposure to hydrogen, for a field evaporated molybdenum emitter at $T_s = 80$ K.

When the surface is at 80 K, exposing the emitter to hydrogen causes immediate adsorption on the emitter as a whole. As shown in Fig. 6.3, the work function of the emitter increases on the average by 0.88 eV to 5.08 eV, at saturation. Although not apparent from this figure, adsorption of hydrogen on the emitter as a whole results in more than one state. This is evident from Fig. 6.4, in which changes in the pre-exponential factor of the F-N curves are plotted as a function of the exposure. (The pre-exponential factor reflects changes in the surface emission properties independently of the more commonly measured work function. See Chap. II.) The pre-exponential factor for the total emitter increases continuously with exposure, and reaches a maximum of $\ln(A/A_0) \approx 2.5$ at an exposure of $\sim 1.5 \times 10^{17}$ molecules/cm². Thereafter it decreases and reaches a stable value, almost the same as that for a clean surface [$\ln(A/A_0) \sim 0$], at an exposure of $\sim 4 \times 10^{17}$ molecules/cm² -- the amount required for the work function to reach its saturation value. At exposures below 1×10^{17} molecules/cm², the total emission current is unstable and shows a strong upward drift. Good data are difficult to obtain in this range, and whether a third state exists in this early stage is not certain. The reason for the upward drift of the emission current is not known. It cannot be the continued adsorption of residual hydrogen -- the residual gas was pumped to below 5×10^{-10} Torr after each exposure before turning on the voltage. It is more likely an indication of the re-distribution of adsorbate caused by the applied electric field. Even by lowering the emission current to the minimum tolerable the drift was not significantly reduced.

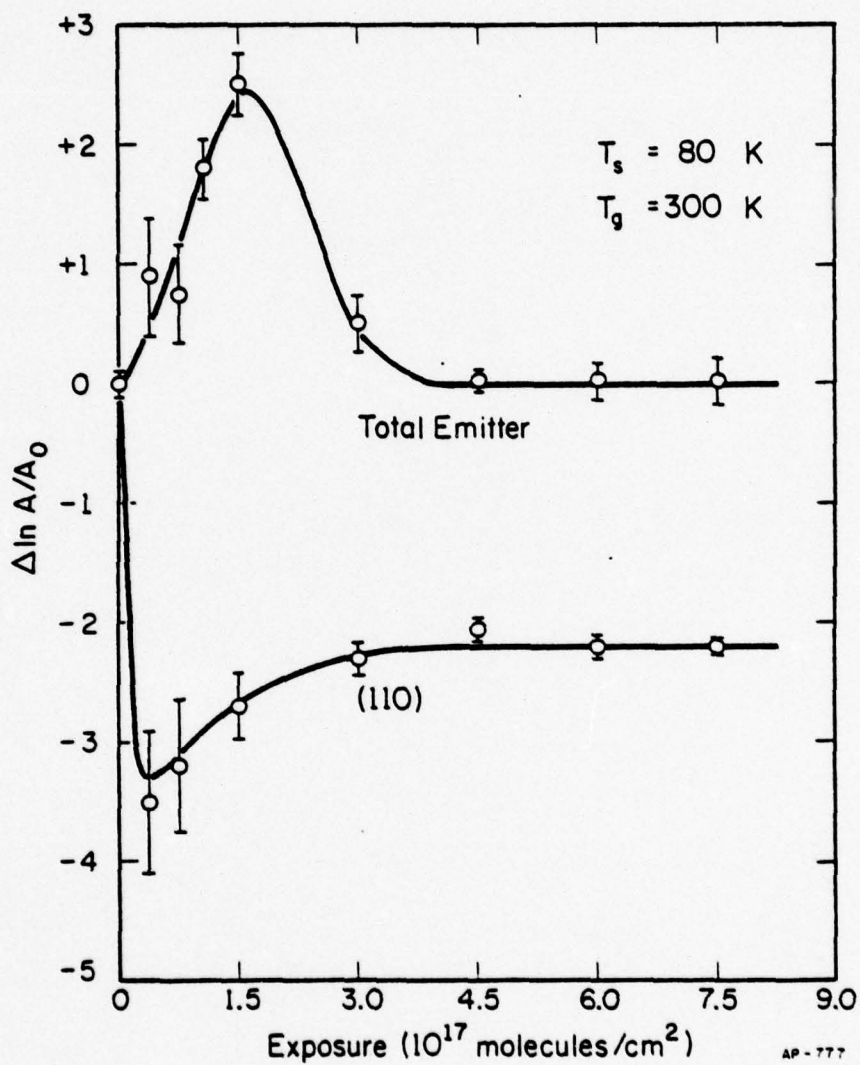


Fig. 6.4. Variation of the total emission and (110) pre-exponential factors with exposure to hydrogen for the same emitter as shown in Fig. 6.3 at $T_s = 80 \text{ K}$.

On the (110) plane, adsorption of hydrogen is also rapid. As shown in Fig. 6.3, the work function of the (110) decreases when first exposed to hydrogen, then gradually rises to 0.1 eV above the clean value. The same trend is also seen in the pre-exponential factor of the F-N curves. As shown in Fig. 6.4, the logarithm of the pre-exponential factor first decreases, and then rises to a stable value of $\ln(A/A_0) \sim -2.2$. The amount of hydrogen necessary to saturate the (110) plane is similar to the amount required to saturate the whole emitter, $\sim 3-4 \times 10^{17}$ molecules/cm². The current drift noted on the total emitter is not observed on the (110) plane. The voltage drop across the electrometer input resistor, however, cannot be properly compensated due to the drifting of the total emission current [118]. Large errors are therefore inherent in the (110) work function for exposures less than 1×10^{17} molecules/cm². At hydrogen exposure of 1.5×10^{17} molecules/cm², the total emission current becomes stable and the (110) work function is 0.1 eV below the clean value; at 5×10^{16} molecules/cm² exposure, the (110) work function is $\sim 0.3 \pm 0.1$ eV below the value for a clean surface.

The most striking feature of hydrogen adsorption on the Mo(110) plane is its speed. No induction period similar to that in the hydrogen-W(110) system is observed. The rate of adsorption of hydrogen on the (110) plane of molybdenum is completely different from that of tungsten, although these metals are isoelectronic. This difference is not caused by defects -- the perfection of the (110) plane of molybdenum in this study is documented, as well as that of tungsten. We must therefore conclude that the difference in the chemical nature of molybdenum and tungsten plays a significant part in chemisorption.

6.2b. Adsorption on thermally annealed emitters

A field emission pattern from a thermally cleaned emitter is shown in Fig. 6.2c. Although the emitter was fabricated from a high purity, zone-refined molybdenum wire (chemical analysis is shown in Table 6, Chap. II), heating in vacuum alone does not appear sufficient to remove surface impurities. Even after the wire is heated above 2500 C, until the tungsten support loop starts to evaporate, the bright spots at the vicinals of the (211) planes still persist, as is evident from Fig. 6.2b. No effort was attempted to further clean the surface by heat treating in oxygen or hydrogen. It must therefore be emphasized that adsorption experiments on thermal emitters were performed under less than perfect conditions.

The smoothness of the (110) plane on a thermally annealed emitter is confirmed by the scanning technique. A scan diagram is shown in Fig. 6.1c. The work function for the (110) plane obtained by comparing slopes of the F-N plots for the (110) with that for the total emitter is 5.4 eV -- higher than for the field evaporated (110). This is expected, since the (110) plane of a thermally cleaned emitter is considerably larger than that of a field evaporated emitter, resulting in a more significant diminution of the field at the center. The work function for the emitter as a whole again increases when exposed to hydrogen. However, the exact values are not known, since the total emission current was plagued by leakage through tungsten films evaporated on the glass insulators during prolonged attempts to clean the surface. Corrections for the systematic errors thus incurred are difficult, and these results are therefore not reported. The work functions of the (110) plane are not seriously affected, since the collector current is not affected by leakage [119].

The adsorption of hydrogen on the Mo(110) at 80 K, as compared to the adsorption on a field evaporated emitter, is plotted in Fig. 6.5. Qualitatively the interaction of hydrogen with a thermally cleaned Mo(110) surface is similar to that with the field evaporated emitters. The work function first decreases by 0.17 eV, then rises again to almost the same value for a clean surface. However, the rate of adsorption on the thermal (110) plane is much lower than that on a field evaporated surface. While the minimum of the work function is reached for a field evaporated emitter at an exposure of 5×10^{16} molecules/cm², very little change is observed at this exposure on the thermal emitter. The lowest work function for a thermal emitter is reached at an exposure of 3×10^{17} molecules/cm², six times more than the amount for the minimum on a field evaporated (110) surface. The amount necessary to reach saturation is also higher, but this effect is less pronounced: 4.5×10^{17} molecules/cm² are required on the thermally prepared surface as compared to $3-4 \times 10^{17}$ molecules/cm² for the field evaporated (110).

The general features of hydrogen adsorption on the annealed (110) surface of molybdenum coincide with those found on the field evaporated emitters. The reason for the quantitative differences is not clear. The larger (110) plane for the annealed samples may be responsible in part. However, the lack of unequivocal proof for the cleanliness of the annealed surfaces imposes serious obstacles to a more detailed explanation.

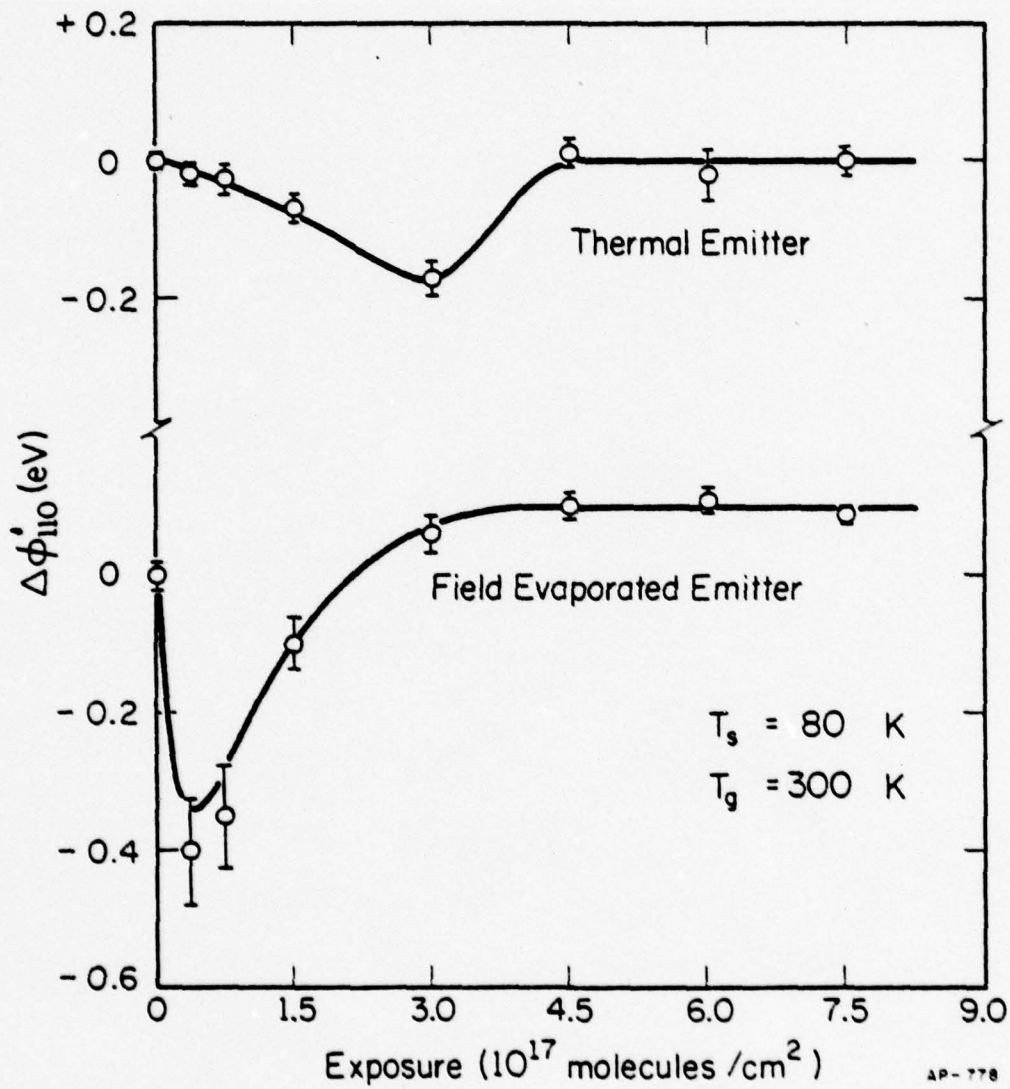


Fig. 6.5. Changes in the total emission and (110) work functions with exposure to hydrogen for a thermally annealed molybdenum emitter at $T_s = 80$ K.

6.2c. Discussion

Our results are consistent with most of the earlier observations on polycrystalline and on single crystal molybdenum surfaces. On polycrystalline molybdenum, Manukova [120], using molecular beam and isotope exchange techniques, found that two hydrogen states, one atomic and one molecular, exist simultaneously between 77 and 100 K. Abon and Teichner [121], using field emission microscopy and thermally annealed emitters, reported work function changes of 0.6 eV initially and 1.2 eV at larger dosage. Chrzanowski [112] using the same technique, reported a work function change of +0.72 eV. He also reported 3 adsorption states as distinguished by the changes in the work function. In our experiments only two states, distinguished mainly by the change in the pre-exponential factor of the F-N curves, are observed. Detection of a possible third state at lower exposure is made difficult by the instability in the emission current. However, the direction and magnitude of the work function changes are roughly comparable.

We don't have the means to measure the sticking coefficient precisely. From the amount of gas required to induce changes on the surface, we can deduce that the rate of sticking on the total emitter is roughly similar to that of tungsten, probably on the order of 0.2. This is somewhat lower than the value obtained by Hayward et al. [122,123] ~ 0.7 for molybdenum films. For the average behavior of all planes, there seems a general agreement that hydrogen adsorbs rapidly on molybdenum and forms more than one state, causing rather large changes in the work function.

On the (110) plane, Mahnig and Schmidt [111] observed two atomic and one molecular states at 80 K. Since no work function was measured in their experiments, the direction of charge transfer in each state is not known. However, the amount of molecular hydrogen in their desorption spectra is rather small ($< 20\%$), and none appears at low coverages. Judging from this, adsorption at 80 K should be primarily in the atomic form, at least initially. The initial decrease in the work function in our experiments therefore should be attributed to the adsorption of atomic hydrogen. The later rise of the work function must also be caused by an atomic state, since warming up to 300 K did not depopulate it appreciably. However, warming up to 300 K appears to cause some rearrangement on the rest of the emitter. This is indicated by an increase of the total emission current by $\sim 40\%$ and by changes in the emission pattern. This is consistent with the observations by Pasternak and Wiesendanger [124]. They have deduced a high mobility of the adsorbed hydrogen between 225 and 410 K from their flash desorption work.

Chrzanowski [112], using field emission, reported an increase of 0.48 eV in the (110) work function at 300 K. This is quite different from the values we observed at 80 K. The conflicting results could be a reflection of the differences in sample preparation. In his experiments, the samples are cleaned by flashing twice to 2200 K for 3 seconds each [125]. From our experience this is not sufficient to really clean the surface. As we have pointed out earlier, heating above 2500 C in vacuum cannot remove some bright spots from the emission pattern. This is evident from Fig. 6.2b, as well as from the field emission pictures shown by Abon and Teichner [121],

and by Oguri and Kanomata [125], all prepared by similar techniques. By heat treating the emitter in 2×10^{-7} Torr of oxygen at 1500 K for 2 hours, followed by heating to 1800 K at ambient pressure in the order of 10^{-9} Torr, Bergeret et al. [127] were able to obtain a much smoother emission pattern. Macroscopic samples prepared following these similar procedures were earlier shown to yield a surface no detectable impurities under Auger spectroscopy [102,128] Bergeret et al., however, only studied the interaction with residual gases (H_2 and CO).

The most interesting feature in the adsorption of hydrogen on the Mo(110) plane is the absence of an induction period as compared to the W(110) plane. Contrary to the very low sticking coefficient ($< 7 \times 10^{-5}$) observed by Polizzotti [3] for hydrogen on the (110) plane of tungsten, the rate of adsorption on the (110) plane of molybdenum is roughly comparable to that on the emitter as a whole. In the flash desorption work by Mahnig and Schmidt [111] a higher sticking coefficient is already observed for the Mo(110) (0.1) than for the W(110) (~ 0.07). The latter value, measured by Tamm and Schmidt [69], is likely to be too large, as the contribution from defects on their crystals was not eliminated. Considering this, the results from desorption work should indicate a much faster rate on Mo(110) than on W(110). This is consistent, at least qualitatively, with our results. The difference in rates is much more pronounced in our experiments, since the results are not affected by defects on the surface.

Apart from the rate of adsorption, the charge transfer on the (110) of molybdenum is also different from that of tungsten. Although the initial decrease of the work function has the same direction and comparable magnitude as that for tungsten, the subsequent increase in the work function is not observed on the W(110). In flash desorption studies [111] two states of equal population have been observed on the (110) surfaces of both molybdenum and tungsten. Since no desorption occurred on Mo(110) when heated to 300 K, both changes in the work function seem caused by atomic hydrogen. The later increase in the work function can be explained either by interactions between the adsorbates, or by sequential filling of the two states. Neither has been examined on the (110) plane of tungsten. It would be very interesting to see if the structure of the adsorbate on the (110) surface of molybdenum is different from that of tungsten. Unfortunately the LEED study by Dooley and Haas [65] failed to reveal the presence of hydrogen and nitrogen on the (110) plane of either molybdenum or tungsten.

A rather pronounced structural effect was reported by Chappell and Hayward [129] using molecular beam techniques. At 300 K they found that hydrogen reflected from the (100) and (111) plane of molybdenum had essentially a cosine distribution in angle, while that from the (110) plane reflected largely at the specular angles. This lack of diffuse scattering from the (110) plane was explained as an indication that thermal accommodation for hydrogen does not occur on this plane. This

explanation is not unequivocal; the lack of diffuse scattering from the (110) might reflect only that hydrogen adsorbed on this surface does not interact strongly with the incoming particles. It is clear, however, that the closest packed plane of molybdenum does show some unusual features in chemisorption, even though the rate of adsorption is comparable to that on other surfaces.

On molybdenum surfaces there is no strong indication in our experiments of any structural dependence of chemisorption, except that the direction of charge transfer on the (110) plane is different from the rest of the emitter. Compared to the close packed plane of tungsten, hydrogen chemisorbed at a rate at least two orders of magnitude faster on the Mo(110) plane. In our experiments surfaces are well characterized and surface perfection is unequivocally established. On these smooth surfaces no surface defects are present to distort experimental results. It is clear from our results that the electronic structure of the substrate does indeed profoundly affect the chemical reactions on the surface.

6.3. Nitrogen on molybdenum

6.3a. Adsorption on field evaporated emitters

The interaction of nitrogen with field evaporated molybdenum surfaces has been studied at 80, 150, and 200 K. At 80 K, nitrogen adsorbs rapidly on both the emitter as a whole and on the (110) plane, as is evident from Fig. 6.6. The work function of the emitter as a whole is raised by 0.3 eV and the work function of the (110) plane is raised by 0.12 eV. On warming

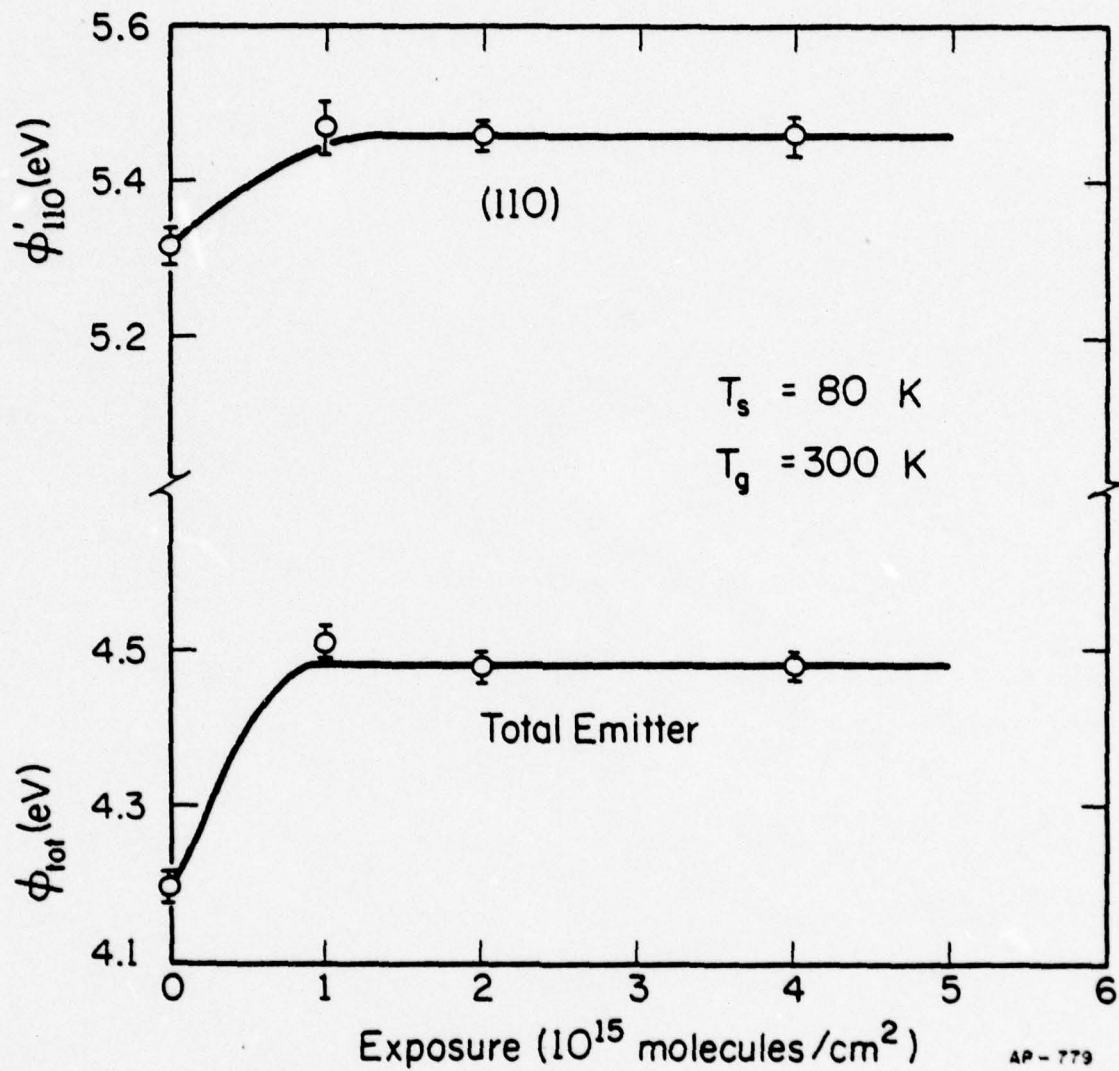


Fig. 6.6. Changes in the total emission and (110) work function with exposure to nitrogen for a field evaporated molybdenum emitter at $T_s = 80$ K.

up to 200 K in vacuum the work function of the (110) plane is further increased by 0.1 eV, but the work function for the total emitter is decreased by 0.1 eV, conforming to the values obtained on exposure to nitrogen at 200 K (Fig. 6.7). The nitrogen adsorbed at 80 K is therefore probably molecular, similar to the γ -nitrogen formed on the tungsten surface at low temperature.

Judging from the amount of gas necessary to saturate the surface, the initial sticking coefficient is high for both the emitter as a whole and the (110) plane, probably approaching unity. This is consistent with the results of King and Tompkins [130]. On a polycrystalline molybdenum film they reported an initial sticking coefficient of 0.9 at 78 K.

At 200 K, nitrogen also adsorbs rapidly on both the emitter as a whole and on the (110) plane, as is evident from Fig. 6.7. The work function of the (110) plane is raised by 0.23 eV, and that for the emitter as a whole by 0.24 eV. The increase in the work function of the (110) when exposed to nitrogen cannot be attributed to the plane edges. The emitters have been cleaned by field evaporation to higher than 20 kV in these experiments, and the contributions from plane edges should be < 0.06 eV (Appendix C). This is also supported by results from thermally cleaned emitters, for which an increase in the (110) work function is also observed, although the size of the plane is much larger. The sticking coefficient, as roughly estimated from the total amount of gas necessary to bring about changes on the surface, is rather high, 0.2-0.5 for both the (110) plane and the whole emitter. This is also in reasonable accord with the value of 0.75 reported by King and Tompkins [130] for polycrystalline films at 300 K.

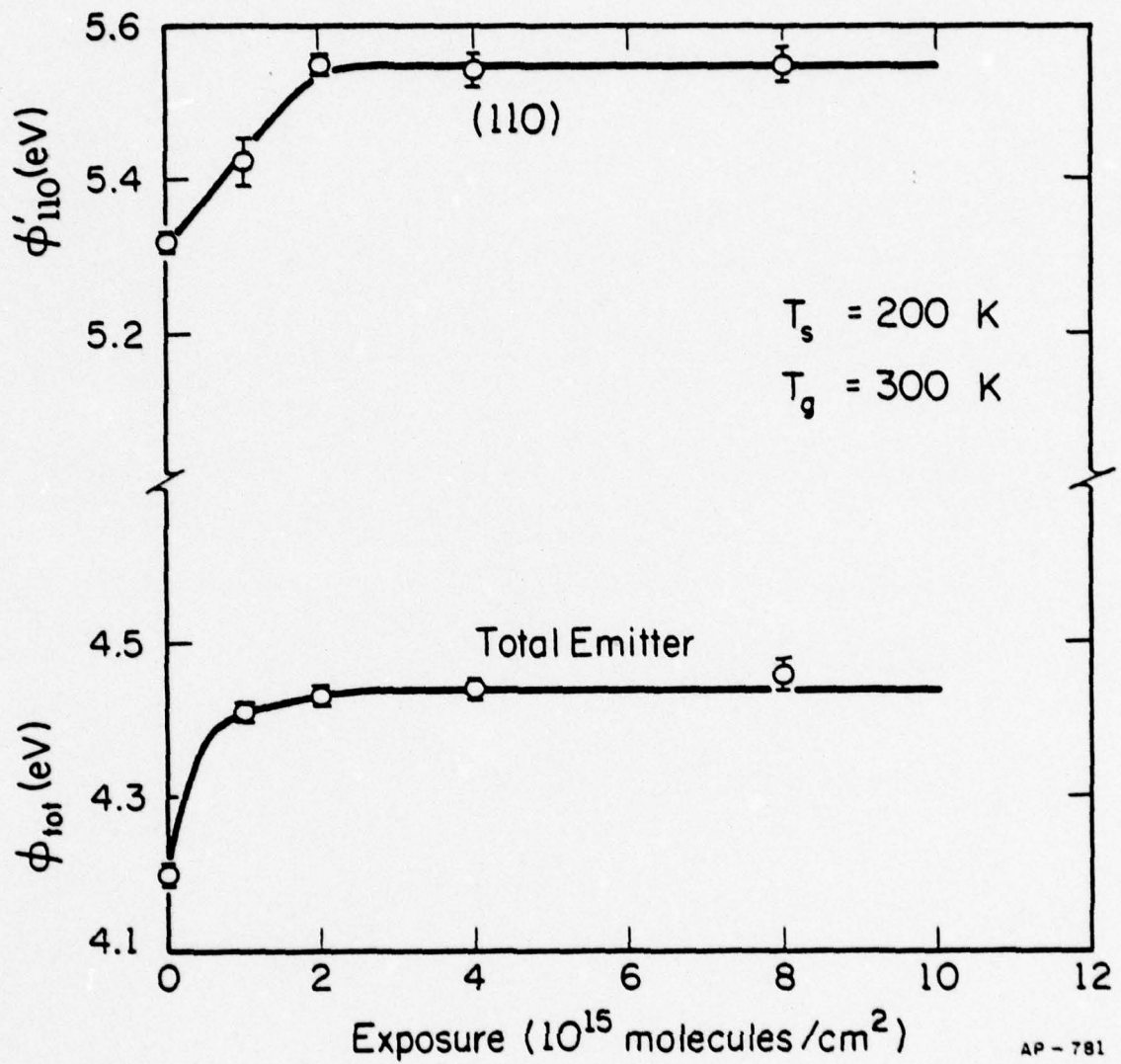


Fig. 6.7. Variation of the total emission and (110) work function with exposure to nitrogen for a field evaporated molybdenum emitter at $T_s = 200 \text{ K}$.

The adsorption of nitrogen on molybdenum at 150 K is more complicated. The adsorption on the emitter as a whole is rapid, as is evident from Fig. 6.8. The rate is comparable to that at 80 K as well as at 200 K. The work function is increased by 0.18 eV, halfway between the increase at 80 and at 200 K. On the (110) plane, the work function gradually rises to ~ 0.2 eV above the clean value. The amount of nitrogen necessary to reach saturation is approximately twice that needed at 200 K. This could be a reflection of the competition between β - and γ -nitrogen. On the (110) plane, the sticking coefficient of γ -nitrogen is about twice that for β -nitrogen (Figs. 6.6, 6.7). The surface is therefore initially covered mostly by γ -nitrogen. Since γ -nitrogen is unstable on the surface above 200 K [120], it cannot be very stable at 150 K. Replacing γ -nitrogen by β -nitrogen should then take place when the surface is further exposed to gas. For the rest of the emitter the sticking coefficients for β - and γ -nitrogen are comparable, and β -nitrogen can adsorb on the surface in an amount comparable to that of γ -nitrogen. This amount of β -nitrogen is probably enough to saturate the molybdenum surface if the saturation coverage on molybdenum [131] is similar to tungsten, for which only about 1/2 of the sites are filled [50]. The dependence of the rate of adsorption on temperature therefore can reasonably be accounted for by the competition between the formation of β - and γ -nitrogen. It is clear from these experiments on field evaporated emitters that the adsorption of nitrogen on the (110) surface of molybdenum is rapid at temperatures between 80 and 200 K.

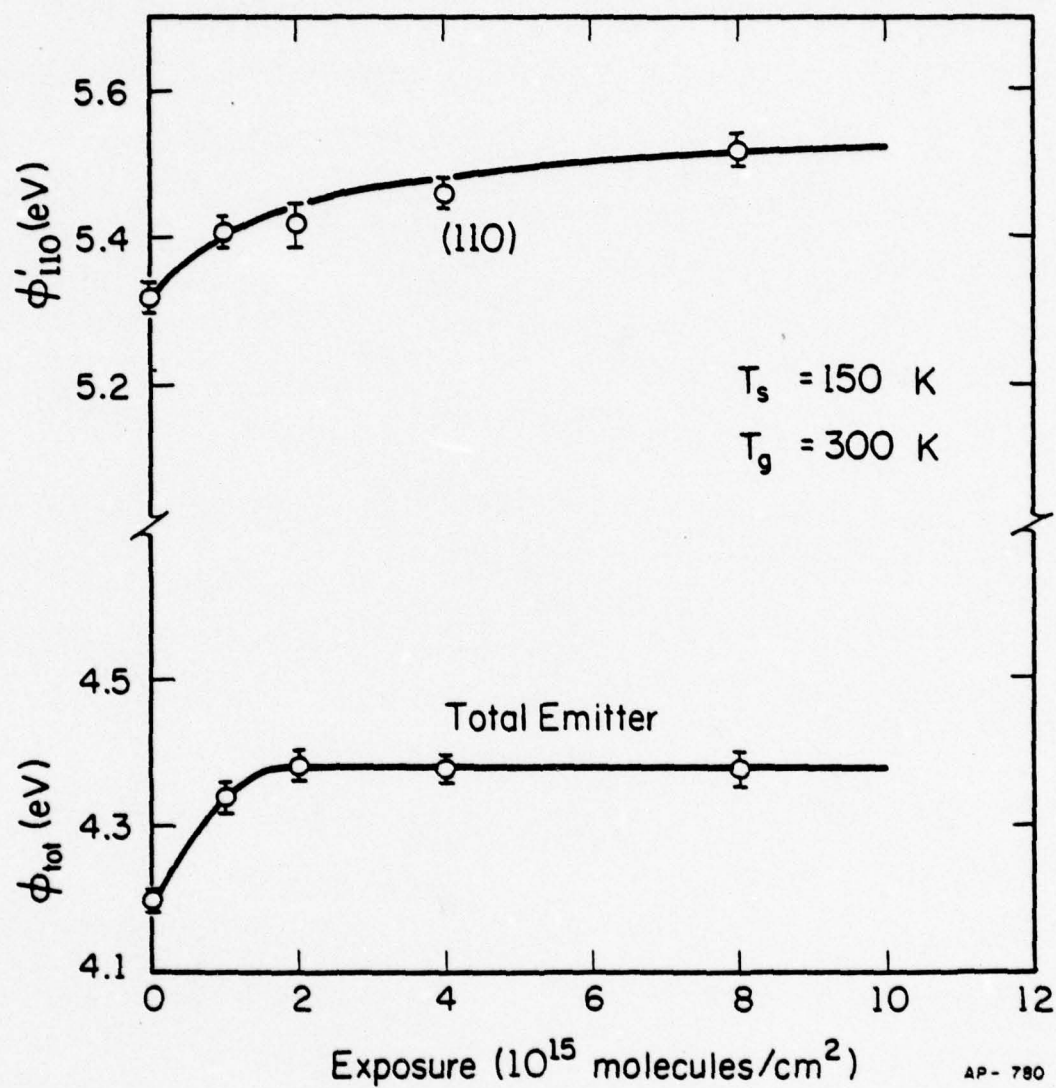


Fig. 6.8. Variation of the total emission and (110) work function with exposure to nitrogen for a field evaporated molybdenum emitter at $T_s = 150$ K.

6.3b. Adsorption on thermally annealed emitters

There are two reasons why the interaction of nitrogen with molybdenum was studied using thermally prepared emitters. The interaction at room temperature and above is of interest, and this cannot be safely done on a field evaporated emitter without risking the possibility of contamination. The other reason was to study the desorption temperature for the adsorbed species. However, we must remain alert to the possibility that the emitter obtained by heating alone may not be unequivocally cleaned, as is evident from the bright spots near the (211) planes (Fig. 6.2c).

The adsorption of nitrogen at 300 K is shown in Fig. 6.9. It is evident from this figure that the adsorption is somewhat slower than on a field evaporated emitter at 200 K. The difference in the rate of chemisorption could be attributed partly to the difference in substrate temperatures [124]. It may also be a reflection of the degree of cleanliness of the two samples. The changes in the work function are in the same direction, but the magnitudes are different. For the emitter as a whole, the work function is increased by 0.12 eV, compared to the 0.24 eV for a field evaporated emitter; on the (110) plane, the work function is increased by 0.15 eV compared to 0.23 eV on the field evaporated sample.

The change of work function over the whole emitter does not coincide with the values reported by other workers. The field emission study by Oguri and Kanomata [126] gave a 0.21 eV decrease in the work function for the whole emitter. Abon and Teichner [121] reported an initial decrease by 0.3 eV and a saturation value of 0.7 eV above the clean value. The discrepancies are probably caused by differences in the substrate conditions. The experiments were all done on surfaces cleaned by heating and the surface impurity concentrations are not known.

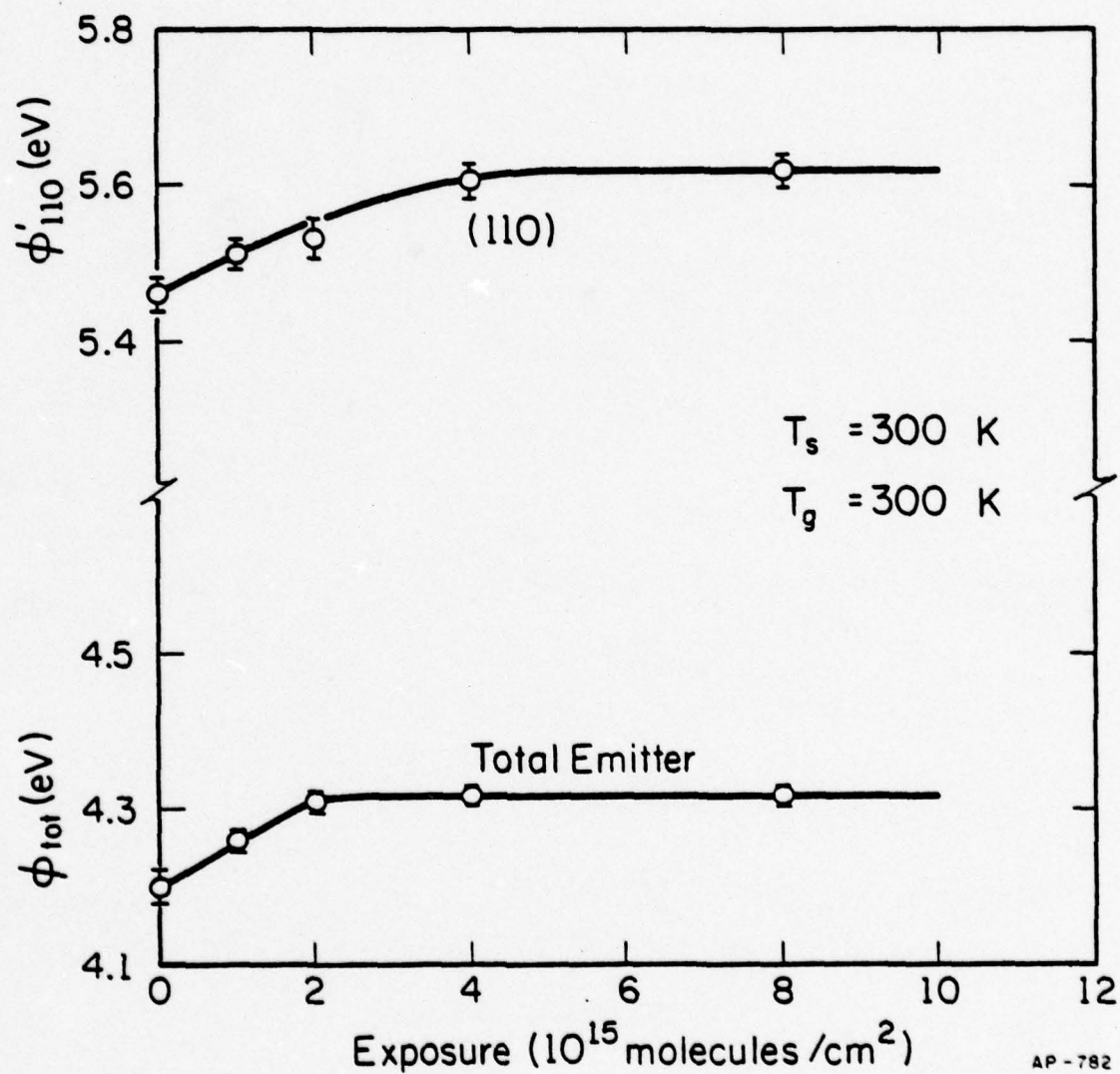


Fig. 6.9. Changes in the total emission and (110) work function with exposure to nitrogen for a thermally annealed molybdenum emitter at $T_s = 300$ K.

To compare the behavior of molybdenum with the nitrogen-W(110) system we also conducted experiments with the surface held at 550 K. As is evident from Fig. 6.10, adsorption at 550 K is not different from that at 300 K. The rate of adsorption on the (110) plane and on the emitter as a whole is about the same as that at 300 K. The changes in work functions are also comparable: +0.15 eV for the (110) plane and +0.09 eV for the emitter as a whole. Contrary to the nitrogen-W(110) system, no temperature dependence of the adsorption is observed.

Desorption of the nitrogen adsorbed at 300 K does not occur until the tungsten support loop is heated to red hot. The temperature as measured by a pyrometer is ~ 1300 - 1500 K. Both the (110) and the emitter as a whole desorb at about the same temperature. The desorption temperature is comparable to that reported by Mahnig and Schmidt [111] and by Abon and Teichner [121]; it is slightly higher than that found by Oguri and Kanomata [126].

6.3c. Discussion

The binding states of nitrogen on molybdenum surfaces are parallel to those on tungsten as observed by flash desorption. The isotope exchange study by Manukova [120] has confirmed that only one state of atomic nitrogen exists above 200 K and that one atomic and one molecular nitrogen state exist between 77 and 200 K for polycrystalline molybdenum. Similar results are reported by flash desorption studies [105,111]. In our experiments these states are also obvious. The bonding strengths of β - and γ -nitrogen are similar to those on tungsten. This is indicated by the desorption temperatures reported in references 111, 121, 124 as well as from our own observations.

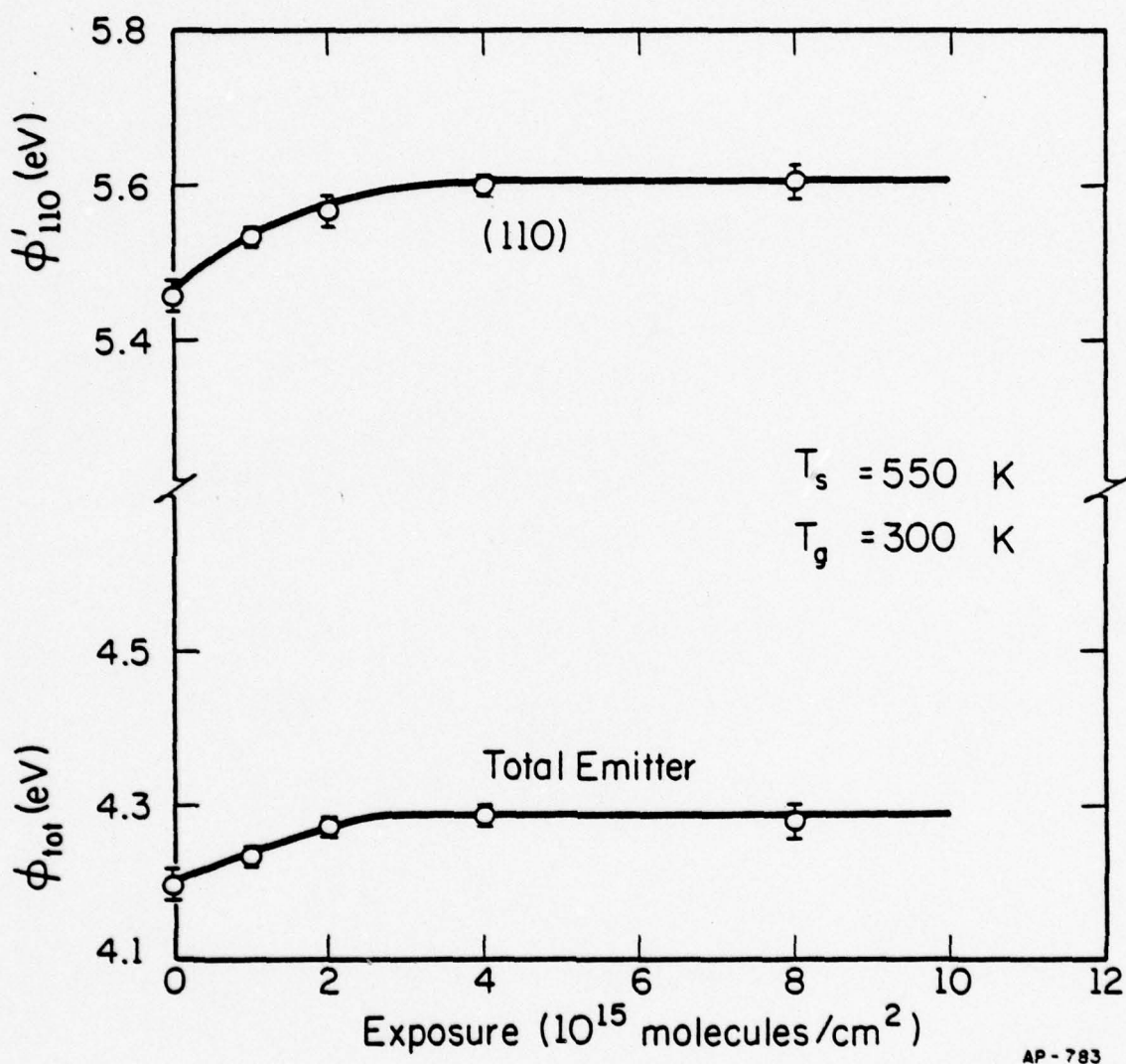


Fig. 6.10. Changes in the total emission and (110) work function with exposure to nitrogen for a thermally annealed molybdenum emitter at $T_s = 550$ K.

The amount of charge transfer during the adsorption of nitrogen on molybdenum reported by different authors is not in good agreement, probably caused by differences in substrate conditions. From our experiments on emitters cleaned by field evaporation it appears that the direction of charge transfer for molybdenum is opposite to that for tungsten, on the emitter as a whole. On the (110) plane, the direction of charge transfer for molybdenum is the same as for tungsten, but the magnitude is different. The change in the work function is 0.23 eV for Mo(110) compared to <0.07 eV for W(110). Hayek et al. [110] reported that nitrogen can interact with the (001) and (110) planes of molybdenum only when activated in N or N^+ . On the (110) plane they found an increase of work function by 0.5 eV. This value is higher than ours. Whether the difference is caused by a new adsorption state, by larger surface concentrations achieved this way, or by differences in surface conditions is not clear.

The rate of adsorption on the molybdenum emitter as a whole is not much different from that on tungsten, both having sticking coefficients on the order of 0.5. More interesting is the much higher rate of adsorption on Mo(110) than on W(110). The rate of adsorption for β -nitrogen is about two order of magnitude higher than that on the (110) plane of tungsten. This difference in rate cannot be attributed to differences in surface conditions in these experiments -- the cleanliness, as well as the perfection, of the (110) plane has been unequivocally established. Just as for hydrogen, the general adsorption behavior of

nitrogen on the (110) plane of molybdenum bears some similarity to that on tungsten. Also like hydrogen, the rate of adsorption for nitrogen on the (110) plane of molybdenum is strikingly different from that on tungsten. From these experiments on perfect planes the importance of the chemical nature of the substrate during chemisorption is quite clear.

CHAPTER VII

THE ROLE OF STRUCTURAL DEFECTS IN CHEMISORPTION

We have seen earlier in Chaps. III and V that densely packed planes of tungsten and rhenium do not dissociatively chemisorb hydrogen and nitrogen effectively; adsorption on these planes appears to be brought about more effectively by the migration of gases dissociated on rougher surfaces. From our experiments it is clear that the stepped areas surrounding the central flat are important for chemisorption on the smooth planes. It is still desirable, however, to observe the effect of defects directly and quantitatively. It is to this goal the present chapter is directed.

Attempts have recently been made to examine the role of defects in chemisorption processes on macroscopic crystals cut in such a way as to expose a sequence of lattice steps [4,6]. Such studies are always open to some doubt, as even the most carefully prepared macroscopic surfaces are marred by steps, dislocations, and other point imperfections. Field emission microscopy, combined with the powerful technique of field evaporation, provides a much better approach to the problem. The microscopic field emitter constitutes a highly perfect crystal specimen with many crystallographic faces exposed. In addition, the degree of perfection of each crystal plane is controllable on the atomic scale. As has been illustrated in Figs. 2.9 and 2.13, we can create through field evaporation a small island in the center of an otherwise perfect plane. By studying the interaction of gas with this surface we should be able to reveal directly the effects of surface imperfections on chemisorption.

Our efforts will be restricted to the interaction of hydrogen with the W(110) surface. This system has shown very low reactivity; the effect of defects should therefore appear more clearly.

7.1. Surface topography

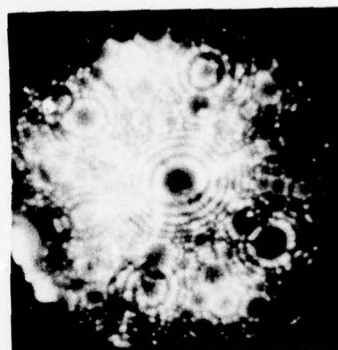
The surface topography of a W(110) plane can be controlled by field evaporation much the same way as that for the Re(0001) plane (Fig. 2.9). This is clear from Fig. 7.1, which shows a sequence of field ion micrographs for the W(110) plane [132]. From these micrographs we see that by controlled field evaporation at low temperature ($< 80\text{K}$), both perfect (110) planes and clusters of various sizes on the (110) plane can be achieved. The ability to create clusters of different sizes is a basic requirement for the direct observation of the effects of surface defects on chemisorption.

7.1a. Determination of surface structures

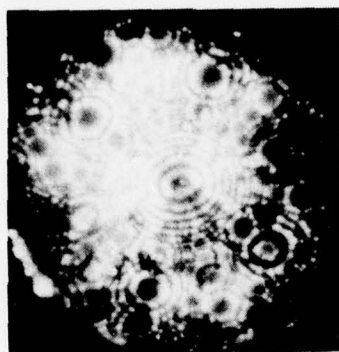
In real adsorption experiments, the surface topography has to be determined by field emission. This is done by the scanning technique described in Chap. II. The sensitivity of this technique increases with the plane size: for smaller emitters less detail can be seen on the (110) plane; for emitters blunted by stripping in vacuum to $< 20\text{ kV}$ (corresponding to a flat (110) plane of diameter $< 60\text{ \AA}$) surface features in the (110) plane can be resolved quite clearly. This is illustrated by the field evaporation of a (110) plane at 27.6 kV , as shown in Fig. 7.2. At 80 K , a smooth (110) plane gives a scan diagram with one single minimum in the probe-hole currents corresponding to the geometrical



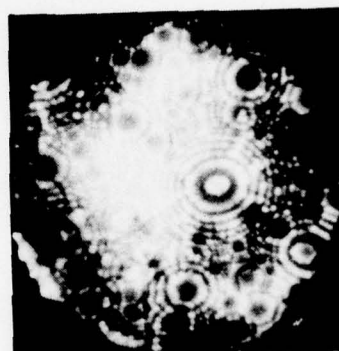
(a)



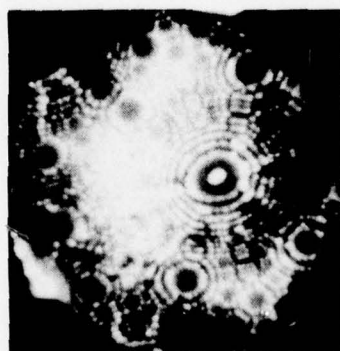
(b)



(c)

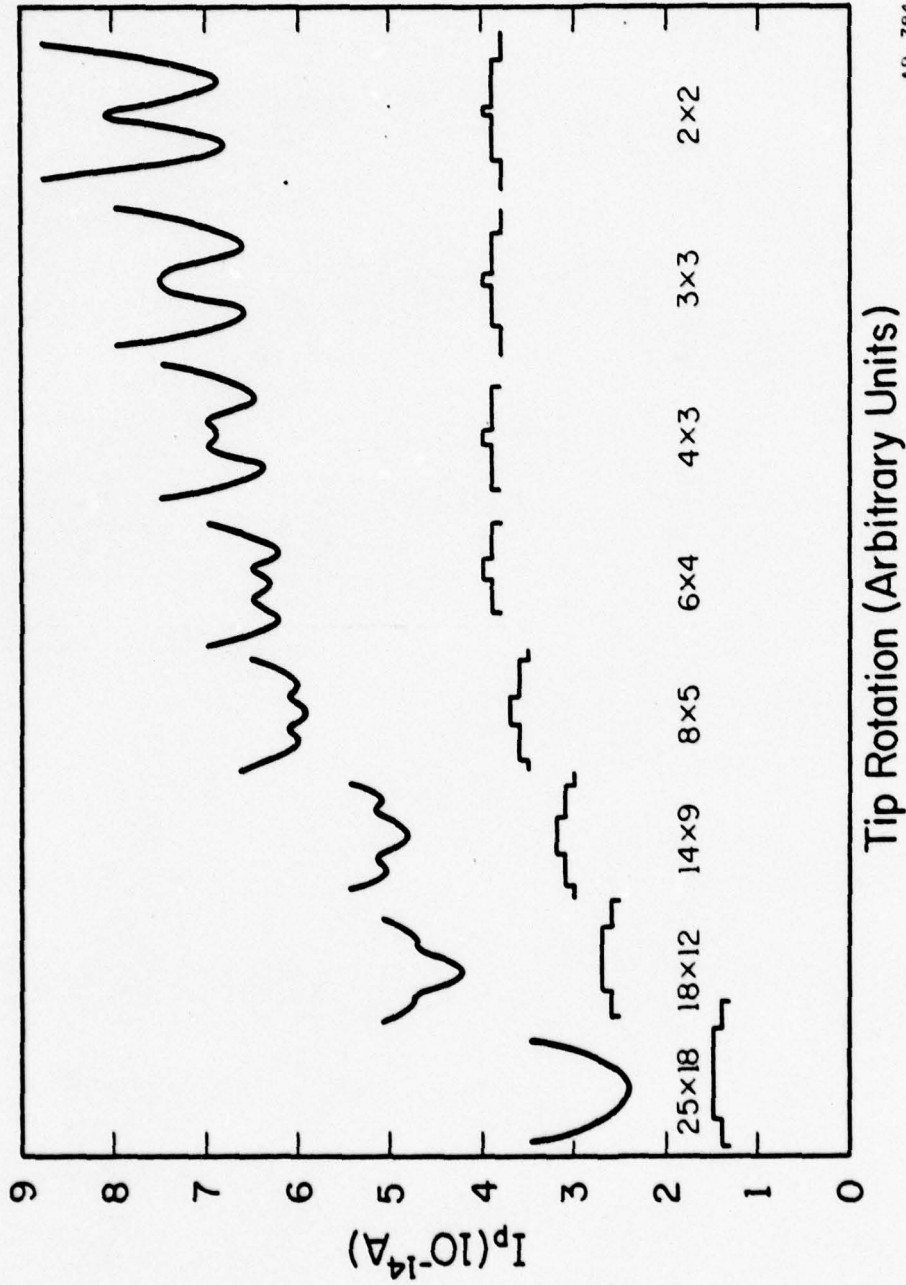


(d)



(e)

Fig. 7.1. Field ion micrographs of a (110)-oriented tungsten emitter at various stages of field evaporation. (a) Large (110) plane; (b), (c) plane shrinks when field evaporation proceeds; (d), (e) atom clusters on the (110) plane. (From Reference 132.)



AP-784

Fig. 7.2. Scan diagrams for W(110) planes on an emitter field evaporated to 27.6 kV at $T_s = 80 \text{ K}$. After each scan diagram is recorded, the evaporation voltage is applied to the emitter to strip off more atoms. The last scan diagram shown here is obtained from a separate experiment.

center of the emission pattern. From the relation between the (110) plane size and field evaporation voltages worked out by Polizzotti [3] the diameter of this plane can be estimated at $\sim 80 \text{ \AA}$. (Also discussed in Appendix C.) This corresponds roughly to a (110) plane with ~ 25 atoms across the [111] zone and ~ 18 atoms across the [100] zone, as the (110) plane is usually elliptical (Fig. 7.1).

A different evaporation procedure than that described in Chap. II is employed here to obtain the scan diagrams shown in Fig. 7.2. Instead of stripping to a pre-determined voltage for a long time (e.g. 5 minutes) to let the surface reach its equilibrium endform, we stripped the emitter under non-equilibrium conditions. In this process the emitter is repeatedly stripped at a fixed voltage for short periods of time (1-10 seconds). During the whole stripping procedure the emitter never reaches its equilibrium endform. This results in the removal of a small amount of material from the emitter surface every time the voltage is raised, giving a much better control over the surface topography than the method described in Chap. II.

After a smooth (110) plane is obtained, raising the voltage to the same value again produces a scan diagram similar to the first diagram in Fig. 7.2, but with a higher probe hole current (not shown in Fig. 7.2). This indicates that the (110) plane has been stripped and has become smaller in size, but is not small enough to produce significant changes in the shape of the scan diagram. Repeating this stripping procedure

two or three times results in the second scan diagram shown in Fig. 7.2. Raising the voltage to the same fixed value again we get the third scan diagram. It is obvious from changes shown in the scan diagrams that each application of the voltage result in the removal of some atoms from the (110) plane.

As the plane gets smaller, the rate of evaporation becomes higher when the same voltage is applied. The time period of evaporation therefore should be decreased as the plane becomes smaller. The fourth and fifth scan diagrams in Fig. 7.2 were obtained in this way. To create even smaller clusters, not only must the time for evaporation be short, the voltage applied to the emitter must also be decreased. The last three scan diagrams in Fig. 7.2 can only be obtained in this way. For these smaller clusters on the (110) plane, evaporation is fast, since the local electric field is stronger. Care must be exercised not to evaporate all the atoms in the cluster at once.

The shape of the last scan diagram in Fig. 7.2 happens to be the same as that obtained after field evaporation at 300 K and allowing enough time for the equilibrium endform. In a separate field ion microscope a cluster thus obtained is recognized as consisting of only 2 to 4 atoms [133]. This defines the smallest cluster obtainable by our technique.

The scan diagrams shown in Fig. 7.2 can be simulated quite successfully by considering electron emission from different areas of the (110) region. The details of this simulation are shown in Appendix B, and typical simulated scan diagrams are shown in Fig. 2.13. As is evident from that figure, essentially all features apparent in the scan diagrams

in Fig. 7.2 can be simulated. It is also clear from this that the satellites in the scan diagrams are caused by emission from plane edges, since varying the strength of emission from edges (by changing the work function, electric field, etc.) changes the intensity of these satellites accordingly. Qualitatively at least, the simulation describes emission for different surface topographies satisfactorily.

7.1b. Estimating the cluster size

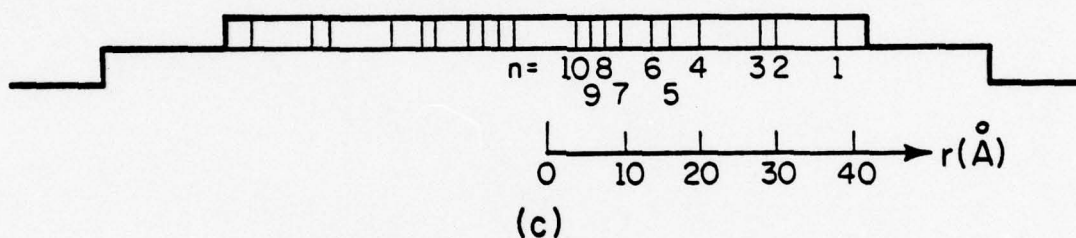
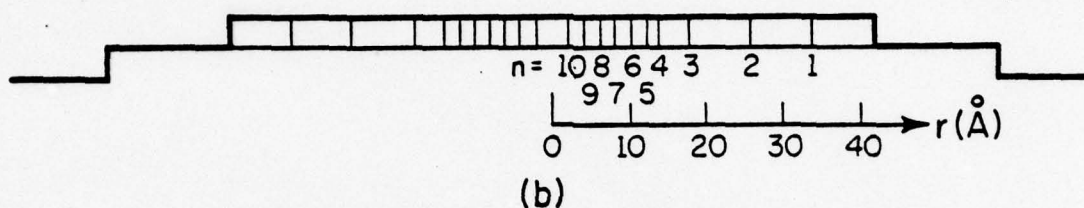
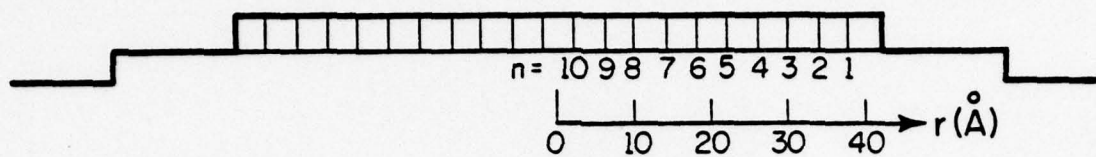
It is not possible to deduce the size of clusters from simulated scan diagrams precisely, since the local variation of electric field on the surface is not known. However, at least some rough estimates can be made based on simulation results. For example, from Fig. 2.13 the radius of the (110) plane is $\sim 25 \text{ \AA}$ when two small satellites appear in the scan diagram. We may deduce from this that the size of the cluster for the third scan diagram in Fig. 7.2, which also shows two satellites, is roughly 25 \AA . Following the same argument we may estimate the radius of clusters for the fifth, seventh, and eighth scan diagrams in Fig. 7.2 as roughly 20, 10, and 5 \AA , respectively.

Estimates for cluster sizes based on the shape of scan diagrams are, of course, endowed with considerable error. The quantitative nature of these estimates, however, emerges clearly from the following consideration. For a (110) plane $\sim 80 \text{ \AA}$ in diameter, there are only about 10-12 concentric rings of atoms in the plane. From the simulation in Appendix B we know that a difference in the cluster radius of at least a few angstroms is necessary in order to change the shape of the scan diagram appreciably. In Fig. 7.2 the surface has been stripped consecutively 10 times, with the scan diagram changing significantly after each stripping. This indicates that some atoms have been removed

during each stripping. On the other hand, during each stripping only a small number of atoms (less than one or two rings of atoms) is removed: it is impossible to remove many atoms (that is, more than two rings of atoms) each time for 10 consecutive strippings and still have any atoms left. We therefore conclude that during the controlled field evaporation leading to the scan diagrams in Fig. 7.2, no more than two rings of atoms were removed during each strip.

From the above argument it follows that the cluster size for each scan diagram in Fig. 7.2 falls within well-defined limits. This is illustrated in Fig. 7.3: assuming that one ring of atoms is evaporated every time the voltage is raised, the size of the clusters can be obtained directly. The diameters for clusters corresponding to each scan diagram in Fig. 7.2 thus estimated are shown in Fig. 7.3a. As a comparison, an alternate evaporation sequence is shown in Fig. 7.3b: in this series two rings of atoms are evaporated during some strippings and one or one-half ring of atoms are evaporated during others. Another alternate evaporation sequence is shown in Fig. 7.3c: this is similar to Fig. 7.3b, but the evaporation occurs more irregularly. The range of the cluster sizes for each scan diagram obtained from these three possible evaporation sequences are shown in Fig. 7.3d. The maximum range of the cluster sizes, obtained by considering all possible combinations of evaporation sequences, is given in Fig. 7.3e.

From Figs. 7.3e, it is clear that the cluster size can be estimated to an accuracy at least a factor of 2 by simply comparing its scan diagram with those in Fig. 7.2. We should point out that this quantitative estimate arises from two basic considerations discussed previously:

Size of plane after n^{th} evaporation

n	1	2	3	4	5	6	7	8	9	10	
$r(\text{max})$	38	34	30	26	22	18	14	10	6	4	\AA
$r(\text{min})$	34	26	18	14	12	10	8	6	4	2	\AA
Δr	4	8	12	12	10	8	6	4	2	2	\AA

(d)

n	1	2	3	4	5	6	7	8	9	10	
$r(\text{max})$	38	34	30	26	24	22	20	18	16	14	\AA
$r(\text{min})$	34	26	18	14	12	10	8	6	4	2	\AA
Δr	4	8	12	12	12	12	12	12	12	12	\AA

(e)

AP-935

Fig. 7.3. Variation of the (110) plane size with n , the number of field strippings. (a) One ring of atoms is evaporated during each application of stripping voltage; (b) two rings of atoms are removed initially, and $1/2$ ring of atoms removed later; (c) number of rings removed during each stripping is randomly selected between $1/2$ and 2; (d) ranges of the (110) plane size determined from possible combinations shown in (a), (b) and (c); (e) ranges of the (110) plane size determined by considering all possible combinations of evaporation sequences.

(a) a considerable number of atoms must be removed from the cluster in order to cause significant changes in its scan diagram; (b) less than two rings of atoms are removed during each stripping for the scan diagrams shown in Fig. 7.2. The quantitative nature of the scan diagram in determining the cluster size therefore really comes from the fact that surface structures can be controlled by careful field evaporation.

In Fig. 7.2 the structure of the surface corresponding to each scan diagram is suggested by a schematic drawing below it. Clusters on the (110) plane are generally elliptical in shape, as evident from Fig. 7.1. The number of atoms estimated to be in each cluster, taking account of this effect, is given below the scan diagram. It is to be understood that these dimensions only represent an estimate, and are accurate only with a factor of two.

7.2. Adsorption on clusters

7.2a. Small clusters

By very careful field evaporation in vacuum at 80 K one can achieve a small cluster consisting of only a few atoms. This cluster can be regarded essentially as a defect lying on top of an otherwise flat (110) surface. This unique configuration gives us a chance to study directly the effect of structural defects on the interaction of gas with a flat surface.

The adsorption of hydrogen on a W(110) surface with such a small cluster of atoms on top of it is shown in Fig. 7.4. There the change in the work function when this surface at 80 K is exposed to hydrogen is compared with that of a perfectly flat (110) plane, as well as with the emitter as a whole. The structures of the relevant surfaces are depicted by schematic drawings accompanying each curve. The scan diagram of the

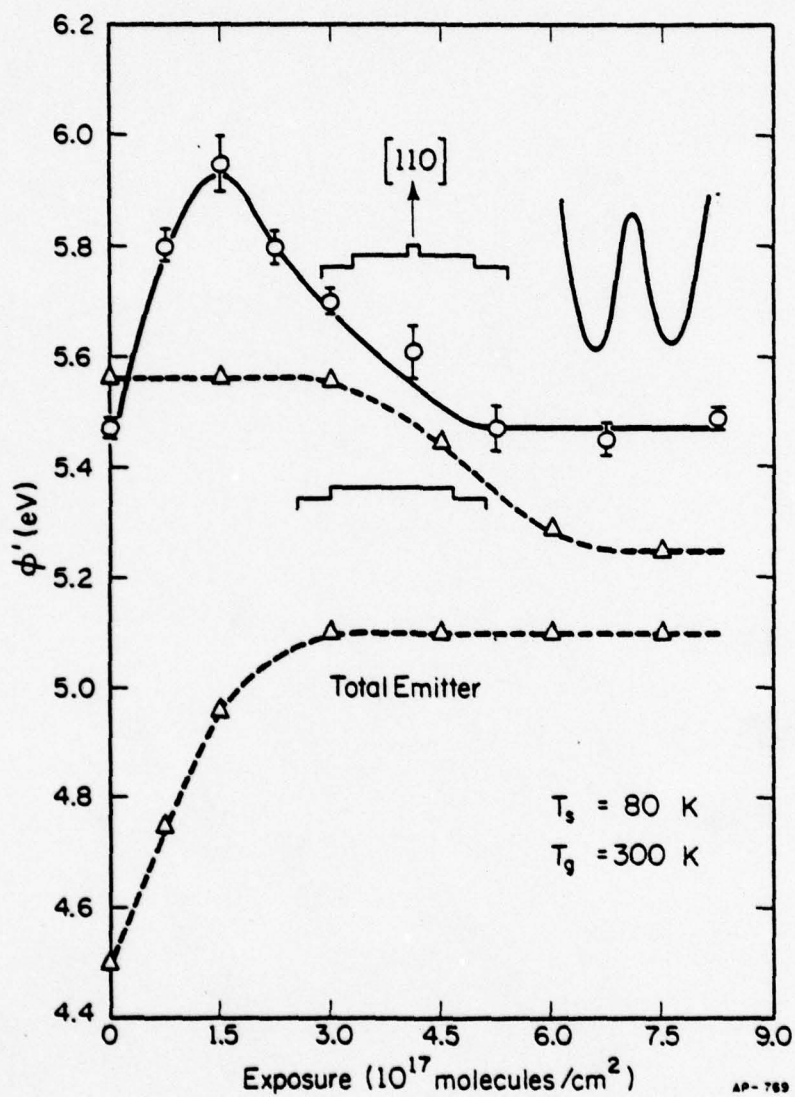


Fig. 7.4. Variation of (110) work function with exposure to hydrogen for a tungsten emitter with a small cluster at the center of the (110) plane. Emitter is field evaporated to 27.62 kV at 80 K.

surface with a small cluster on it is shown in the upper right corner of Fig. 7.4. It features a maximum at the geometrical center of the emission pattern and a minimum at each side. At a total emission current of 6×10^{-8} A, the probe-hole current at the maximum is 0.81×10^{-13} A and at the minimum 0.68×10^{-13} A. These values are much higher than the probe hole current for a flat (110) plane, which amounts to only 0.21×10^{-13} A at the same total emission current. It is obvious that the strong local field and the lower work function of the cluster edges make the emission from the cluster dominant over that from the flat (110) plane.

When the surface is held at 80 K and exposed to hydrogen, the work function for the emitter as a whole increases steadily from 4.5 eV to 5.1 eV. The saturation value is reached at an exposure of approximately 3×10^{17} molecules/cm². The changes for the emitter as a whole are independent of the shape of the (110) plane, since the emission from the (110) area is weak in any event. Hereafter we shall plot the changes on the emitter as a whole only as a reference.

The adsorption of hydrogen on the flat W(110) plane has been studied extensively by Polizzotti [3]. Similar experiments at 80 K are duplicated here, however, so that results for surfaces with and without clusters may be compared under identical conditions. For a large enough, flat (110) plane (diameter $> 70 \text{ \AA}$), the work function does not change appreciably at 80 K when first exposed to hydrogen, as is evident from the dashed curve in Fig. 7.4. The work function of the (110) remains unchanged up to the saturation value. The length of the incubation period is almost

the same as that necessary for the whole emitter to reach saturation. These results are in complete agreement with Polizzotti's, and have been reproduced for emitters field evaporated at 20.8, 23.7, and 30.6 kV. It is therefore safe to assume that the adsorption behavior for flat (110) planes field evaporated between 21 and 30 kV is essentially constant.

The adsorption of hydrogen on a flat surface with a small cluster on top is shown by the solid curve in Fig. 7.4. When exposed to hydrogen, the work function of the (110) region (the apparent work function determined from the F-N plots for the (110) plane plus cluster) increases rapidly; the changes are almost parallel to those for the emitter as a whole. At an exposure of 1.5×10^{17} molecules/cm², the work function of the (110) regions increases by ~ 0.4 eV, compared to ~ 0.5 eV on the emitter as a whole. After that, the work function decreases gradually, and reaches saturation at an exposure of $\sim 5 \times 10^{17}$ molecules/cm². When saturated, the work function from the (110) region is about the same as that for the initially clean (110) region.

It must be emphasized that the work function value deduced from the F-N plots does not represent the actual work function for either the cluster or the flat. When the physical size of the probe-hole and the resolution of the microscope are considered, the region surveyed by the probe-hole is found to be ~ 45 Å in diameter [3]. The current through the probe-hole consists of almost all the emission from the cluster, together with most of the emission from the flat area. The work function obtained from F-N

plots therefore represents contributions from both the cluster and the (110) flat. The value of the work function thus obtained depends largely on the relative dominance of the emission from the cluster and from the flat, as well as on the local electric field.

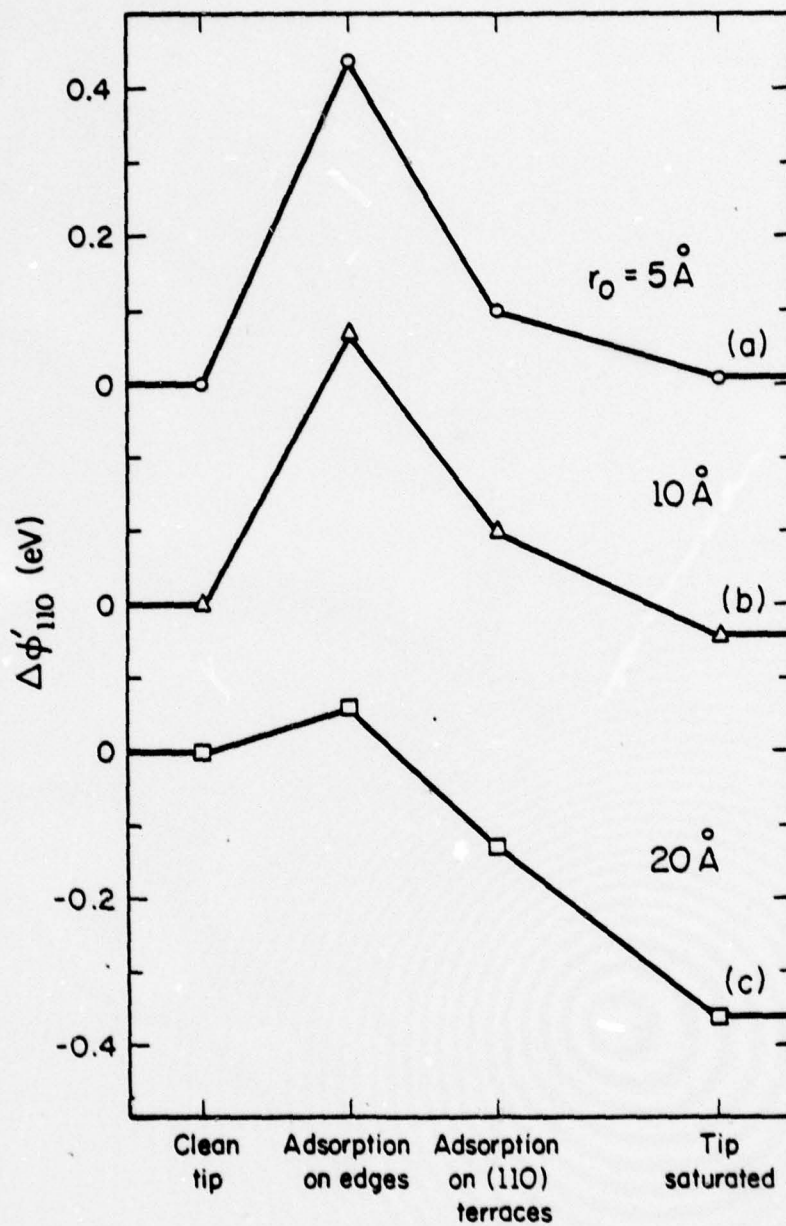
Despite the difficulty in relating the work function changes to actual chemical events on the surface, it is easily seen from Fig. 7.4 that saturation of the (110) region by hydrogen on a surface with a cluster is faster than on a perfectly flat (110) plane. On a surface with a cluster, saturation is reached at a total exposure of $\sim 5 \times 10^{17}$ molecules/cm², compared to $\sim 7 \times 10^{17}$ molecules/cm² on a flat (110). Even without knowing the detailed mechanism, it is clear that the rate of chemisorption on the flat surface is increased appreciably by the presence of the cluster.

A more detailed analysis for the experiments shown in Fig. 7.4 requires some help from the computer simulation of adsorption on field emitters. The details of these simulations are discussed in Appendix B. The contribution to the field emission current from a small cluster on top of a flat surface comes from two sources: the lower work function of the edges of the cluster, and the stronger electric field caused by the protrusion near the edge. These result in strong emission from the center of the (110) region, as evident from the prominent maximum in the scan diagram. This effect can be simulated readily, as shown in Fig. 2.13f. Adsorption of gas on a surface can be simulated by changing the emission characteristics (work function, pre-exponential factor) on different regions of the surface according to previously gathered data. (For example, when hydrogen is adsorbed, the work function of a flat (110) surface decreases while the

work function of rough surfaces increases.) For the adsorption of hydrogen on tungsten (110) surfaces, the following changes in the emission characteristics are assumed: ϕ for the (110) plane is decreased by 0.4 eV. ϕ for the (110) plane edges is increased by 0.4 eV. The pre-exponential factor for the (110) plane is also decreased according to experimental values, $\Delta \ln A/A_0 \sim -2$. The pre-exponential factor for the (110) plane edges is assumed unchanged. Using these emission characteristics simulated experiments can be performed on a computer.

The result of a simulated experiment on a (110) plane with a small cluster is shown in Fig. 7.5. In this simulation, changes in the work function (as deduced from F-N plots) of the (110) region are derived for the following situations: (a) the edges of the cluster, as well as the edges of the (110) plane, are covered by hydrogen; (b) in addition to the edges, the (110) terraces outside of the (110) plane are also covered by hydrogen; and (c) the whole (110) region, including the top of the cluster, is saturated. When the edges are covered by hydrogen, the work function of the (110) region rises sharply by ~ 0.4 eV; after that the work function drops by ~ 0.15 eV when the (110) plane is covered by hydrogen, and a drop by 0.2 eV follows when the top of the small cluster is also covered by hydrogen, as evident from Fig. 7.5a.

Quantitatively we cannot expect the simulation to match our experimental results completely, as important parameters such as the local electric field are essentially unknown. Qualitatively, however, the simulation fits quite well with our results. The initial rise in the work function in our experiments is of a magnitude comparable to that



AP-938

Fig. 7.5. Computer simulated work function changes for tungsten (110) planes with different size clusters on top. Diameter of the (110) plane is 80 Å. Diameter of cluster is: (a) 10 Å; (b) 20 Å; (c) 40 Å.

obtained in the simulation when the cluster edges are covered by hydrogen. This suggests that the edges of the cluster adsorb hydrogen at a rate faster than the rest of the (110) region. The later drop in the work function can be explained by the adsorption of hydrogen on the (110) flat and on top of the cluster; from Fig. 7.5a it is clear that both lead to a decrease in the work function. Whether adsorption on the (110) flat and on the top of the cluster occurs sequentially or not cannot be discerned from our experiments, as the drop in the work function appears quite continuous in Fig. 7.4.

From these experiments on surfaces with a small cluster we reach the following conclusions: (a) the rate of chemisorption of hydrogen on a (110) surface with a cluster is faster than that on a perfectly flat (110) surface; and (b) chemisorption on the edges of a cluster is faster than on the rest of the (110) region. The faster rate on a surface with a cluster must be caused by the presence of the cluster, since all other surface as well as experimental conditions are identical. Considering the faster rate of chemisorption on the cluster edges, it is likely that chemisorption on the flat (110) plane is catalyzed by the adsorption on cluster edges. However, to confirm this conclusion more quantitative evidence must be obtained.

7.2b. Intermediate clusters

In our experiments, intermediate clusters consist of a small plane made up of about 15 atoms (accuracy within a factor of 2) on top of a large, flat (110) plane. Clusters of this size are of interest since

the number of edge sites (defects) is greater than for a small cluster. By studying clusters of different sizes (hence different number of edge sites) we may get some quantitative information about the effect of defects on chemisorption.

1. Work function changes

The adsorption of hydrogen on a W(110) plane with such a cluster is shown in Fig. 7.6. The dashed curves indicating adsorption on the emitter as a whole, and on the perfect (110) plane, are used as reference. Also shown are a schematic drawing for the structure of the (110) region, and the scanning diagram. Judging from the shape and magnitude of the scan diagram, the size of the cluster is within the range we described earlier ($r_0 \sim 10 \text{ \AA}$). When exposed to hydrogen, the work function (deduced from F-N plots) of the (110) region immediately rises by $\sim 0.15 \text{ eV}$. It stays at that value during the next dose ($7.5 \times 10^{16} \text{ molecules/cm}^2$). After that, it decreases again by $\sim 0.15 \text{ eV}$ when exposed to another dose of $1.5 \times 10^{17} \text{ molecules/cm}^2$ of hydrogen. Upon further addition of hydrogen, the work function decreases only slowly, showing a change of $\sim 0.05 \text{ eV}$ at exposures between 3 and $4.5 \times 10^{17} \text{ molecules/cm}^2$. Saturation of the (110) work function is reached at an exposure of $\sim 6 \times 10^{17} \text{ molecules/cm}^2$. At saturation, the work function is 0.25 eV below that for the clean surface.

Reproducing the experiment shown in Fig. 7.6 is rather difficult, since with d.c. field evaporation it is almost impossible to reproduce a cluster of exactly the same size. The general adsorption behavior described above, however, is quite reproducible. The adsorption of hydrogen on a (110) surface with a slightly different size cluster is

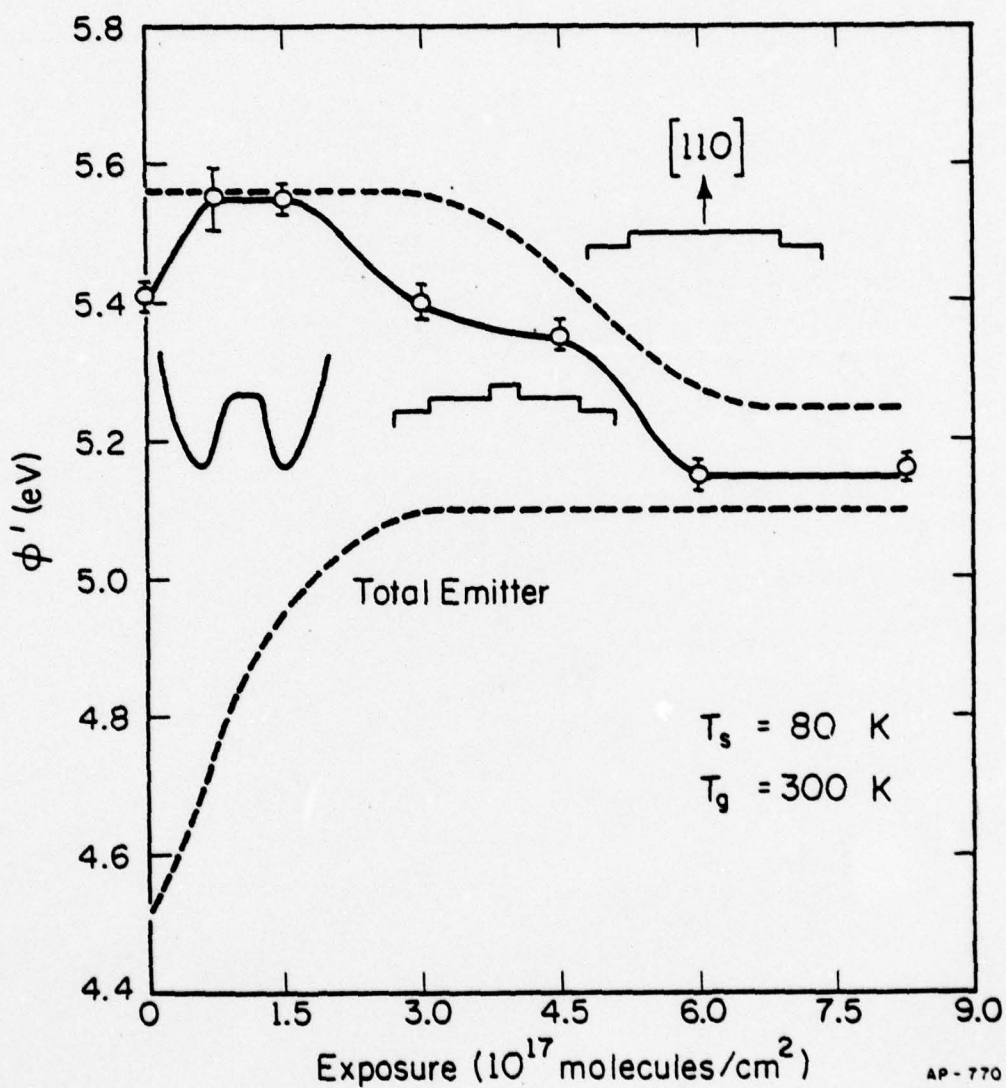


Fig. 7.6. Variation of (110) work function with exposure to hydrogen for a tungsten (110) surface with an intermediate size cluster on top at $T_s = 80 \text{ K}$. Emitter field evaporated to 25.7 kV at $T_s = 80 \text{ K}$.

shown in Fig. 7.7. From the magnitude and shape of the scan diagram the size of the cluster is judged slightly larger than that in Fig. 7.6. However, the general features of adsorption on this surface are reminiscent of those in Fig. 7.6. The initial rise of the work function is somewhat smaller, 0.1 eV compared to 0.15 eV, but the rate of adsorption is not significantly different from that shown in Fig. 7.6.

Again the rather complicated changes in the work function on the (110) can be better understood through computer simulation. Adsorption of hydrogen on a W(110) surface with a cluster ~ 20 Å in diameter has been simulated. As shown in Fig. 7.5b, the work function of the (110) region rises when the edges of the cluster are covered by hydrogen, similar to the behavior of a small cluster. Adsorption on the (110) plane, as well as adsorption on top of the cluster, decreases the work function. Therefore the initial rise of the work function must be caused by adsorption on the edges of the cluster; the subsequent drop in the work function is then an indication of adsorption on the (110) flat and on top of the cluster.

The most striking feature in the chemisorption on a (110) surface with a cluster on it is the disappearance of the long incubation period observed on a flat (110). As shown in both Figs. 7.6 and 7.7, after the initial rise in the work function, an incubation period only about 1/4 of that for a perfectly flat (110) plane is seen. The work function starts to decrease at an exposure only about 1/2 that for a perfect (110) surface. It is clear that the rate of chemisorption on the (110) region is increased at least twofold by the presence of a cluster.

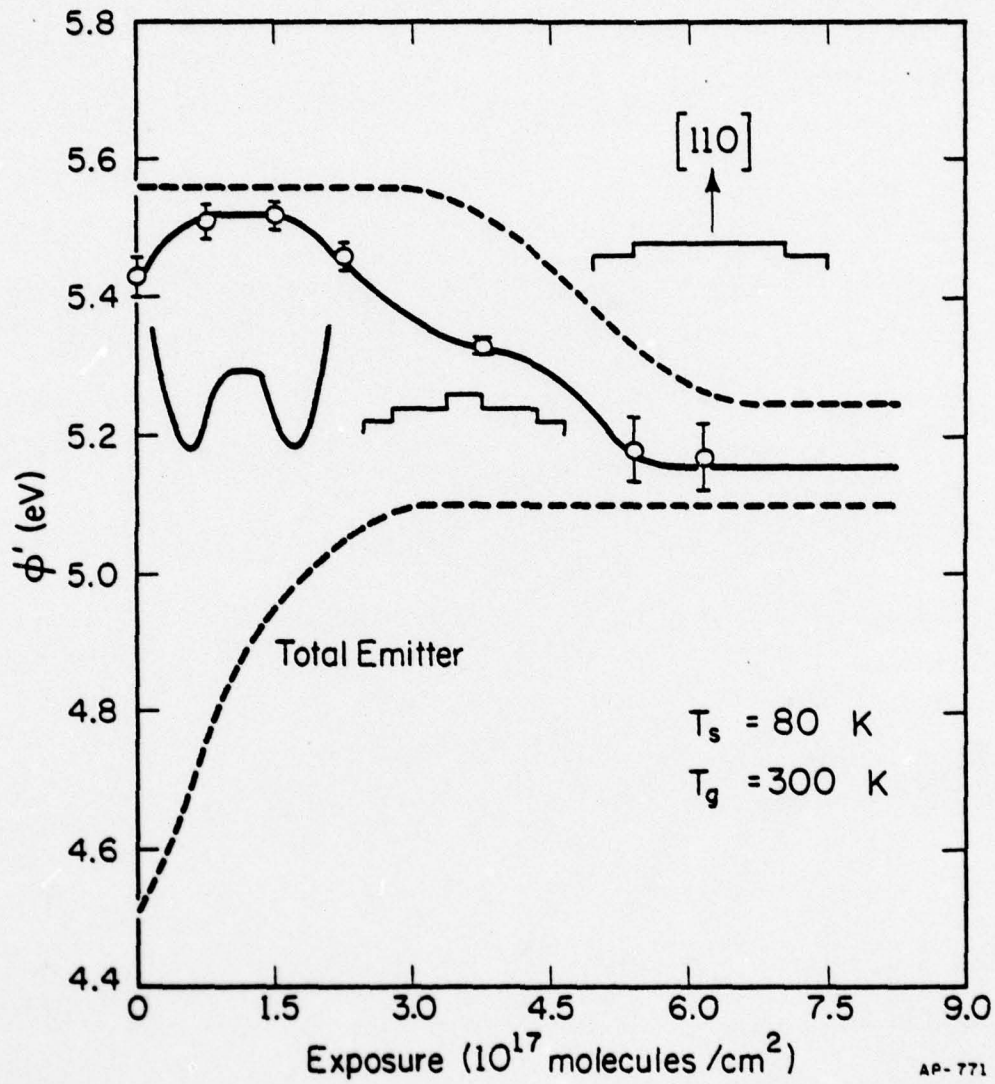


Fig. 7.7. Variation of (110) work function with exposure to hydrogen for a tungsten (110) surface with an intermediate size cluster on top at $T_s = 80$ K. Emitter vacuum field evaporated to 28.52 kV at 80 K.

Furthermore, even the short incubation period in Figs. 7.6 and 7.7 is probably fortuitous: for a small cluster, the initial rise of the work function stops at an exposure of $\sim 1.5 \times 10^{17}$ molecules/cm²; for an intermediate cluster the rate of chemisorption on edge sites should not differ from that for a small cluster. Therefore the saturation of the edges should also occur at a total exposure of $\sim 1.5 \times 10^{17}$ molecules/cm² on an intermediate cluster. The fact that the initial work function rise for this surface stops at a lower exposure (7.5×10^{16} molecules/cm²) indicates clearly that chemisorption on the (110) flat or on top of the cluster begins at exposures less than 1.5×10^{17} molecules/cm². The lack of work function change between exposures of 0.75 - 1.5×10^{17} molecules/cm² therefore is probably caused by a trade-off between adsorption on cluster edges (which increases the work function) and on the (110) flats (which decreases the work function).

Compared to a small cluster, the initial rise in the work function on an intermediate cluster is much smaller in magnitude; at an exposure of 7.5×10^{16} molecules/cm² it amounts to only 0.1 - 0.15 eV compared to 0.32 eV. This probably reflects the relative dominance of the work function and the electric field on these clusters. The strong emission from the cluster is a result of both the lower work function and the stronger electric field at the cluster edges, as discussed earlier. When the cluster becomes smaller, the emitting area from the cluster diminishes, but the local electric field becomes stronger. Therefore for a small

cluster the strong emission is caused largely by the strong local electric field; for an intermediate cluster the lower work function of the edges probably plays a dominant role. If this is assumed in our computer simulation a small cluster remains strongly emitting even after the edges are covered by hydrogen. On an intermediate cluster, however, adsorption of hydrogen on cluster edges makes them less dominant in emission. The (110) work function then reflects largely the true value of the (110) flats. As a result, the simulated work function change has a magnitude smaller than for a small cluster, as is clear from Fig. 7.5a,b.

In Fig. 7.6 the decrease of the work function appears halted at a total exposure of 3×10^{17} molecules/cm², the work function drops by only 0.05 eV. Further exposures beyond 4.5×10^{17} molecules/cm² bring about a larger drop, 0.2 eV in the work function, and the (110) region is saturated. A unique explanation for this behavior is not available at this time. There are, however, two possible ways to rationalize this phenomenon: (a) the formulation of a new adsorption state at exposures higher than 4.5×10^{17} molecules/cm²; and (b) the sequential filling in of the (110) flat and the top of the cluster. Both can explain the break in the adsorption curve. If a new state forms after the (110) region is saturated by atomic hydrogen, the work function can conceivably be changed further. If adsorption on top of the cluster is appreciably faster or slower than on the (110) flat, then it can also cause a break in the adsorption curve. We shall not attempt to resolve these two possibilities until the next chapter, when a more quantitative analysis can be made.

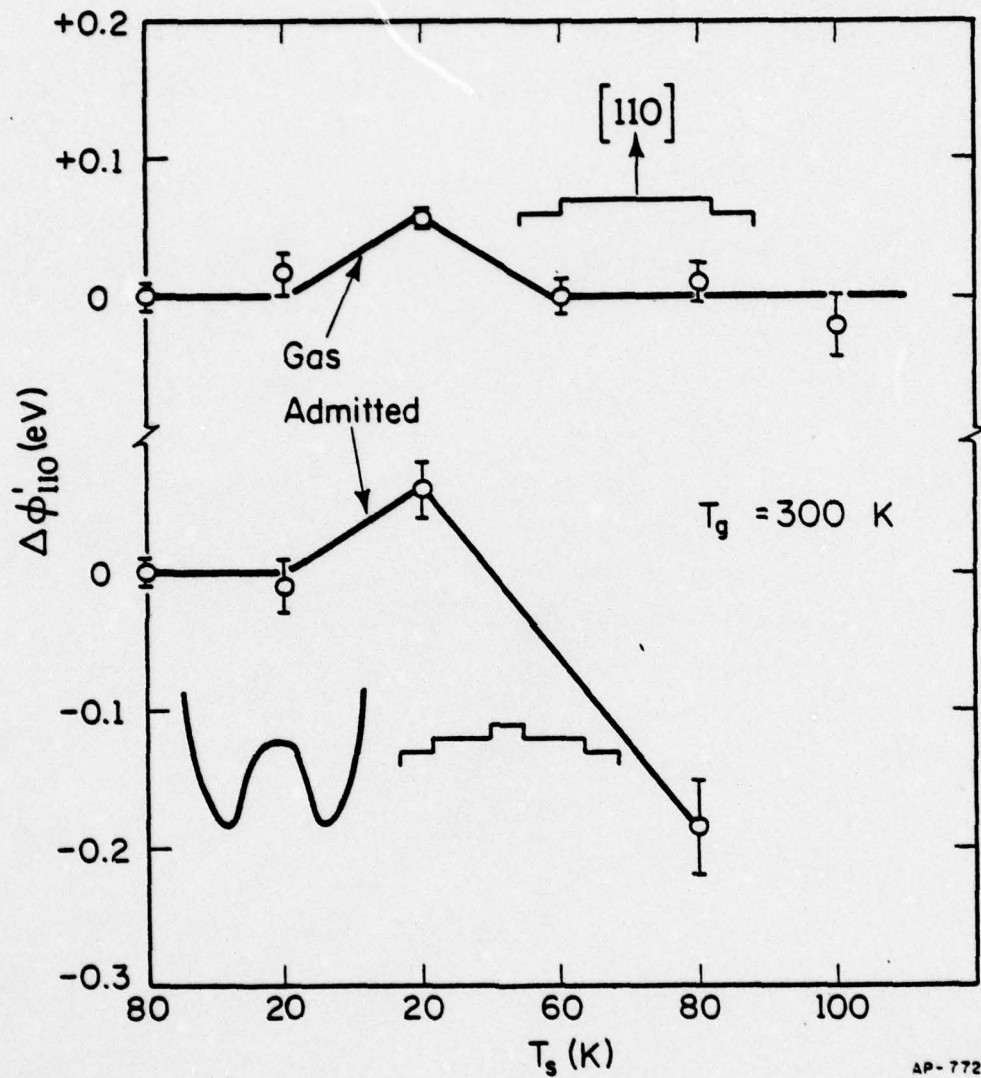
In summary, by monitoring the work function change on a (110) surface with an intermediate cluster we have learned that: (a) adsorption of hydrogen on the edges of the cluster is much faster than on the (110) flats; (b) the presence of the cluster reduces the incubation period on the (110) surface at 80 K by at least a factor of two. It is clear that the chemisorption of hydrogen on the (110) surface is substantially promoted by the cluster.

ii. Studies at $T_s < 80$ K

It has been shown by Polizzotti [3] that on a perfect W(110) plane hydrogen can be adsorbed at low temperature (~ 38 K) in a form different from that adsorbed at 80 K. On warming up the emitter the hydrogen adsorbed in this form desorbed below ~ 66 K. From this low desorption temperature he concluded that the hydrogen adsorbed at low temperature is bound as undissociated molecules. The fact that molecular hydrogen, adsorbed at low temperature, desorbs rather than converts into tightly bound atomic hydrogen indicates that W(110) is inert in dissociating hydrogen. The molecules evaporate before they can find a suitable dissociation site on the W(110) surface. If this view is correct then one should be able to promote chemisorption on the (110) plane by simply furnishing some high activity sites. This can easily be done by creating a cluster of atoms on top of the flat surface. As we have seen earlier in this chapter, such a cluster appears to be highly effective in dissociating hydrogen into atoms.

The results of two similar low temperature experiments, with and without a cluster at the center, are shown in Fig. 7.8. At the top half is an experiment similar to Polizzotti's except for slight differences in the temperatures. In this, a flat (110) plane is created by field evaporation at 24.9 kV and 80 K. The emitter is then cooled to ~ 20 -30 K and exposed to hydrogen. The exact exposure is not known, since pumping by the walls at this temperature is pronounced. Adsorption of molecular hydrogen is indicated by an increase in the work function, rather than in a decrease as for atomic hydrogen. After this adsorption, the emitter is warmed to ~ 60 K by passing a d.c. current of 0.8 A through the tungsten support loop. The molecular hydrogen appears to desorb, as indicated by a return to the clean value of the (110) work function. Heating the emitter to ~ 80 K and ~ 100 K thereafter does not bring about further changes. These results are in complete agreement with Polizzotti's findings.

Shown in the lower half of Fig. 7.8 is a similar experiment but for a (110) plane with an intermediate size cluster on top of it. The emitter was field evaporated at 24.2 kV and 80 K. The size of the (110) plane should be similar to that in the last experiment described above. When exposed to hydrogen at ~ 20 -30 K, the work function also increases. However, when the surface is then warmed to ~ 80 K, the work function dropped by 0.25 eV, to 0.18 eV below its clean value. It appears that molecular hydrogen can convert to tightly bound atomic hydrogen on this surface. Judging from the shape and magnitude of the scanning diagram, the size of this cluster is similar to that shown in Fig. 7.6. According



AP-772

Fig. 7.8. Changes in (110) work function with surface temperatures T_s for tungsten. Emitters are cooled to 20-30 K, exposed to H_2 at this temperature, and then warmed slowly to 60-80 K. Upper curve: a flat (110) plane obtained by vacuum field evaporation to 24.9 kV at 80 K. Lower curve: a (110) plane with an intermediate size cluster on top, obtained by vacuum field evaporation to 24.42 kV at 80 K.

to the data in Fig. 7.6, a drop of 0.18 eV in the work function corresponds to $\sim 3/4$ of the change at saturation. Therefore not only the edges of the cluster, but most of the flat area, must have been covered by atomic hydrogen upon warming the initial deposit of molecular hydrogen. It is evident that the presence of the cluster greatly enhanced the rate of dissociation of hydrogen on the flat (110).

7.2c. Large clusters

A large cluster is itself a small plane. A large cluster can be envisioned as a small plane sitting on top of a larger one. Judging from simulated scanning diagrams, the diameter of the smaller plane is probably less than 40 Å, that of the larger plane ~ 80 Å. Such a cluster provides a rather large defect area along its edges, and a considerable flat surface on its top. A study of the interaction of a larger cluster with gas may reveal the relative rate of chemisorption on top of the cluster and on the (110) flat.

Adsorption of hydrogen on a W(110) surface with a large cluster on it is shown in Fig. 7.9. From the magnitude and shape of the scan diagram, the size of the cluster can be estimated at $\sim 10 \times 7$ atoms, or approximately 20 Å in radius. The changes in the work function of a large cluster are quite different from those of smaller clusters. When exposed to hydrogen, the work function initially drops by ~ 0.05 eV rather than increasing. The work function then stays unchanged after the second exposure; thereafter it drops slowly until saturation. Saturation is reached at $\sim 6 \times 10^{17}$ molecules/cm² of exposure, only slightly earlier than that for a perfect (110) plane. The work function at saturation is ~ 0.25 eV below that for the clean surface.

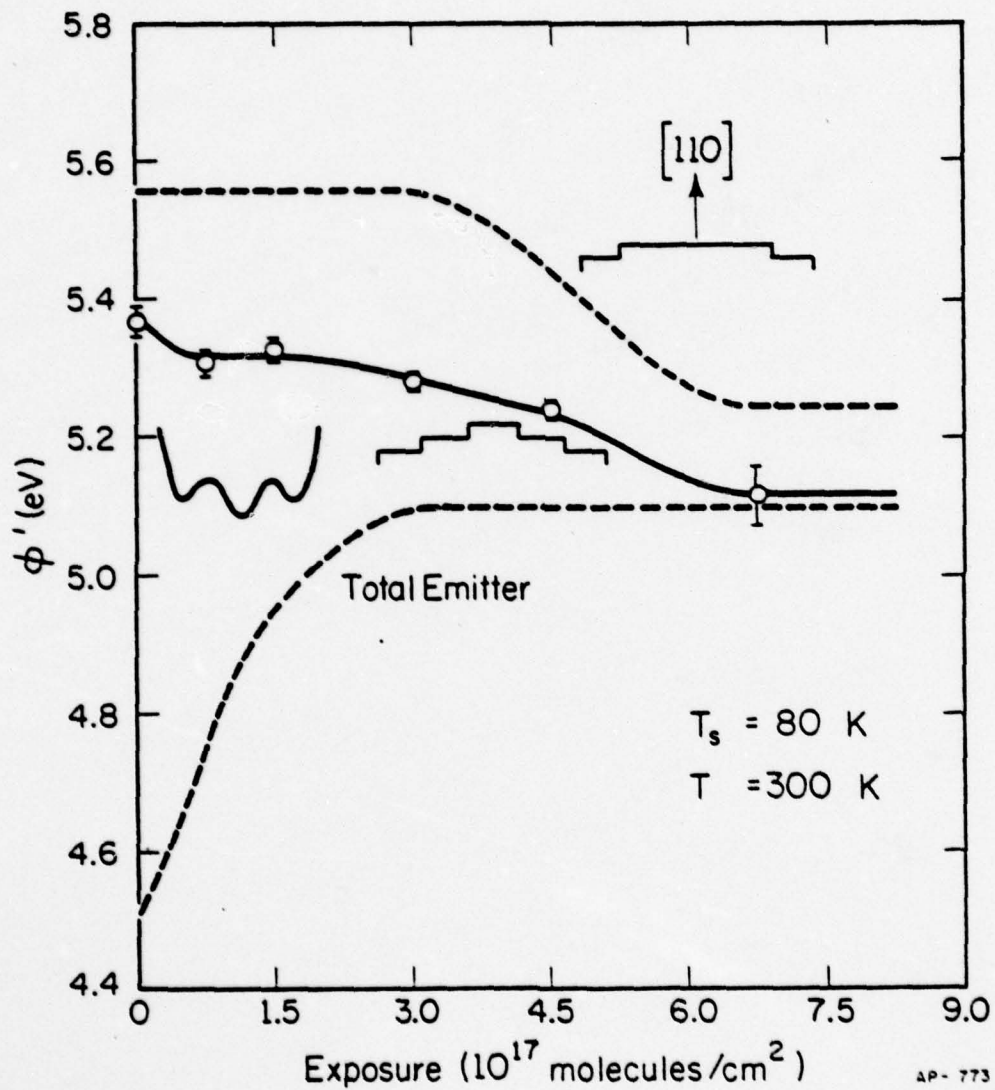


Fig. 7.9. Variation of (110) work function with exposure to hydrogen for a W(110) surface with a large cluster on top at $T_s = 80$ K. Emitter vacuum field evaporated to 21.82 kV at 80 K. ^s

As in the case of smaller clusters, changes in the work function can be better understood with the help of computer simulation. From our simulation, shown in Fig. 7.5c, the work function of the (110) region should also increase for a large cluster when the edges of the cluster are covered by hydrogen. In the actual experiment, however, a decrease in the work function is observed initially. This behavior can be explained only if chemisorption of hydrogen occurs both on the edges of the cluster and on the flat (110): the lowering of the work function by the adsorption on the (110) flats then overcompensates the rise of the work function at the cluster edges. This is expected, since: (a) the contribution from cluster edges is relatively weak compared to smaller clusters, as the local electric field is weaker; (b) the defect area (cluster edges) is larger for large clusters yet the total flat area remains essentially unchanged. Therefore on a surface with a large cluster the rate of chemisorption on the (110) flats is faster due to the catalytic action on the larger defect area provided by the cluster.

After the initial drop, the work function changes only slowly on further exposure to hydrogen. This is considerably different from the situation for smaller clusters. For a small cluster, the work function drops continuously after the initial rise; for an intermediate cluster, the work function decreases rapidly after the initial rise, but slows down after the exposure reaches 3×10^{17} molecules/cm². These differences must be caused by differences in the surface structure alone, as all other experimental parameters are identical.

AD-A056 535

ILLINOIS UNIV AT URBANA-CHAMPAIGN COORDINATED SCIENCE LAB F/G 7/4
CHEMISORPTION ON PERFECT SURFACES AND STRUCTURAL DEFECTS.(U)

OCT 77 R LIU

DAAB07-72-C-0259

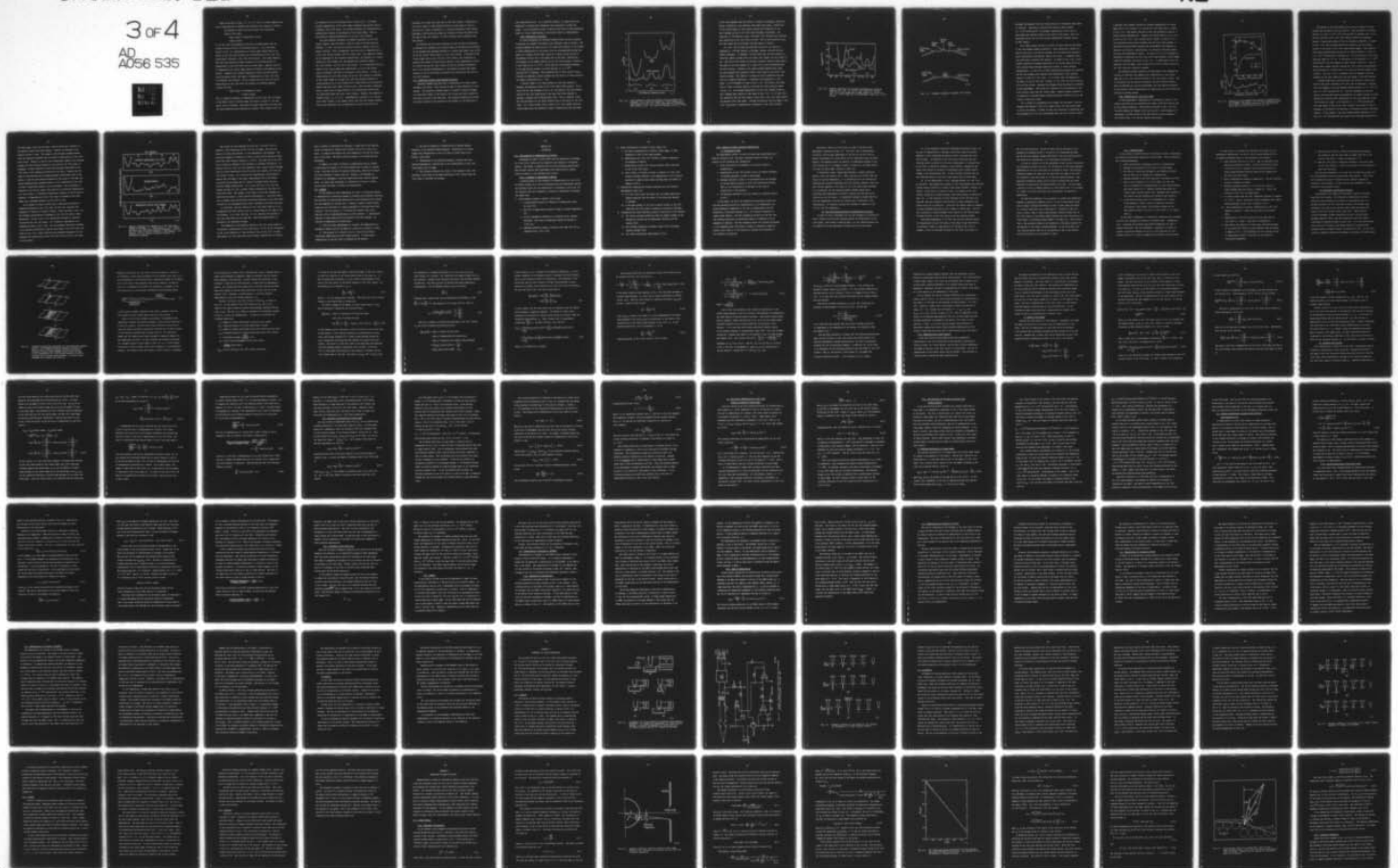
NL

UNCLASSIFIED

R-790

3 of 4

AD
A056 535



Based on the data in Figs. 7.4, 7.6, 7.7, and 7.9, we may summarize the rate of chemisorption on surfaces with different size clusters as follows:

the exposure at which the work function stops increasing
stands in the order:

large cluster < intermediate cluster

< small cluster.

It is clear that the dependence of the rate of chemisorption upon the surface structure follows a well-defined pattern. As we have shown earlier in Fig. 7.5, chemisorption on cluster edges brings about an increase in the (110) work function, while chemisorption on the (110) flat brings about a decrease in the (110) work function. The actual change in the (110) work function therefore depends on the relative amount of chemisorption on the (110) flats and on cluster edges. However, the rate of chemisorption on cluster edges should not depend on the geometry of the surface. Therefore the different exposures at which the work function stops increasing reflect the amount of chemisorption on the (110) flats for different size clusters. We can conclude from this that the rate of chemisorption on the (110) flats for surfaces of different geometry follows the order:

large cluster > intermediate cluster

> small cluster.

This is completely expected if chemisorption on the (110) flat is induced by the defect sites at cluster edges; the larger a cluster is, the more defect sites it provides. This view is further supported by the fact that the long incubation period observed on a perfect (110) surface at 80 K is

not observed on any of the surfaces with a cluster on it. For these surfaces chemisorption on the (110) region commences much earlier than on a perfectly flat (110) plane. We conclude therefore that chemisorption on surfaces with clusters is accelerated by the cluster edges. That is, these defects catalyze chemisorption on the flat (110) surfaces.

The total exposure necessary for complete saturation of the (110) region, however, does not follow a trend as clear as the work function increase. In fact, the rate for complete saturation appears faster for smaller clusters. This is unexpected, since the rate of chemisorption on a flat (110) should increase with the cluster size. This behavior, however, may be understood by the following consideration: the presence of a cluster divides the (110) surface into two geometrically different regions -- the (110) terrace, and the top of the cluster. It is conceivable that the effect of the cluster edges upon chemisorption on top of the cluster would be different from that on the adjacent (110) terrace. In fact, if chemisorption on top of the cluster and on the (110) terrace is catalyzed by the cluster edges at an equal rate, then the exposure necessary to bring saturation for a (110) surface with a large cluster on top should be smaller than that with a small cluster on top. This is easily visualized, since a surface with a large cluster on top provides more active sites for dissociation than that with a small cluster. However, the opposite is observed (Figs. 7.4, 7.6, 7.9). Experimentally, saturation of a surface with a small cluster on top appears faster than that with larger clusters. This can be understood only if chemisorption on top of the cluster is

catalyzed in a slower rate than that on the (110) terrace. Adsorption on top of the cluster is then delayed relative to other parts of the tip, resulting in a delay of saturation. A detailed examination would require knowledge of the activation energy for an adatom to leave the defect site and jump to the (110) surface. We shall postpone such an analysis until next chapter.

We conclude this section by pointing out that the rate of saturation on surfaces with different size clusters cannot be satisfactorily accounted for by assuming that hydrogen adsorbed on a cluster edge tends to go to the top of the cluster rather than go to the (110) terrace. If adatoms on the cluster edges tend to go to the top of the cluster, then saturation on surfaces with larger clusters would be faster, since chemisorption on both the cluster top and the (110) terrace can now be catalyzed effectively. This is not observed experimentally. We therefore conclude that chemisorption on top of the cluster is promoted less effectively than that on the (110) terraces.

7.3. Adsorption studies using scanning techniques

Scanning diagrams have been used to characterize the clean surface throughout this study. They can also be used to study adsorption on this surface. The probe-hole technique makes it possible to monitor changes on a particular region of the crystal, but it does not allow a survey of more than one place at the same time. The scanning technique can provide an overall profile of the situation on the surface, at the sacrifice of

truly quantitative data. It is possible, however, to combine these two techniques to acquire more information than accessible to either one singly. In the following we shall illustrate this point by some experiments aimed at a better understanding of structural effects in chemisorption.

7.3a. Adsorption on clusters

In these experiments the scanning diagrams before and after exposure to hydrogen are compared for surfaces with different types of defects. The scanning diagrams are shown in Fig. 7.10; there the structure of the surface is drawn schematically at the bottom, with the corresponding scanning diagrams for a perfect W(110) plane; those for a large cluster and for an intermediate cluster are in the middle and at the right, respectively. The diagrams at the higher currents are for the clean surfaces, scanned at a total emission of 6×10^{-8} A. Below them are the diagrams determined at the same applied voltage, but after exposure to 7.5×10^{16} molecules/cm² of hydrogen. The reproducibility of these curves is good, although the mechanical motion assembly has some play in it which restricts the angular reproducibility to $\sim 10\%$.

A feature common to all three surfaces is that once exposed to hydrogen, the emission outside of the (110) region drops greatly. As is clear from the scan diagrams in Fig. 7.10, the emission from the terraces outside of the (110) plane drops to the same level after exposed to hydrogen, although quite different when clean. This is expected, since the only difference for the three surfaces lies in the center of the (110) plane. For a clean surface with a cluster on it, the strongly emitting cluster edges raise the probe-hole current, forming satellites and bumps

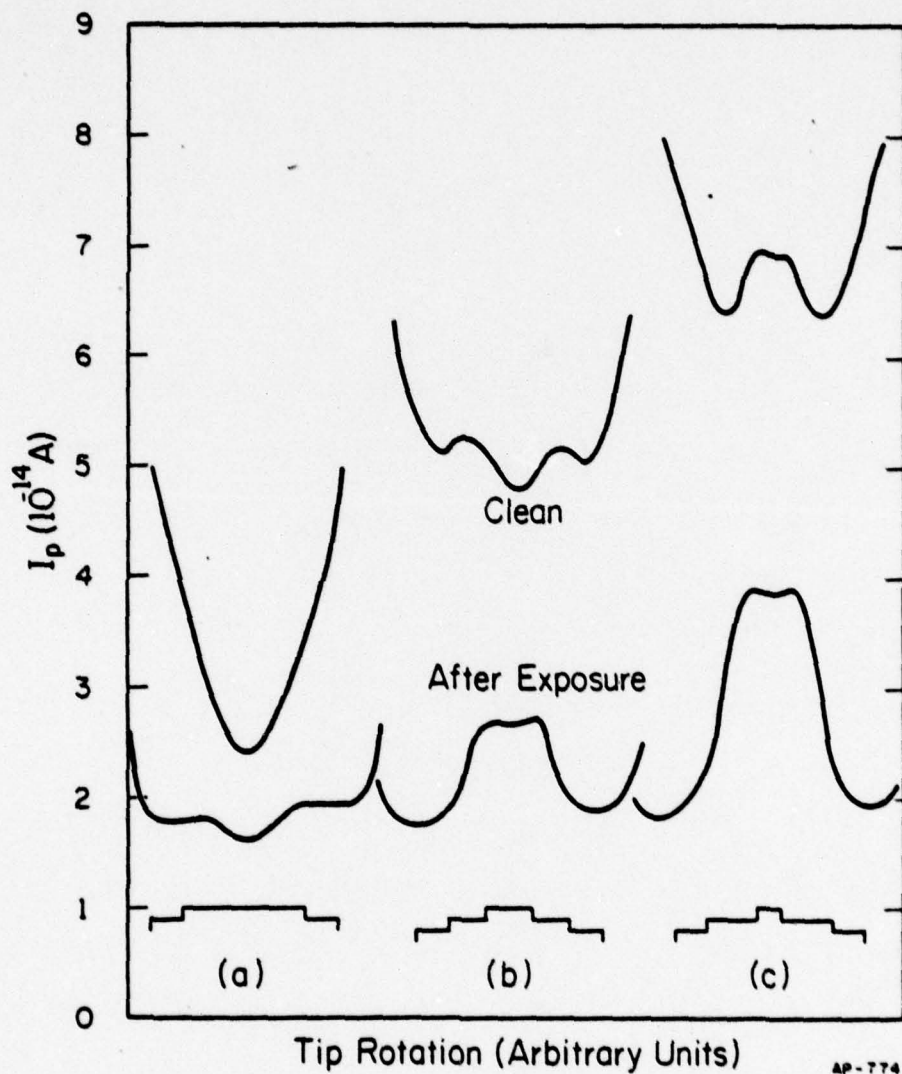
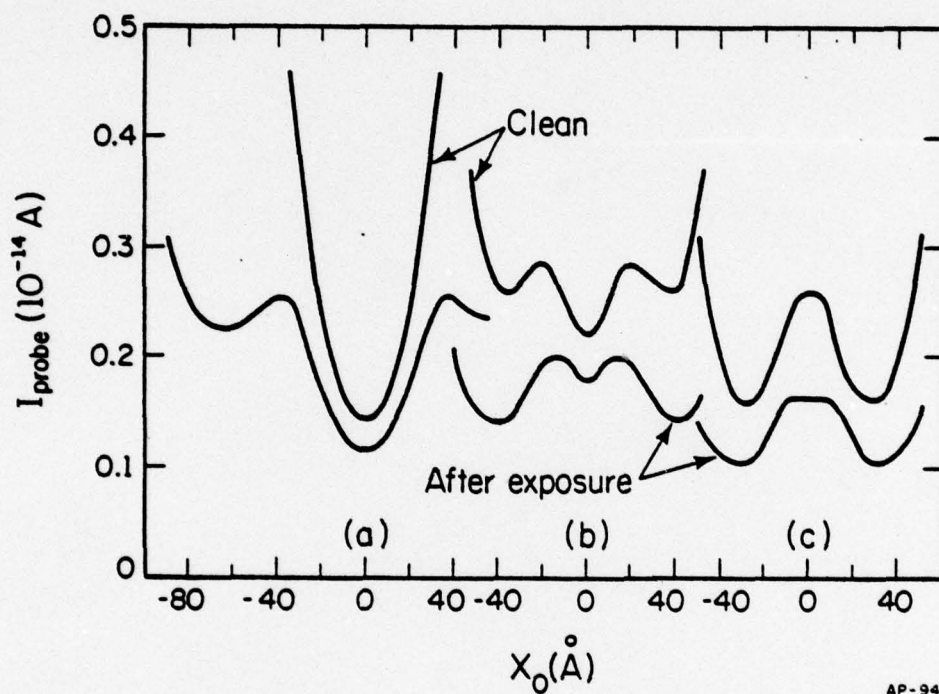


Fig. 7.10. Scan diagrams for clean and hydrogen covered tungsten (110) surfaces. (a) A flat (110) plane; (b) a (110) plane with a large cluster on top; (c) a (110) plane with an intermediate size cluster on top. All scans and exposures are at $T_s = 80$ K.

in the scan diagrams; when the surface is exposed to hydrogen, adsorption causes a diminution in the emission from these plane edges. Effects due to the cluster edges are thus greatly reduced and differences in the scan diagrams outside of the (110) plane disappear accordingly. The large drop in the emission current from these (110) terraces also indicates that adsorption on the (110) steps is rapid. This is also expected, since the (110) steps are not different from the edges of clusters.

On a flat (110) surface the probe-hole current at the center is decreased by $\sim 25\%$ when exposed to hydrogen; however, the work function remains unchanged. In Appendix C we have shown that the work function is relatively immune to edge effect for large (110) planes, but the current is not. The drop in the current is therefore probably caused by edge effects. The shape of the scan diagram for a large (110) is more interesting than the work function. Instead of the single minimum apparent when clean, the scan diagram after adsorption shows a small bump at each side of the central minimum. This behavior can again be better understood with the help of a computer simulation. A simulated scan diagram for a (110) plane $\sim 70 \text{ \AA}$ in diameter is shown in Fig. 7.11a. For clarity, the terms used to refer to various regions on and near the (110) plane are shown in Fig. 7.12. By assuming chemisorption on the (110) terraces alone we get a diagram quite similar to that shown in Fig. 7.10. It is clear from our simulation that the small bumps on each side of the (110) plane reflect the emission from plane edges. Although the emission from the edges of the (110) plane drops on chemisorption, adsorption on the (110) vicinals



AP-941

Fig. 7.11. Computer simulated scan diagrams corresponding to surfaces shown in Fig. 7.10. (a) A flat (110) plane with radius = 35 \AA ; (b) a (110) plane with a large cluster ($r_0 = 20 \text{ \AA}$) on top; (c) a (110) plane with an intermediate cluster ($r_0 = 10 \text{ \AA}$) on top.

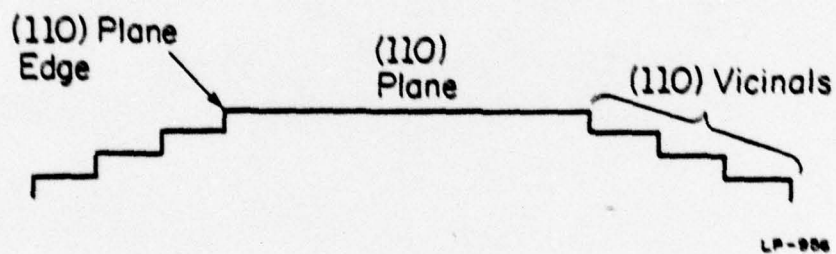
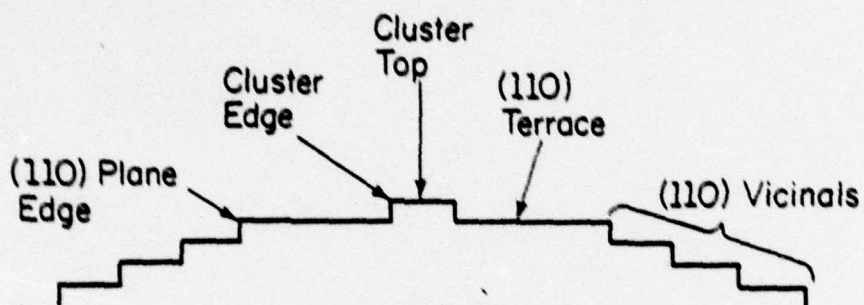


Fig. 7.12. Schematic diagrams of tungsten (110) planes.

decreases the emission from that region even more, causing the plane edges to stand out. Therefore on exposing the surface to small amounts (7.5×10^{16} molecules/cm²) of hydrogen, chemisorption occurs only on plane edges and terraces outside of the central (110) plane. This is in reasonable accord with the work function measurement discussed earlier in this chapter.

For a large cluster the drop in current is quite large and the shape of the scan diagram changes drastically. After adsorption, instead of a bump on each side of the central minimum, the scan diagram now features a broad, essentially structureless, bump at the center. A computer simulation also helps to explain this behavior. As shown in Fig. 7.11b, a scan diagram simulated by assuming adsorption on the cluster edges and on the (110) vicinals shows features essentially similar to those obtained experimentally. At the (110) vicinals chemisorption decreases the emission and the scan diagram (both simulated and experimental) shows features similar to those for a flat (110). It is evident that the dominance of the edges, as well as the (110) vicinals, is lost after the first exposure. On top of the cluster, simulated scan diagram shows structures not observed in real experiments. This could be a reflection of the difference in the local electric field near the cluster edges. Without further evidence it is impossible to conclude whether chemisorption has occurred on top of the cluster at this early stage.

For a cluster of intermediate size changes are also great. The scan diagram looks similar to that for a large cluster, but the central bump is taller and broader. We have not been very successful in simulating this scan diagram due to our lack of knowledge about the local electric fields.

A simulated scan diagram, obtained by assuming chemisorption on cluster edges and on (110) vicinals, but leaving the (110) plane bare, is shown in Fig. 7.11c. The general features of this scan diagram are similar to those obtained experimentally. However, the central bump is not as tall as that in Fig. 7.10c. For a surface with a cluster of radius $\leq 10 \text{ \AA}$, the probe-hole current varies strongly with the local field assumed. A quantitative match between simulated and experimental scan diagrams is therefore not possible. Qualitatively, our simulation coincides reasonably well with experimental results. As shown in Fig. B.8 of Appendix B, simulation of adsorption on top of the (110) plane produces a scan diagram completely different from those in Fig. 7.11. It seems that at this low exposure, only the edges of the cluster and the (110) vicinals outside of the (110) plane are covered by hydrogen.

The similarity between simulated and experimental scan diagrams for clusters of different size suggests that chemisorption on the cluster edges and on the (110) terraces outside of the (110) plane is rapid. This is consistent with our earlier conclusions from work function studies. Thus by combining work function measurement with the scanning technique we can achieve a better understanding of chemisorption on flat surfaces as affected by surface defects.

7.3b. Adsorption on a flat (110) plane

In these experiments, chemisorption of hydrogen on a perfect (110) plane is monitored both by measuring the change in the work function and by the scanning technique. These results are given in Fig. 7.13, with the inset showing the changes in the work function. Scan diagrams corresponding to various points in the work function curve are drawn at the bottom of Fig. 7.13, and are labelled accordingly.

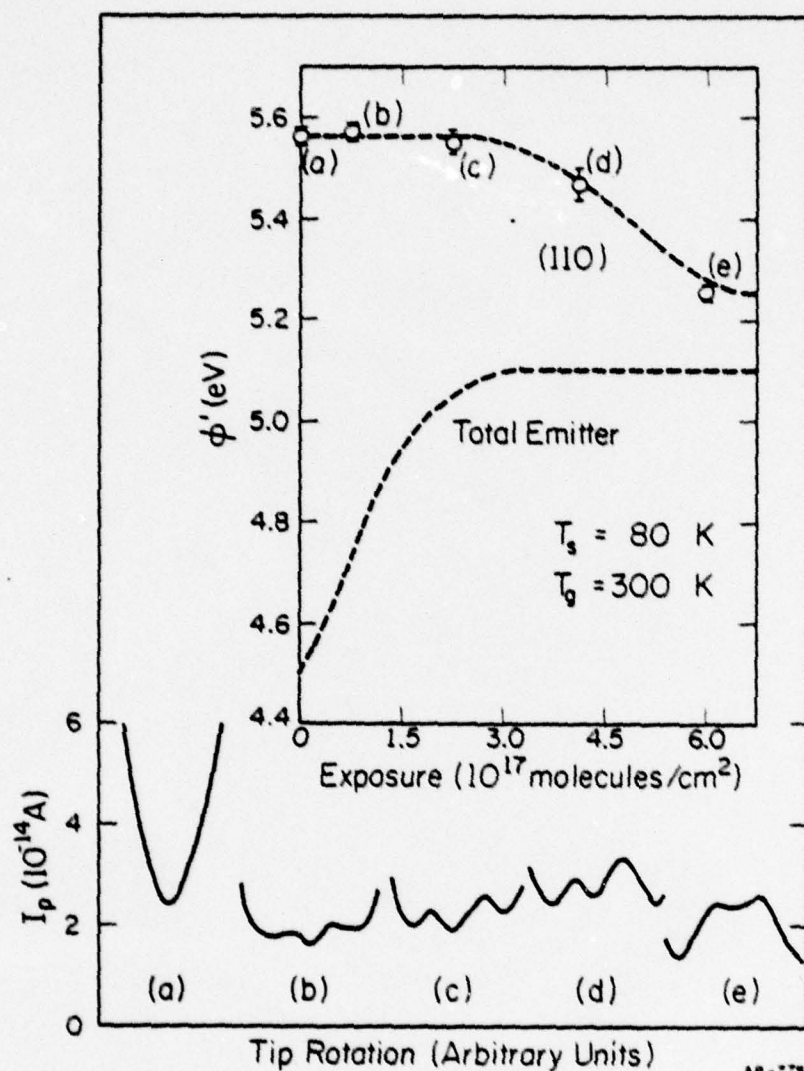


Fig. 7.13. Variation of scan diagrams with exposure to hydrogen for a flat tungsten (110) plane. Work function changes are shown in the inset. Hydrogen exposures in 10^{17} molecules/cm²: (a) 0; (b) 0.75; (c) 2.25; (d) 4.25; (e) 6.0.

The changes in the scan diagram after the first exposure (b) have already been discussed in the last section. When the emitter is further exposed to a total of 2.25×10^{17} molecules/cm² of hydrogen (Fig. 7.13c), the work function of the (110) plane remains essentially unchanged. However, a significant change in the scan diagram is observed. As shown in Fig. 7.13c, the two maxima become more prominent and the emission current at the center of the (110) plane becomes higher. This trend becomes more pronounced when the emitter is further exposed to a total of 4.13×10^{17} molecules/cm² of hydrogen (d). The work function of the (110) plane now drops by ~ 0.1 eV. At saturation, at an exposure of $\sim 7 \times 10^{17}$ molecules/cm², the scan diagram (e) again changes drastically. The two maxima seem to merge together although they still remain distinguishable. More pronounced is a further drop of the emission from the outside (110) terraces. From Fig. 7.13 it is apparent that the changes in the scan diagrams are far more complicated than the changes in the work function.

Although quantitative interpretations are difficult, we may still extract some useful information from this type of experiment. Consider first the changes in the scan diagrams between exposure of 7.5×10^{16} (b) and 2.25×10^{17} molecules/cm² (c). From the experiments in the last section, and from work function measurements on surface clusters, we have reached the conclusion that chemisorption on the plane edges and on the (110) vicinals is rapid. At an exposure of 7.5×10^{16} molecules/cm², the plane edges, as well as the (110) vicinals, are already covered by hydrogen, as indicated by the decrease in the emission current from these regions. If the changes in the scan diagram between exposures of 0.75 and 2.25×10^{17} molecules/cm² are caused by the continued adsorption on

the plane edges or the (110) vicinals, then we should see a decrease in the emission current from these regions. However, an increase in the emission current is seen. The changes in the scanning diagrams between these two exposures therefore must be caused by chemisorption on the (110) plane itself. However, in spite of this significant change in the scanning diagram, the work function measured at the center of the (110) plane is unchanged. We must therefore conclude that hydrogen chemisorbed on the (110) plane is not uniformly distributed on the plane. Regions near the edges of the plane must have a higher hydrogen concentration than at the center, so that the work function measured at the center of the plane can remain unaffected while enough hydrogen is still chemisorbed on the (110) to cause a significant change in the scan diagram. This explanation is supported by our earlier results that defects can accelerate chemisorption on a flat surface. An adsorbate concentration gradient is exactly what is expected, if chemisorption on the (110) plane is promoted by the plane edged, and if hydrogen diffusion on the (110) is slow.

As an attempt to further confirm such a concentration gradient of chemisorbed hydrogen on the (110) plane, we have also simulated scan diagrams as a function of surface coverage. These are shown in Fig. 7.14. Two different distributions of hydrogen on the (110) are used in these simulations. In Fig. 7.14a, it is assumed that hydrogen is uniformly distributed over the (110) plane. As a reference, experimental scan diagrams are shown in Fig. 7.14b. The scan diagrams obtained by assuming a step function distribution along the outer edges of the (110) plane are given in Fig. 7.14c. These simulated scan diagrams approximate the real diagrams only qualitatively, since the local electric field is not known to any accuracy.

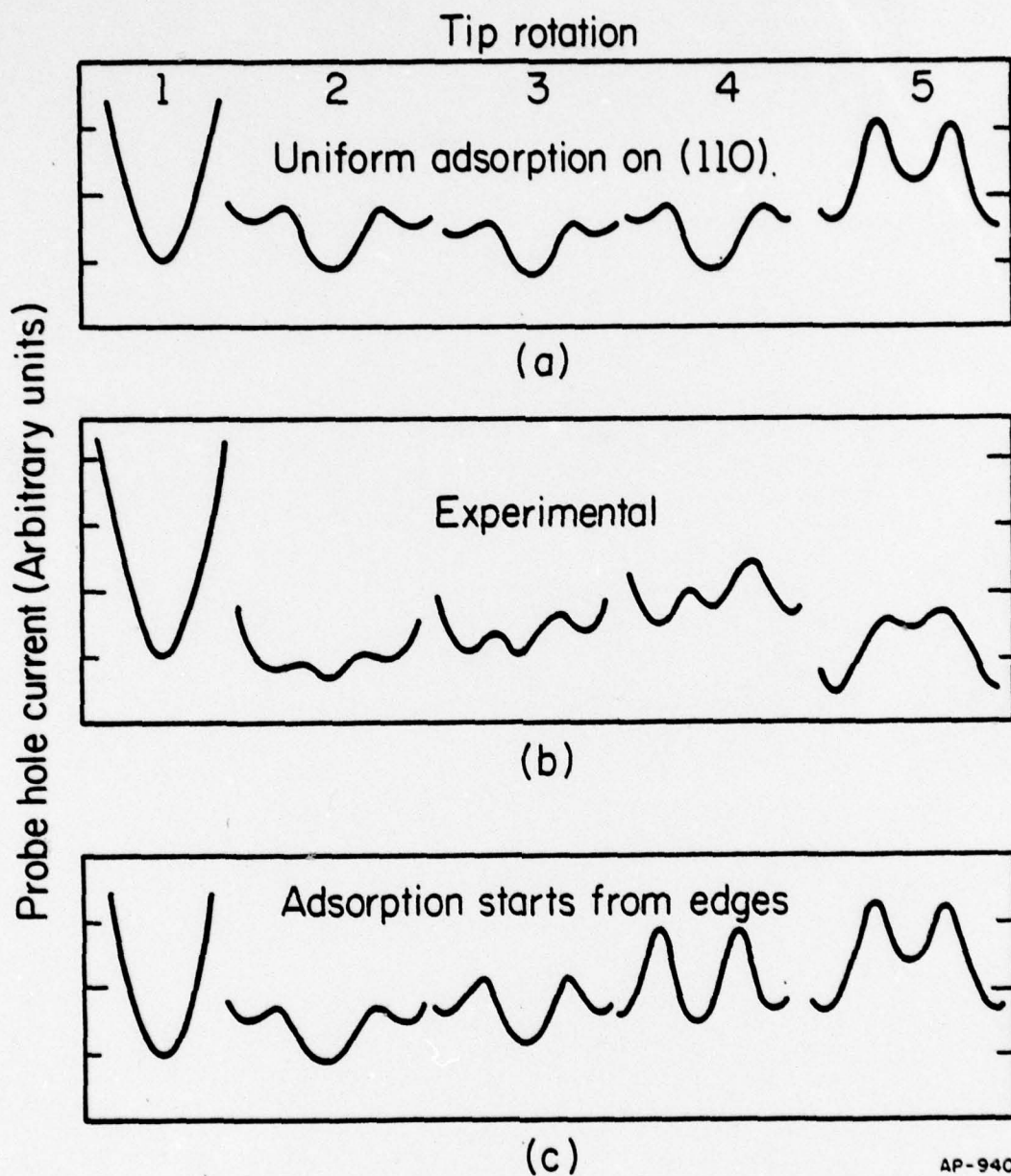


Fig. 7.14. Computer simulated scan diagrams for a flat (110) plane exposed to hydrogen. 1. Clean surface; 2. (110) terraces outside of the (110) plane covered by hydrogen; 3. 10% of the (110) plane covered by hydrogen; 4. 30% covered; 5. 90% covered. (a),(c): computer simulated diagrams; (b): experimental diagrams.

The initial two scan diagrams for both Fig. 7.14a and 7.14c are identical, since adsorption on the (110) has not begun; they are also similar, at least qualitatively, to the experimental scan diagrams. The third scan diagram is different: in order to keep the work function change within the value actually observed (< 0.05 eV), less than 10% of the (110) can be covered by hydrogen if the adsorbate is uniformly distributed. As evident from Fig. 7.14a, the scan diagram for such a small surface coverage does not differ significantly from the second scan diagram, for which the (110) plane is clean. For a surface with chemisorption concentrated on regions near the edges of the plane, approximately 10% of the radius (starting from the edges) may be covered by hydrogen before the work function changes significantly. As is clear from Fig. 7.14c, the scan diagram obtained for such a surface differs substantially from that of a clean (110) plane. The changes in the shape of these scan diagrams are qualitatively similar to those observed experimentally. From this simulation it appears that non-uniformly distributed adsorbate on the (110) plane accounts for our experiments better than a uniformly distributed adsorbate.

At saturation, the work function of the (110) plane drops by 0.3 eV. Accompanying this work function drop is a large change in the shape of the scan diagram. As is clear from Fig. 7.13 (e), emission from outside of the (110) plane drops by more than 50%. This scan diagram cannot be produced by our simulation program.

The diminution of the emission outside of the (110) plane cannot be attributed to chemisorption on the (110) alone. It can only be interpreted as due to the formation of a new adsorption state on the (110) vicinals. Some support for this view comes from the direct observations on clusters;

after a surface is saturated with hydrogen, a large drop in the emission current is observed on surfaces with clusters, but not on a flat (110) plane. It appears that defects also have something to do with the formation of this state. The exact relation, however, is not known from our experiments.

In summary, the effect of defects on chemisorption may be studied by monitoring the changes in the scan diagrams when a surface is exposed to gas. Even with the help of computer simulations, quantitative results are still difficult to obtain this way. However, scan diagrams are valuable as a supplement to the more quantitative work function measurements. By using these techniques in combination we can get a clearer picture about the effect of defects on chemisorption.

7.4. Summary

In this chapter we have investigated the effect of structural defects on chemisorption by monitoring changes on surfaces with different structures. The influence of steps during chemisorption in the hydrogen-Pt(111) system has been suggested in the past [4,6]. However, studies in which surface conditions are controlled to a degree comparable to ours have never been reported. From our results, it is evident that defects play a very important role in promoting adsorption on flat surfaces. A quantitative analysis of these results will be presented in the next chapter. We conclude by summarizing our observations:

1. From our direct measurements on clusters, the chemisorption of hydrogen on defects such as the edges of a plane (or a cluster) is rapid.
2. The presence of a cluster on top of a flat W(110) surface accelerates chemisorption on this surface greatly. In other words, chemisorption on the flat (110) is promoted by the defects.

3. The rate of promotion of chemisorption by defects appears dependent on the detailed surface geometry. Observations on clusters suggest that chemisorption on top of a plane is slower than on the adjacent (110) flats.

4. Observations by the scanning technique, combined with work function measurements, indicate that at 80 K chemisorption on the (110) plane begins near its edges.

5. The scanning technique also leads to the impression that a new adsorption state forms on the high-step-density (110) terrace after the (110) plane is saturated by hydrogen.

CHAPTER VIII

DISCUSSION

8.1. The promotion of chemisorption by defects

Experiments in Chap. VII have shown that the adsorption of hydrogen on a flat W(110) surface can be promoted by the presence of structural defects. The extent of promotion has only been discussed qualitatively. Here we shall analyze these experiments more quantitatively, paying special attention to the hydrogen-W(110) system.

8.1a. A summary of experimental findings

A detailed model for the promotion of chemisorption on a flat (110) by defects present on it can be constructed from the experimental results. The relevant results for the chemisorption of hydrogen on the W(110) can be classified into four categories, according to experimental techniques and sample size:

A. Field emission studies on perfect (110) planes

1. A long incubation period is observed for chemisorption when $T_s \leq 80 \text{ K}$ [3].
2. The rate of chemisorption depends strongly on surface temperature [3].
3. At 38 K, hydrogen is adsorbed in a different state, probably molecular. This state is completely removed by heating to $< 66 \text{ K}$ [3].
4. Hydrogen adsorbed as atoms on surfaces other than the (110) is immobile below $\sim 150 \text{ K}$ [134].

B. Direct observations on surface clusters (Chap. VII)

5. The rate of chemisorption on defects (plane edges) is fast, comparable to that on the rough surfaces.
6. Chemisorption on a flat (110) surface is greatly enhanced by the presence of defects.
7. Chemisorption on the (110) terraces appears faster than that on top of the (110) plane.
8. When a defect (a cluster of atoms) is present on a flat (110) surface, hydrogen adsorbed at low temperatures (~ 30 K) converts partially to tightly bound atomic hydrogen when the surface is warmed to ≤ 80 K.

C. Observations combining the scanning technique with work function measurements (Chap. VII)

9. On a flat (110) plane, the region near the edges appears more densely populated than the center of the plane when exposed to hydrogen.
10. A new state appears on the (110) terraces outside of the (110) plane when the (110) plane is completely saturated by hydrogen.

D. Condensation and flash desorption studies on macroscopic (110) surfaces

11. The initial sticking coefficient does not depend strongly on the pressure of the gas and the temperature (80-300 K) of the surface [135].
12. The sticking coefficient decreases linearly with increasing surface coverage [135].
13. Two atomic states exist simultaneously [136].

8.1b. Models for defect promoted chemisorption

1. Polizzotti's model

The experimental results 1-4 and 11-13 have been incorporated into a model by Polizzotti [3]. His model, discussed briefly in Chap. III, consists of the following four assumptions:

1. Direct dissociation of hydrogen on the W(110) surface is insignificant.
2. Chemisorption on the (110) surface occurs via surface diffusion of hydrogen adsorbed on steps or plane edges.
3. Hydrogen adsorbed on steps is in equilibrium with the hydrogen in the gas phase according to first order desorption kinetics. That is, the concentration of hydrogen on the steps is proportional to the pressure.
4. The hydrogen adsorbed on the (110) surface is completely mobile at 80 K.

In this model, the first two assumptions successfully account for the long incubation period for chemisorption at low temperatures, the strong temperature dependence of the rate of chemisorption, and the evaporation of molecular hydrogen at $T_g < 66$ K without conversion to tightly bound species. The third assumption accounts for the fact that the sticking coefficient on macroscopic samples is observed to be independent of pressure. The last assumption gives the sticking coefficient a $(1-\theta)$ dependence upon the surface coverage, as observed by Tamm and Schmidt [135], where θ is the fraction of occupied sites relative to the coverage at saturation.

Polizzotti's model can also account for some of the more recent experiments, presented in Chap. VII. The faster rate of chemisorption on defects, and the great enhancement of the rate on the flat (110) by defects (experiments 5-8 listed above) are all predictable from this model. However, the assumption about the mobility of chemisorbed hydrogen on the (110) surface has to be changed in order to account for the higher population near the plane edges, detected in Chap. VII.

In Polizzotti's model, chemisorbed hydrogen is assumed completely mobile on the (110) plane at 80 K. While this does not conflict with the results of earlier experiments, it is incompatible with our observations combining work function measurement with the scanning technique: there the work function measured at the center of the (110) plane stayed unchanged at low exposures, but the scanning diagrams changed significantly, indicating that chemisorption occurred on regions near the edge of the plane but not at the center. If chemisorbed hydrogen is highly mobile at this low temperature, we should not observe such a difference in the concentration. We therefore conclude that hydrogen is immobile on the (110) at this low temperature.

ii. The rate limiting process for chemisorption on W(110)

In order to find a replacement for the last assumption in Polizzotti's model, consider first the rate limiting process for chemisorption on the (110) plane. Even without a detailed model, the rate limiting process can be singled out by the experiments discussed earlier in this thesis:

(a) In the sequential adsorption experiments discussed in Chap. III, the rate of chemisorption of hydrogen on the W(110) plane was greatly enhanced by first saturating the emitter surface, excluding the (110), with nitrogen. If diffusion on the (110) plane itself were the rate limiting process we should not see such an enhancement; if chemisorption on the (110) is limited by diffusion on that surface, changing the gas supply from outside by altering its environment cannot produce drastic changes in the chemisorption rate. We must therefore conclude that the rate limiting process is the rate of gas supply from the plane edges.

(b) At low temperatures (< 50 K), hydrogen adsorbs on a flat (110) as molecules. Upon warming the surface to ≤ 80 K the hydrogen thus adsorbed desorbs without conversion to tightly bound atomic hydrogen. However, if defects, in the form of a cluster of atoms, are present on the (110) surface, conversion to atomic hydrogen occurs upon warming, as detected in Chap. VII. If the diffusion of atomic hydrogen on the (110) were rate limiting, then the conversion from molecular to atomic hydrogen by the defects could not be effective -- sites near the defects would be congested by atomic hydrogen which had not had a chance to diffuse away. The fact that conversion to atomic hydrogen occurs readily on this surface again excludes diffusion on the (110) plane as the rate limiting process.

From these experiments, it is clear that the rate limiting process for chemisorption on the (110) plane is the supply of gas from defects. In Polizzotti's model, a high mobility for the gas on the (110) is assumed, so that in this model diffusion on the (110) plane cannot be

the rate limiting process. Should we simply replace Polizzotti's last assumption by assuming instead a low mobility for chemisorbed hydrogen then we have also changed, though inadvertently, the rate limiting process. This would be in contradiction to our experimental observations.

In order to account for all the experiments we must replace Polizzotti's last assumption in such a way that: (a) the mobility of the atomic hydrogen chemisorbed on the (110) plane must be low enough to allow a concentration difference between the center and the region near the edges of the plane; (b) diffusion on the (110) plane is not the rate limiting process. This apparently paradoxical problem can be solved by invoking the well known mechanism of precipitation following diffusion [137,138]. In this scheme, a particle is able to rapidly diffuse in a solid matrix until it is trapped by a defect or by other particles; once precipitated, the particle is immobilized.

To adapt this mechanism to our processes, we assume that chemisorbed hydrogen is essentially immobile at 80 K. On top of this tightly bound layer, however, hydrogen dissociated at steps or plane edges may adsorb in a loosely bound state and is quite mobile. Diffusion in this overlayer is rapid. When a loosely bound hydrogen reaches an empty site on the (110) surface it may become tightly adsorbed and lose its mobility; in other words, it precipitates when trapped at an empty site. The distribution of the adsorbate formed by this mechanism is determined primarily by the mobility of the tightly adsorbed hydrogen. On the other hand, the rate limiting process need not be the migration of gas on the surface, since now diffusion in the overlayer is rapid.

iii. A modified model

We now outline a modified version of Polizzotti's model, incorporating the diffusion-precipitation mechanism described above. This is defined by the following assumptions:

1. Direct dissociation of hydrogen on W(110) is insignificant.
2. Hydrogen can dissociate only on steps or on plane edges.
3. The ability to dissociate hydrogen is not completely blocked when an edge site is occupied by a hydrogen atom.
4. Hydrogen adsorbed on the (110) plane has a low mobility at 80 K.
5. Once a site, no matter if it is at an edge or on the (110) flat, is occupied by a hydrogen adatom, no other atomic hydrogen may adsorb tightly on it. However, hydrogen may adsorb in a loosely bound, and more mobile form. Hydrogen atoms adsorbed in this mobile form may recombine into molecules and evaporate.
6. An activation energy V_s has to be surmounted for a loosely bound hydrogen to leave a step or an edge site and jump to the adjacent (110) terrace; the activation energy for the same adatom to jump to the top of a (110) plane, V_t , is larger than V_s .

In this model, assumptions 1-3 essentially reformulate more precisely the first two statements of Polizzotti's original model. Assumptions 4 and 5, containing the diffusion-precipitation mechanism, are used to replace Polizzotti's last two assumptions. Assumption 6 is added to provide a distinction between the top of a (110) plane and the (110) terrace outside of it, which is geometrically different from the former.

Our next task is to elucidate how this model can account for the experimental observations. We shall do this by going through the list of relevant experiments given at the beginning of this chapter.

1. Long incubation period at $T_s = 80$ K -- may be explained in the same way as Polizzotti's model. No direct dissociation occurs on the (110); rate is limited by the activated process for a loosely bound hydrogen leaving an edge site and jumping onto the top of the (110) plane.
2. Rate of chemisorption depends on temperature -- the rate limiting process is thermally activated.
3. Molecular hydrogen adsorbed at ~ 38 K does not convert to atomic hydrogen when the surface is warmed up -- direct dissociation on the (110) is insignificant.
4. On surfaces other than the (110), chemisorbed hydrogen is immobile at ~ 150 K -- this is consistent with our assumption that tightly adsorbed hydrogen on the (110) is immobile at 80 K.
- 5,6. Rapid chemisorption on defects; chemisorption on flat (110) enhanced by defects -- these are the bases for the present model.
7. Chemisorption on the (110) terrace is faster than that on top of the (110) plane -- this leads to assumption 6.
8. When defects are present on a (110) plane, molecular hydrogen on the surface can convert to atomic hydrogen when the surface is warmed to 80 K -- this determines the rate limiting process of chemisorption, which in turn leads to the diffusion-precipitation mechanism.

9. Before the (110) plane is completely saturated with hydrogen, the population near the plane edges is higher than that at the center of the plane -- leads to assumptions 4, 5.
10. When the (110) plane is completely saturated, a new state forms on the (110) terraces -- neutral with respect to both Polizzotti's model and this model.

From the above discussion, it is clear that our model can account for all the experimental results on microscopic field emitters. Macroscopic (110) surfaces have quite a different surface geometry compared to microscopic field emitters. We shall discuss the experiments on these crystals in the following section.

iv. Extension to macroscopic surfaces

A macroscopic (110) sample will inevitably consist of alternate steps and (110) terraces. The promotion of chemisorption on such a surface by steps according to our model is illustrated in Fig. 8.1. Hydrogen molecules can only dissociate on steps; the hydrogen atoms adsorbed on the steps in this way are tightly bound and cannot move freely to the (110) terrace at 80 K (Fig. 8.1a). When steps are filled by hydrogen, further dissociation results in loosely bound hydrogen (shown in black); this may diffuse onto the (110) terrace, overcoming an activation energy V_s (Fig. 8.1b). If it can find an empty site on the (110) terrace it may become adsorbed as strongly bound hydrogen, which is assumed to have a low mobility at 80 K. As the (110) terrace is gradually populated by hydrogen, an overlayer of loosely bound

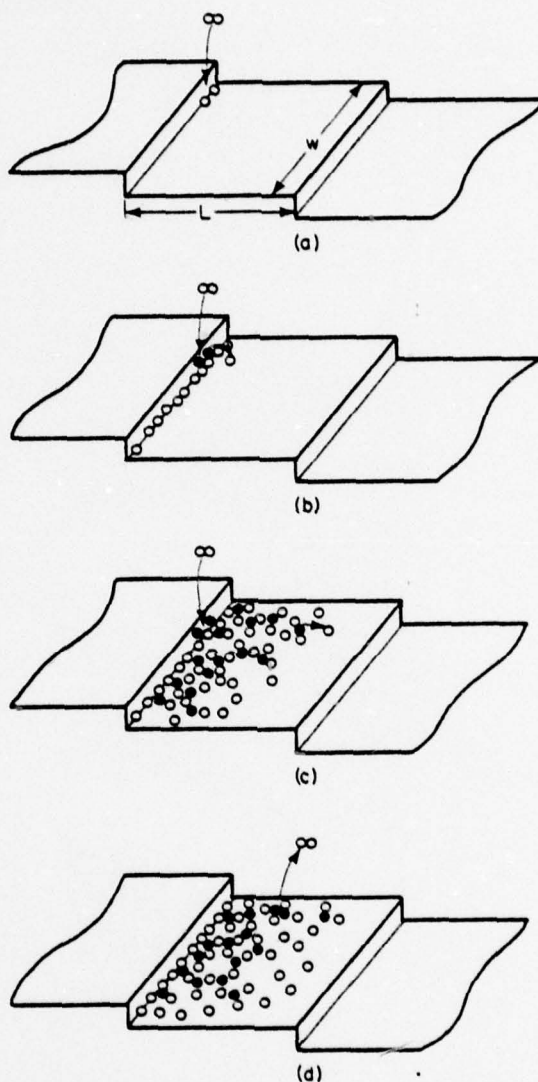
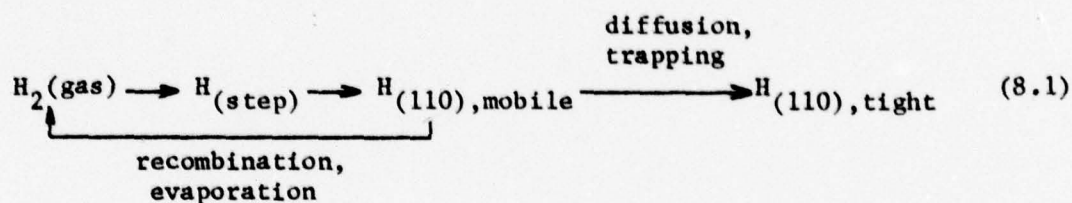


Fig. 8.1. Diffusion-precipitation mechanism on a one-dimensional stepped surface. (a) Hydrogen molecules dissociate on steps; (b) after a step is filled by adatoms, further dissociation produces a loosely bound hydrogen (black) which can jump to the (110) terrace; (c) (110) terrace gradually filled by diffusion of the loosely bound hydrogen; (d) loosely bound hydrogens may recombine and evaporate.

hydrogen is also built up. The rest of the (110) terrace is filled by the diffusion of these mobile hydrogens over the primary layer (Fig. 8.1c). As the population in the overlayer grows, evaporation through the recombination of two loosely bound hydrogen atoms becomes possible, as shown in Fig. 8.1d. According to this model, the adsorption of hydrogen on the (110) surface at $T_s = 80$ K may be represented by the following scheme:



In this reaction scheme, evaporation from steps is ignored, since the area covered by steps is much smaller than the (110) terrace.

From Eq. (8.1) we may estimate approximately the dependence upon temperature, pressure, and surface coverage, of the sticking coefficient on the (110) surface. We shall derive these relations in some detail, since the kinetic processes on macroscopic surfaces are the same as those on field emitters, which we shall discuss later on. For simplicity, assume that the tightly bound atomic hydrogen is completely immobile at the temperature of concern. We shall estimate the sticking coefficient for a geometry similar to that shown in Fig. 8.1, i.e., a (110) surface with steps of infinite length, which can be treated as a one dimensional problem. The filling of the (110) terrace on such a surface is analogous

to the unrolling of a carpet [137]: starting from a step, a uniform layer of tightly bound hydrogen is gradually formed by diffusion from the loosely bound hydrogen in the overlayer. We shall assume that diffusion in this overlayer is rapid and not rate-limiting, to comply with the experimental results. For reasons that will become clear in the next section, we shall ignore the jumping of loosely bound atoms from a step to the top of the adjacent (110). Therefore, in this analysis, a step only promotes chemisorption on the (110) terrace adjacent to it.

Consider a section of the (110) terrace of width wa_0 , as shown in Fig. 8.1. Let the length of the (110) terrace be La_0 , and let the length of the region covered by tightly bound hydrogen, measured from the step, be ya_0 . The unit a_0 is chosen to represent one interatomic distance so that w , L , and y are dimensionless. In addition, we introduce the following definitions:

n_s = number of loosely bound atoms on steps per unit length;

n_{s0} = saturation density of loosely bound atoms on steps;

n_t = number of loosely bound atoms on the (110) terrace per unit area;

n_{t0} = saturation density of loosely bound atoms on the (110) terrace;

θ = fractional coverage = $\frac{ya_0 wa_0}{La_0 wa_0} = y/L$;

R_0 = rate of total impingement on the (110) terrace

= $\frac{P}{\sqrt{2\pi mkT}}$ (total area);

R_{110} = rate of filling on the (110) terrace (atoms/sec).

It is easy to see that the number of mobile hydrogens on the (110) terrace, n_t , must be a function of the loosely bound atoms on the steps, n_s . n_t must increase with increasing n_s , as the loosely bound hydrogen at the step is the only source for the mobile hydrogen on the (110) terrace. We may express n_t as a function of n_s by

$$\frac{n_t}{n_{to}} = b \left(\frac{n_s}{n_{so}} \right)^c, \quad (8.2)$$

where b, c are two dimensionless constants. This particular form is chosen because n_t must vanish when n_s becomes zero.

The rate of change of the number of loosely bound atoms on a step may be obtained by considering the detailed balance

$$\begin{aligned} \frac{d}{dt}(n_s w_{s0}) &= (\text{Rate of dissociation from the gas phase}) \\ &- (\text{Net rate of leaving the step}) \\ &= 2R_o \frac{N_s}{N} s' \left(1 - \frac{n_s}{n_{so}} \right) - (n_s w_{s0}) v_s \exp(-V_s/kT) \cdot \left(1 - \frac{n_t}{n_{to}} \right) \cdot K \quad (8.3) \end{aligned}$$

In this formula, N_s/N is the ratio of sites on the step to the total sites on the surface, s' the sticking coefficient for dissociation on steps, and v_s the attempt frequency for a loosely bound hydrogen leaving the step. Evaporation from steps has been ignored for reasons stated previously. The factor 2 in the first term on the right hand side signifies that such hydrogen molecule dissociates into two atoms. The factor $K \leq 1$ in the second term accounts for the transport of adatoms from the (110) terrace back to the step. The terms $(1 - n_s/n_{so})$ and $(1 - n_t/n_{to})$ give

the probability of finding an available site on the step and on the (110) terrace, respectively. (An "available site" means an empty site in the overlayer. Adatoms in the overlayer are mobile, and are hence randomly distributed.) The ratio N_s/N can be obtained from purely geometrical considerations. For the geometry shown in Fig. 8.1 we have

$$\frac{N_s}{N} = \frac{1}{L}. \quad (8.4)$$

Assuming that a steady state can be approximately established, so that

$\frac{dn_s}{dt} \approx 0$ and $\frac{dn_t}{dt} \approx 0$, then using Eq. (8.4) we may write Eq. (8.3) as

$$R_o \approx \frac{L w a_o n_s v_s \exp(-V_s/kT)}{2s'} \cdot \frac{\left(1 - \frac{n_t}{n_{to}}\right)}{\left(1 - \frac{n_s}{n_{so}}\right)}. \quad (8.5)$$

The rate of change for loosely bound hydrogen on the (110) terrace, n_t , may also be obtained from detailed balance

$$\begin{aligned} \frac{d}{dt}(n_t w a_o^2) &= (\text{Rate of supply from the step}) \\ &- (\text{Rate of recombination and evaporation}) \\ &- (\text{Rate of conversion into tightly bound hydrogen}) \\ &= K(n_s w a_o) v_s \exp(-V_s/kT) \cdot \left(1 - \frac{n_t}{n_{to}}\right) \\ &- \alpha_2 n_t^2 v_2 \exp(-V_2/kT) \cdot (w a_o^2) - R_{110}. \end{aligned} \quad (8.6)$$

In this formula, α_2 is a constant with appropriate dimensions, v_2 is the attempt frequency for a hydrogen molecule to evaporate from the overlayer, and V_2 is the activation energy for evaporation. The dependence of the second term upon the area covered by strongly bound hydrogen is given explicitly by (wya_o^2) , since evaporation can occur only from the overlayer. The left hand side of Eq. (8.6) may be expressed as

$$\begin{aligned} \frac{d}{dt}(n_t wya_o^2) &= wya_o^2 \frac{dn_t}{dt} + \frac{n_t}{n_o} \frac{d}{dt}(wya_o^2 n_o) \\ &= wya_o^2 \frac{dn_t}{dt} + \frac{n_t}{n_o} R_{110}. \end{aligned} \quad (8.7)$$

In this formula, the last term comes from our assumption that the tightly bound hydrogen is completely immobile. The number of tightly bound hydrogens on the surface is therefore given by the area covered times the saturation concentration, n_o . When a steady state is approximately established, $\frac{dn_t}{dt} \approx 0$. We have, from Eqs. (8.6) and (8.7)

$$\begin{aligned} R_{110} &\approx \frac{1}{\left(1 + \frac{n_t}{n_o}\right)} [Kwa_o n_s v_s \exp(-V_s/kT) \cdot \left(1 - \frac{n_t}{n_{to}}\right) - \alpha_2 n_t^2 (wya_o^2) v_2 \exp(-V_2/kT)] \\ &= \frac{1}{\left(1 + \frac{n_t}{n_o}\right)} [Kwa_o n_s v_s \left(1 - \frac{n_t}{n_{to}}\right) \exp(-V_s/kT) - \alpha_1 n_t^2 v_{2L} \exp(-V_2/kT)] \end{aligned} \quad (8.8)$$

where α_1 is defined as $\alpha_1 = \alpha_2 wLa_o^2$.

The sticking coefficient for adsorption on the (110) terrace now can be obtained from Eqs. (8.5) and (8.8) as

$$s = \frac{R_{110}}{R_o} = 2s' \frac{\left(1 - \frac{n_s}{n_{so}}\right)}{L\left(1 + \frac{n_t}{n_o}\right)} \left[1 - \alpha_1 \frac{n_t^2}{Kwa_o n_s} \cdot \frac{\theta}{\left(1 - \frac{n_t}{n_o}\right)} \exp((-V_2 + V_s)/kT) \right]. \quad (8.9)$$

In the above formula we have replaced y/L by θ , the fractional coverage of strongly bound hydrogen. Eq. (8.9) may be further simplified by considering Eq. (8.2). When the (110) terrace is completely saturated, R_{110} must be zero. From Eq. (8.8) we have

$$n_s \left(1 - \frac{n_t}{n_{to}}\right) \propto n_t^2 \quad (8.10)$$

Since n_t/n_{to} is likely to be small, as a first approximation the loosely bound hydrogen on the step n_s must be proportional to the square of the concentration of the loosely bound hydrogen on the (110), n_t . We may therefore rewrite Eq. (8.2) by assigning $c = 1/2$ as

$$\frac{n_t}{n_{to}} \approx b \left(\frac{n_s}{n_{so}}\right)^{1/2}. \quad (8.11)$$

Substituting Eqs. (8.10), (8.11) into Eq. (8.9), we have

$$\begin{aligned}
 s &\approx \frac{2s' \left(1 - \frac{n_s}{n_{so}}\right)}{L \left[1 + b \left(\frac{n_{to}}{n_o}\right) \left(\frac{n_s}{n_{so}}\right)^{1/2}\right]} \left\{1 - \frac{\alpha_1 b v_2}{k n_{so} w a_o v_s} \theta \exp((-V_2 + V_s)/kT)\right\} \\
 &= \frac{2s' \left(1 - \frac{n_s}{n_{so}}\right)}{L \left[1 + b \left(\frac{n_{to}}{n_o}\right) \left(\frac{n_s}{n_{so}}\right)^{1/2}\right]} \left[1 - \gamma \theta \exp((-V_2 + V_s)/kT)\right] \quad (8.12)
 \end{aligned}$$

where $\gamma = \frac{\alpha_1 b v_2}{k w a_o n_{so} v_s}$.

In Eq. (8.12) the constants b and γ depend on the mobility of the loosely bound hydrogen on the (110) terrace, the mechanism for recombination, and other details of surface kinetic processes. Even without knowing these details, however, simply from the form of Eq. (8.12) we can already deduce important features of the sticking coefficient on macroscopic (110) surfaces. It is clear that the sticking coefficient depends linearly on the surface coverage, as experimentally found [139]. Also, the sticking coefficient s depends only weakly on the pressure of gas, as found by Tamm and Schmidt [135]. This follows from the $\left(1 - \frac{n_s}{n_{so}}\right) / \left[1 + b \left(\frac{n_{to}}{n_o}\right) \left(\frac{n_s}{n_{so}}\right)^{1/2}\right]$ dependence on n_s in Eq. (8.12). From Eq. (8.5) we see that n_s is proportional to the rate of impingement R_o , which in turn is proportional to the gas pressure. Assume that $b \approx 1$ and $n_{to} \approx n_o$, then

$$\frac{\left(1 - \frac{n_s}{n_{so}}\right)}{1 + b\left(\frac{n_{to}}{n_o}\right)\left(\frac{n_s}{n_{so}}\right)^{1/2}} = \frac{1 - \frac{n_s}{n_{so}}}{1 + \left(\frac{n_s}{n_{so}}\right)^{1/2}} = 1 - \left(\frac{n_s}{n_{so}}\right)^{1/2}. \quad (8.13)$$

Let $n_s/n_{so} = 0.05$ for a given hydrogen pressure. If we increase the pressure 10 times, then n_s/n_{so} becomes ~ 0.5 ; the sticking coefficient as obtained from Eq. (8.12), using Eq. (8.13), is changed by only a factor of 2. It is thus clear the sticking coefficient does not depend strongly upon the pressure.

The initial sticking coefficient s_o on the (110) surface may be obtained by substituting $\theta = 0$ into Eq. (8.12). We then have

$$s_o = \frac{2s' \left(1 - \frac{n_s}{n_{so}}\right)}{L \left[1 + b\left(\frac{n_{to}}{n_o}\right)\left(\frac{n_s}{n_{so}}\right)^{1/2}\right]}. \quad (8.14)$$

It is clear from this equation that the initial sticking coefficient is independent of the temperature of the surface, as observed by Tamm and Schmidt [135].

From the above discussion it appears that the diffusion-precipitation model for the filling in of the (110) flats from surface defects can describe experimental findings satisfactorily, not only on microscopic surfaces but also on macroscopic samples. In addition, Eq. (8.12) gives a $1/L$ dependence for the sticking coefficient upon the length of the (110) terrace. That is, the shorter a (110) terrace is, the higher the sticking coefficient becomes. This dependence of the sticking

coefficient on surface geometry explains fully the difference in rates observed on macroscopic crystals and on field emitters. For a field emitter, a rather large, perfect (110) plane can be achieved with no defects on it; on macroscopic crystals elimination of all surface defects and steps is impossible. Therefore, the rate of chemisorption on a perfect (110) plane of a field emitter at low temperature is very slow.

We can estimate the initial sticking coefficient for a macroscopic surface from Eq. (8.14). Let the sticking coefficient of dissociation on the steps s' be the same as that measured on rough surfaces, ~ 0.2 [135, 136]. Consider a surface with a step density of about one step per 10 atoms, or $L \sim 10$. Assign quite arbitrarily $b = 1$, $n_{to} = n_o$, and $n_s/n_{so} \sim 0.1$ in Eq. (8.14), we get $s_o \approx 0.03$. This is comparable to the value of 0.07 obtained experimentally [135], but is much larger than the sticking coefficient of hydrogen on the perfect (110) plane of field emitters, ~ 0.002 . It is clear that the higher values observed on macroscopic samples only reflect defect-promoted chemisorption on the surface, rather than the actual rate of dissociation on the (110) plane.

8.1c Chemisorption on field emitters

In the last section we have demonstrated that experimental observations on the (110) terrace may be rationalized if dissociation occurs at steps. On a field emitter, with the help of field evaporation, the number of defects on the (110) surface is controllable. The rate of chemisorption on the surface should vary accordingly. This provides an excellent way of testing our model quantitatively.

The general formulation for the chemisorption rate on field emitters does not differ from that for macroscopic surfaces, except that now the geometry is different. The (110) plane of a field emitter is surrounded by rings of steps and (110) terraces. The promotion of chemisorption on the (110) plane by steps is therefore governed by the activation energy V_t for a loosely bound hydrogen on the step jumping to the top of the (110) plane. Also, the ratio of defects to sites in the (110) plane varies with the size of the plane, roughly as $2/r$, where r is the radius of the plane. The rate of chemisorption on the (110) plane of a field emitter therefore depends critically upon its size and perfection. In the following we shall derive the rate of chemisorption on perfect (110) planes, as well as on surfaces with a cluster on top.

1. Perfect (110) planes

Consider the (110) plane of a field emitter. According to our model, the edges of the plane act as active sites for chemisorption on this plane. The rate of chemisorption on this plane and on the adjacent (110) terraces may be obtained following the same outline as in the last section. Assuming that a steady state can be established, we get, from detailed balance considerations similar to Eq. (8.3), the relation

$$\begin{aligned}
 0 = \frac{d}{dt} (n_s A_s) = & 2R_0 \frac{N_s}{N} s' \left(1 - \frac{n_s}{n_{so}} \right) \\
 & - n_s A_s v_s \exp(-V_s/kT) \cdot \left(1 - \frac{n_t}{n_{to}} \right) \\
 & - n_s A_s v_s \exp(-V_t/kT) \cdot \left(1 - \frac{n_t'}{n_{to}} \right). \quad (8.15)
 \end{aligned}$$

In this formula N_s/N is the ratio of defect sites relative to the total number of available sites in the (110) area, and A_s is the area of the defect. The last term in Eq. (8.15) accounts for the jumping of loosely bound hydrogen from the step onto the top of the (110) plane with an activation energy V_t . In this, n'_t is the density of loosely bound hydrogen on the (110) plane, and n'_{to} is the saturation density of loosely bound hydrogen on the same plane. The rate of chemisorption on the (110) terrace can be obtained following the same arguments as in the last section. In analogy with Eq. (8.6), we now have

$$\frac{d}{dt} [n_t \pi(r_2^2 - r_o^2)] = n_s A_s v_s \exp(-V_s/kT) \left(1 - \frac{n_t}{n_{to}}\right) - \alpha_2 n_t^2 v_2 \exp(-V_2/kT) \cdot \pi(r_2^2 - r_o^2) - R_{110}^{\text{terrace}}, \quad (8.16)$$

where r_o is the radius of the (110) plane, and $r_2 (> r_o)$ is so defined that the region between r_o and r_2 of the (110) terrace is covered by hydrogen. Following the same reasoning leading to Eq. (8.7), we have

$$\frac{d}{dt} [n_t \pi(r_2^2 - r_o^2)] = \pi(r_2^2 - r_o^2) \frac{dn_t}{dt} + \frac{n_t}{n_o} R_{110}^{\text{terrace}} \quad (8.17)$$

When a steady state is approximately established, $\frac{dn_t}{dt} \approx 0$. We have, from Eqs. (8.16) and (8.17), in analogy with Eq. (8.8):

$$R_{110}^{\text{terrace}} \approx \frac{1}{\left(1 + \frac{n_t}{n_o}\right)} \left\{ n_s A_s v_s \exp(-V_s/kT) \cdot \left(1 - \frac{n_s}{n_{so}}\right) - \alpha_1 n_t^2 v_2 \theta_2 \exp(-V_2/kT) \right\}, \quad (8.18)$$

where θ_2 is the fractional coverage for strongly bound hydrogen on the (110) terrace outside of the (110) plane. In order to simplify the appearance,

we may rewrite Eq. (8.18) as

$$R_{110}^{\text{terrace}} \approx \frac{1 - \frac{n_s}{n_{so}}}{1 + \frac{n_t}{n_o}} n_s A_s v_s \exp(-V_s/kT) f(\theta_2). \quad (8.19)$$

In this formula all dependence on the coverage θ_2 has been absorbed into the function $f(\theta_2)$. Substituting Eq. (8.15) into Eq. (8.19), we have

$$R_{110}^{\text{terrace}} \approx 2R_o s' \frac{N_s}{N} f(\theta_2) \frac{1 - \frac{n_s}{n_{so}}}{1 + \frac{n_t}{n_o}} \left[1 + \exp((V_s - V_t)/kT) \cdot \frac{1 - \frac{n_t'}{n_{to}}}{1 - \frac{n_t}{n_o}} \right]^{-1}. \quad (8.20)$$

The rate of chemisorption on top of the (110) plane may be obtained by simply replacing Eq. (8.19) with

$$R_{110}^{\text{top}} \approx \frac{1 - \frac{n_t'}{n_{to}}}{1 + \frac{n_t}{n_o}} n_s A_s v_s \exp(-V_t/kT) f(\theta_1), \quad (8.21)$$

where θ_1 is the fractional coverage on top of the (110) plane. Substituting this into Eq. (8.15), we have

$$R_{110}^{\text{top}} \approx 2R_o s' \frac{N_s}{N} f(\theta_1) \frac{1 - \frac{n_s}{n_{so}}}{1 + \frac{n_t}{n_o}} \left[1 + \exp((V_t - V_s)/kT) \cdot \frac{1 - \frac{n_t}{n_{to}}}{1 - \frac{n_t'}{n_{to}}} \right]^{-1}. \quad (8.22)$$

The ratio of the rate of chemisorption on top of the (110) plane, and that on the (110) terrace, both caused by the defects along the plane edges, is given by

$$\begin{aligned}
 \frac{R_{110}^{\text{top}}}{R_{110}^{\text{terrace}}} &\approx \frac{f(\theta_1)}{f(\theta_2)} \cdot \frac{1 + \frac{n_t}{n_o}}{1 + \frac{n_t}{n_o}} \cdot \exp((-V_t + V_s)/kT) \cdot \frac{1 - \frac{n_t'}{n_{to}'}}{1 - \frac{n_t}{n_{to}}} \\
 &\approx \frac{f(\theta_1)}{f(\theta_2)} \exp((-V_t + V_s)/kT). \quad (8.23)
 \end{aligned}$$

In the last equation, we have assumed that $n_{to} \approx n_{to}'$. That is, the saturation density of loosely bound hydrogen is the same as that of strongly bound hydrogen.

From Eq. (8.23) it is clear that the relative rate of adsorption on top of the (110) plane and that on the adjacent (110) terrace is governed by the difference in the activation energies, $V_t - V_s$. If this value is significantly larger than the thermal energy $\sim kT$, then the rate of chemisorption on top of the (110) becomes very small. Defects surrounding this plane then do not effectively promote chemisorption on the plane. The actual value of $V_t - V_s$, however, cannot be determined from experiments on perfect (110) planes alone. We shall therefore postpone the estimation of the sticking coefficient on the (110) until after we get a value for the activation energies $V_t - V_s$ from studies on surface clusters.

ii. Surfaces with clusters

For a surface with a cluster on top the rate of chemisorption may be obtained by combining Eqs. (8.20) and (8.22). Hydrogen dissociated on the edges of the (110) plane must climb up the step in order to reach the (110) plane; those dissociated on the edge of the cluster can jump onto the (110) with a smaller activation energy V_s . Therefore chemisorption on

the (110) plane caused by the cluster must obey Eq. (8.20), while that caused by the plane edges must be described by Eq. (8.22). As usual, define N as the number of total sites on the (110) area. Let N_c be the number of sites on the cluster edges, and let N_p be the number of sites on the plane edges. The probabilities that a hydrogen molecule impinging on the (110) area will hit the cluster edges, and the (110) plane edges, are given by N_c/N and N_p/N , respectively. Substituting these for N_s/N in Eqs. (8.20) and (8.22), we get the rate of chemisorption on the (110) plane as

$$\begin{aligned}
 R_{110} &= R_{110}(\text{cluster edges}) + R_{110}(\text{plane edges}) \\
 &= R_{110}^{\text{terrace}}(N_s = N_c) + R_{110}^{\text{top}}(N_s = N_p) \\
 &= 2R_o s' \frac{N_c}{N} f(\theta_c) \frac{1 - \frac{n_c}{n_{co}}}{1 + \frac{n_t}{n_o}} \left[1 + \exp((-V_t + V_s)/kT) \frac{1 - \frac{n'_t}{n'_{to}}}{1 - \frac{n_t}{n_{to}}} \right]^{-1} \\
 &\quad + 2R_o s' \frac{N_p}{N} f(\theta_p) \frac{1 - \frac{n_p}{n_{po}}}{1 + \frac{n_t}{n_o}} \left[1 + \exp((V_t - V_s)/kT) \frac{1 - \frac{n_t}{n_{to}}}{1 - \frac{n'_t}{n'_{to}}} \right]^{-1}. \quad (8.24)
 \end{aligned}$$

In this formula, θ_c is the fractional coverage of strongly bound hydrogen on the (110) plane caused by the cluster edges, and θ_p the fractional coverage caused by the plane edges; n_c , n_p are the density of loosely bound hydrogen on the cluster edges and on the plane edges, and n_{co} , n_{po} are the saturation densities of loosely bound hydrogen on the cluster and plane edges. Since the cluster edge is not different from the plane edge,

$n_{co} = n_{po} = n_{so}$. Assume, in addition, $n_c \approx n_p \approx n_s$, and $\frac{n'_t}{n_{to}} \approx \frac{n_t}{n_{to}}$ [140].

We can then approximate Eq. (8.24) by

$$R_{110} \approx 2R_{os'} \frac{1 - \frac{n_s}{n_{so}}}{1 + \frac{n_t}{n_o}} [1 + \exp((V_t - V_s)/kT)]^{-1} \cdot \left\{ \frac{N_c}{N} f(\theta_c) \exp((V_t - V_s)/kT) + \frac{N_p}{N} f(\theta_p) \right\}. \quad (8.25)$$

A comparison with Eq. (8.22) indicates that the second term in Eq. (8.25) is just the rate of chemisorption on a perfect (110) plane. Therefore, the first term in this equation represents the contributions from the cluster to the rate of chemisorption on the (110) plane. The ratio of contributions from cluster edges to that by the plane edges is

$$\frac{R_{110}^{cluster}}{R_{110}^{plane}} = \frac{N_c}{N_p} \cdot \frac{f(\theta_c)}{f(\theta_p)} \cdot \exp((V_t - V_s)/kT). \quad (8.26)$$

From this equation, and from the experiments discussed in Chap. VII, we may estimate the difference between the activation energies V_t and V_s . As we have discussed in Chap. VII, the rate of chemisorption on the (110) is significantly accelerated by a cluster. For a small cluster, the number of edge sites on the cluster, N_c , is much smaller than the number of edge sites of the (110) plane, N_p . In order for the rate on the (110) plane to be significantly altered by the cluster, $\exp((V_t - V_s)/kT)$ must be quite large.

Quantitative values for $V_t - V_s$ may be obtained from the experiments on a small cluster shown in Fig. 7.4. In these experiments a cluster $\sim 6 \text{ \AA}$ in diameter was created on top of an otherwise perfect (110) plane with a diameter of $\sim 80 \text{ \AA}$. For such a surface N_c/N_p is ~ 0.075 . We shall ignore the dependence on coverage of the chemisorption rate, since our measurement of work function is not accurate enough to account for it in any event. Eq. (8.26) may be approximated by

$$\frac{R_{110}^{\text{cluster}}}{R_{110}^{\text{plane}}} \approx \frac{N_c}{N_p} \cdot \exp((V_t - V_s)/kT). \quad (8.27)$$

The rate of chemisorption on a surface with a small cluster on top as compared to that on a perfect (110) plane is then given by

$$\begin{aligned} \frac{\text{Rate on (110) with cluster}}{\text{Rate on a perfect (110)}} &= \frac{R_{110}^{\text{plane}} + R_{110}^{\text{cluster}}}{R_{110}^{\text{plane}}} \\ &= 1 + \frac{N_c}{N_p} \cdot \exp((V_t - V_s)/kT). \end{aligned} \quad (8.28)$$

From Fig. 7.4 the rate of chemisorption on the (110) surface with a small cluster is roughly 30% higher than that on a perfect (110), judging from the total exposure at saturation. Substituting this fact into the above equation, we have:

$$\frac{N_c}{N_p} \cdot \exp((V_t - V_s)/kT) \sim 0.3. \quad (8.29)$$

However, we also have $N_c/N_p \sim 0.075$ and $T = 80$ K, so that $V_t - V_s \sim 0.2$ kcal/mole. It follows that at 80 K, approximately 80% of the loosely bound hydrogen on a plane edge goes to the adjacent (110) terrace, and only about 20% goes to the top of the (110) plane. Therefore, even a small cluster, which has only a few defect sites along its edges, can accelerate the chemisorption on a (110) plane significantly.

iii. The rate of dissociation on plane edges

Now that we know an approximate value for $V_t - V_s$, we can estimate the sticking coefficient s' on plane edges using Eq. (8.22). We shall again ignore the θ dependence, since the coverage of the (110) estimated from the work function change is not accurate enough to account for it. Also, we shall assume that n_t/n_{to} , n'_t/n'_{to} and n_s/n_{so} are all small, so that we can ignore the terms $(1 - n_s/n_{so})$, etc. For a perfect (110) plane, we may then approximate Eq. (8.22) as

$$R_{110} \sim 2R_o s' \frac{N_p}{N} [1 + \exp((V_t - V_s)/kT)]^{-1}. \quad (8.30)$$

Multiplying both sides of the above equation by the time the sample is exposed to gas, t , we get the number of hydrogen atoms on the (110) plane as

$$N_{110} \sim 2N_o s' \frac{N_p}{N} [1 + \exp((V_t - V_s)/kT)]^{-1} \quad (8.31)$$

where $N_{110} = R_{110} t$ = total number of adsorbate atoms on the (110), and $N_o = R_o t$ is the total number of molecules that have struck the (110) region.

From the dashed curve in Fig. 7.4 we estimate that an exposure of roughly 2×10^{17} molecules/cm² is necessary to bring the work function change from zero to $\sim 50\%$ of its saturation value. Since hydrogen adsorbed on the (110) plane is not uniformly distributed, the work function does not necessarily vary linearly with surface coverage. Using the computer simulated $\Delta\phi$ -coverage curve shown in Fig. D.2a, we estimate that $\sim 40\%$ of the (110) plane is covered by hydrogen when the work function reaches $\sim 50\%$ of its saturation value. For a (110) plane ~ 80 Å in diameter we get $N_p/N \sim 0.15$ and $N_{110} \sim 160$. At 80 K we have $1 + \exp((V_t - V_s)/kT) \approx 5$, and

$$N_o = 2 \times 10^{17} \text{ (molecules/cm}^2\text{)} \times 5000 \text{ (Å}^2\text{)} \times 10^{-16} \text{ (cm}^2\text{/Å}^2\text{)} = 10^5 \text{ molecules.}$$

Substituting these values into Eq. (8.31), we find $s' \sim 0.03$.

The sticking coefficient on plane edges s' obtained from our experiments and Eq. (8.31) is about an order of magnitude smaller than that on rough surfaces [135]. This is unexpected, since surfaces with high step densities generally show a high sticking coefficient comparable to that on rough surface. This discrepancy may arise partially from ignoring the θ dependence in our estimates. It may also be caused by an inaccurate calibration of the hydrogen exposure -- the hydrogen pressure cannot be directly measured by ionization gauge owing to its interaction with hot filaments [141]. In the following we shall estimate the sticking coefficient on the total emitter so that we can make a comparison between the rate on plane edges and on rough surfaces in our experiments alone.

The sticking coefficient of hydrogen on the emitter as a whole can be estimated from the $\Delta\phi$ -exposure curve in Fig. 7.4, assuming that the change in work function is proportional to the surface coverage θ . Assume a $(1 - \theta)^2$ dependence for the dissociative chemisorption on the emitter as a whole. The average rate of chemisorption on the total emitter is then given by

$$R'_t = 2R'_0 s'_0 (1 - \theta)^2, \quad (8.32)$$

where R'_t is the rate of chemisorption per unit area on the emitter as a whole, R'_0 the rate of impingement per unit area, and s'_0 the initial sticking coefficient on the emitter as a whole. The number of hydrogen adatoms per unit area on the emitter surface is given by integrating Eq. (8.32) with respect to time:

$$n_{te} = \int_0^t R'_t dt = 2R'_0 s'_0 \int_0^t (1 - \theta)^2 dt. \quad (8.33)$$

Substituting $\theta = n_{te}/n_{teo}$, where n_{teo} is the saturation adsorbate density on the total emitter, into the above equation, we have

$$\theta n_{teo} = 2R'_0 s'_0 \int_0^t (1 - \theta)^2 dt. \quad (8.34)$$

We can solve for θ as a function of time by differentiating Eq. (8.34), we get

$$\frac{d\theta}{dt} = \frac{2R'_0 s'_0}{n_{teo}} (1 - \theta)^2. \quad (8.35)$$

This differential equation can be solved by rearranging variables:

$$\frac{d\theta}{(1 - \theta)^2} = \frac{2s'_0}{n_{teo}} R'_0 dt. \quad (8.36)$$

Integrating both sides, we get

$$(1 - \theta)^{-1} + C = \frac{2s'_0}{n_{teo}} \chi, \quad (8.37)$$

where C is an integration constant, and $\chi = \int R'_0(t) dt$ is the total exposure.

The integration constant C can be determined from the initial condition

$\theta(0) = 0$. We then get the fractional coverage θ as a function of total exposure

$$\theta(\chi) = \frac{2s'_0 \chi}{n_{teo} + 2s'_0 \chi}. \quad (8.38)$$

From this relation, and from the $\Delta\phi - \chi$ curve in Fig. 7.4, we estimate the initial sticking coefficient of hydrogen on the emitter as a whole as $s'_0 \sim 0.01$.

The sticking coefficient on plane edges s' estimated from Eq. (8.31) therefore is comparable to that on the total emitter estimated from our experiments. The discrepancies between our values and others' are probably caused by differences in the exposure calibration. However, it is the relative rate of chemisorption on plane edges and on smooth planes that is most interesting in our work. Since the hydrogen exposure in our experiments is highly reproducible, the relative rate of chemisorption is not affected by inaccuracies in the calibration. In the following discussions, we shall pay attention only to the rate of chemisorption relative to that on the total emitter.

iv. The rate of chemisorption on flat (110)
planes as promoted by plane edges

From last section we get the sticking coefficient for dissociation on plane edges as $s' \sim 0.03$, comparable to that on the emitter as a whole. The rate of chemisorption on a perfect (110) plane caused by defects can be estimated, using this s' , from Eq. (8.22). Ignore again, the θ dependence and the concentration dependence of the rate. That is, let $f(\theta_1) = 1$, $n_t/n_{to} \approx n'_t/n'_{to}$, and let $n_s/n_{so} \ll 1$. Eq. (8.22) then becomes Eq. (8.30):

$$R_{110} \approx 2R_0 s' \frac{N_p}{N} [1 + \exp((V_t - V_s)/kT)]^{-1}.$$

The sticking coefficient for defect-promoted chemisorption on the (110) plane is given by

$$s = \frac{R_{110}}{R_0} \sim 2s' \frac{N_p}{N} [1 + \exp((V_t - V_s)/kT)]^{-1}. \quad (8.39)$$

For a (110) plane with a diameter $\sim 80 \text{ \AA}$ we get $N_p/N \sim 0.15$. Substituting this, and $1 + \exp((V_t - V_s)/kT) \sim 5$, into the above equation, we get the sticking coefficient on the (110) due to the edges as $s \sim 0.002$. This is about 15 times smaller than the sticking coefficient on plane edges.

It is interesting to compare this sticking coefficient with that obtained experimentally, so that the percentage of direct dissociation on the (110) plane may be determined. For this purpose, assume a $(1 - \theta)$ dependence of the sticking coefficient, according to experiments on macroscopic crystals [135]. The rate of direct chemisorption on the (110) plane is then given by

$$\frac{dn_{110}}{dt} = R'_0 s_0 (1 - \theta) \quad (8.40)$$

where n_{110} is the number of adatoms per unit area on the (110) plane, R'_0 the rate of impingement per unit area, and s_0 the initial sticking coefficient on the (110). Using $\theta = n_{110}/n_0$, where n_0 is the saturation density of adatoms on the (110) plane, we may rewrite Eq. (8.40) as

$$\frac{d\theta}{1 - \theta} = \frac{s_0}{n_0} R'_0 dt. \quad (8.41)$$

Integrating both sides, and using the initial condition $\theta(0) = 0$, we get

$$\theta(X) = 1 - \exp\left(-\frac{X}{n_0} s_0\right), \quad (8.42)$$

where X is the total exposure per unit area. From experiments in Chap. VII, an exposure of approximately 2×10^{17} molecules/cm² of hydrogen is necessary to bring about a work function change $\sim 50\%$ of saturation. From Fig. D.2a [Appendix D], this work function change corresponds to a $\theta \sim 0.4$. Let $n_0 \sim 1.4 \times 10^{15}$ atoms/cm². From Eq. (8.42) we get the value for s_0 as $s_0 \sim 0.003$.

Thus, the sticking coefficient obtained experimentally ($s_0 \sim 0.003$) is comparable to that estimated from defect-promoted chemisorption, $s \sim 0.002$. We conclude, therefore, that direct dissociation of hydrogen on the (110) plane does not contribute significantly. The observed change on the (110) surface is primarily due to chemisorption promoted by plane edges. We shall, however, derive an upper limit for the sticking coefficient on the (110) caused by direct dissociation in a later section.

8.1d. The variation of sticking coefficient with surface geometry

In the last section we have estimated the sticking coefficient on plane edges s' as comparable in magnitude to that on the rough surfaces of the emitter. The rate of chemisorption on a smooth (110) plane, as promoted by plane edges, was found much lower than that on plane edges. According to our model, the rate of chemisorption on the (110) should vary with different defect geometries; the rate of chemisorption on the plane edges, however, should be independent of surface geometry. If our model is correct, then these effects should be revealed in experiments on surfaces with different size clusters on top. In Chap. VII, this trend is indeed observed. Here we shall analyze these experiments on surface clusters again, and prove that our model can quantitatively account for these results.

i. Sticking coefficient on cluster edges

The sticking coefficient s' on cluster edges and on plane edges should not depend on the geometry of the surface. Surface with clusters on top should have an s' on the same order as that on the edges of a flat (110) plane. For a surface with a cluster on top, the number of adatoms on the (110) can be derived from Eq. (8.25) as

$$N_{110} \approx 2N_0 s' [1 + \exp((V_t - V_s)/kT)]^{-1} \cdot \left\{ \frac{N_c}{N} \exp((V_t - V_s)/kT) + \frac{N_p}{N} \right\}, \quad (8.43)$$

where N_{110} and N_0 are defined in the same way as in Eq. (8.31). In this formula, the θ dependence of the rate of chemisorption has been ignored.

Also we have assumed that $n_s/n_{so} \ll 1$, and $n_t/n_{to} \approx n'_t/n'_{to}$.

For a small cluster at the center of the (110) plane, the exposure necessary to bring about a 50% decrease in the work function from its maximum value is $\sim 1.5 \times 10^{17}$ molecules/cm² (Fig. 7.4). Corresponding to this work function change, approximately 16% of the (110) surface is covered by hydrogen according to our computer simulation shown in Fig. D.5. From this we estimate the number of hydrogen adatoms on the (110) as roughly $N_{110} \sim 65$. The total number of molecules that have struck the (110) is

$$N_o \sim 1.5 \times 10^{17} (\text{molecules/cm}^2) \times 5000 (\text{\AA}^2) \times 10^{-16} (\text{cm}^2/\text{\AA}^2) = 7.5 \times 10^4 \text{ molecules.}$$

For a (110) plane ~ 80 \AA in diameter and a cluster ~ 6 \AA in diameter, we have $N_c \sim 4$, $N_p \sim 60$, and $N \sim 400$. Substituting these, as well as $\exp((V_t - V_s)/kT) \sim 4$, into Eq. (8.43), we get a value for the sticking coefficient on plane edges s' as ~ 0.02 . This is quite close to the value of 0.03 obtained from experiments on a perfect (110) plane.

For a surface with an intermediate size cluster on it, the sticking coefficient on plane and cluster edges can be estimated from experiments shown in Fig. 7.6, and from computer simulations shown in Fig. D.4. For a (110) plane ~ 80 \AA in diameter and a cluster ~ 20 \AA in diameter, we have $N_c \sim 60$, and $N_p \sim 60$, and $N \sim 400$. The exposure necessary to bring about a $\sim 50\%$ change in the (110) work function, estimated from Fig. 7.6, is $\sim 7.5 \times 10^{16}$ molecules/cm². Corresponding to this change, $\sim 34\%$ of the (110) region is covered by hydrogen, according to our simulation shown in Fig. D.4. We can estimate the number of hydrogen adatoms on the (110) as $N_{110} \sim 135$, and the total number of molecules that have struck the (110) as

$$N_0 \sim 0.75 \times 10^{17} (\text{molecules/cm}^2) \times 5000 (\text{\AA}^2) \times 10^{-16} (\text{cm}^2/\text{\AA}^2) = 3.75 \times 10^4 \text{ molecules.}$$

Substituting these, as well as $\exp((V_c - V_s)/kT) \sim 4$, into Eq. (8.43), we get $s' \sim 0.05$. This sticking coefficient, obtained from experiments on a surface with an intermediate cluster, has the same order of magnitude as those obtained from experiments on perfect (110) planes, and on surfaces with a small cluster on top.

If our model describes surface events properly, we should expect a similar value for s' on surfaces with a large cluster on top. For a large cluster, such as in the experiments shown in Fig. 7.9, the diameter of the cluster is probably $\sim 40 \text{ \AA}$. Consider the diameter of the (110) plane as $\sim 80 \text{ \AA}$, we have $N_c \sim 30$, $N_p \sim 60$, and $N \sim 400$. As discussed in Chap. VII, from the initial decrease in the work function we conclude that an appreciable area of the (110) plane has already been covered by hydrogen after the first exposure. From our simulation results, shown in Fig. D.3, roughly 35% of the (110) region must be covered before the decrease in the work function becomes appreciable ($|\Delta\phi| > 0.04 \text{ eV}$). Assuming that this is actually the case on the surface, we can estimate N_{110} at ~ 140 . The hydrogen exposure corresponding to a decrease in the work function of $\sim 0.05 \text{ eV}$ is $\sim 7.5 \times 10^{16} \text{ molecules/cm}^2$ (Fig. 7.9). We get $N_0 \sim 3.75 \times 10^4 \text{ molecules}$. Substituting these into Eq. (8.43), we get the sticking coefficient on the edges, $s' \sim 0.02$. Again, this value for s' is quite close to the values we obtained from surfaces having other geometries.

From this discussion it is clear that the rate of chemisorption on the (110) plane depends on the presence of defects on the surface as predicted by our model. The degree to which chemisorption on the (110) surface is promoted is directly proportional to the number of active sites

on the (110) plane. From the fact that the sticking coefficient for dissociation on the edges of clusters and planes obtained from surfaces with different defect geometries is the same, it is evident that our model can quantitatively account for the experiments discussed in Chap. VII.

ii. Sticking coefficient on surfaces with different
size clusters on top

If chemisorption on a flat (110) surface is indeed promoted by dissociation on defects, then the rate of chemisorption on a surface with defects on top should be faster than that on a perfect surface. Also, a surface with a large number of defects on top should react with hydrogen faster than that with a small number of defects. This should be reflected in the sticking coefficient of hydrogen on surfaces with different size clusters on top. We can obtain the sticking coefficient on a surface with a cluster on top simply by rearranging Eq. (8.25). Ignoring again the θ dependence, and assuming that $n_s/n_{so} \ll 1$, and that $n_t/n_{to} \approx n'_t/n'_{to}$, we get

$$s = \frac{R_{110}}{R_o} \approx 2s' [1 + \exp((V_t - V_s)/kT)]^{-1} \cdot \left\{ \frac{N_c}{N} \exp((V_t - V_s)/kT) + \frac{N_p}{N} \right\}. \quad (8.44)$$

Let $s' = 0.03$, and let the radius of the (110) plane be 40 Å. For a (110) plane with a small cluster on it, $N_c \sim 4$, $N_p \sim 60$, and $N \sim 400$. Using $\exp((V_t - V_s)/kT) \sim 4$, we get from Eq. (8.44) the sticking coefficient on this surface, $s \sim 0.0025$. This value is larger than the sticking coefficient on a perfect (110) plane of the same radius 0.0018. For a plane with an intermediate size cluster, $N_c \sim 15$, $N_p \sim 60$, and $N \sim 400$,

we get a sticking coefficient $s \sim 0.0036$ from Eq. (8.44). For a (110) plane with a large cluster on it, $N_c \sim 30$. For such a surface the chemisorption on top of the cluster amounts to $\sim 25\%$ of the total. To include this, we simply add another term to Eq. (8.44):

$$\begin{aligned}
 s &= \frac{R_{110} + R_{110}^{\text{cluster top}}}{R_o} \\
 &\approx 2s' [1 + \exp((V_t - V_s)/kT)]^{-1} \cdot \left\{ \frac{N_c}{N} \exp((V_t - V_s)/kT) + \frac{N_c}{N} + \frac{N_p}{N} \right\} \\
 &= 2s' \left\{ \frac{N_c}{N} + \frac{N_p}{N} [1 + \exp((V_t - V_s)/kT)]^{-1} \right\}. \quad (8.45)
 \end{aligned}$$

From this equation, we get the sticking coefficient on a (110) surface with a large cluster as $s \sim 0.006$.

The variation of the sticking coefficient with surface geometry is expected from our model, since a larger cluster provides more defect sites along its edges. This is observed experimentally on surfaces with different size clusters on top. The initial rate of chemisorption on large clusters is indeed faster than that on smaller clusters. It is from these measurements on surface clusters we are able to establish positively the role of defects on chemisorption.

8.1e. Direct dissociation on the W(110) plane

On a flat (110) plane, hydrogen adsorbs as undissociated molecules at temperatures below ~ 38 K. The hydrogen adsorbed in this form desorbs rather than converting to tightly bound atomic hydrogen when the surface is then warmed to ~ 80 K. This is clear from the return to the clean

value of the (110) work function, as shown in Fig. 7.8. From this we may estimate the activation barrier that must be overcome for direct dissociation on the (110) plane.

Consider a flat (110) surface covered by a monolayer of molecular hydrogen at low temperature. When the surface is warmed to $\lesssim 80$ K, the molecules become unstable. Assuming that no defect is involved, then the molecules can either evaporate or dissociate on the (110) plane and form tightly bound atomic hydrogen. The rate of disappearance for these molecules may be expressed by

$$-\frac{dn_m}{dt} = n_m \nu \exp(-V/kT) + n_m \nu' \exp(-Q/kT). \quad (8.46)$$

In this formula, n_m is the number of hydrogen molecules per unit area, and ν , ν' the attempt frequency for evaporation and dissociation, respectively; V and Q stand for the activation energy for evaporation and dissociation. From our experiments, the rate of evaporation is much higher than the rate of dissociation. As an approximation we may solve Eq. (8.46) without the second term and get the number of hydrogen molecules on the (110) surface as a function of time as

$$n_m \sim n_{m0} \exp(-\nu t \exp(-V/kT)), \quad (8.47)$$

where n_{m0} is the original concentration for molecular hydrogen on the surface. The rate of chemisorption on the (110) caused by direct dissociation is given by the standard rate equation

$$\frac{dn_{110}}{dt} = 2n_m \nu' \exp(-Q/kT), \quad (8.48)$$

where n_{110} is the number of hydrogen adatoms per unit area. The factor 2 on the right hand side of this equation comes from the fact that each hydrogen molecule dissociates into two atoms. Substituting Eq. (8.47) into (8.48) and integrating over time t , we get the number of hydrogen adatoms on the (110) as a function of time

$$n_{110} = 2n_{mo} \frac{v'}{v} - \exp((-Q+V)/kT) \cdot [1 - \exp(-vt \exp(-V/kT))] \quad (8.49)$$

A lower limit for the activation energy for dissociation on the (110) surface, Q , may be estimated from Eq. (8.49). Assume that we can detect the existence of 1/100 monolayer of hydrogen on the surface. Then the fact that no adsorption was observed after warming up the surface indicates that $n_{110}/n_{mo} < 0.01$. The heat of evaporation for hydrogen molecules from a tungsten surface, V , has been determined experimentally both on field emitters [142] and on evaporated films [143]. The value varies from 3 to 4 kcal/mole. Assume further that $v \sim v' \sim kT/h$
 $\sim 2 \times 10^{12} \text{ sec}^{-1}$, and let $t = 10 \text{ sec}$. Substituting these, as well as $V = 4 \text{ kcal/mole}$, and $T = 80 \text{ K}$, into Eq. (8.49), we have

$$\exp((-Q + V)/kT) < 0.0051.$$

From this we get a lower limit for the activation energy for the direct dissociation on the (110) plane $Q > 4.9 \text{ kcal/mole}$.

The lower limit estimated for the activation energy of dissociation Q is about 20% higher than the activation energy for evaporation. Even if the actual activation energy for dissociation is quite close to this minimum value, this 20% edge over the activation energy for evapora-

tion is enough to prevent chemisorption on the (110) plane. The probability that a hydrogen molecule adsorbed on the (110) plane will evaporate compared to the probability that it will dissociate is given by $\frac{v}{v^*} \exp((Q - V)/kT)$. At 80 K, at least 99% of the molecules will evaporate; less than 0.5% will dissociate on the (110). Assume quite arbitrarily that the probability that a hydrogen impinged on the surface will be adsorbed as a molecule is 0.5. Then we can estimate a sticking coefficient for dissociative chemisorption on the (110) plane at $T_s = 80$ K as $s < 0.002$.

A direct comparison between the sticking coefficient for direct dissociation and that caused by defect-promoted chemisorption is difficult from our experiments. The sticking coefficient for direct dissociation estimated above does not depend upon experimental exposure calibrations, but that for defect-promoted chemisorption is affected by errors in the exposure calibration. To solve this problem, we shall compare only the sticking coefficients relative to that on rough surfaces. The ratio of the upper limit for the sticking coefficient for direct dissociation on the (110) relative to that on rough surfaces at 80 K is

$$\frac{s(\text{direct dissociation})}{s(\text{rough surfaces})} \sim \frac{0.002}{0.2} = 0.01.$$

The sticking coefficient for defect-promoted chemisorption on the (110) plane relative to that on rough surfaces, obtained from the analysis shown in previous sections, is

$$\frac{s(\text{defect-promoted, expt.})}{s(\text{rough surfaces, expt.})} \sim \frac{0.002}{0.03} \sim 0.07$$

Therefore, the upper limit to the rate of direct dissociation on the (110) plane at 80 K is at least one order of magnitude lower than the rate of defect-promoted chemisorption. The rate of direct dissociation thus estimated is at least 100 times slower than the rate of chemisorption on rough surfaces and on plane edges. We conclude that on the (110) plane of tungsten, direct dissociation of hydrogen is insignificant compared to defect-promoted chemisorption.

8.1f. Diffusion on the (110) plane

Even with the help of computer simulation, the variation of the scanning diagrams with adsorption is not quantitative enough to yield information about the actual concentration profile for hydrogen on the (110) plane. This makes it impossible to estimate with any accuracy the rate of diffusion for hydrogen on the (110) plane. However, merely from the fact that the mobility of hydrogen on the (110) is limited we may already get some feeling about the diffusion coefficient.

If the diffusion length of hydrogen during the time of one exposure is larger than the radius of the (110) plane, then the surface should be covered by gas quite uniformly, even though dissociation can only occur at plane edges. The fact that this is not observed indicates that the diffusion length $\sqrt{\overline{r^2}}$ must be smaller than $\sim 40 \text{ \AA}$, the radius of the (110) plane. The diffusion length is related to the diffusion coefficient D via the formula [144]

$$\overline{r^2} \sim 4D \tau, \quad (8.50)$$

where $\tau \sim 100$ sec is the time for one exposure. We therefore can get the upper limit for the diffusion coefficient as $D = 4 \times 10^{-16} \text{ cm}^2/\text{sec}$. Writing as usual $D = D_0 \exp(-V_d/kT)$, with $D_0 \sim 10^{-3} \text{ cm}^2/\text{sec}$, yields an activation energy $V_d > 4.6 \text{ kcal/mole}$.

The migration of hydrogen on tungsten surfaces other than the (110) becomes appreciable at surface temperatures from 150 - 180 K. On the (110) plane, the temperature for the onset of diffusion should be lower, as the surface potential is smoother. Assuming quite arbitrarily that the diffusion length for hydrogen on the (110) is $\sim 100 \text{ \AA}$ at 150 K, then we may estimate the upper limit for the activation energy for diffusion. Using again Eq. (8.50), and letting $\tau \sim 100$ sec, we get $D \sim 2.5 \times 10^{-15} \text{ cm}^2/\text{sec}$. With $D_0 \sim 10^{-3} \text{ cm}^2/\text{sec}$, we get the upper limit for the activation energy $V_d \lesssim 8.0 \text{ kcal/mole}$. From these rough estimates, the activation energy for diffusion on the (110) plane lies within the range $4.6 < V_d < 8 \text{ kcal/mole}$.

8.1g. Summary

In this section we have analyzed the experiments in Chap. VII more quantitatively, according to a refined version of Polizzotti's model. All the experimental results, both on macroscopic and on microscopic surfaces, can be fully explained by dissociation on defects. From our experiments on surfaces whose geometry have been controlled to an unprecedented degree, we have been able to deduce for the first time the rate of dissociation on surface steps and on plane edges. On the (110) plane the rate of dissociation at plane edges is found at least two orders of magnitude higher than that on the flat (110). Therefore, chemisorption on the (110) flats can be promoted effectively by defects.

The lower limit for the activation barrier which prevents dissociation on the (110) plane has been estimated as $Q \geq 4.9$ kcal/mole. From this, and from the heat of evaporation, $V \sim 4$ kcal/mole, the upper limit for the sticking coefficient for direct dissociation on the (110) has been estimated as $s \sim 0.002$. The value is lower than the sticking coefficient on the (110) plane for chemisorption caused by defects.

Finally, the activation energy for the diffusion of hydrogen on the (110) plane has been estimated as $4.6 < V_d < 8$ kcal/mole.

8.2. Chemisorption of hydrogen on Re(0001)

The adsorption of hydrogen on the (0001) plane of rhenium is quite similar to that on the W(110) plane. It is therefore reasonable to assume that the mechanism of chemisorption on the Re(0001) is the same as that on the W(110). The chemisorption of hydrogen on the (0001)Re has not been studied by the methods discussed in Chap. VII. However, some information may still be obtained from experiments presented in Chap. V.

8.2a. Mechanism of chemisorption

Two experiments discussed in Chap. V give direct support for the diffusion-precipitation model proposed earlier in this chapter. After a rhenium emitter is saturated with hydrogen, heating to ~ 900 K desorbs the hydrogen from the (0001) plane almost completely, but leaves the rest of the emitter still covered by hydrogen. If this same emitter is then cooled to 80 K and re-exposed to hydrogen, the rate of chemisorption on the (0001) plane is much faster than on a (0001) plane of a clean rhenium emitter, as shown in Fig. 5.6. The condition of the (0001) plane on the

clean emitter and on the emitter dosed by hydrogen and then heated to 900 K is essentially the same. If chemisorption on the flat surface is caused by direct dissociation on that surface, we should not observe any difference in the rate of chemisorption between these two (0001) planes. The difference in the rate of chemisorption observed thus cannot be explained by any direct process; it must be attributed to changes in the state of adsorption on the rest of the emitter surface. This is in direct support of the first assumption of our model, namely that the direct dissociation on the flat surface is negligible.

The (0001) plane of rhenium is quite inert to nitrogen adsorption at 300 K, as discussed in Chap. V. If a rhenium emitter is first saturated with nitrogen at 300 K and then cooled to 80 K, the (0001) plane remains bare. When this emitter is then exposed to deuterium, the rate of chemisorption of deuterium on the (0001) plane becomes much faster than that for a clean emitter, as evident from Fig. 5.12. This change in the rate of chemisorption must be attributed to the change in the state of adsorption on the rest of the emitter surface. Direct dissociation on the (0001) plane cannot be the significant process for the chemisorption on this plane.

The strong temperature dependence of the rate of chemisorption of hydrogen on the (0001) plane may be explained in a manner similar to that for the hydrogen-W(110) system. At high enough temperatures ($\geq 200\text{K}$) the migration of hydrogen adatoms is fast enough that the (0001) plane may be filled in by the equilibration of adsorbate on the

surface. At low temperatures (≤ 80 K) the migration of adatoms on the surface is probably too slow so that the (0001) plane has to be filled in by a mechanism similar to the diffusion-precipitation model discussed earlier. A long incubation period is therefore observed at low temperature, as evident from Fig. 5.3.

The chemisorption of hydrogen on the Re(0001) plane is essentially parallel to that on the W(110). The Re(0001) surface has not been studied in as much detail as the W(110), and hence quantitative results are less complete. However, all the experimental results presented in Chap. V can be explained by the model discussed earlier in this chapter. We shall therefore adopt the same mechanism as for the hydrogen-W(110) system, and use it to derive quantitative informations from the experiments discussed in Chap. V.

8.2b. Rate of chemisorption

Without direct observations on surfaces with clusters on top we don't know with certainty whether the activation energy for a loosely bound hydrogen at an edge site jumping to the top of the (0001) plane, V_t , is different from that for jumping to the adjacent (0001) terrace, V_e . A rough idea about the order of magnitude for $V_t - V_e$ may be obtained by considering the temperature dependence of the sticking coefficient from Eq. (8.17); ignoring the θ dependence this may be written as

$$s_{0001} = \frac{R_{0001}}{R_0} \sim \frac{N_p}{N} s' [1 + \exp((+V_t - V_e)/kT)]^{-1}. \quad (8.51)$$

The initial sticking coefficient on the (0001) plane at 200 K roughly estimated from the work function changes in Fig. 5.3, is ~ 2.5 times

that at 80 K. Substituting this into Eq. (8.51) we get $V_t - V_e \sim 0.1$ kcal/mole. This value is only about 1/2 that for the hydrogen-tungsten system, and is somewhat marred by the fact that at 200 K some atomic hydrogen may already diffuse onto the (0001) plane. It nevertheless indicates that the potential barrier that a loosely bound hydrogen must overcome to climb to the top of the plane is still larger than that to go to the adjacent (0001) terraces. At 80 K, approximately 1/3 of the atoms dissociated on the plane edges go to the top of the plane, while 2/3 go to the (0001) terraces.

The sticking coefficient on the edge of the (0001) can also be estimated from Eq. (8.27) once $V_t - V_e$ is known. The initial sticking coefficient on the (001) plane at 80 K may be derived from the work function changes shown in Fig. 5.3 as $s_{0001} \sim 0.0003$. The diameter of the (0001) plane is $\sim 500 \text{ \AA}$ for the thermally formed emitter; this rough value is obtained from its field emission voltage as compared to that for field evaporated emitters, we thus get the sticking coefficient on the plane edges as $s' \sim 0.07$. This value is comparable to that obtained on the tungsten-hydrogen system, ~ 0.03 . From the fact that the rate of dissociation on plane edges (given by $s' \sim 0.07$) is more than 200 times larger than the upper limit on the (0001) plane ($s_{0001} \sim 0.0003$), we conclude that chemisorption on the (0001) plane can be effectively promoted by defects.

8.3. Chemisorption of hydrogen on Ir(111)

The rate of chemisorption for hydrogen on the (111) plane of iridium is quite different from that on both the W(110) and the Re(0001) planes. No induction period is observed for chemisorption on the Ir(111) at low temperatures. The rate of chemisorption on the (111) plane is as rapid as on other surfaces of the emitter, and little temperature dependence is observed.

Whether chemisorption on the (111) plane is through direct molecular dissociation on this plane or by an indirect mechanism, such as described by the model discussed earlier, is not known. Chemisorption on iridium is quite similar to that observed on rhodium, another fcc metal. The adsorption of hydrogen on the (111) plane of rhodium has been studied by Polizzotti [3] and no obvious structural specificities were found. An interesting implication comes from the surface diffusion experiments reported by Ayrault and Ehrlich [145]. They found that the surface self-diffusion of rhodium atoms on the (111) plane of rhodium is rapid even at temperatures as low as 50 K; the activation energy for diffusion on this close packed surface is very low, ~ 3.6 kcal/mole. We should expect an even lower activation energy for the diffusion of hydrogen on the surface, as this quantity is generally lower than the activation energy for self-diffusion. If this is also true for iridium then the (111) plane may be filled in by hydrogen dissociated on other surfaces of the emitter even at low temperatures.

Although the activation energy for the diffusion of hydrogen on iridium surfaces is not available, some qualitative values for the self-diffusion on iridium [146] show the same trend as that on rhodium. If iridium is like rhodium, then the rapid hydrogen adsorption may be explained by either the direct dissociation on the (111) plane itself or by the rapid migration of hydrogen dissociated on rougher surfaces. We cannot distinguish between these two processes from our experiments alone.

No matter which mechanism operates in hydrogen adsorption on iridium, the effect of defects on the surface reaction would be difficult to observe. If hydrogen dissociates rapidly on the (111) surface, then the presence of defects would not help much. On the other hand, if hydrogen cannot dissociate directly on the close packed planes of iridium, but migrates rapidly over the surface, then a small number of defects would be enough to promote chemisorption on the whole surface. At 80 K the upper limits for the number of defects required may be estimated from our results. Our emitter contains an almost circular (111) plane, approximately 80 Å in diameter as estimated in Appendix C. The ratio N_e/N is about 1/10 for this surface. Judging from the rate of chemisorption on this (111) surface at 80 K, we conclude that a ratio of defects to surface atoms of $< 1/10$ is enough to produce adsorption on the entire surface. At higher temperature an even lower value for N_e/N would be enough, since the rate of diffusion becomes higher.

The promotion of chemisorption by defects on fcc metals has been of particular interest, since these metals constitute an important class of catalysts. However, from Polizzotti's results on rhodium and from our results on iridium, promotion by defects is either not necessary or else so effective that even a small number of defects is enough to bring about chemisorption on the entire surface. At this point it seems that these fcc metals are poor candidates for studying the effects of structural defects on surface reactions.

8.4. Chemisorption of nitrogen on W(110)

In Chap. III we showed that nitrogen adsorbs in the atomically bound β -state on the W(110) plane; although this produces only a small change in the work function, it results in a significant change in the emission current. The adsorption of nitrogen between 150-300 K is slow, but becomes rapid at 550 K.

It is difficult to exclude a slow rate of dissociation on the (110) plane; in fact, conversion from γ - to β -nitrogen has been observed on the (110). The rate of direct dissociation, however, is rather slow compared to adsorption through other mechanisms. This is evident from the temperature dependence of the rate of chemisorption. As shown in Figs. 3.2 and 3.4, at 300 K the rate of chemisorption is about 2-3 times faster than that at 150 K, judging from the changes in the emission current. At 550 K, the rate of chemisorption is almost as fast as on the emitter as a whole.

The rapid adsorption at 550 K may be understood by the migration of β -nitrogen on the emitter surface, as discussed in Chap. III. Work [22] in the past has shown that the onset for the diffusion of nitrogen on the (111) and (110) regions is 400-500 K. The higher rate of chemisorption at 300 K compared to that at 150 K may be understood by a mechanism similar to that proposed for the hydrogen-W(110) system. The promotion of chemisorption on the (110) plane by the plane edges presumably follows a mechanism similar to our model discussed earlier. A loosely bound layer of nitrogen is probably responsible for the promotion of chemisorption on the (110) plane by plane edges, since the mobility of β -nitrogen on this surface is too small at 150-300 K [45]. If this is correct then the rate of chemisorption on the W(110) should be described at least approximately by Eq. (8.30).

Without observations on surface clusters it is not certain that the (110) terraces outside of the (110) plane are filled by nitrogen first. Assume that our model correctly describes the actual mechanism, then from experiments at 150 and 300 K we can estimate the difference between the activation energies for a loosely bound nitrogen atom at a plane edge jumping to the top of the (110) plane and to the adjacent (110) terraces, $V_t - V_e$, as ~ 0.7 kcal/mole. This is, however, an underestimate, as direct dissociation at 150 K is more important than at 300 K.

The rate of dissociation at the (110) plane edges may also be estimated from Eq. (8.30). From experiments shown in Fig. 3.4 the initial sticking coefficient on the (110) plane at 300 K may be roughly estimated from the changes in the emission current as ~ 0.003 . If the

diameter of the (110) plane is $\sim 400 \text{ \AA}$ (thermally formed emitter), we get a value for $s' \sim 0.3$; this is in reasonable agreement with the sticking coefficient for heavily stepped surfaces [147]. From the fact that the rate of dissociation on plane edges is about two orders of magnitude higher than the upper limit on the (110) plane we conclude that chemisorption on this plane can be promoted effectively by defects.

From our experiments it is not possible to exclude the possibility of an activated, but direct, dissociation on the (110) surface. The rate of chemisorption on the (110) plane as a function of surface geometry must be studied in order to distinguish between activated process at the plane edges, and that on the (110) plane itself. If activated dissociation on the (110) plane is the actual mechanism leading to the observed chemisorption, the activation energy may be estimated by considering the fraction of molecules dissociated on the surface. This fraction is given by $\frac{\nu}{\nu'} \cdot \exp((-Q + V)/kT)$, where ν , ν' are the attempt frequencies for dissociation and evaporation, respectively, and Q , V are the activation energies for dissociation and for evaporation. Take the value of V as $\sim 9 \text{ kcal/mole}$ [62]; we estimate, from the fact that the rate of chemisorption on the (110) plane at 300 K is about 2-3 times faster than that at 150 K, an activation energy $Q \sim 9.6 \text{ kcal/mole}$. Such an activation energy, however, would imply $\sim 40\%$ direct conversion from molecular to atomic nitrogen on the (110) surface. This would result in a sticking coefficient on the (110) on the order of 0.4, in contradiction to experimental results. It appears that activated dissociation on the (110) cannot explain experimental results satisfactorily. An unequivocal conclusion cannot be reached, however, without further experiments.

8.5. Chemisorption of nitrogen on Re(0001)

The chemisorption of nitrogen on the Re(0001) plane is somewhat similar to that on the W(110). The change in the work function is small but positive; the change in the emission current is significant. Also similar to the nitrogen-W(110) system is the strong temperature dependence of adsorption. At temperatures between 200-300 K, no adsorption on the Re(0001) is observed long after the total emitter is saturated. Adsorption on the (0001) can be observed, however, when the surface is heated to ~ 550 K. It is obvious from the lack of adsorption at 300 K that nitrogen does not chemisorb on the (0001) plane directly. The complete lack of adsorption also indicates that the activation energy for a nitrogen adatom to climb up a step, V_t , is much higher than that for tungsten. From the fact that no changes in the emission characteristics have been observed for exposure up to 3×10^{19} molecules/cm², the sticking coefficient on the (0001) plane at 300 K must be less than 3×10^{-16} . Assuming a value of ~ 0.1 for s' and a (0001) plane of diameter ~ 500 Å, we get from Eq. (8.51) the difference between activation energies $V_t - V_e$, as ~ 2.5 kcal/mole. This is about 3 times larger than that for tungsten.

The higher rate of chemisorption on the Re(0001) at 550 K may be understood by the same mechanism as that for the W(110) surface. The speed of migration of β -nitrogen at 550 K must be high enough that some nitrogen may enter the (0001) plane. This is supported by the fact that even at 550 K, the adsorption on the (0001) still lags behind that for

the emitter as a whole. The adsorption on the (0001) plane cannot be accounted for by the activated dissociation on this plane. As shown in Chap. V, adsorption on the (0001) plane may be brought about by heating a nitrogen covered emitter in vacuum from 300 and 550 K. This can be explained only by the redistribution of adsorbate on the surface, since the supply from the gas phase is inadequate to bring about this change. The promotion of adsorption on the (0001) plane by the plane edges also does not contribute significantly at 550 K. The rate, as estimated from Eq. (8.17), is increased by only a factor of 10 on increasing the temperature from 300 to 550 K. Therefore, the higher rate of chemisorption at 550 K can only be explained by the redistribution of adsorbate on the surface at this temperature.

At low temperature, nitrogen does adsorb on the (0001) plane as molecules. When the surface is warmed to room temperature, the molecular nitrogen simply evaporates without conversion to tightly bound atomic nitrogen. This further reflects the inertness of the (0001) toward the dissociation of nitrogen. The ability to convert molecular nitrogen to atomic nitrogen on the W(110) surface suggests that this molecular nitrogen may be related to the precursor for dissociative chemisorption. On the Re(0001) surface, the presence of molecular nitrogen does not lead to dissociative chemisorption. From this we conclude that the difficulty in dissociation, rather than the difficulty for molecular accommodation, is responsible for the inertness of this surface.

Suppose that the dissociation on the (0001) is prevented by a potential barrier Q ; from the evaporation experiments we have just discussed the lower limit for this activation energy barrier may be estimated from Eq. (8.49). Let $v \sim v' \sim \frac{kt}{h} \sim 3.10^{12}/\text{sec}$, $\tau = 10 \text{ sec}$, and $T = 150 \text{ K}$. The activation energy for molecular nitrogen on the surface to desorb, V , has been measured as $\sim 9 \text{ kcal/mole}$ [95]. We then get the minimum activation energy for dissociation on the (0001) plane as $\sim 11 \text{ kcal/mole}$. The highest rate of dissociation on the (0001), compared to the rate of evaporation, is given by $\exp((-Q+V)/kT)$. At 150 K , less than 0.2% of the nitrogen that is adsorbed as molecules on the (0001) plane will dissociate into atomic nitrogen. The majority of the nitrogen will re-evaporate into the gas phase.

At 300 K , however, $\sim 3\%$ of the nitrogen molecules can dissociate on the (0001) plane if $Q = 11 \text{ kcal/mole}$. From the experimental fact that no such conversion is observed, we must conclude that the activation energy for dissociation, Q , is considerably higher than this minimum value of 11 kcal/mole . From experiments shown in Chap. V, no appreciable changes in the emission characteristics are observed after exposure to $3 \times 10^{19} \text{ molecules/cm}^2$ of nitrogen at 300 K . Assume rather arbitrarily that 10% of these molecules stick on the (0001) plane temporarily, and that the technique is sensitive enough to detect 0.01 monolayer of coverage on the surface. Then a 0.0003% conversion of the nitrogen molecules to atoms on the (0001) can produce a detectable change in the emission characteristics. Equating this (0.0003%) to $\exp((-Q+V)/kT)$, and let $T = 300 \text{ K}$, we estimate the activation energy Q as roughly 17 kcal/mole .

The chemisorption of hydrogen and nitrogen on the Mo(110) surface not only is much faster than that on the W(110), but it also changes the work function differently. From the very high sticking coefficient it seems that promoted adsorption by defects does not play an important role on molybdenum. Even if it does, a small defect concentration should be enough to bring about adsorption on the entire surface. In any case, the rate of chemisorption on the (110) is not controllable by varying the defect concentration on the surface.

8.7 Summary

In this study the role of structural defects has been explored by direct observations on surfaces possessing defects of different sizes. From these observations we conclude that defects play a decisive role on the rate of chemisorption on the W(110) surface. A model for the promotion of chemisorption by surface defects is proposed. Experimental results on the densely packed plane of tungsten, as well as rhenium, can be explained quantitatively by this model.

We have shown that the chemisorption of hydrogen on densely packed planes of tungsten and rhenium cannot occur via direct dissociation on these surfaces. The rate of chemisorption on these planes can be completely understood by the promotion of chemisorption at the edges of these planes.

We have introduced the scanning technique as a new method of monitoring chemisorption on the emitter surface. This technique has allowed us to deduce that the speed of diffusion of hydrogen on the W(110) is rather limited at 80 K.

The direct dissociation on the W(110) plane has been found not to be an important process for the chemisorption of nitrogen. At temperatures between 150-300 K, the promotion of chemisorption by the edges of the (110) plane is a more important process for the adsorption of nitrogen than the direct dissociation.

Chemisorption of nitrogen on the Re(0001) plane at 300 K does not occur, leading us to conclude that promotion by the edges of this plane is ineffective. From our results, we can also conclude that the lack of chemisorption on the (0001) plane is caused by difficulties involved in dissociating hydrogen on this surface, rather than by any difficulty in the thermal accommodation of molecules.

We have investigated the interaction of hydrogen with the close packed (111) of iridium. For this surface the promotion of chemisorption is either too effective, so that it is hardly controllable, or not important at all.

For the interaction of hydrogen and nitrogen with the Mo(110) plane, we have found that the electronic structure and the minor difference in the chemical nature of the substrate have profound effects in the chemisorption behavior.

In conclusion, in our systematic investigation we found that chemisorption is a sensitive function of the structure of the substrate surface, as well as the chemical nature of the substrate.

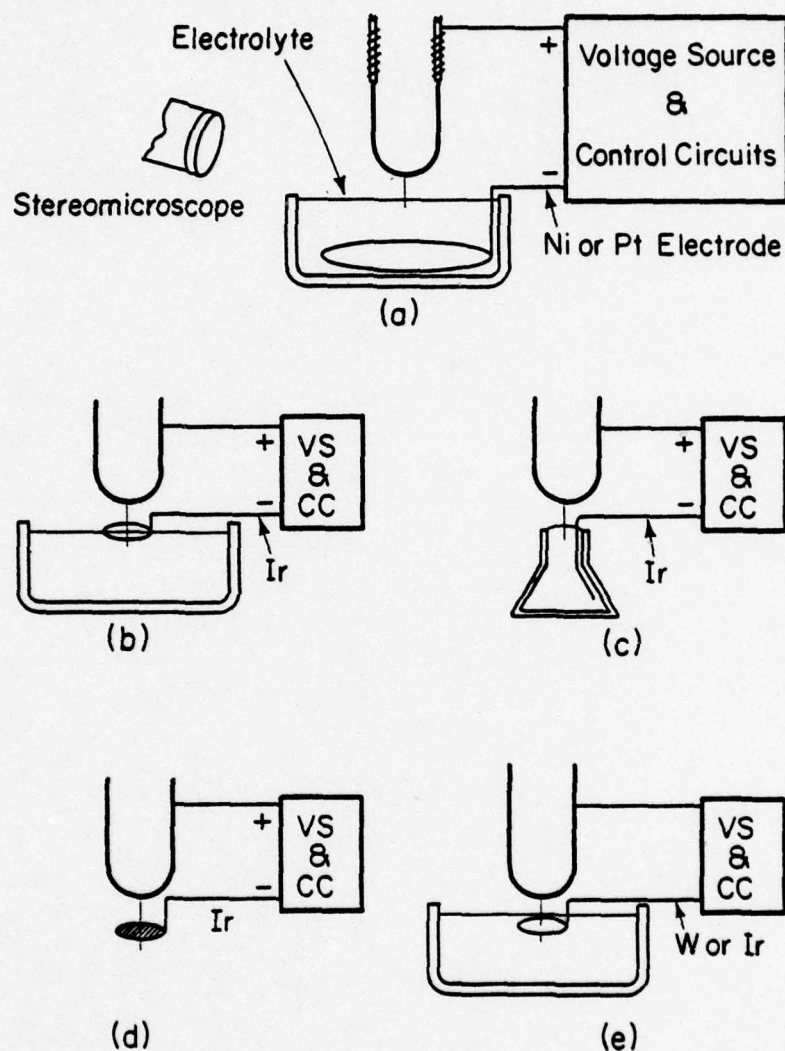
APPENDIX A
TECHNIQUES OF SAMPLE PREPARATION

Three conditions have to be met for a good field emitter specimen:

- (a) The end of the specimen, that is the tip, has to be sharp enough so that strong electric fields can be attained at reasonable voltages;
- (b) The tapered section, or the shank, has to be smooth and devoid of large defects or undercuts, so that the emitter can withstand field stresses;
- and (c) The whole shank and tip should be smooth and symmetric to avoid serious distortion of the image. In this Appendix we describe in some detail the techniques for emitter preparation, and compare different techniques following the above guidelines, for five metals: tungsten, molybdenum, rhenium, iridium, and platinum.

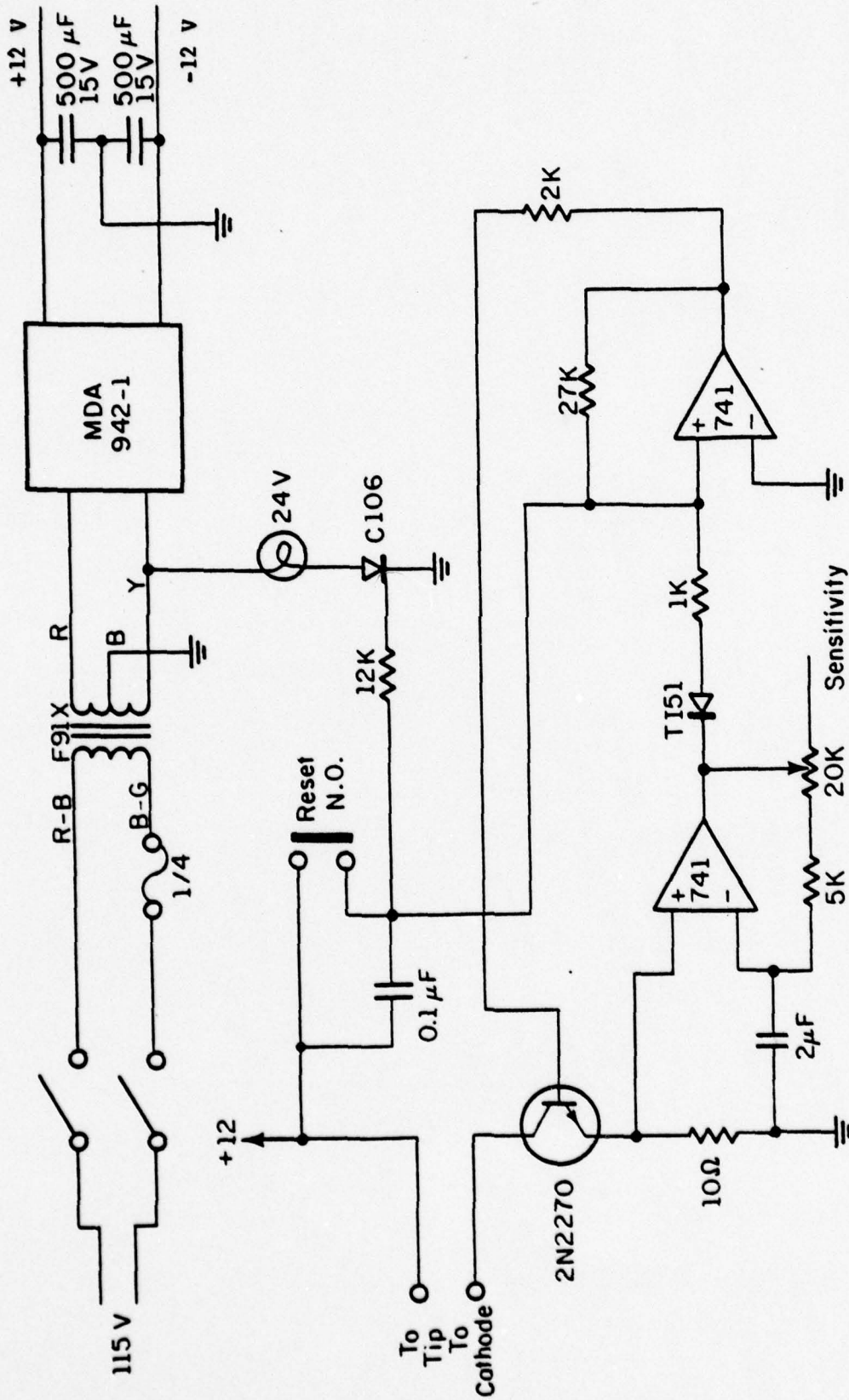
A.1. Tungsten

The easiest and most successful method for preparing tungsten emitters is the drop-off technique. In this method a small section of 0.005 in. diameter wire is dipped in 2N NaOH solution, using a ring-shaped platinum or nickel wire as counter-electrode, as shown in Fig. A.1a. Approximately 12 V dc is applied across the cell by an automatic shut-off circuit, shown in Fig. A.2. [148]. The tungsten wire is attacked most rapidly at the air-liquid interface, forming a neck there, as shown in Fig. A.3a. As polishing proceeds, the portion of the wire below the liquid level is thinned and finally pinched-off at the thinnest place. When this happens the polishing current suddenly drops, as the surface interacting with the solution is greatly reduced; at this moment the



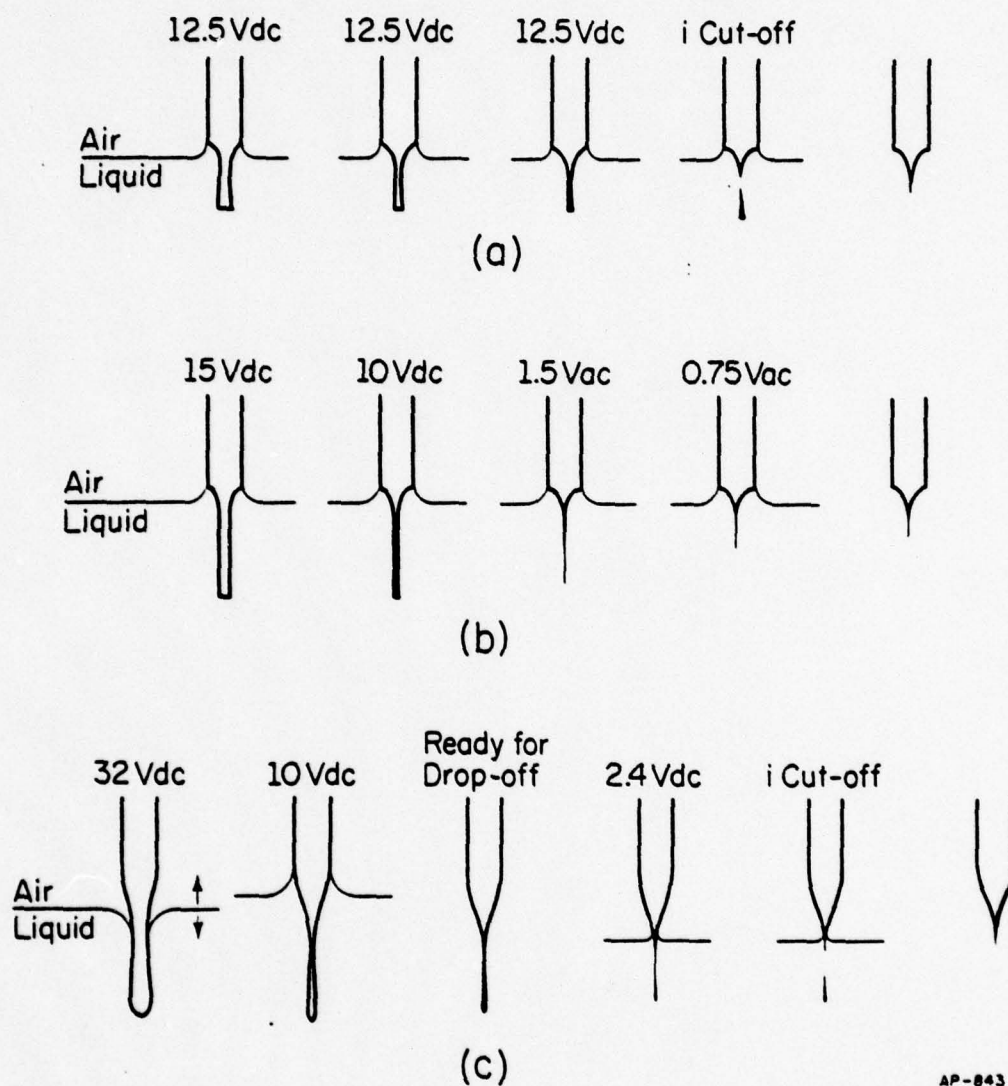
AP-845

Fig. A.1. Arrangements for electrochemically preparing field emission specimens. (a) Tungsten and molybdenum; (b) (1120)-oriented rhenium; (c) drop-off arrangement for rhenium emitters; (d) (0001)-oriented rhenium; (e) iridium and platinum.



AP-387

Fig. A.2. Schematic diagram of electrical circuit for tip etching by the drop-off technique. (From Ref. 148).



AP-843

Fig. A.3. Schematic drawings of tip etching for (a) tungsten; (b) molybdenum; (c) (1120)-oriented rhenium.

potential across the cell is switched off immediately by the shut-off circuit to stop the back-etching. The wire is then lifted out of the solution and rinsed with distilled water, followed by ethyl alcohol, to remove the residual polishing solution still on the surface. The emitter tips obtained following this procedure ordinarily have a diameter of a few hundred angstroms, and the general result is very satisfactory.

A.2. Molybdenum

Molybdenum is located immediately above tungsten in the periodic table; chemically it is quite similar to tungsten [149]. The polishing solution for tungsten (2N NaOH) also polishes molybdenum, but at a much higher rate. When the polishing conditions for tungsten are applied to molybdenum, the large ion currents cause turbulence in the solution which breaks the wire before it is properly dropped off. Attempts to reduce the current by either reducing the potential across the cell or the concentration of the polishing solution were unsuccessful: both lead to uneven etching of the wire.

There is an established method [150] for preparing molybdenum emitters: immerse 1/8 in. of 0.003 in. diameter molybdenum wire in 3.57N KOH, using nickel as counter-electrode. Then apply 4.0 V a.c. across the cell and polish until the lower section of the immersed wire acquires a long, uniformly thin shape. The potential is then reduced to 1.0 V a.c. and is applied as intermittent, short pulses while the shape of the wire is monitored with a stereomicroscope. At a magnification of 70X the end of the wire seem to vanish as the wire is attacked from both the side and bottom. The rate of disappearance of the wire is directly related to the

Rhenium does not react readily with acids other than nitric. Most electrochemical polishing solutions cited in the literatures [151] are fairly slow and time consuming. Besides this, rhenium responds to electrochemical polishing quite differently depending upon its heat treatment, increasing further the difficulty in developing an efficient and versatile etching technique.

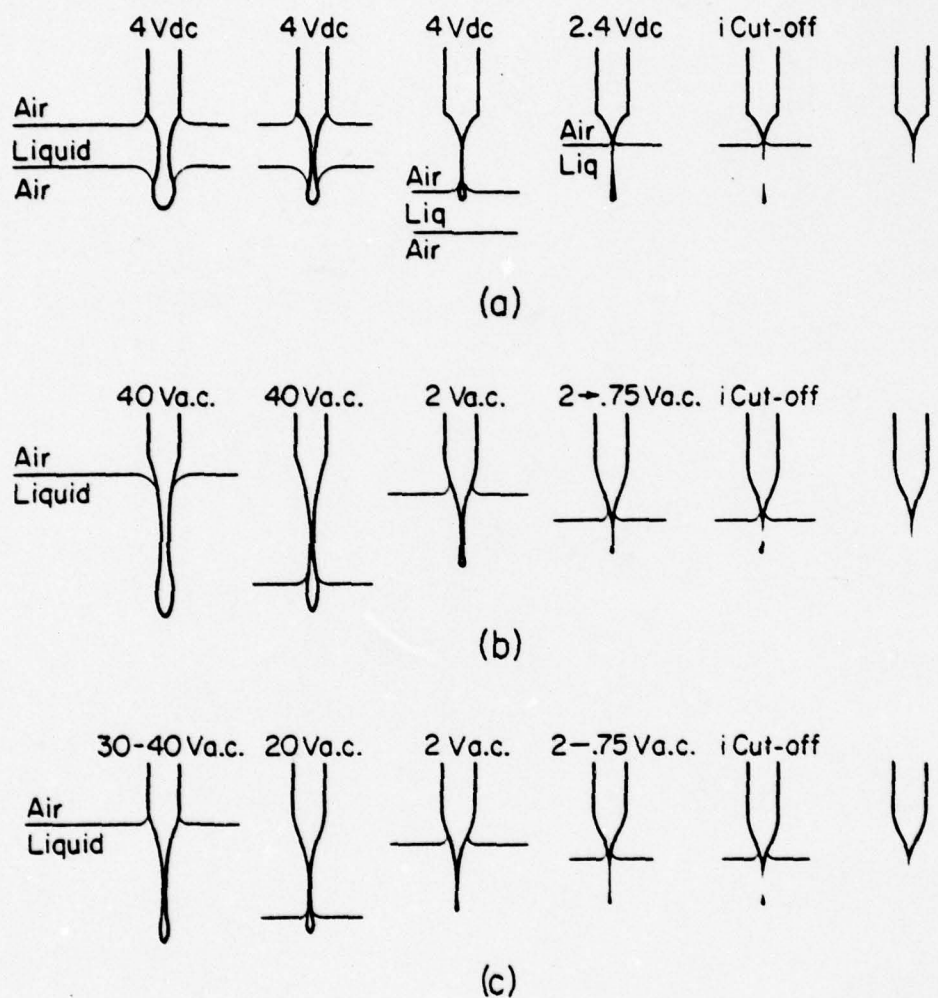
To resolve these difficulties, we have developed two methods for etching rhenium. For unheated wires, which are usually (11 $\bar{2}$ 0) oriented, the polishing solution consists of freshly mixed 20% H₂O, 40% conc. HNO₃, and 40% HF (48% wt. conc.). In the cell, an iridium counter-electrode in the shape of a small loop about $\frac{1}{4}$ in. in diameter is immersed in the above electrolyte, as shown in Fig. A.1b. A Petri dish is used as the cell container and is filled with electrolyte up to the level of the iridium loop. When a 32 V d.c. potential is applied across the cell, polishing is rapid and the attack fastest at the interface. Frequent moving of the wire up and down results in a long, thin neck as shown in Fig. A.3c. The potential is then dropped to ~ 10 V d.c. and the polishing becomes uniform along the whole immersed section. Excessive bubbling at the anode (rhenium) is normal at this stage and should not be a matter of concern. After the wire is thinned and appears barely visible under stereomicroscope, the old solution is abandoned and the final drop-off stage starts. In this stage a different electrolyte and cell are used: the latter is a narrow necked (5/16 in. diameter) flat bottom glass flask containing ~ 2 c.c. of the electrolyte; the electrolyte consists of 4 parts conc. H₃PO₄, 1 part glycerin, 1 part ethyl alcohol, and 1 part 10% aqueous HF.

Rhenium does not react readily with acids other than nitric. Most electrochemical polishing solutions cited in the literatures [151] are fairly slow and time consuming. Besides this, rhenium responds to electrochemical polishing quite differently depending upon its heat treatment, increasing further the difficulty in developing an efficient and versatile etching technique.

To resolve these difficulties, we have developed two methods for etching rhenium. For unheated wires, which are usually $(11\bar{2}0)$ oriented, the polishing solution consists of freshly mixed 20% H_2O , 40% conc. HNO_3 , and 40% HF (48% wt. conc.). In the cell, an iridium counter-electrode in the shape of a small loop about $\frac{1}{4}$ in. in diameter is immersed in the above electrolyte, as shown in Fig. A.1b. A Petri dish is used as the cell container and is filled with electrolyte up to the level of the iridium loop. When a 32 V d.c. potential is applied across the cell, polishing is rapid and the attack fastest at the interface. Frequent moving of the wire up and down results in a long, thin neck as shown in Fig. A.3c. The potential is then dropped to ~ 10 V d.c. and the polishing becomes uniform along the whole immersed section. Excessive bubbling at the anode (rhenium) is normal at this stage and should not be a matter of concern. After the wire is thinned and appears barely visible under stereomicroscope, the old solution is abandoned and the final drop-off stage starts. In this stage a different electrolyte and cell are used: the latter is a narrow necked (5/16 in. diameter) flat bottom glass flask containing ~ 2 c.c. of the electrolyte; the electrolyte consists of 4 parts conc. H_3PO_4 , 1 part glycerin, 1 part ethyl alcohol, and 1 part 10% aqueous HF.

A single iridium wire serves as counter-electrode, as shown in Fig. A.1c. A d.c. potential of 2.2 to 2.4 V is applied through the circuits shown in Fig. A.2. The total current should be restricted to below 100 μ A. The position of the air-liquid interface is essential for the success of the drop-off method. The interface should be located just above the thinnest portion of the wire, as shown in Fig. A.3c. Ordinarily a macroscopic undercut is left at the position of the meniscus (Fig. A.3c), since the drop-off solution also attacks the interface preferentially. This does not affect the performance of the tip: we have never lost an emitter due to this.

For the (0001) oriented zone-refined wires the final drop-off method is the same as described above. The initial thinning solution is different, however; it is made up from freshly mixed 40% glycolic acid, 30% conc. HNO_3 , and 30% HF (10% aqueous sol.). The counter electrode is still the $\frac{1}{4}$ in. iridium loop, but the cell now consists only of a thin layer of electrolyte suspended on the loop, and the rhenium wire. The rhenium wire pierces the electrolyte layer, a small section protruding below it, as shown in Fig. A.1d. Only the section in the solution is etched. The potential across the cell varies from 3 to 4 V d.c., depending upon the thickness of the electrolyte layer. Maximum polishing effect is reached when the ion current is 25 to 30 mA. Polishing is then rapid and smooth; a highly polished surface and a long, narrow section suitable for final drop-off are produced in a couple of minutes. Changes of the wire during polishing are shown schematically in Fig. A.4a.



AP-844

Fig. A.4. Schematic drawings of tip etching for (a) (0001)-oriented rhenium; (b) iridium; (c) platinum.

If incorrect proportions of electrolyte constituents are used, maximum polishing conditions cannot be achieved. This ordinarily results in preferential etching along certain crystallographic directions and hence the creation of deep furrows on the surface. Such undesirable effects usually can be removed by adding some conc. HNO_3 to the electrolyte. The field emitters prepared in this way are very sharp. A perfectly smooth surface and clear field ion image can usually be obtained below 5 KV, using He as imaging gas.

A.4. Iridium

Iridium is famous for its inertness toward virtually all chemicals, including aqua regia. Reasonably rapid etching of iridium can be accomplished in molten NaCl or KCl salts [14], but control is difficult and the set-up is inconvenient. Chromic acid and ammonium carbonate have been used sequentially to make iridium field emitters [152]. This technique is quite slow and the chance of success is rather poor. Quite a simple method was reported by Graham et al. [153]; this uses dilute HF to achieve a thin, narrow taper and 4N HCl to finally sharpen the emitter. The results are generally satisfactory, except that the thinning solution has no effect on heat treated iridium wires.

To etch zone-refined wires we have developed a technique which yields excellent specimens with a high chance of success. This technique employs three different etchants. For convenience, the following solution can be made in advance and stored for indefinitely long periods of time: deposit iridium complex in 4% HF by electrochemically dissolving an iridium wire at 10 V d.c. and 2-3A for about 1 hour, until the solution acquires a

purple-bluish color. The initial polishing solution is made of 1 part of the above solution, 1 part distilled water, and 2 parts of conc. HNO_3 . The cell consists of a $\frac{1}{4}$ in. diameter tungsten loop as counter-electrode, immersed slightly below the electrolyte, as shown in Fig. A.1e. A section of 1/16 in. length of 0.005 in. diameter iridium wire is inserted into the electrolyte, and a potential ~ 40 V a.c. is applied across the cell. There should be appreciable noise due to sparking. Raise the voltage if this is not heard. The polishing is generally smooth and relatively fast compared to other methods. After 7 or 8 minutes a slender neck is formed below the interface, as shown in Fig. A.4b. The wire is then raised and the excess wire below the neck etched off. (If this stage is allowed to proceed, etching tends to localize near the meniscus.)

The second step is to continue thinning in saturated $(\text{NH}_3)_2\text{CO}_3$ solution. This is done simply by replacing the polishing solution and applying 2 V a.c. for two or three minutes, until the wire is barely visible under 70X magnification. The last stage is to drop off the lower section. This is done with an electrolyte which has been developed for preparing samples for transmission electron microscopy [154]: 1 part conc. H_3PO_4 , 1 part conc. HNO_3 , and 1 part conc. H_2SO_4 . Start out at 2 V a.c. and gradually decrease to 0.75 V a.c. as the wire gets thinner. The etching rate of this solution is fairly slow; approximately one hour is needed for the lower section to drop off. A bluish iridium complex tends to form near the anode in this final stage, blocking the view of the iridium wire. This complex does not affect the performance of the emitter, and can usually be removed by blowing air lightly on the solution surface.

The above etching procedures are somewhat lengthy [155]. However, the rewards are considerable: if the procedures are followed correctly a good specimen is guaranteed. Also, the sharpness of the tip can be controlled by controlling the size of the portion dropped off. Usually a good helium field ion image can be obtained at voltages ranging from 3 to 15 KV.

20% KCN can also be used for the final drop-off method. This saves considerable time since KCN attacks iridium at a much faster rate than the solution we used. However, KCN tends to leave a rough instead of a finely polished surface. Undercutting of the shank and uneven etching are more frequent and a good specimen is not always achieved. The chance of success is about 30% with KCN.

A.5. Platinum

Platinum is similar to iridium chemically except that it is less resistant to acids. Procedures for etching iridium can be applied to platinum directly. However, we have discovered a much better and faster method to replace the lengthy procedures used with iridium. The construction of the electrolytic cell is similar to iridium, except that now an iridium counter-electrode is used. The electrolyte is replaced by a solution composed of equal volumes of water and saturated NH_4Cl . The surface is highly polished and the etching is smooth and rapid when a potential of 30-40 V a.c. is applied across the cell. A thin slender neck is, as shown in Fig. A.4c, formed within one or two minutes. The potential is then dropped to 20 V a.c. and excess wire at the end etched off. The wire is further etched in the same solution at 2 V a.c. until the thin section becomes barely visible at 70X. Next the wire is taken out and immersed in distilled water

to rinse off the ammonium chloride. The final drop-off procedure is the same as with iridium, but since platinum is less resistant than iridium, the time required is only 15 to 30 minutes. Field emitters prepared by this method ordinarily produce excellent helium ion images between 4 to 10 KV.

The mechanical strength of platinum is much less than of tungsten or iridium. In order for a platinum specimen to withstand the stress of the applied field, which corresponds to a negative pressure of 10^5 atmosphere [14], it has to be very smooth and free of mechanical defects. The above procedures yield consistently successful specimens. 20% KCN can also be used for preparing platinum tips. However, the surface finish is far inferior to our method. Due to the roughness of the surface, less than 30% of the field emitters prepared by KCN survive the rigors of field evaporation even when exercising great care.

APPENDIX B

SIMULATION OF PROBE HOLE SCANS

Characterizing a surface by scanning the emitter across the probe hole is the most important process we have used to identify surface topography. Scan diagrams thus obtained give a good qualitative description of the surface. The scanning technique can also be used to monitor chemical processes on a surface, as discussed in Chapter VII. This method, however, produces complicated results which are not yet fully understood. It is the desire to achieve a better understanding of these results, and to describe the surface topography more quantitatively, that stimulates this computer simulation of scan diagrams. In this Appendix, we shall simulate the scan diagrams by considering electron emission from various regions of the emitter surface, first for clean emitters, and then for gas covered emitters.

B.1. Clean Surfaces

B.1a. Principle of Simulation

We can simulate a scan diagram by calculating the electron current passing through the probe hole as a function of the probe hole location relative to the tip apex. According to Fowler-Nordheim theory, the field emission current density is given by Eq. (2.1). If the probe hole is infinitely large, the collector current (or the probe hole current I_p) is given by simply integrating over all emitting area

$$I_p^{\text{inf.}} = \int J(\vec{r}) d^2r, \quad (\text{B.1})$$

where $J(\vec{r})$ is the field emission current density. In this case the collector

current has the same value as the total emission current. For a probe hole of finite size, not all electrons from the emitter surface are detected by the collector. The probe hole current then must be expressed by

$$I_p = \int J(\vec{r}) P(\vec{r}) d^2r, \quad (\text{B.2})$$

where $P(\vec{r})$ is the probability that an electron emitted at position \vec{r} will be detected. The probability $P(\vec{r})$ depends sensitively on the relative position of the probe hole and the emitting site. If this is known, and if the total energy and the tangential momentum of the electron and the accelerating potential are known, then the probability $P(\vec{r})$ can be determined theoretically.

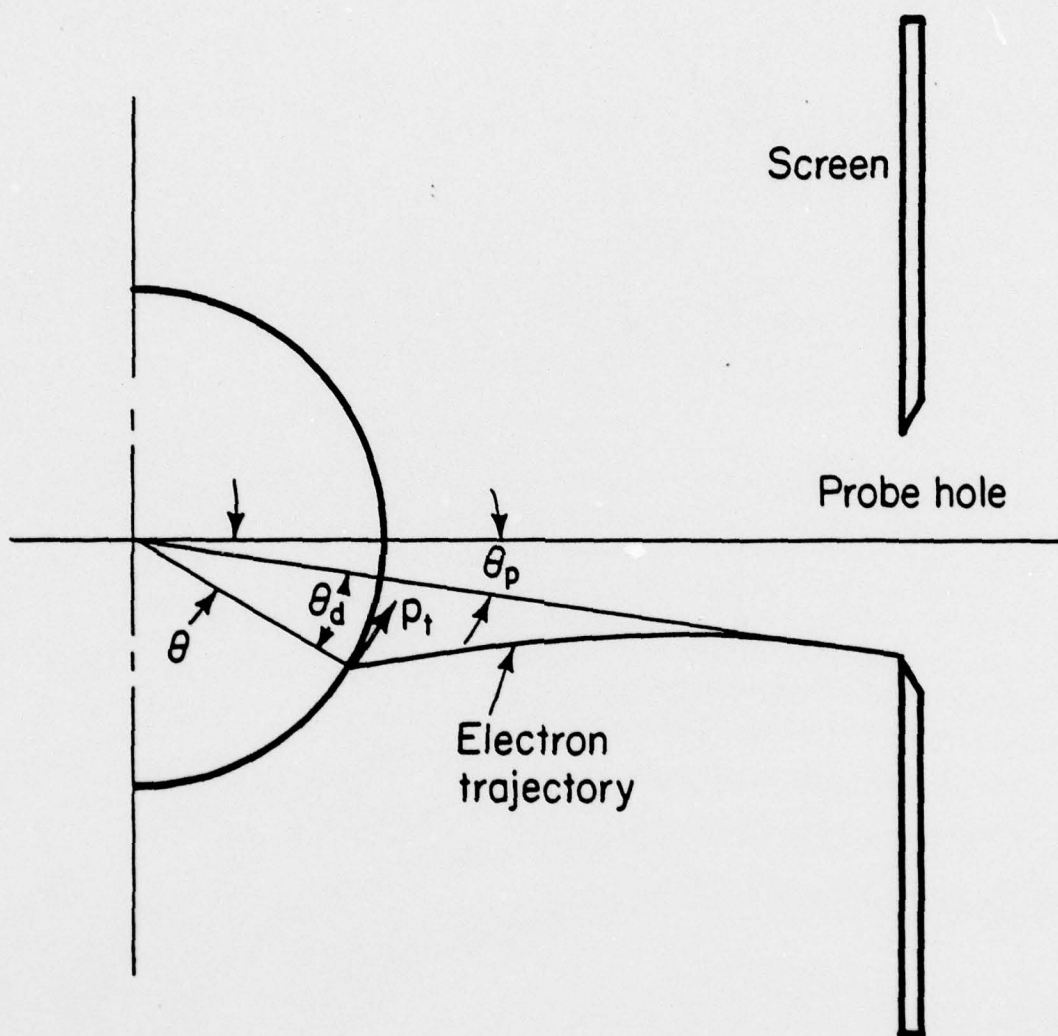
The trajectory of an electron emitted at an angle θ from the probe hole (Fig. B.1), with an initial tangential momentum p_t , has been calculated by Plummer and Gadzuk [30]. Their argument is simple: the conservation of angular momentum (rp_t) requires that p_t continuously decreases while the electron is accelerated away from the emitter surface; after travelling a short distance, p_t has to have fallen so much that the trajectory becomes radial, as shown in Fig. B.1. The angle of deviation can therefore be calculated as

$$\theta_d \approx \sqrt{\frac{4E_t}{eV}}, \quad (\text{B.3})$$

where $E_t = p_t^2/2m$, and V is the accelerating potential. The angle θ_d defines the effective probe size via

$$\theta = \theta_p + \theta_d, \quad (\text{B.4})$$

where θ_p is the half angle obtained by geometrically projecting the probe hole onto the surface, as shown in Fig. B.1; θ is the half angle of the area



AP-933

Fig. B.1. Schematic diagram of electron trajectory from a semi-spherical tip. The size of the emitter and the probe hole is greatly exaggerated.

actually probed. Contributions from the uncertainty principle are neglected here. The actual probe size therefore varies with the tangential momentum of the emitted electrons. To estimate the probe hole current we need to know not only the geometrical relation between the probe hole and the emitter, but also the energy distribution of the electrons.

The energy distribution of field emitted electrons has been studied before [28,29,117]. Inside a free electron metal, the number of electrons with total energy between E and $E+dE$, and "normal energy" [156] between W and $W+dW$ is given by:

$$N(W,E)dWdE = \frac{4\pi m}{h^3} \frac{dWdE}{1 + \exp[(E-E_f)/kT]}, \quad (B.5)$$

where E_f is the Fermi energy. The tunneling probability, $D(W)$, is a function of normal energy W only, and has been calculated using the WKB approximation by Murphy and Good [157] as

$$D(W) = \left\{ 1 + \exp \left[-\frac{2\sqrt{2}}{h^3} \left(\frac{Fh}{2e} \right)^{-\frac{1}{2}} y^{-\frac{3}{2}} v(y) \right] \right\}^{-1}, \quad (B.6)$$

where $y = \sqrt{e^3 F/W}$, and $v(y)$ is a special elliptical function discussed in Chapter II. The energy distribution $P(W,E)dWdE$ for emitted electrons can then be expressed by

$$P(W,E)dWdE = N(W,E)D(W)dWdE. \quad (B.7)$$

Since $E_t = E - W$, the above equation can be written in terms of E_t :

$$\begin{aligned} P(E_t,E)dE_t dE &= N(E_t,E)D(E_t)dE_t dE \\ &= \frac{4\pi m}{h^3} \frac{dE}{1 + \exp[(E-E_f)/kT]} \frac{dE_t}{1 + \exp \left[\frac{2\sqrt{2}}{3} \left(\frac{Fh}{2e} \right)^{-\frac{1}{2}} y'^{-\frac{3}{2}} v(y') \right]}, \end{aligned} \quad (B.8)$$

where $y' = \sqrt{e^3 F / (E - E_t)}$. As is clear from Eq. (B.3), the actual probe size depends only on the tangential energy E_t . We can therefore integrate Eq. (B.8) over the total energy E , and obtain the energy distribution with respect to E_t :

$$\begin{aligned} P(E_t) dE_t &= \int_E P(E_t, E) dE_t dE \\ &= \frac{4\pi m}{h^3} dE_t \int_E \frac{dE}{\{1 + \exp[(E - E_f)/kT]\} - \{1 + \exp[\frac{2\sqrt{2}}{3} (\frac{Fm^4}{2e^5})^{-\frac{1}{2}} y'^{-\frac{3}{2}} v(y')]\}} \end{aligned} \quad (B.9)$$

Integration of Eq. (B.9) cannot be carried out analytically. The energy distribution $P(E_t) dE_t$ is therefore evaluated by numerically integrating the right hand side of Eq. (B.9). The values of $P(E_t) dE_t$ as a function of E_t thus obtained are plotted in Fig. B.2. Fortunately, the plot of $\ln(P(E_t) dE_t)$ vs. E_t is almost a straight line. The tangential energy distribution $P(E_t) dE_t$ can therefore be approximated very accurately by:

$$P(E_t) dE_t \simeq 8.5955 \exp(-8.5955 E_t) \quad , \quad (B.10)$$

where E_t is measured in eV. Equation (B.10) has been normalized properly to meet the requirement $\int_{E_t} P(E_t) dE_t = 1$ so that the energy distribution $P(E_t) dE_t$ represents the probability of finding an emitted electron having "tangential energy" [156] between E_t and $E_t + dE_t$.

If an electron emitted from a position which is θ rad. away from the center of the probe hole is to be captured by the collector, then according to Eqs. (B.3) and (B.4) it must have a "tangential energy" $E_t \geq \frac{1}{4} (\theta - \theta_p)^2 \cdot (eV)$. The probability that an electron will have a tangential momentum such that the corresponding energy is larger than E_t is given simply by

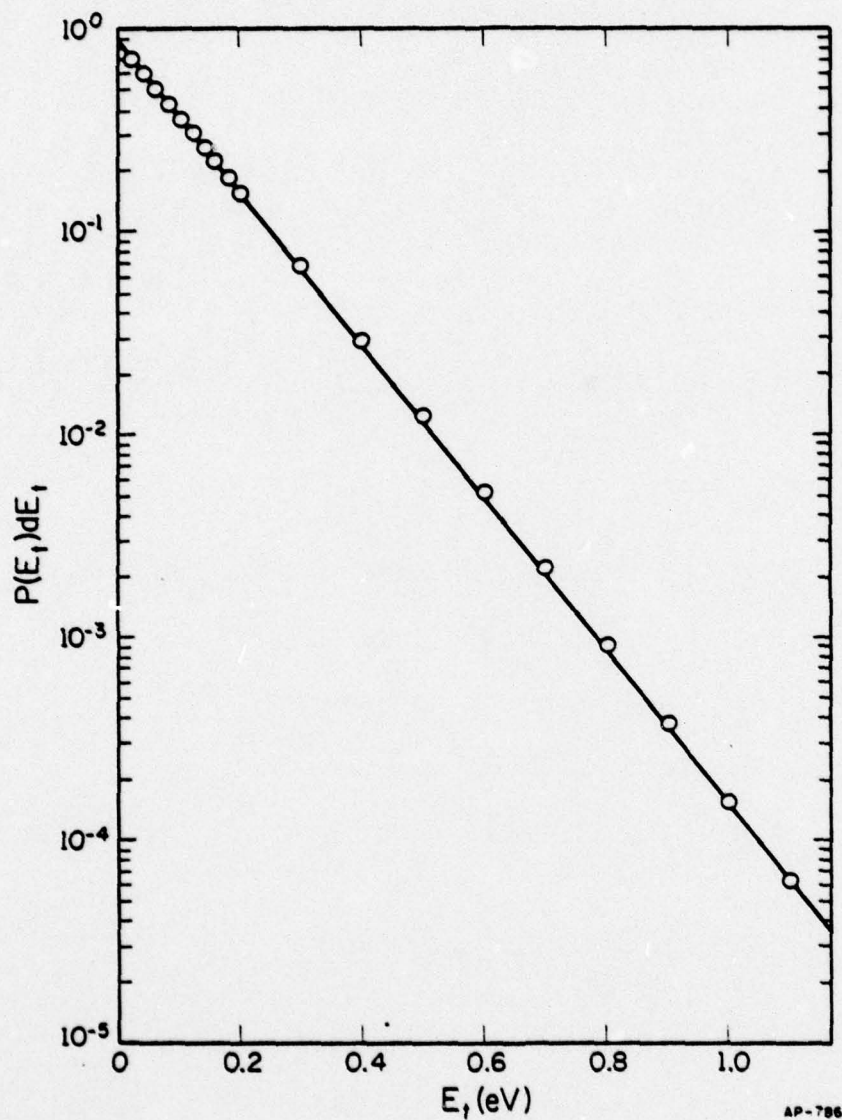


Fig. B.2. The "tangential energy distribution" of field emission electrons calculated from Eq. (B.9). See footnote 156 for the meaning of "tangential energy".

$$P_{>}(E_t) = \int_{E_t}^{\infty} P(E_t) dE_t = \exp(-8.5955 E_t) \quad . \quad (\text{B.11})$$

In terms of these expressions, the probability of an electron reaching the probe hole, $P(\vec{r})$, can be written as

$$P(\vec{r}) = P_{>}(E_{\theta}) \cdot G \quad , \quad (\text{B.12})$$

where $E_{\theta} = \frac{1}{4} (\theta - \theta_p)^2 \cdot \text{eV}$, and G is a geometrical factor which accounts for the percentage of electrons whose initial tangential momentum is favorably oriented toward the probe hole. In obtaining Eq. (B.12), a circularly symmetric surface geometry has been assumed so that \vec{r} can be represented by the angle θ alone. As a first approximation, G can be expressed by $G \approx \tan^{-1}(\theta_p/\theta)/\pi$. The probability $P(\vec{r})$ then becomes

$$\begin{aligned} P(r) &= \frac{\tan^{-1}(\theta_p/\theta)}{\pi} \exp[-8.5955 \cdot \frac{1}{4} (\theta - \theta_p)^2 \cdot \text{eV}] \\ &= \frac{\tan^{-1}(r_p/r)}{\pi} \exp[-8.5955 \cdot \frac{1}{4} (\frac{r-r_p}{r_a})^2 \cdot \text{eV}] \quad , \quad (\text{B.13}) \end{aligned}$$

where r_p is the projection of the radius of the probe hole on the surface, and r_a is the average radius of curvature of the emitter.

As mentioned earlier, Eq. (B.13) correctly describes the probability of detecting the electrons only when the emitter surface is spherically symmetric. The surface of a real field emitter is quite complicated, and emission depends strongly on the local work function and electric field. While the local variation of work function only affects the current density, the local electric field distribution affects both the current density and the probability of electron collection. The reason for this is simple: the electron emerging

from the surface follows the direction of the electric field initially. The local variation of surface curvature changes the initial direction of electron emission. The trajectory of the electron is thus affected and so is the collecting probability. The exact form of the field distribution over the emitter surface is not known. We can only describe the work function and field distribution qualitatively and the rest of this Appendix can therefore only be considered qualitative.

Let F_0 be the electric field for a hemi-spherical emitter. Consider a step of single atomic height on the surface: the field near the step is enhanced because of the local increase of curvature. Let ΔF be the magnitude of field enhancement, and η the angle between the tip apex and the normal to the equi-potential on the surface, as shown in Fig. B.3. Assuming that the enhanced field near the edge obeys a cosine law, then the electric field can be written as

$$\vec{F} = \vec{F}_0 + \Delta \vec{F} \cos(2\eta - \frac{\pi}{2}). \quad (B.14)$$

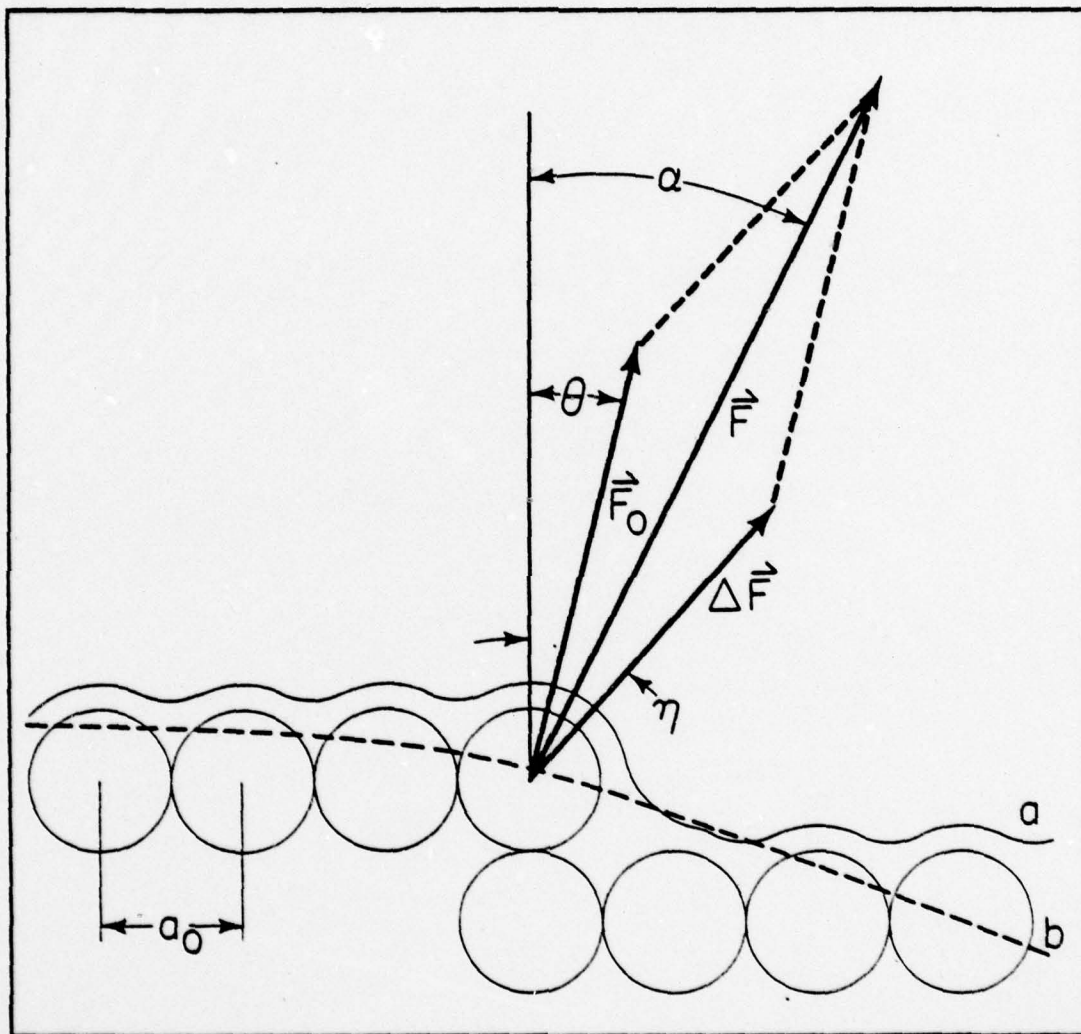
To find the magnitude and direction of the electric field on the surface, we simply decompose \vec{F}_0 and $\Delta \vec{F}$ into their Cartesian components according to Fig. B.3. We get

$$\vec{F} = [F_0 \sin\theta + \Delta F \cos(2\eta - \frac{\pi}{2})\sin\eta]\hat{x} + [F_0 \cos\theta + \Delta F \cos(2\eta - \frac{\pi}{2})\cos\eta]\hat{y} \quad (B.15)$$

and

$$F^2 = F_0^2 + [\Delta F \cos(2\eta - \frac{\pi}{2})]^2 + 2F_0\Delta F \cos(2\eta - \frac{\pi}{2})\sin(\theta + \eta) \quad (B.16)$$

The direction of the electric field at \vec{r} relative to the tip apex is given by the angle



AP-786

Fig. B.3. Local electric field near a plane edge. Solid circles depicts surface atoms. Solid curve (a) depicts equipotential near the surface. Dashed curve (b) depicts the macroscopic shape of the emitter.

$$\alpha = \tan^{-1} \frac{F_0 \sin \theta + \Delta F \cos(2\eta - \frac{\pi}{2}) \sin \eta}{F_0 \cos \theta + \Delta F \cos(2\eta - \frac{\pi}{2}) \cos \eta} \quad (B.17)$$

The probe hole current I_p can now be evaluated using Eq. (B.2). The probability $P(\vec{r})$ is obtained simply by replacing θ with α in Eq. (B.13):

$$P(\vec{r}) = \frac{\tan^{-1}(r_p/r)}{\pi} \exp[-8.5955 \cdot \frac{1}{4} \text{eV}(\alpha - \theta_p)^2] \quad (B.18)$$

The emission current density can be calculated still using the Fowler-Nordheim equation (Eq. (2.1)), but with F replacing F_0 . Let (x_0, y_0) be the projection of the center of the probe hole on the surface. The contribution from any place (x, y) on the emitter can be calculated by assigning $r = [(x - x_0)^2 + (y - y_0)^2]^{\frac{1}{2}}$ in Eqs. (B.16), (B.17), and (B.18). The probe hole current is obtained by numerically evaluating the double integral in Eq. (B.2).

A scan diagram can be simulated by calculating a series of probe hole currents corresponding to various probe locations. For example, by keeping y_0 constant and varying x_0 through a range of values we can simulate a horizontal scan across the surface at a latitude y_0 . The numerical simulations are performed by a computer program, SCAN, listed in Appendix E. The parameters used in this simulation are discussed in the next section.

B.1b. Simulation Parameters

Before the double integral in Eq. (B.2) can be evaluated numerically, parameters describing surface geometry and electric field must be provided. The parameters describing surface geometry are the radius of the central plane r_0 , and the step density on the terraces outside of the central plane. The step density on the terraced region can be estimated approximately from field ion micrographs. In our simulation, the step density near the central plane is roughly estimated from field ion micrographs of a (110) oriented

AD-A056 535

ILLINOIS UNIV AT URBANA-CHAMPAIGN COORDINATED SCIENCE LAB F/G 7/4
CHEMISORPTION ON PERFECT SURFACES AND STRUCTURAL DEFECTS. (U)

OCT 77 R LIU

DAAB07-72-C-0259

UNCLASSIFIED

R-790

NL

4 of 4

AD
A056 535



tungsten emitter of a size comparable to those in our experiments. Considerable errors are involved in such rough estimates. However, this should not affect the qualitative features of the simulated scan diagram.

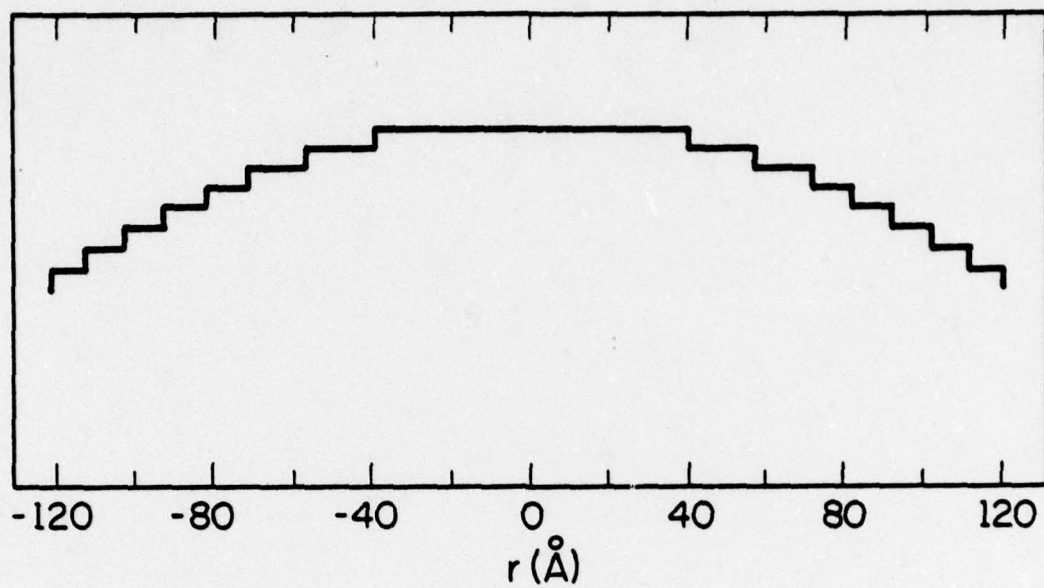
The radius of the central plane, r_0 , can be estimated with reasonable accuracy from field ion micrographs using the standard ring counting technique [14]. The size of the tungsten (110) plane as a function of field evaporation voltage has been determined by Polizzotti [3]. From his results, we estimate the radius of the (110) plane of the tungsten emitters in our experiments at $\sim 40\text{\AA}$. In our simulation, the maximum r_0 used ranges from 40 to 50\AA , and the minimum r_0 used is 5\AA . A schematic drawing for the surface geometry of a typical emitter used in our simulation is shown in Fig. B.4a.

Local variation of electric field on an emitter is not well-known, and hence more difficult to simulate. In our simulation, the following factors affecting the electric field on the surface are considered:

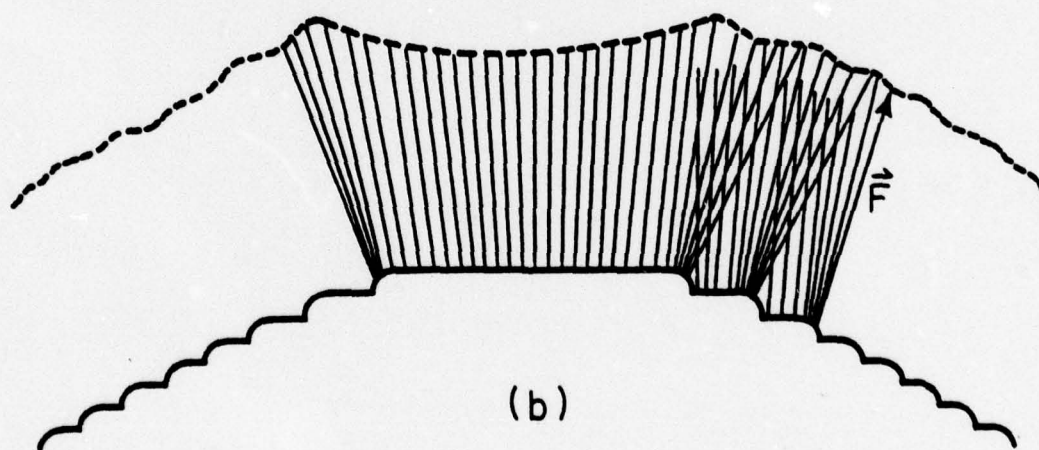
- (1) the electric field at the center of a large plane is "depressed" compared to that near its edges;
- (2) the strong local electric field near a step also affects neighboring areas;
- (3) the non-hemi-spherical shape of the emitter [71]. That is, the local protrusion and depression on the emitter.

In our simulation, these contributions are represented by the following:

- (1) The field depression at the center of a plane -- a field of the form $(\frac{r}{r_0} - 1)F_1$ (which is always ≤ 0) is added to F_0 . F_1 is a variable parameter which depends on r_0 . F_1 ranges from 1 to 5% of F_0 .



(a)



(b)

AP-937

Fig. B.4. Schematic diagrams of a typical surface used in the computer simulation. (a) Topography of the surface. Step height is one interatomic distance. (b) Typical electric field distribution on the surface.

- (2) The electric field near a step--a field of the form

$\Delta F \exp[-((r-r_k-a_0/2)/\delta)]$ is assumed, since this is short-ranged.

In this formula, a_0 is the lattice constant, r_k the position of the k -th step from the plane, and δ a variable parameter. ΔF is usually 5 to 10% of F_0 .

- (3) The local protrusion on the surface--a field of the form $(\frac{r}{a_0})^2 F_2$ is used. F_2 is a variable parameter.

Quantitative contributions from these factors are largely unknown. Therefore influences from these local fields are simulated parametrically. That is, these parameters are varied in a trial-and-error fashion until the simulated scan diagrams resemble the experimental ones reasonably well.

Another parameter that must be determined is the equipotential surface near a step (Fig. B.2). The angle η between the normal of the equipotential surface and the tip apex must be known in order to evaluate the electric field and the collection probability from Eqs. (B.14)-(B.17). Since no experimental, nor theoretical values are available, this parameter has to be determined again by trial and error. An equipotential surface described by a parabolic equation $y = \gamma(x^2 + \epsilon)$ was found most satisfactory. For such an equipotential surface, the angle η is given by:

$$\eta = \frac{\pi}{2} - \tan^{-1} \left[\frac{a_0}{2\gamma(r-r_k)} \right] \quad , \quad (B.19)$$

where γ is a variable parameter, a_0 the lattice constant, and r_k the position of the k -th step from the central plane.

The electric field on the emitter surface is therefore quite complicated. A typical surface field distribution is shown in Fig. B.4b. We must emphasize that the local electric fields used in this simulation are largely guesses. This practice is justified only by the ability to simulate

scan diagrams similar to those actually observed experimentally.

B.1c. Results

Simulated scan diagrams for r_0 ranging from 40 to 5\AA have already been shown in Fig. 2.13. As discussed in Chapter II, all major features of these scan diagrams have been observed experimentally. Qualitatively at least, the simulation has been successful. Some quantitative information can also be obtained from these simulated scan diagrams if the size of the central plane is known. This is discussed in Chapter VII.

For the scan diagrams in Fig. 2.13, the following parameters were used in simulation: $F_1 = 0.003 \text{ V/\AA}$; $F_2 = 0.0006 \text{ V/\AA}$, $\Delta F = 0.02 \text{ V/\AA}$, $\delta = 15\text{\AA}$, and $\gamma = 6$. The surface geometry used in the simulation can be described by the position of steps: $(r_0, r_1, r_2, \dots) = (r_0, 57\text{\AA}, 71\text{\AA}, 81\text{\AA}, 91\text{\AA}, 101\text{\AA}, \dots)$, where r_0 is the radius of the central plane, and r_k the k -th step outside of this plane. As a comparison, two sets of scan diagrams of slightly different parameters and surface geometry are shown in Figs. B.5 and B.6. For the scan diagrams in Fig. B.5, the parameters for local electric fields are: $F_1 = 0.003 \text{ V/\AA}$, $F_2 = 0.001 \text{ V/\AA}$, $\Delta F = 0.01 \text{ V/\AA}$, $\delta = 7\text{\AA}$, and $\gamma = 6$. The surface geometry for these scan diagrams is defined by $(r_0, r_1, r_2, \dots) = (r_0, 62\text{\AA}, 76\text{\AA}, 86\text{\AA}, 96\text{\AA}, 106\text{\AA}, \dots)$. The scan diagrams in Fig. B.5 are quantitatively different compared to those in Fig. 2.13. However, even though the parameters F_2 , ΔF , and δ differ by a factor of two, the scan diagrams are quite similar qualitatively. Essential features are the same in these two sets of scan diagrams.

The parameters for local electric fields for the scan diagrams in Fig. B.6 are: $F_1 = 0.003 \text{ V/\AA}$, $F_2 = 0.0006 \text{ V/\AA}$, $\Delta F = 0.04 \text{ V/\AA}$, $\delta = 8\text{\AA}$, and

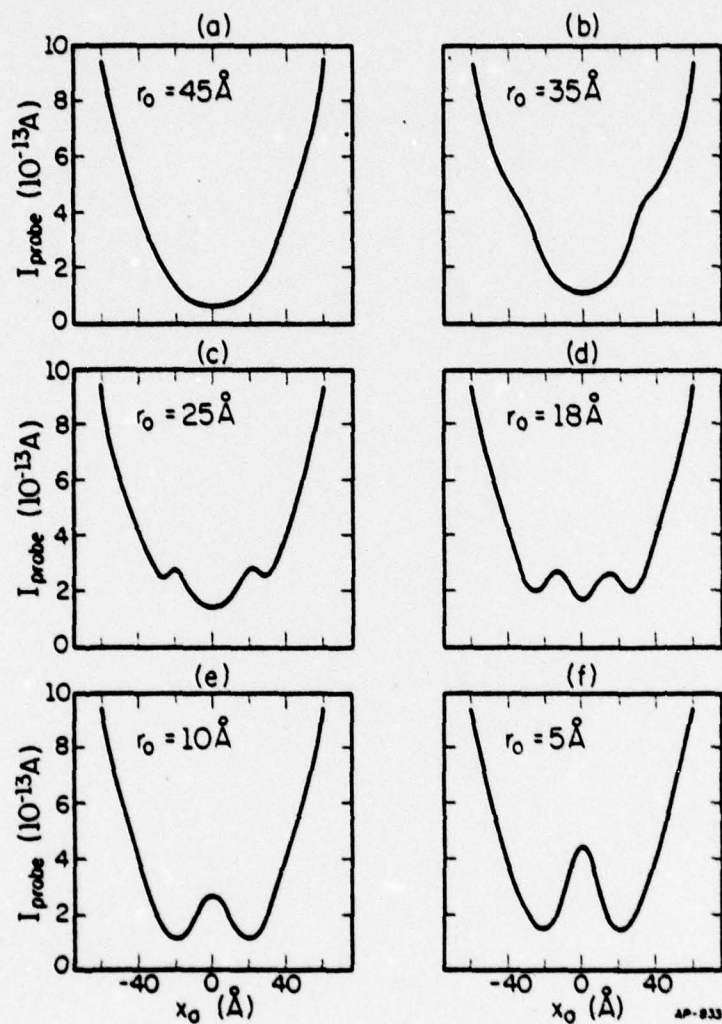


Fig. B.5. Computer simulated scan diagrams for tungsten (110) surfaces. Contributions from local electric fields are assumed smaller than that in Fig. 2.13.

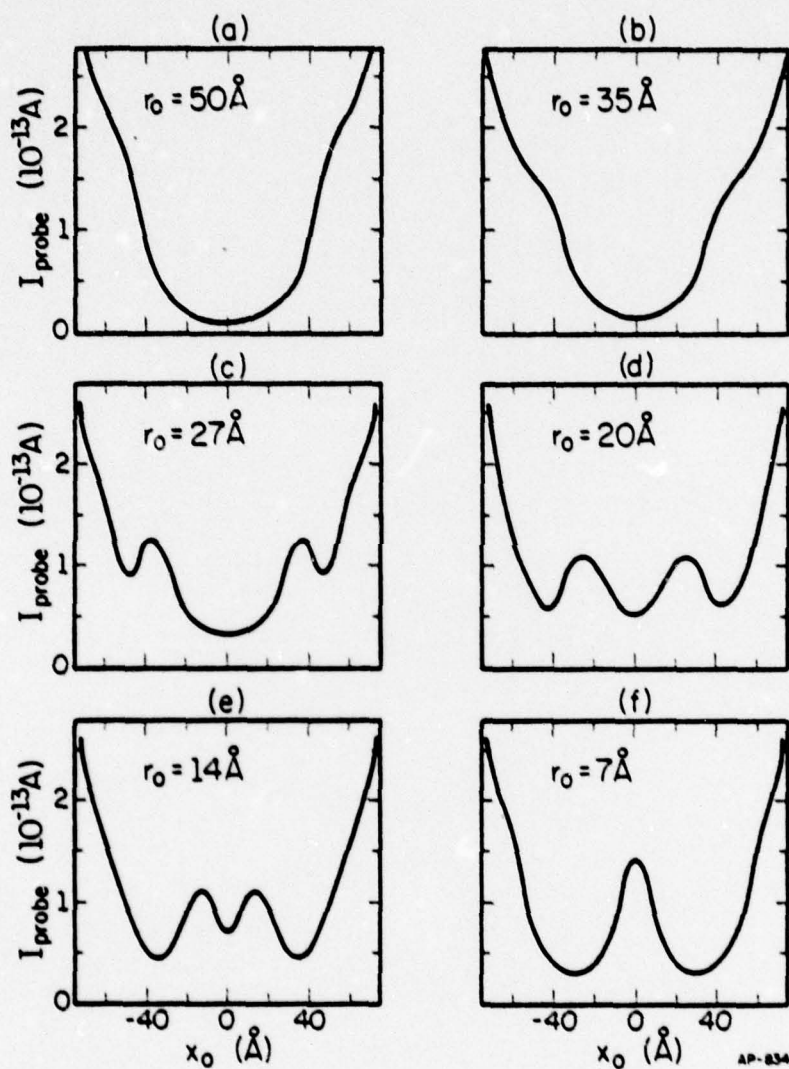


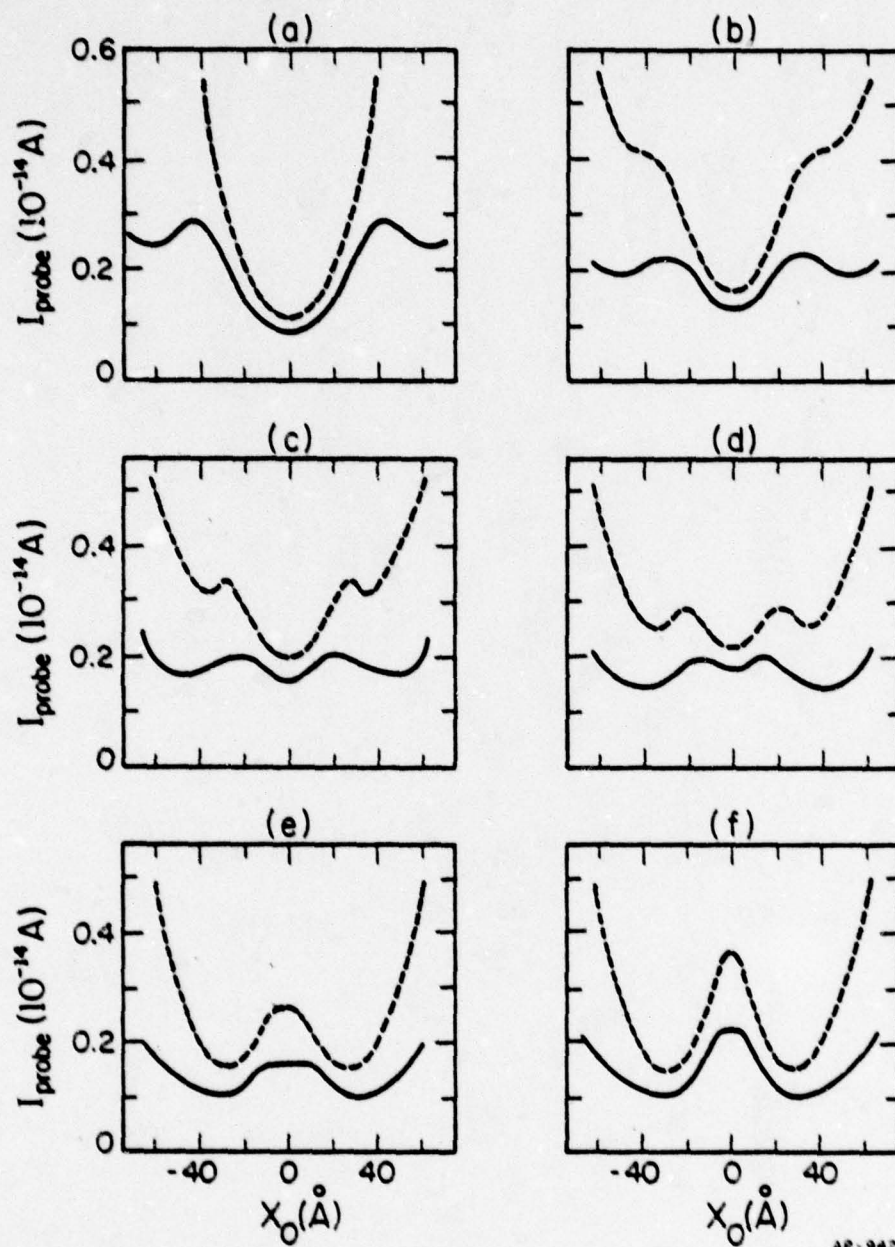
Fig. B.6. Computer simulated scan diagrams for tungsten (110) surfaces with different surface geometries. Contributions from local electric fields are assumed larger than that in Fig. 2.13.

$\gamma = 6$. The surface geometry is the same as that in Fig. B.5. Compared to the scan diagrams in Fig. B.5, those in Fig. B.6 have much larger bumps corresponding to plane edges. Again, essential features in the scan diagrams in Figs. B.5 and B.6 are the same. A comparison of the scan diagrams in Figs. 2.13, B.5 and B.6 indicates that the general features of the scan diagrams do not depend critically on the local electric field. Therefore, even without knowing exactly the local electric field distribution on a surface, considerable information can still be obtained from scan diagrams. This enables us to deduce some quantitative information from scan diagrams, as discussed in Chapter VII.

B.2. Gas Covered Surfaces

Scan diagrams for gas covered surfaces are simulated in much the same way as those for clean surfaces, except that the work function and the pre-exponential factor for the F-N equation must be changed. In our simulation, these changes are made according to experimental results. Take the example of hydrogen adsorption on tungsten: the work function of the rough surface is increased by adsorption, but that for the smooth (110) is decreased. The F-N pre-exponential factor for both rough surfaces and the (110) decreases with adsorption, but with different magnitude. These have been determined by Polizzotti, also by us (Chapter VII). Scan diagrams for gas covered surfaces can be simulated simply by substituting these values into the computer program.

Typical scan diagrams for the hydrogen covered tungsten emitter are shown in Fig. B.7. The parameters determining the surface geometry and the local fields are identical with those shown in Fig. 2.13. In Fig. B.7,



AP-942

Fig. B.7. Computer simulated scan diagrams for tungsten (110) surfaces covered by 1.5×10^{17} molecules/cm² of hydrogen. Solid curves represent gas-covered surfaces; dashed curves represent clean surfaces. Size of the plane in Angstroms: (a) 40; (b) 30; (c) 25; (d) 20; (e) 10; (f) 5.

the scan diagrams for clean surfaces are drawn by dashed lines, and those for gas covered surfaces are shown by solid lines. Hydrogen adsorption was assumed on the plane edges and rough surfaces, but not on the (110) plane nor on top of the cluster. According to the analysis in Chapter VIII, these scan diagrams would represent surfaces exposed to $< 1.5 \times 10^{17}$ molecules/cm² of hydrogen.

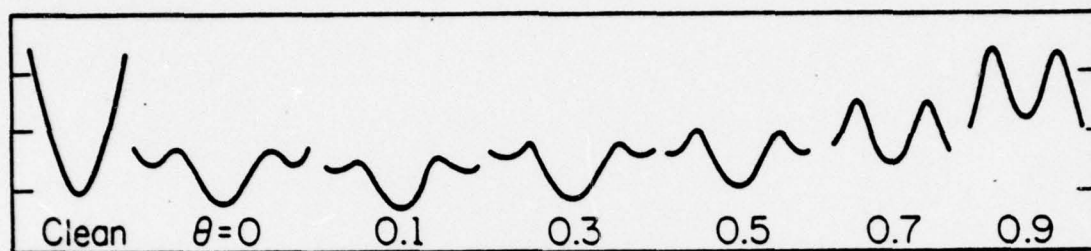
Qualitatively, the scan diagram of gas covered surfaces thus simulated are quite similar to those obtained experimentally. At low exposures, the experimental scan diagram of a flat W(110) plane shows two small satellites on each side of the central minimum. As is clear from Fig. B.7a, two satellites also appear in the scan diagram for a (110) plane of radius $\sim 40\text{\AA}$ when the edges and the (110) terraces are covered by hydrogen. The magnitude of these bumps, however, is much larger than those experimentally observed. This is not surprising, since quantitative simulation is still difficult owing to our lack of information on local fields. Simulated scan diagrams for W(110) planes of radius 30 and 25\AA are shown in Figs. B.7b and c; experimental scan diagrams for gas covered surfaces of similar sizes are not available for comparison. Scan diagrams for large, intermediate, and small clusters on the W(110) plane are shown in Fig. B.7d-f. Again, qualitatively the scan diagrams for large and for intermediate clusters are quite similar to those obtained experimentally, as discussed in Chapter VII. Experimental scan diagrams for small clusters are not available for comparison. For surfaces on which experiments are available for comparison, the simulated scan diagrams agree well qualitatively gas covered surfaces.

Adsorption on a flat surface as a function of surface coverage can also be simulated. This is done by assigning an approximate work function and pre-exponential factor to the flat surface according to experimental results and according to the mechanism of adsorption. For the adsorption of hydrogen on the (110) plane of tungsten, scan diagrams corresponding to two different mechanisms have been simulated. Shown in Fig. B.8a are scan diagrams obtained by assuming a uniformly distributed adsorbate on the (110) plane. In these, the degree of saturation is expressed by the surface fractional coverage θ . Shown in Fig. B.8b are scan diagrams obtained by assuming that adsorption starts at plane edges and that tightly adsorbed hydrogen is completely immobile, following the model proposed in Chapter VIII. The degree of saturation in these scan diagrams is expressed by the region covered by gas, $1 - \frac{r}{r_0}$, where r_0 is the radius of the (110) plane, and r is so defined that the region between r and r_0 is covered by hydrogen. For scan diagrams shown in Figs. B.8a and B.8b, a value of -0.4 eV was assigned to the work function change at saturation, and the pre-exponential change, $\ln(A/A_0)$, was -2.3 , according to experimental results.

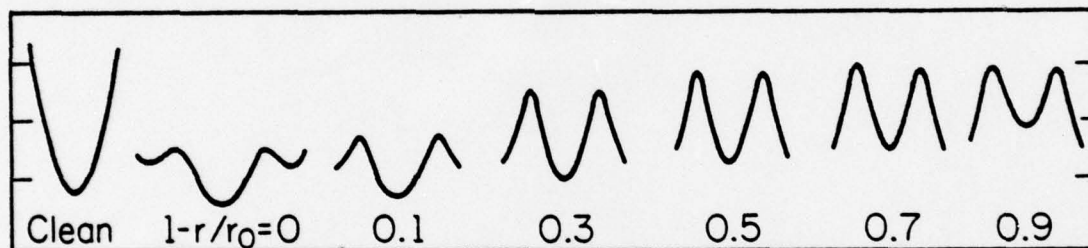
If it is assumed that adsorbate on the (110) plane is uniformly distributed, as in Fig. B.8a, adsorption of hydrogen up to a fractional coverage $\theta \approx 0.5$ does not change the shape of the scan diagram radically from that for which edges and the (110) terraces are covered by hydrogen. However, at a coverage of $\theta = 0.5$, the work function of the (110) regions has already decreased by 0.16 eV (Fig. D.2b). At higher surface coverages, the satellites at each side of the central minimum become prominent. If, however, adsorption starts from the plane edges, as in Fig. B.8b, then

Adsorption on a flat surface as a function of surface coverage can also be simulated. This is done by assigning an approximate work function and pre-exponential factor to the flat surface according to experimental results and according to the mechanism of adsorption. For the adsorption of hydrogen on the (110) plane of tungsten, scan diagrams corresponding to two different mechanisms have been simulated. Shown in Fig. B.8a are scan diagrams obtained by assuming a uniformly distributed adsorbate on the (110) plane. In these, the degree of saturation is expressed by the surface fractional coverage θ . Shown in Fig. B.8b are scan diagrams obtained by assuming that adsorption starts at plane edges and that tightly adsorbed hydrogen is completely immobile, following the model proposed in Chapter VIII. The degree of saturation in these scan diagrams is expressed by the region covered by gas, $1 - \frac{r}{r_0}$, where r_0 is the radius of the (110) plane, and r is so defined that the region between r and r_0 is covered by hydrogen. For scan diagrams shown in Figs. B.8a and B.8b, a value of -0.4 eV was assigned to the work function change at saturation, and the pre-exponential change, $\ln(A/A_0)$, was -2.3 , according to experimental results.

If it is assumed that adsorbate on the (110) plane is uniformly distributed, as in Fig. B.8a, adsorption of hydrogen up to a fractional coverage $\theta \approx 0.5$ does not change the shape of the scan diagram radically from that for which edges and the (110) terraces are covered by hydrogen. However, at a coverage of $\theta = 0.5$, the work function of the (110) regions has already decreased by 0.16 eV (Fig. D.2b). At higher surface coverages, the satellites at each side of the central minimum become prominent. If, however, adsorption starts from the plane edges, as in Fig. B.8b, then



(a)



(b)

AP-934

Fig. B.8. Computer simulated scan diagrams for a flat tungsten (110) surface covered by various amounts of hydrogen. (a) Hydrogen adatoms on the (110) are uniformly distributed. θ = fractional coverage. (b) Adsorption starts from plane edges. Hydrogen covers the region between r and r_0 .

even for $1 - \frac{r}{r_0} = 0.1$ the scan diagram changes significantly. The satellites become prominent at this low coverage despite the fact that the (110) work function changes by < 0.03 eV, hardly a significant change. The prominence of the satellites persists at higher coverages, until near saturation, then the scan diagram becomes relatively smooth. The satellites, however, still remain distinguished.

The scan diagrams in Fig. B.8 do not resemble those obtained experimentally quantitatively no matter which adsorbate distribution is used. Qualitatively the scan diagrams obtained by assuming immobile hydrogen are closer to the experimental ones than for a uniform distribution, as is clear from Fig. 7.13. By combining the shape change of the scan diagram with work function measurements, however, we have been able to deduce that the former mechanism is more favorable, as discussed in Chapter VII.

The scanning technique has the advantage of probing the whole emitter surface at one scan, and therefore could contribute a tremendous saving in experimental effort. In Chapter VII we have illustrated that by combining this technique with work function measurements, unique information about surface kinetic processes can be obtained. In this simulation, attempts to obtain truly quantitative information have not been stressed, owing to the limited knowledge of the field distribution at the surface. In order to fully utilize the potential of this technique, a more quantitative understanding of the scan diagrams is still desirable, however.

APPENDIX C

EFFECTS OF EDGES ON SINGLE PLANE WORK FUNCTION

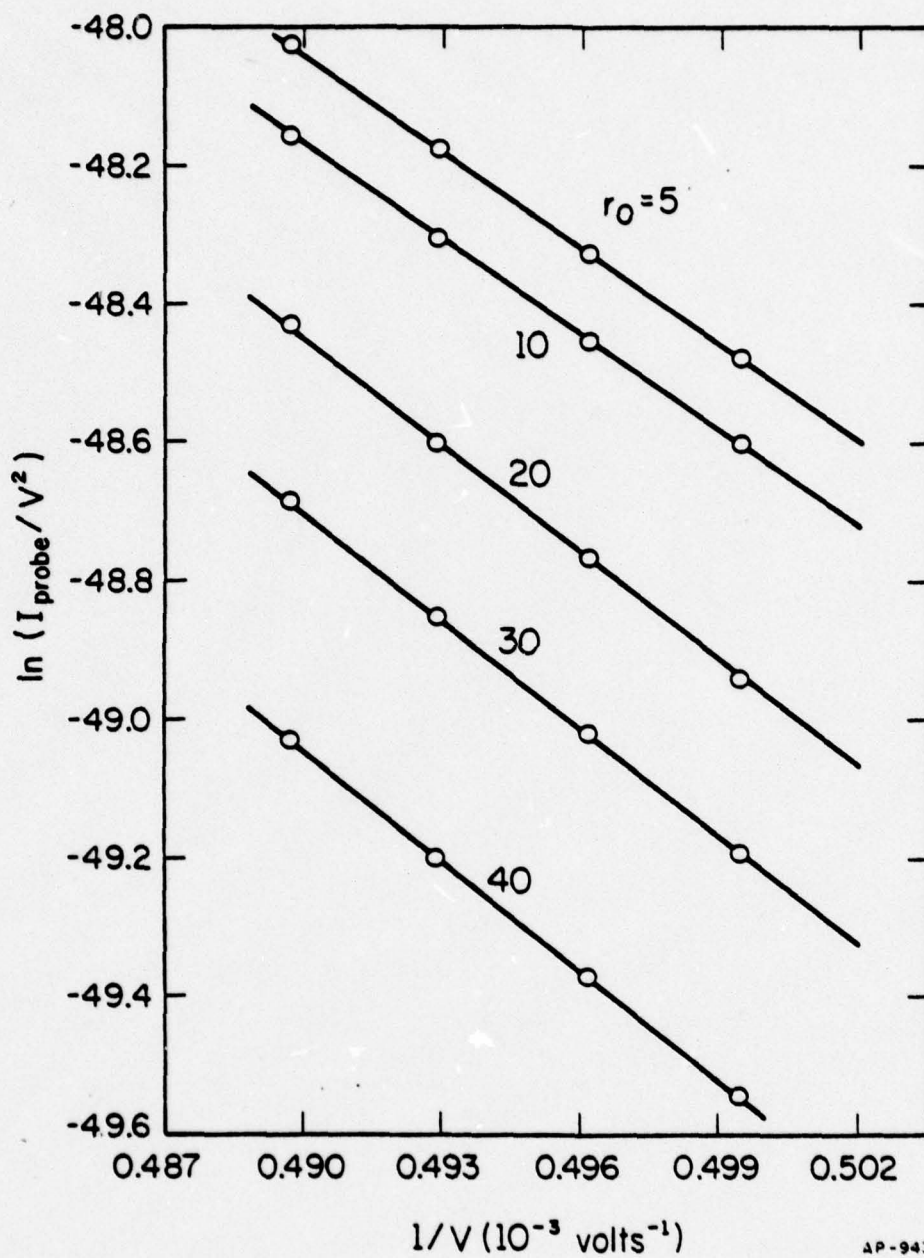
Field evaporation is an ideal way to prepare a surface since both cleanliness and smoothness of the surface are guaranteed. However, the single crystal planes obtained by field evaporation are no larger than 100\AA in diameter. Due to the finite size of the probe hole and the finite resolution in field emission microscopy, contributions from the strongly emitting plane edges could be significant enough to obscure the experimental results. In this Appendix we estimate contributions from plane edges and determine if the experimental conditions routinely achievable are such as to exclude this obscuring effect.

During an experiment intended to detect a chemical reaction on a single crystal plane, the probe hole is focused at the center of the plane. The collector current, however, measures not only the emission from this particular plane but also some of the electrons emitted from the edges of the plane. The work function obtained from FN plots by the procedures described in Chapter II may therefore be affected by edge effects. It is important to distinguish real adsorption on a single crystal plane from changes caused by electron emission from edges.

Except for a few cases where adsorption on a flat surface is delayed relative to rougher surfaces, contributions from plane edges are difficult to determine experimentally. We shall, therefore, estimate the edge contributions by simulation. In Appendix B, we have already calculated the current passing through the probe hole in detail. From this, an FN plot is easily obtained by fixing the probe hole location and generating a series

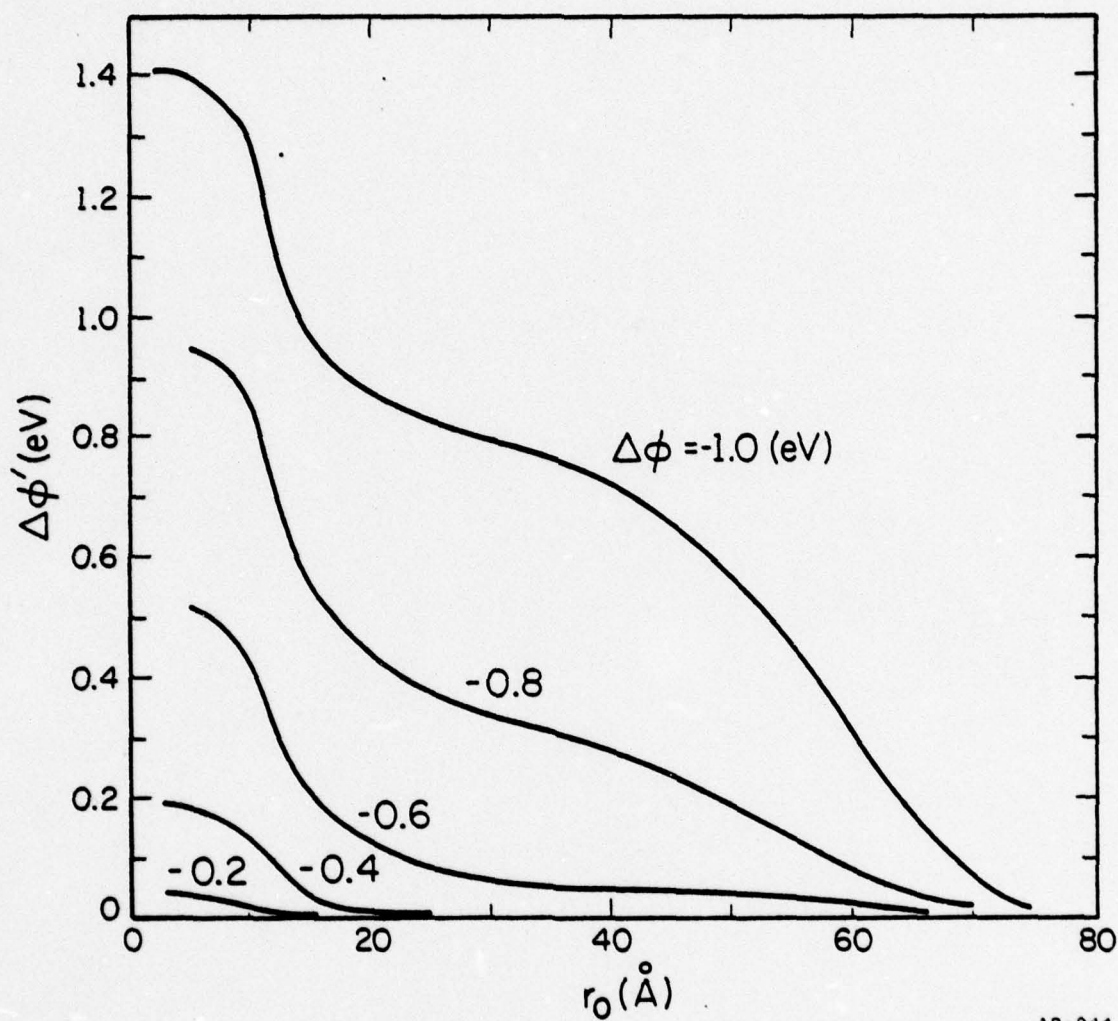
of current-voltage points. The work function ϕ' for the plane, as affected by edge contributions, can then be obtained from the slope of the FN plot by the procedures described in Chapter II. A typical set of FN plots thus obtained for planes of different sizes ($r_0 = 5$ to 40 \AA) is given in Fig. C.1. The FN plot is always a straight line, even for small planes where contributions from plane edges are great. To simulate the work function change caused by adsorption on plane edges, we only have to assign appropriate work functions for plane edges. The apparent work function change $\Delta\phi'$ thus obtained is shown in Fig. C.2. In this figure, the work function change $\Delta\phi'$ caused by edges is plotted as a function of the plane size, r_0 , and as a function of $\Delta\phi$, the difference in the work function of the plane and the edges. These simulation results can only be considered as semi-quantitative, since the local electric field is not known exactly. The general trend of edge contributions, however, is quite clear: the work function of the plane is more strongly affected by plane edges if (a) the size of the plane is small, and (b) the work function difference $|\Delta\phi|$, is large. For a large work function difference, $|\Delta\phi| \geq 0.8 \text{ eV}$, the work function of the plane is strongly affected by plane edges even for the largest plane ($r_0 \sim 50\text{-}60 \text{ \AA}$) achievable by field evaporation. For $|\Delta\phi| < 0.4 \text{ eV}$, edge contributions are negligible for planes of radius $r_0 > 20 \text{ \AA}$. For planes of radius $r_0 < 20 \text{ \AA}$, contributions from plane edges are significant even for small $|\Delta\phi|$.

The work function of a stepped W(110) surface is typically 0.3eV lower than for the flat region [158]. Our measurements on the (0001) terraces of a field evaporated rhenium emitter yielded a value 0.5eV below that of (0001) plane, comparable to the above value. Assuming that $\Delta\phi = -0.6 \text{ eV}$,



AP-943

Fig. C.1. Computer simulated Fowler-Nordheim plots for tungsten (110) surfaces with different geometries.



AP-944

Fig. C.2. Variation of apparent work function changes, due to hydrogen adsorption on plane edges, with plane size. The parameter $\Delta\phi$ is the difference between the clean work functions of the plane edges and the plane.

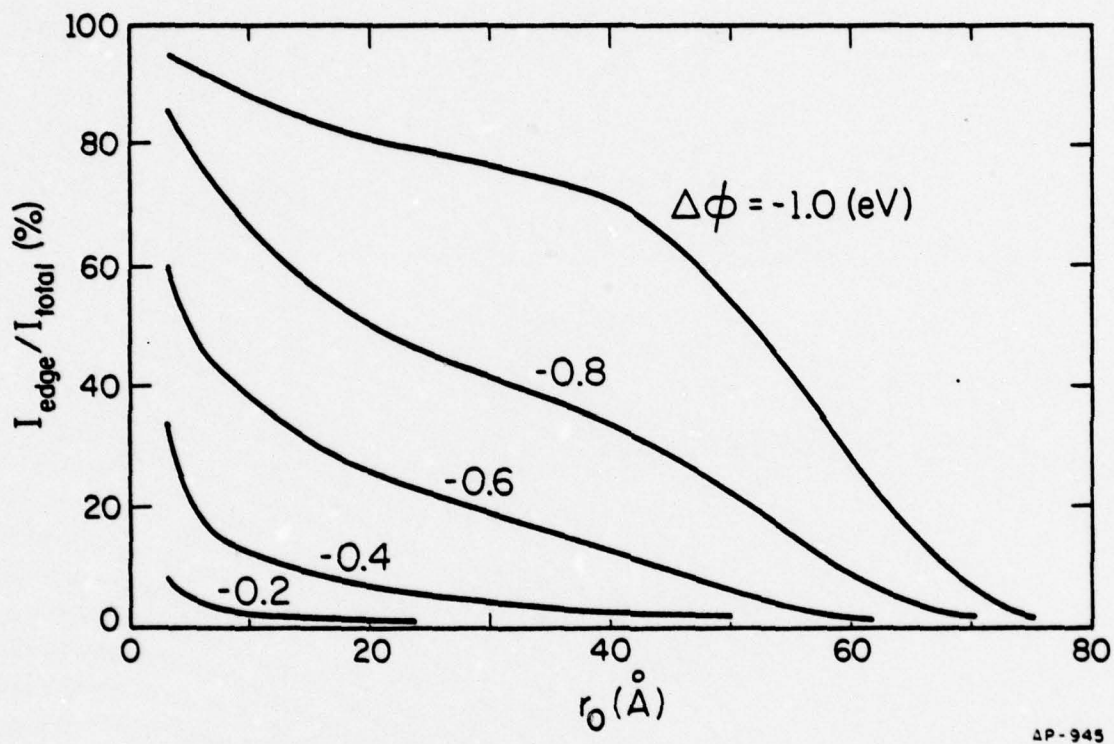
then from Fig. C.2 we conclude that a plane of radius 30-40Å is enough to restrict the edge contributions to work function changes $\Delta\phi'$ below 0.05 eV.

Contributions of plane edges to the probe hole current are much more significant than to the work function. As is evident in Fig. C.3, contributions from plane edges for a surface with $\Delta\phi = -0.6\text{eV}$ become insignificant only when the radius of the plane is larger than 60Å. For a plane of radius $\sim 30\text{Å}$, the electrons emitted from the edges constitute about 20% of the probe hole current, but the work function change $\Delta\phi'$ is still less than 0.05eV. According to our estimates from this simulation, contributions of plane edges to the probe hole cannot be eliminated completely even for the largest planes achievable by field evaporation.

From Figs. C.2 and C.3, we may estimate contributions of plane edges to the single plane work function for materials studied in Chapters. III-VII. The apparent work function change caused by plane edges, $\Delta\phi'$, for the densely packed planes of these materials are shown in Table C1. Only the values corresponding to the highest evaporation voltage are given. The size of the (110) plane of tungsten is determined from the plane size-evaporation voltage relation derived by Polizzotti [3]. At the maximum evaporation voltage of 31 kV, the radius of the (110) plane is $\sim 40\text{Å}$. The size of the densely packed planes of molybdenum, rhenium, and iridium is estimated by comparing with the W(110) plane according to the formula [159]

$$r_0 \approx \alpha \frac{V}{F},$$

where V is the evaporation voltage, r_0 the radius of the plane, F the evaporation field for the particular plane and material, and α a constant independent



AP-945

Fig. C.3. Contribution of plane edges to the emission current, as a function of plane size and $\Delta\phi$.

of geometry and material. The evaporation fields for materials studied in this thesis have been determined by Nakamura [160], and are shown in the first column of Table C1.

Table C1
Contributions of plane edges to the work function

	Evaporation field	Evaporation voltage	r_o (Å) (estimated)	$\phi_{ave} - \phi_{flat}$	$\Delta\phi$ (eV)	$\Delta\phi'$ (eV) (estimated)
W(110)	5.70 V/Å	31.0 kV	40	-1.1 eV	-0.6	0.04
Mo(110)	4.50	22.0	35	-1.1	-0.6	0.06
Re(0001)	4.80	26.0	40	-0.9	-0.5	0.02
Ir(111)	5.00	26.0	38	-0.7	-0.4	0.01

The radius of the densely packed planes thus estimated ranges from 30 to 40 Å. The work function difference between a plane and its edges, $\Delta\phi$, is not generally known. For each material we assign a value approximately 60% the difference between the flat surface and the total emitter work function. This gives a $\Delta\phi \sim -0.6$ eV for W(110) and ~ -0.5 eV for Re(0001), consistent with previous observations. The work function changes caused by plane edges thus estimated are shown in column 6; they are generally ≤ 0.06 eV and are usually within the accuracy of FN measurements. We therefore conclude that by carefully controlling the size of the plane, the single plane work functions are not seriously affected by the plane edges.

Experimental estimates for edge contributions can be obtained only for W(110) and for Re(0001) planes. As discussed in Chapters III and V,

adsorption of hydrogen and nitrogen on these surfaces is extremely slow. For thermally annealed emitters, which have large, flat planes, exposure to $< 1 \times 10^{17}$ molecules/cm² of hydrogen or nitrogen does not bring about any changes in the work function or the emission current, indicating no contributions from plane edges. For field evaporated rhenium and tungsten emitters, however, exposure to small amounts of hydrogen and nitrogen brings about a decrease of 20 to 30% in the probe hole current. The work function change for both the W(110) and the Re(0001) plane with radius larger than $\sim 30 \text{ \AA}$ is less than 0.04 eV at low exposures. Except for the initial decrease in the probe hole current, the adsorption of hydrogen and nitrogen on field evaporated surfaces is not significantly different from that on thermally annealed emitters. We must, therefore, conclude that the initial diminution in the probe hole current on field evaporated emitters is caused by contributions from plane edges. A comparison between estimated edge contributions from our simulation and those from our experiments is given in Table C2. Experimental estimates for edge contributions for Mo(110) and Ir(111) are not possible, since adsorption occurs rapidly.

From Table C2 it is clear that contributions from plane edges estimated from our simulation are comparable to those observed experimentally. The contribution from edges are the smallest for Ir(111), since the work function difference is the smallest. The effect of plane edges is the greatest for Mo(110). However, even for this surface, the estimated work function change caused by plane edges is still far smaller than actually observed. We conclude that the experiments shown in Chapters III-VII are not obscured by effects of plane edges.

Table C2

Comparisons for edge contributions

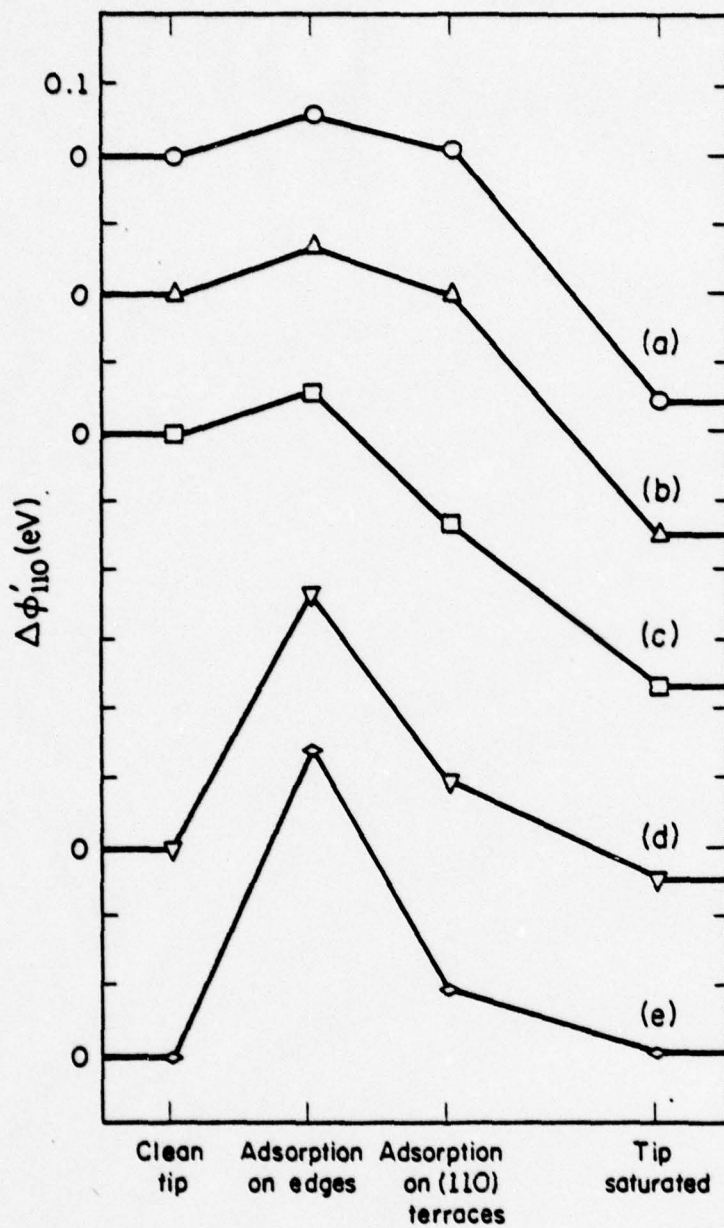
	r_o	$\Delta\phi'$		$\Delta I/I$	
	estimated	estimated	observed	estimated	observed
W(110)	40 Å	0.04 eV	0.04 eV	15%	20%
Mo(110)	35	0.06	—	18%	—
Re(0001)	40	0.02	0.04	10%	30%
Ir(111)	38	0.01	—	4%	—

APPENDIX D

SIMULATION OF WORK FUNCTION CHANGES

In Chapter VII, the promotion by defects of chemisorption on a flat tungsten (110) surface has been studied by direct measurement on surface clusters. For this kind of surface, contributions from strongly emitting cluster edges are not negligible. Experimental results can be interpreted quantitatively only if the change in the work function can be related to the coverage of the surface by gas. For a surface with a cluster, the change in the work function does not necessarily vary linearly with surface coverage. We must, therefore, establish new $\Delta\phi'$ -surface coverage relations for these surfaces. For this purpose we shall simulate the work function change during adsorption on surfaces of various geometries.

The probe hole current for gas covered surfaces can be simulated by the same method as that in Appendix B, and work functions can be obtained by the method described in Appendix C. The work function changes for W(110) planes with different regions covered by hydrogen thus simulated are shown in Fig. D.1. For all surfaces with $r_0 = 5 - 40\text{\AA}$, the work function increases when the plane edges chemisorb hydrogen. The magnitude of the change varies. For a smooth plane the work function increases by only $\sim 0.05\text{eV}$; for a surface with a small cluster the work function increases by 0.45eV . Adsorption on the (110) terraces decreases the work function; again, the change is the greatest for the small cluster. The work function change at saturation also varies with surface geometry: for a flat (110) and for large clusters, the work function at saturation is $\sim 0.3\text{eV}$ below the clean surface; for smaller clusters the work function at saturation is comparable

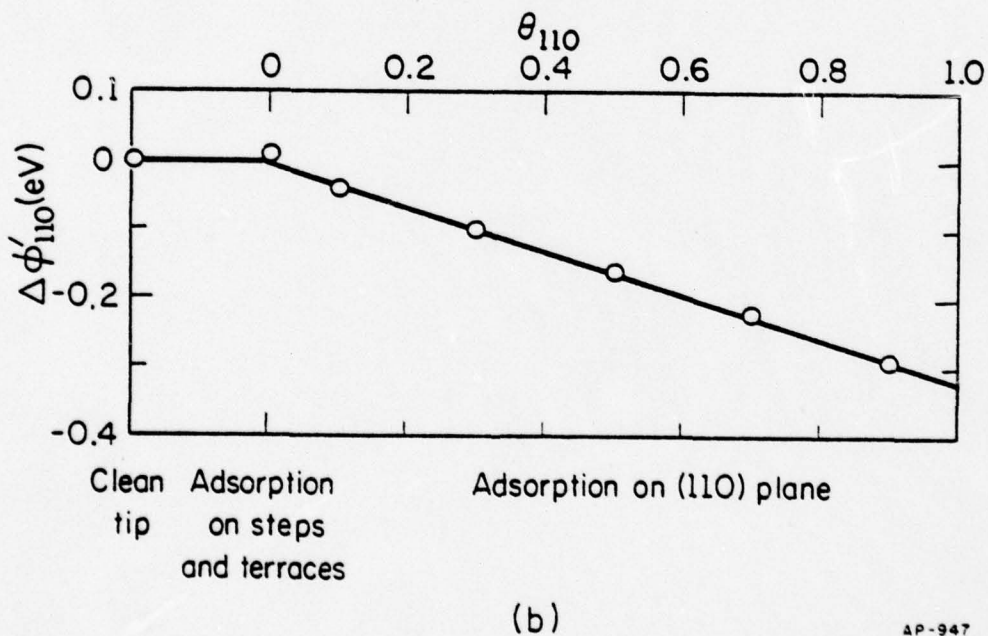
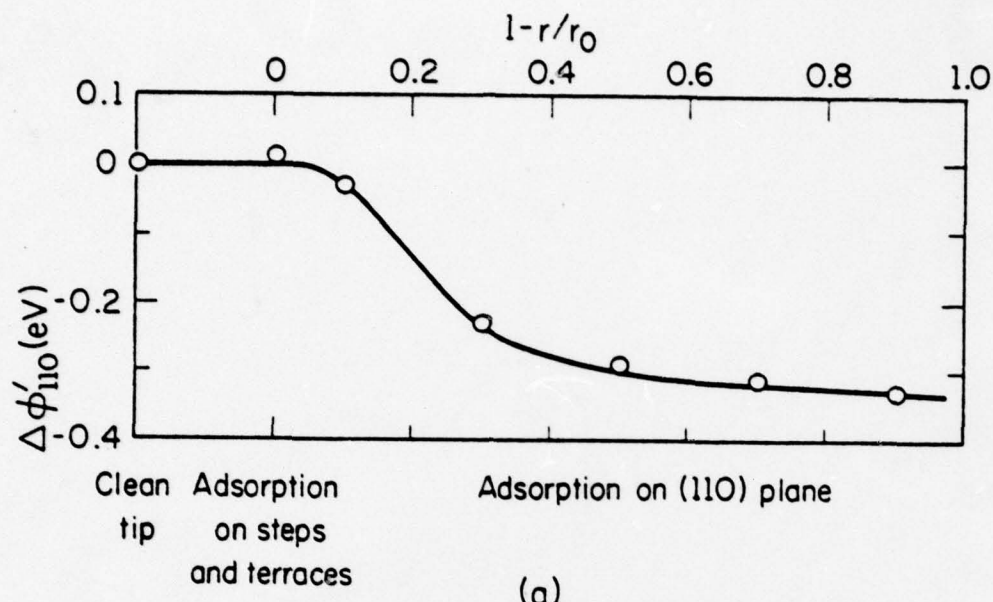


AP-946

Fig. D.1. Variation of computer simulated work function with hydrogen adsorption for tungsten (110) planes. The size of the plane in Angstroms: (a) 40; (b) 35; (c) 20; (d) 10; (e) 5.

to the clean surface. These are in reasonable accord with experimental results, as discussed in Chapter VII.

Work function changes on the (110) can also be simulated when chemisorption on this plane is still proceeding. This is done by assigning an appropriate work function, pre-exponential factor, and adsorbate distribution to the (110) plane. Two possible adsorbate distributions on the (110) are used in our simulation, according to the discussion in Chapter VIII. In Fig. D.2a are shown the work function changes for the (110) plane as a function of surface coverage when hydrogen adatoms are assumed immobile on this surface. Following the model proposed in Chapter VIII, hydrogen adsorption is assumed to start from the plane edges and to spread onto the (110) plane. In this figure surface coverage is measured by $1 - \frac{r}{r_0}$, where r_0 is the radius of the plane, and r is so defined that hydrogen covers the region between r and r_0 . It is evident from this figure that the work function does not vary linearly with surface coverage. Even for such a smooth plane, the work function change need not be proportional to surface coverage if adsorbate on this plane is not uniformly distributed. The work function changes for a (110) plane with mobile hydrogen adatoms, hence uniformly distributed adsorbates, are shown in Fig. D.2b. In this, the surface coverage is measured by θ , the fractional coverage. The work function changes linearly with surface coverage, as expected. Mobile hydrogen adatoms, however, cannot explain the experiments shown in Chapter VII, as discussed in Chapter VIII. In the simulations hereafter we shall always assume that hydrogen adsorbed on the (110) plane is immobile.



AP-947

Fig. D.2. Variation of computer simulated work function with surface coverage by hydrogen for a tungsten (110) plane with radius = 40 Å. (a) Adsorption starts from plane edges; (b) adsorption on the (110) plane is uniform.

Work function changes on surfaces with clusters can be simulated in the same manner as for smooth (110) planes. The direct dissociation on the (110) plane is ignored; chemisorption on the (110) is assumed caused only by dissociation on cluster edges and on plane edges. Tightly bound hydrogen is assumed immobile at the temperature of interest. Therefore, adsorption on the (110) plane is assumed to start from the plane edges and cluster edges, and to spread according to the mechanism described in Chapter VIII. According to the same mechanism, chemisorption on top of a cluster is assumed promoted by its edges, but at a lower rate. The work function changes thus simulated for (110) planes with clusters of radius 20, 10 and 5 Å are shown in Figs. D.3-D.5.

In Fig. D.3a is shown the work function change of the (110) region for a plane with a large cluster ($r_0 = 20\text{Å}$) on top. Adsorption on the plane edges and the cluster edges brings about an increase in the work function. Thereafter the work function decreases almost lineally until $\sim 90\%$ of the (110) is covered, then it decreases sharply to saturation. This sharp change in the slope may be understood by considering the work function changes as a function of coverage on the (110) terrace, and on top of the cluster, shown in Figs. D.3b and D.3c. According to the mechanism described in Chapter VIII, chemisorption on the (110) terrace proceeds at a faster rate than on top of the cluster. As a result, the (110) plane is saturated by hydrogen before the top of the large cluster reaches saturation. As shown in Fig. D.3b the simulated (110) work function decreases only by $\sim 0.2\text{eV}$ when the (110) terrace is saturated by hydrogen. The work function reaches saturation only when the top of the cluster is covered by hydrogen. This is more clearly shown by plotting the fractional coverage on the (110)

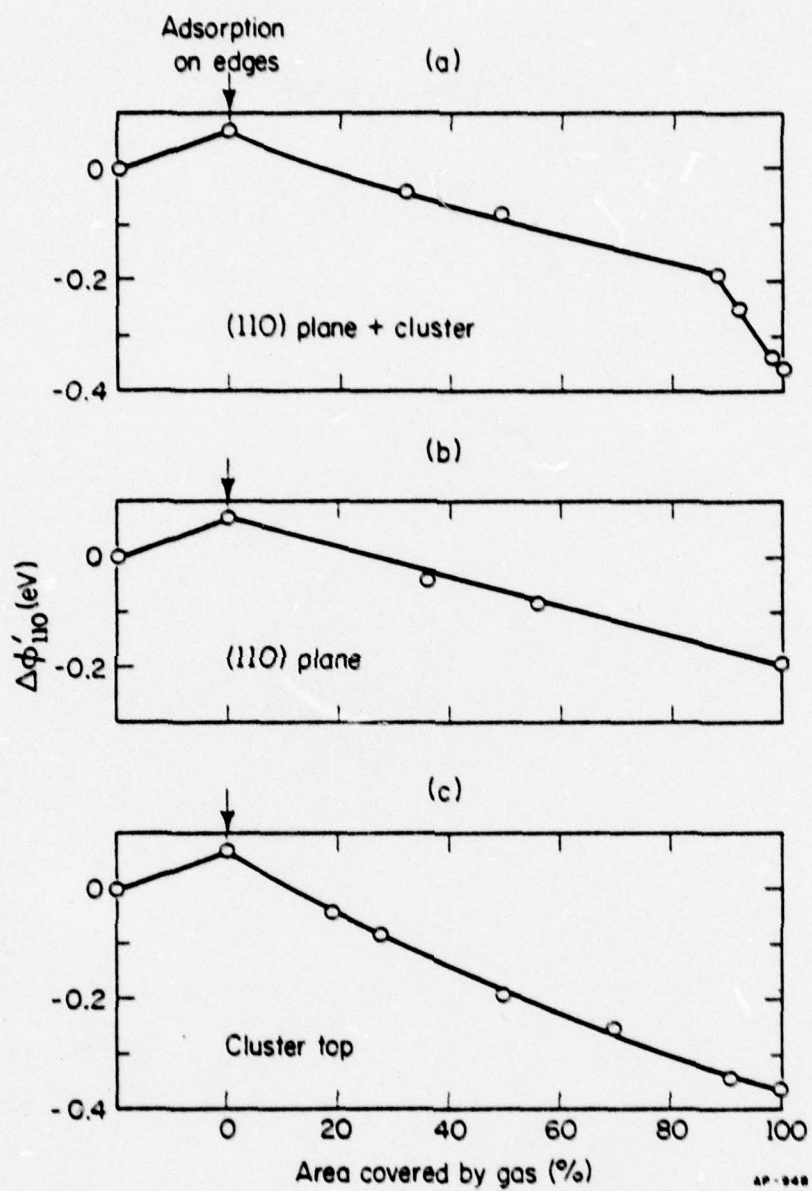


Fig. D.3. Variation of work function with a large cluster on top. Abscissas indicate percentage coverages: (a) (110) + cluster; (b) (110) plane only; (c) cluster only.

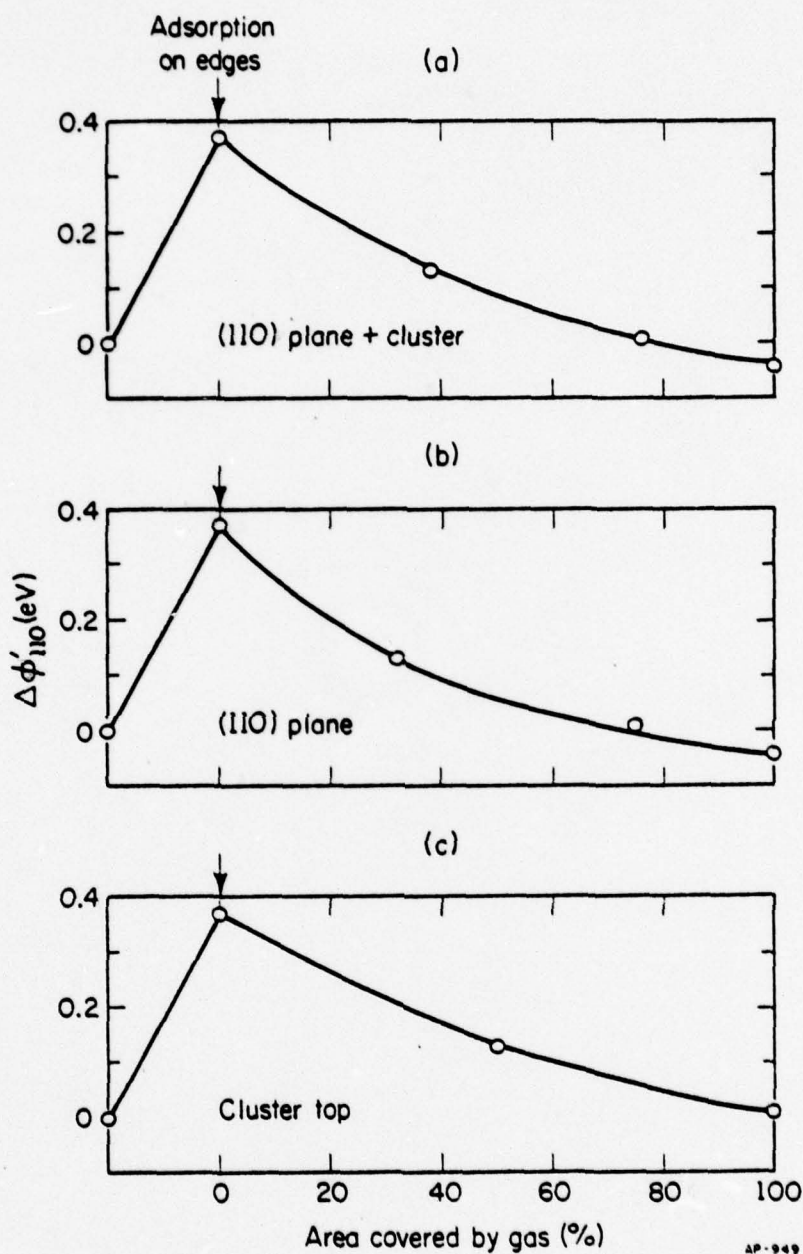


Fig. D.4. Changes of simulated work function with surface coverage for a tungsten (110) surface with an intermediate cluster on top. Abscissas indicate percentage coverage by hydrogen: (a) (110) + cluster; (b) (110) only; (c) cluster top only.

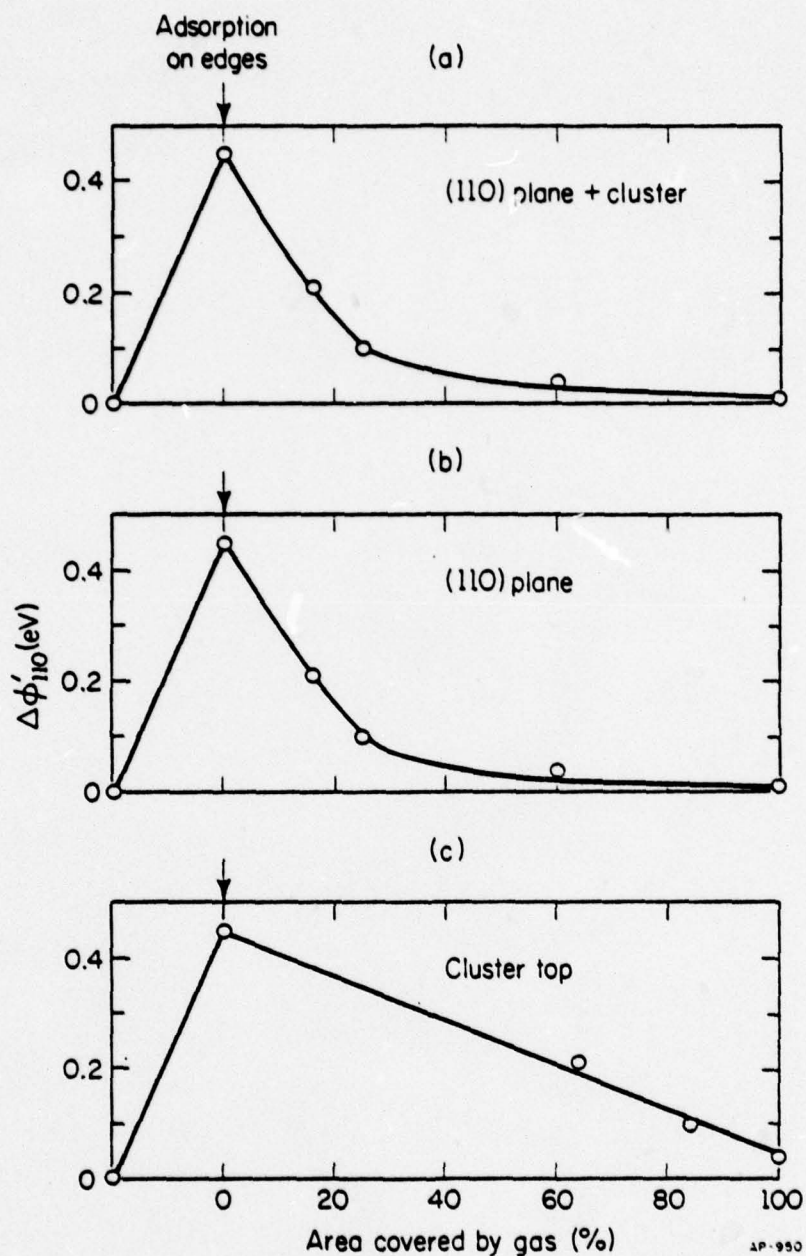
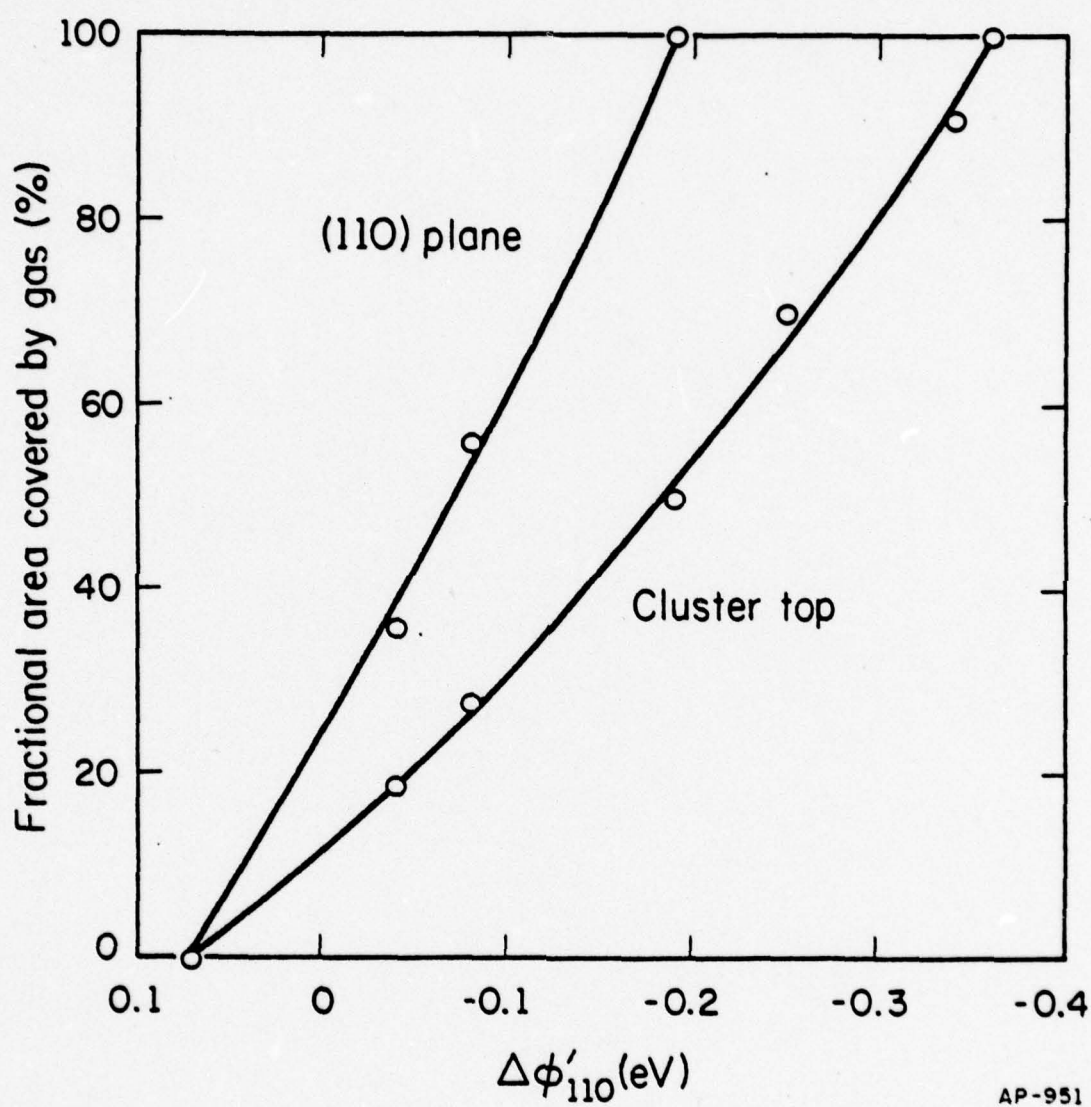


Fig. D.5. Changes of computer simulated work function with surface coverage for a tungsten (110) surface with a small cluster on top. Abscissas indicate percentage coverage by hydrogen: (a) (110) + cluster top; (b) (110) plane only; (c) cluster top only.

terrace and on top of the cluster as a function of $\Delta\phi'$, as in Fig. D.6. Only $\sim 50\%$ of the cluster top is covered by hydrogen when the (110) terrace is saturated. The work function change corresponding to the saturation of the (110) terrace, 0.19eV, is the same as that when the sharp change in slope occurs in Fig. D.3a. The change in slope therefore corresponds to the saturation of the (110) terrace. This is expected, since adsorption on top of a large cluster is responsible for most of the work function changes, as is evident from Fig. D.1c.

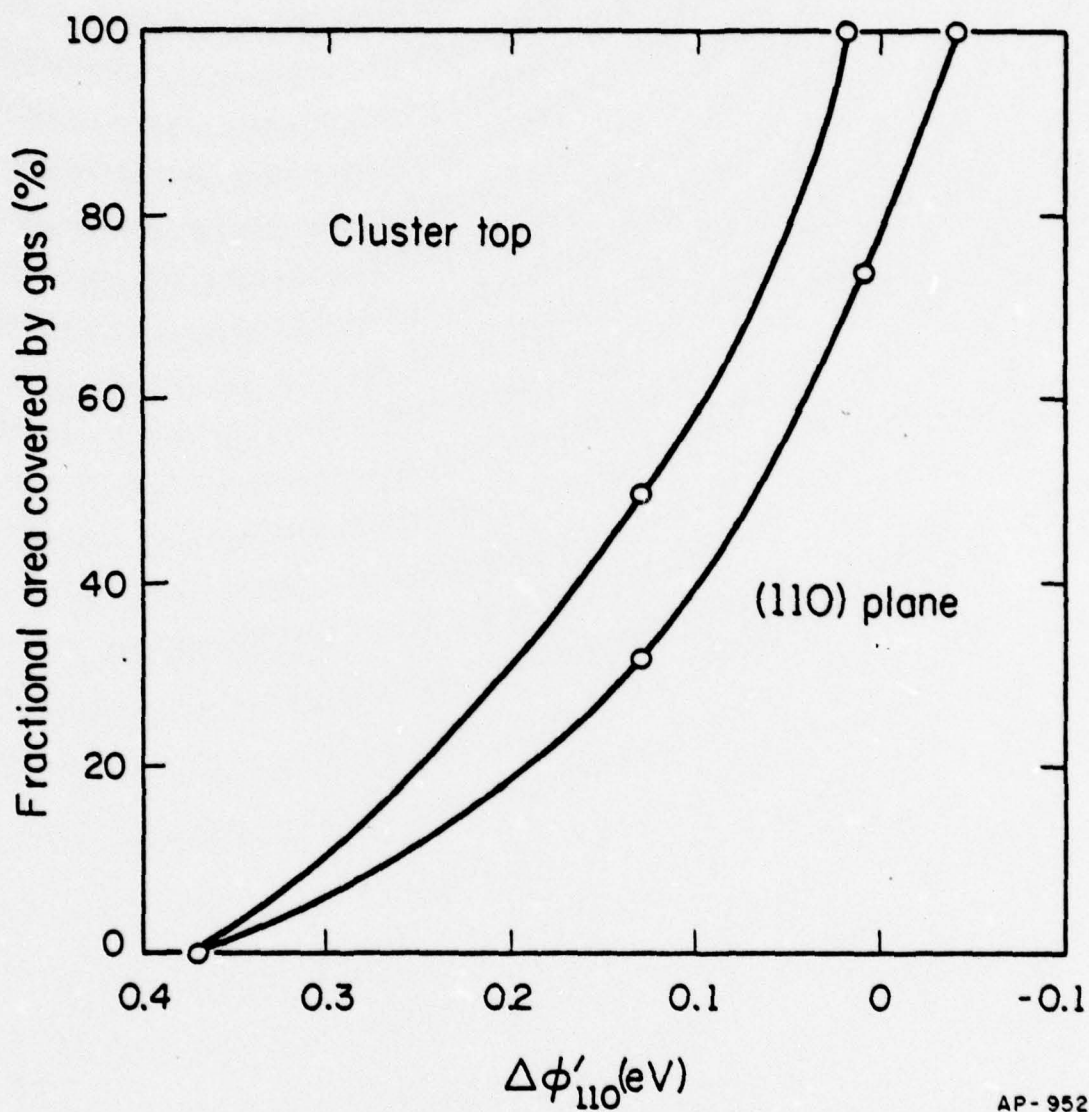
Simulated work function changes for a (110) with an intermediate cluster ($r_o = 10\text{\AA}$) are shown as a function of coverage for the whole (110) region in Fig. D.4a, for the (110) plane in Fig. D.4b, and on top of the cluster in Figs. D.4c. In these simulations, the relative rate of filling for the (110) plane and for the top of the cluster is estimated according to the mechanism described in Chapter VIII. It appears that the top of the cluster is saturated when only about 70% of the (110) plane is covered by hydrogen, as shown in Fig. D.7.

Work function changes on a (110) plane with a small cluster ($r_o = 5\text{\AA}$) on top as a function of coverage are shown in Fig. D.5a, b, c. Adopting again the mechanism in Chapter VIII, the top of the cluster is saturated when less than 50% of the (110) plane is covered by hydrogen, as shown in Fig. D.8. In Figs. D.5a and b, 90% of the work function drop occurs before the (110) plane is half saturated. This is expected, since the top of the cluster, as well as the region near the cluster, is saturated by hydrogen earlier than the rest of the (110) plane. The effect of adsorption on regions far away from the probe hole is quite small.



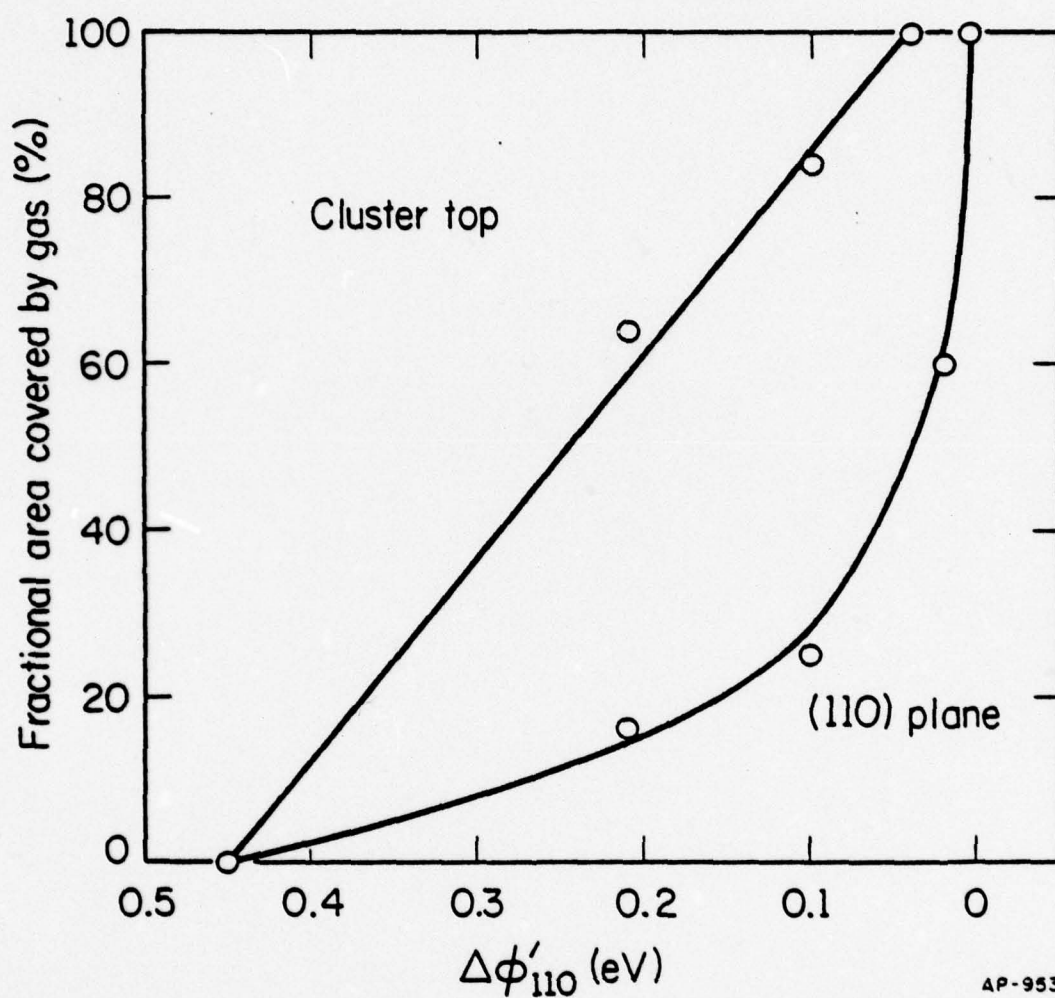
AP-951

Fig. D.6. Variation of percentage coverage by hydrogen on various regions of tungsten (110) plane with computer simulated work function changes. The (110) consists of a flat plane with a radius of 40 Å, with a large cluster with radius 20 Å on top.



AP-952

Fig. D.7. Variation of hydrogen coverage on various regions of a tungsten (110) plane with computer simulated work function changes. The (110) surface consists of a flat plane (radius = 40 Å) with an intermediate cluster (radius = 10 Å) on top.



AP-953

Fig. D.8. Variation of hydrogen coverage on the tungsten (110) plane with computer simulated work function changes. The (110) region consists of a flat plane (radius = 40 Å) with a small cluster (radius = 5 Å) on top.

The simulated work function changes shown in Figs. D.2-D.5 do not resemble real experimental curves, since they are plotted against surface coverages while experimental curves are drawn as a function of exposure. In order to achieve some feeling about how the simulation conforms to real experiments, we have drawn the work function changes versus exposures to hydrogen. This is done by deriving a coverage-exposure relation from Eq. (8.19). If we integrate Eq. (8.19) with respect to time, we get

$$\begin{aligned}
 N_{110} &= \int_0^t R_{110} dt \\
 &= R_o s_o' [1 + \exp((-V_t + V_e)/kT)]^{-1} \cdot \left[\frac{N_c}{N} + \frac{N_p}{N} \cdot \exp((-V_t + V_e)/kT) \right] \int_0^t f(\theta) dt \\
 &= R_o s_o \int_0^t f(\theta) dt , \tag{D.1}
 \end{aligned}$$

where $s_o = s_o' [1 + \exp((-V_t + V_e)/kT)]^{-1} \cdot \left[\frac{N_c}{N} + \frac{N_p}{N} \cdot \exp((-V_t + V_e)/kT) \right]$ is the initial sticking coefficient. Let $\theta = N_{110}/N$, then Eq. (D.1) becomes an integral equation,

$$\theta = \frac{R_o}{N} s_o \int_0^t f(\theta) dt , \tag{D.2}$$

where θ is a function of time. By differentiation, we get the differential equation

$$\frac{d\theta}{dt} = \frac{R_o s_o}{N} f(\theta) . \tag{D.3}$$

Assuming $f(\theta) \approx 1 - \theta$, Eq. (D.3) can be solved explicitly, giving

$$\theta(t) = 1 - \exp\left(-\frac{R_o s_o}{N} t\right) . \tag{D.4}$$

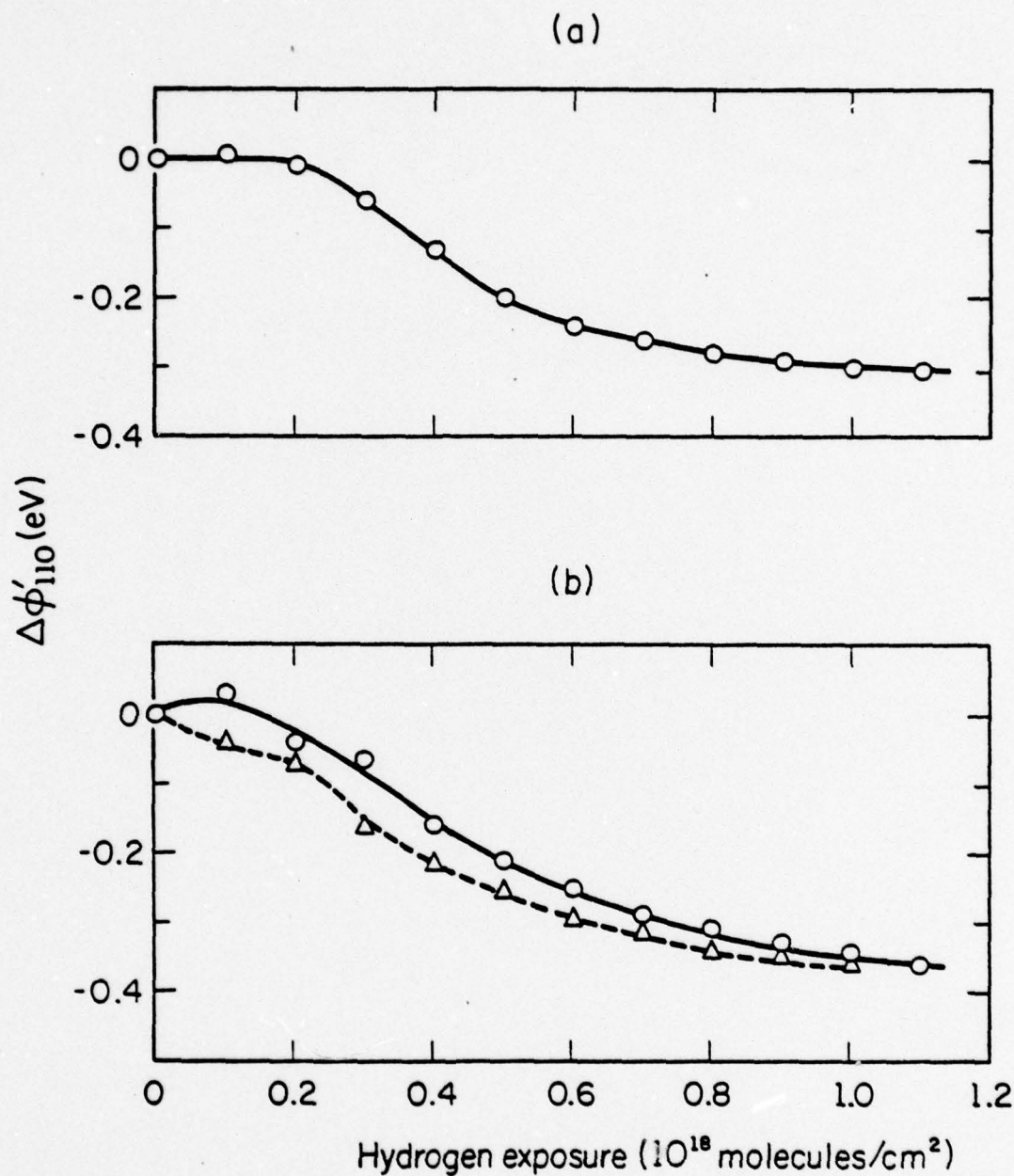
Let χ be the total exposure. At a constant pressure the total exposure χ is given by $\chi = R_0 t$. In terms of this, the fractional coverage on the (110) becomes

$$\theta(\chi) = 1 - \exp\left(-\frac{\chi s_0}{N}\right). \quad (D.5)$$

The work function change on the (110) as a function of exposure can now be plotted according to the following procedures: for a given exposure χ , the surface coverage $\theta(\chi)$ can be estimated from Eq. (D.5); the work function change $\Delta\phi'$ corresponding to this surface coverage may be obtained from Figs. D.2-D.5, depending on the geometry of the surface.

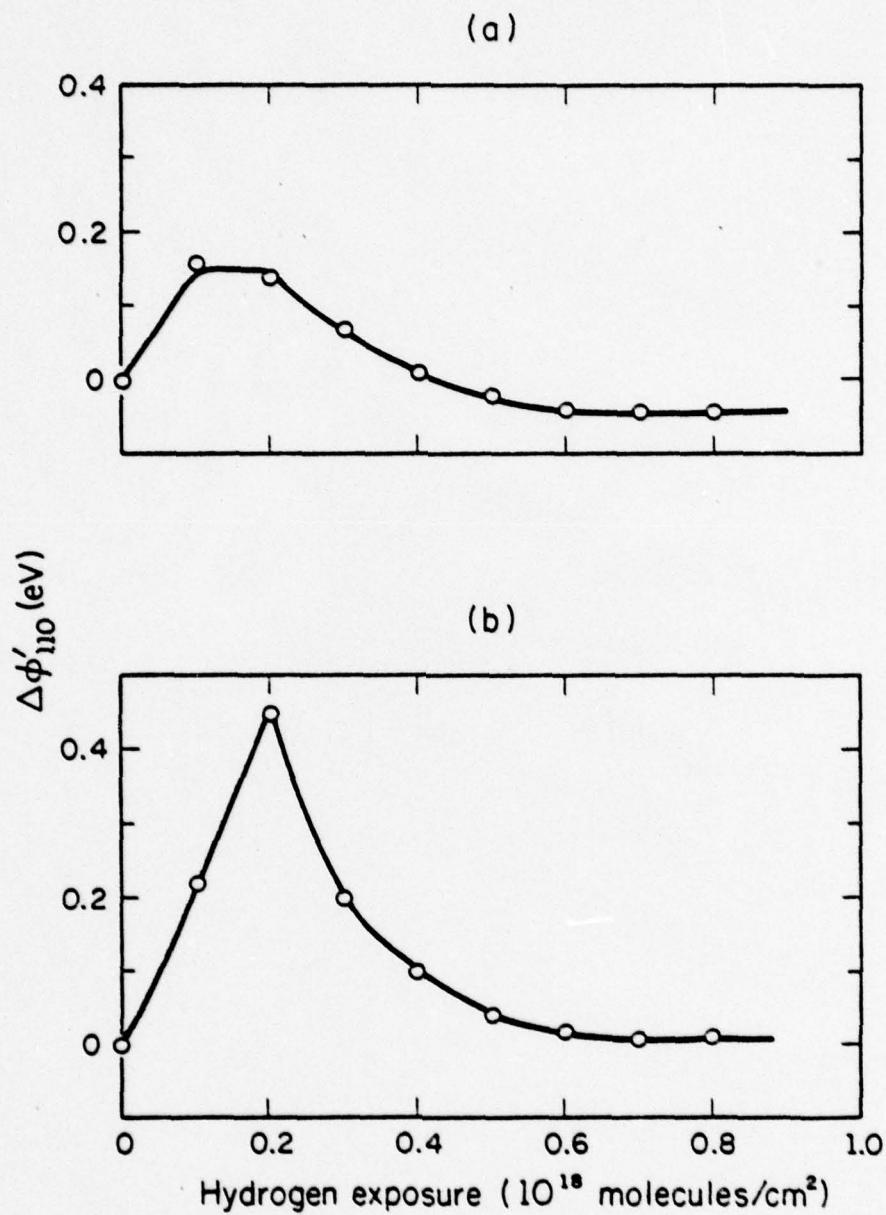
Adsorption curves ($\Delta\phi'$ vs. exposure curves) thus obtained are shown in Figs. D.9 and D.10. The following assumptions have been used: the sticking coefficient s' is assumed ~ 0.04 , following the discussion in Chapter VIII; the plane edges saturate at a total exposure of 2.3×10^{17} molecules/cm², according to experiments shown in Chapter VII; the promotion of adsorption on the flat (110) by defects is assumed to start when $\sim 50\%$ of the edge sites are occupied by hydrogen. In this last assumption, the value of 50% was chosen arbitrarily, since neither theoretical nor experimental data are available. In Fig. D.9a is shown the work function change as a function of exposure for a smooth (110) plane of radius $r_0 = 40\text{\AA}$. Hydrogen adatoms are assumed immobile at the temperature of interest, and work function changes are obtained from Fig. D.2a. An incubation period is clear in this adsorption curve. The general shape of this curve is similar to those obtained experimentally, shown in Figs. 7.4-7.9.

The work function changes for a (110) plane of radius 40\AA with a large cluster of radius 20\AA on it are shown in Fig. D.9b. The solid curve



AP-954

Fig. D.9. Variation of computer simulated work function changes with hydrogen exposure for tungsten (110) planes: (a) for a flat (110) plane with radius = 40 Å; (b) for (110) plane (radius = 40 Å) with a large cluster (radius = 20 Å) on top. The dashed curve in (b) is obtained by assuming immediate defect-promoted adsorption on the (110). For solid curves, defect-promoted adsorption does not occur until after a total exposure of 1×10^{17} molecules/cm².



AP-955

Fig. D.10. Variation of computer simulated work function changes with hydrogen exposure for tungsten (110) planes: (a) for a (110) plane ($r = 40$ Å) with an intermediate cluster ($r = 10$ Å) on top; (b) with a small cluster ($r = 5$ Å) on top.

represents the changes in the work function when defect-promoted adsorption on the (110) flats is assumed to start after a total exposure of 1×10^{17} molecules/cm². This assumption is the same as that used in obtaining Fig. D.9a. The dashed curve shows the work function change if defect-promoted adsorption on the (110) flats occur immediately on exposure to hydrogen. According to Chapter VIII, the rate of adsorption on this surface has been assumed faster than that on a smooth (110) plane, since now the cluster edges also contribute to promote adsorption on the flats. However, this is not reflected in the work function changes shown in Fig. D.9b. Except for the initial rise (decrease, for the dashed curve), the work function does not change appreciably faster than that for a smooth (110) plane. From our simulation, we understand that this is caused primarily by the non-linear dependence of work function change upon coverage for the smooth (110) plane (Fig. D.2a). The $\Delta\phi'$ -coverage relation for the surface with a large cluster is essentially linear, as evident from Fig. D.3c. It is interesting to note that this actually shows up in our experiments (Fig. 7.9): for a surface with a large cluster, the exposure necessary to saturate the entire (110) region is about the same as that for a smooth (110) plane. Our simulation seems to describe the real surface events reasonably. In fact, the experimental adsorption curve is quite similar to the dashed curve in Fig. D.9b.

In Figs. D.10a and b are shown the work functions changes for surfaces with an intermediate cluster (radius = 10\AA) and for a small cluster (radius = 5\AA). A comparison between Fig. D.10a and Fig. 7.6 proves that they are quite similar, except at higher exposures. As discussed in Chapter VIII, at high exposures a new state, which cannot be simulated by

our program, probably forms. Fig. D.10b is obtained by assuming that defect-promoted adsorption occurs after the edges are saturated by hydrogen. This assumption is made partly because a small cluster is less effective in promoting chemisorption on the (110) flats, and partly because the adsorption curve thus obtained looks more similar to the experimental ones. A comparison with Fig. 7.4 shows that it does in fact resemble the experimental adsorption curve.

Therefore, by adopting the mechanism in Chapter VIII, the work function change on surfaces of various geometry can be simulated. From the correspondence between simulated and experimental adsorption curves this simulation seems reasonable. The work function thus simulated can only be regarded as semi-quantitative, owing to the unknown local fields. However, these can already help us to understand surface kinetic processes. The work function change vs. surface coverage relation, even in this semi-quantitative form, is important for the explanation of direct measurements on surface clusters.

APPENDIX E

COMPUTER PROGRAMS

Listed in this Appendix is a FORTRAN program, SCAN, used for simulating scan diagrams for clean and gas covered surfaces. It is designed to run on a time-sharing terminal of a CYBER-175 computer (made by Control Data Corp.). The program used for data analysis, FNWORK, is a FORTRAN program designed to run on a PDP-10 computer (made by Digital Equipment Corp.). FNWORK has been listed in Reference 3.

PROGRAM SCAN

```

00050 PROGRAM SCAN(INPUT,OUTPUT)
00060 THIS PROGRAM SIMULATES THE PROBE HOLE SCAN OF AN EMITTER
00070 ALL INPUTS SHOULD BE IN INTEGERS
00080 THIS PROGRAM INVOLVES MANY DOUBLE INTEGRATIONS
00090 BEWARE OF COMPUTER TIME
00100 INTEGER R3,X5,Y5,Q5
00110 REAL LEDGE(100),J0,J1,M1,L
00120 DIMENSION ANGLE(200),RADIAL(200),RING(100)
00130 DIMENSION B(10,10),CCC(10,10)
00134 FREEX=1.
00135 EDG=2.
00136 PREF=0.2
00137 STEP=2.
00138 ALPHA=6.
00139 GAMMA=3.
00140 DO 398 I=1,10
00150 DO 397 J=1,10
00160 B(J,I)=0
00170 CCC(J,I)=0
00180 397 CONTINUE
00190 398 CONTINUE
00200 P0=5.4
00205 P0 IS THE WORK FUNCTION OF THE PLANE
00210 WRITE 402
00220 402 FORMAT(15H A8?,A9? IN I3:)
00225 A8,A9,A10 DEFINE LOCAL ELECTRIC FIELD
00230 READ 404,L10,L11,L14
00240 404 FORMAT(3I3)
00250 WRITE 406
00260 406 FORMAT(22H MULTIPLICATION FACTOR)
00265 MULTIPLICATION FACTOR DEFINES FIELD SURROUNDING THE CENTRAL PLANE
00270 READ 408,L12
00275 408 FORMAT(I2)
00280 P1=-0.8
00285 P1=DIFFERENCE IN WORK FUNCTION BETWEEN PLANE AND EDGES
00290 V1=2000.
00295 V1=APPLIED VOLTAGE
00300 P9=3.14159
00310 T0=1800.
00315 T0=RADIUS OF THE TIP
00320 M1=5.5E+8/T0
00325 M1=MAGNIFICATION
00330 R0=.375E+7/M1
00335 R0=PROBE SIZE
00340 G0=R0/T0
00350 N=50
00360 N1=40
00370 N2=24
00380 N5=24
00390 512 WRITE 513
00400 513 FORMAT(13H INPUT FIELD )
00410 READ 515,L7
00415 L7/300.=AVERAGE FIELD
00420 515 FORMAT(I3)
00430 IF (L7.LE.0) GO TO 4700
00440 Q4=0
00450 1600 WRITE 1603
00460 1603 FORMAT(23H INPUT RADIUS OF PLANE:)
00465 R9=RADIUS OF PLANE IN ANGSTROM
00470 Q5=0
00480 Q4=Q4+1
00490 READ 1612,R8
00500 1612 FORMAT(I2)

```

```

00490 READ 1612,R8
00500 1612 FORMAT(I2)
00510 IF (R8.LE.0) GO TO 512
00520 RING(1)=R8
00530 IF (RING(1).GT.45)GO TO 1645
00535 DEFINE TIP GEOMETRY
00540 RING(2)=62
00550 LEDGE(2)=62-RING(1)
00560 GO TO 1670
00570 1645 RING(2)=RING(1)+17
00580 LEDGE(2)=17
00590 1670 LEDGE(3)=14
00600 RING(3)=RING(2)+14
00610 LEDGE(1)=RING(1)
00620 DO 1720 I=1,4
00630 RING(I+3)=RING(I+2)+10
00640 LEDGE(I+3)=10
00650 1720 CONTINUE
00660 DO 1760 I=1,4
00670 RING(I+7)=RING(I+6)+8
00680 LEDGE(I+7)=8
00690 1760 CONTINUE
00700 DO 1800 I=1,4
00710 RING(I+11)=RING(I+10)+6
00720 LEDGE(I+11)=6
00730 1800 CONTINUE
00740 DO 1840 I=1,4
00750 RING(I+15)=RING(I+14)+4
00760 LEDGE(I+15)=4
00770 1840 CONTINUE
00780 F0=L7/1000.
00790 F3=0.0001*L12*L7/300./35.
00800 A6=0.001*L7/300.
00810 A7=10.
00820 A6=A6/3./A7
00830 A8=L10/100.*(L7/300.)
00840 A9=L11/10.
00841 IF (RING(1).GT.9) GO TO 2001
00842 A10=L14/100.
00843 GO TO 2002
00844 2001 A10=A8
00845 2002 CONTINUE
00850 2030 WRITE 2035
00860 2035 FORMAT(30H INPUT PROBE LOCATIONS X0Y0: )
00870 READ 2042,X5,Y5
00880 2042 FORMAT(2I2)
00890 X0=X5
00900 Y0=Y5
00910 Q5=Q5+1
00920 IF (Y0.LT.0) GO TO 1600
00930 Q2=0
00940 Z0=SQRT(X0*X0+Y0*Y0)
00950 R2=Z0+80.
00960 IF (Z0.LE.80) GO TO 2110
00970 C0=ATAN(80/SQRT(Z0*Z0-6400.))
00980 R1=Z0-80.
00990 GO TO 2120
01000 2110 R1=0.
01010 C0=P9
01015 DECIDE RANGE OF PROBE
01020 2120 DO 2140 I=1,18
01030 IF (R1.LT.RING(I)) GO TO 2150
01040 2140 CONTINUE
01050 2150 II=I

```



```

01060 DO 2180 I=1,18
01070 IF (R2.LT.RING(I)) GO TO 2190
01080 2180 CONTINUE
01090 2190 I2=I-1
01100 2210 DO 4500 K=I1,I2
01110 IF (K.GT.1) GO TO 3400
01115 NM=N+1
01120 DO 2620 J=1,NM
01125 CALCULATE CONTRIBUTIONS FROM PLANE
01130 R=(J-1)*(RING(1)-EDG)/N
01140 F1=A6*LEDGE(1)*(R/LEDGE(1)-1.)*2
01150 U=((LEDGE(1)-EDG/2.-R)/A9)**2
01160 IF (U.LT.15) GO TO 2260
01170 F2=0.
01180 GO TO 2280
01190 2260 IF (RING(1).LE.10) GO TO 2268
01200 F2=A8*EXP(-U)
01210 GO TO 2280
01220 2268 F2=A8*(A7/RING(1))*0.8*EXP(-U)
01230 2280 F=F0+F3*R*R+F1
01240 F=F+F2
01250 Y=3.7946*F**0.5/P0
01260 Z=(1-SQRT(1-Y*Y))/(1+SQRT(1-Y*Y))
01270 CALL FNT1(Z,FNT,FNV)
01280 J0=1.54E-6*F*F/P0/(FNT**2)
01290 J0=J0*EXP(-.683066*P0**1.5*FNV/F)
01295 NM1=N1+1
01300 DO 2560 I=1,NM1
01310 C=(I-1)*P9/N1
01320 X1=R*COS(C)
01330 Y1=R*SIN(C)
01340 X2=X1-X0
01350 Y2=Y1-Y0
01360 R9=SQRT(X2*X2+Y2*Y2)
01370 IF (R9.GT.R0) GO TO 2490
01380 P8=1.
01390 GO TO 2550
01400 2490 G1=R9/T0
01410 G8=8.5955*V1/4.*(G1-G0)**2
01420 IF (G8.LT.20) GO TO 2540
01430 P8=0.
01440 GO TO 2550
01450 2540 P8=EXP(-G8)*ATAN(R0/R9)/P9
01460 2550 ANGLE(I)=P8
01470 2560 CONTINUE
01480 R5=0.
01490 R6=0.
01495 NM12=N1/2-1
01500 DO 2575 I=1,NM12
01510 R5=R5+ANGLE(2*I)
01520 R6=R6+ANGLE(2*I+1)
01530 2575 CONTINUE
01540 A=(ANGLE(1)+ANGLE(N1+1)+4*(R5+ANGLE(N1))+2*R6)
01550 A=A/3./N1
01560 RADIAL(J)=2*A*J0*R
01570 M=J-1
01580 IF (R.GT.RING(1)-EDG) GO TO 2630
01590 2620 CONTINUE
01600 Z7=M
01610 2630 IF (Z7/2.EQ.M/2) GO TO 2650
01620 M=M-1
01630 2650 M=M
01640 H2=RING(1)-2
01650 H1=0.
01660 N3=M
01670 H=(H2-H1)/N3

```

```

01660 N3=M
01670 H=(H2-H1)/N3
01680 R5=0.
01690 R6=0.
01695 NM32=N3/2-1
01700 DO 2688 I=1,NM32
01710 R5=R5+RADIAL(2*I)
01720 R6=R6+RADIAL(2*I+1)
01730 2688 CONTINUE
01740 A=H*(RADIAL(1)+RADIAL(N3+1)+4*(R5+RADIAL(N3))+2*R6)
01750 A=A/3.
01760 B(Q5,K)=1
01770 Q1=A
01780 WRITE 2699,A
01790 2699 FORMAT(6HPLANE ,E14.7)
01800 DO 3100 J=1,NM
01805 CALCULATE CONTRIBUTIONS FROM PLANE EDGES
01810 R=RING(1)-EDG+EDG*(J-1)/N
01820 F1=A6*LEDGE(1)*(R/LEDGE(1)-1.)*2
01830 F2=A10*EXP(-((LEDGE(1)-EDG/2.-R)/A9)**2)
01832 IF (RING(1).GE.10) GO TO 101
01834 F2=F2
01836 101 CONTINUE
01840 F=F3*R*R+F1
01850 F=F0+F+F2
01860 CONTINUE
01950 Y=3.7946*F**.5/(P0+P1)
01960 IF (Y.LT.1) GO TO 2820
01970 Y=0.99999999
01980 2820 Z=(1-SQRT(1-Y*Y))/(1+SQRT(1-Y*Y))
01990 CALL FNT1(Z,FNT,FNV)
02000 J1=1.54E-6*F*F/(P0+P1)/(FNT**2)*PREP
02010 J1=J1*EXP(-.683066*(P0+P1)**1.3*FNV/F)
02020 DO 3070 I=1,NM1
02030 Q=(I-1)*F9/N1
02040 X1=R*COS(Q)
02050 Y1=R*SIN(Q)
02060 X2=X1-X0
02070 Y2=Y1-Y0
02080 R9=SQRT(X2*X2+Y2*Y2)
02090 IF (R9.GT.R0) GO TO 3000
02100 P8=1.
02110 GO TO 3060
02120 3000 G1=R9/T0
02130 G8=8.5955*V1/4.*(G1-G0)**2
02140 IF (G8.LT.20) GO TO 3050
02150 P8=0.
02160 GO TO 3060
02170 3050 P8=EXP(-G8)*ATAN(R0/R9)/P9
02180 3060 ANGLE(I)=P8
02190 3070 CONTINUE
02200 R5=0.
02210 R6=0.
02220 DO 3085 I=1,NM12
02230 R5=R5+ANGLE(2*I)
02240 R6=R6+ANGLE(2*I+1)
02250 3085 CONTINUE
02260 A=ANGLE(1)+ANGLE(N1+1)+4*(R5+ANGLE(N1))
02270 A=A+2*R6
02280 A=A/3./N1
02290 RADIAL(J)=2*A*J1*R
02300 3100 CONTINUE
02310 H2=RING(1)
02320 H1=RING(1)-EDG
02330 N3=N
02340 H=(H2-H1)/N3
02350 R5=0.
02360 R6=0.

```

```

02365 NM32=N3/2-1
02370 DO 3147 I=1,NM32
02380 R5=R5+RADIAL(2*I)
02390 R6=R6+RADIAL(2*I+1)
02400 3147 CONTINUE
02410 A=RADIAL(1)+RADIAL(N3+1)
02420 A=A+R*(R5+RADIAL(N3))+2*R6
02430 A=A/H/3.
02440 Q1=Q1+A
02450 WRITE 3156,A
02460 3156 FORMAT(SHEDGE ,E14.7)
02470 CCC(Q5,K)=A
02480 3160 GO TO 4500
02490 3400 IF (K.EQ.2) GO TO 3440
02495 CALCULATE CONTRIBUTIONS FROM PLANE VICINALS
02500 N4=N5
02505 NM4=N4+1
02510 GO TO 3500
02520 3440 N4=N
02525 NM4=N4+1
02530 3500 DO 3800 J=1,NM4
02540 R=RING(K-1)+(J-1)*(LEDGE(K)-EDG)/N4
02550 R3=R-RING(K-1)
02560 F1=A6*LEDGE(K)*(R3/LEDGE(K)-1)
02570 U=((LEDGE(K)-EDG/2.-R3)/A9)**2
02580 IF (U.LT.15) GO TO 3540
02590 F2=0.
02600 GO TO 3550
02610 3540 F2=AB*EXP(-U)
02620 3550 F=F0+F3*R*R+F1+F2
02630 Y=3.7946*F**5/F0
02640 Z=(1-SQRT(1-Y*Y))/(1+SQRT(1-Y*Y))
02650 CALL FNT1(Z,FNT,FNV)
02660 J0=1.54E-6*F*F/F0/(FNT**2)
02670 J0=J0*EXP(-.683066*F0**1.5*FNV/F)
02680 DO 3770 I=1,NM1
02690 C=(I-1)*C0/N1
02700 X1=R*COS(C)
02710 Y1=R*SIN(C)
02720 X2=X1-X0
02730 Y2=Y1-Y0
02740 R9=SQRT(X2*X2+Y2*Y2)
02750 IF (R9.GT.R0) GO TO 3700
02760 P8=1.
02770 GO TO 3760
02780 3700 G1=R9/T0
02790 G8=8.5955*U1/4.*(G1-G0)**2
02800 IF (G8.LT.20) GO TO 3750
02810 P8=0.
02820 GO TO 3760
02830 3750 P8=EXP(-G8)*ATAN(R0/R9)/F9
02840 3760 ANGLE(I)=P8
02850 3770 CONTINUE
02860 R5=0.
02870 R6=0.
02880 DO 3785 I=1,NM12
02890 R5=R5+ANGLE(2*I)
02900 R6=R6+ANGLE(2*I+1)
02910 3785 CONTINUE
02920 A=ANGLE(1)+ANGLE(N1+1)
02930 A=A+4*(R5+ANGLE(N1))+2*R6
02940 A=A/3./N1
02950 RADIAL(J)=2*A*J0*R
02960 3800 CONTINUE
02970 H2=RING(K)-EDG
02980 H1=RING(K-1)
02990 N3=N4
03000 H=(H2-H1)/N3

```



```

02970 H2=RING(K)-EDG
02980 H1=RING(K-1)
02990 N3=N4
03000 H=(H2-H1)/N3
03010 R5=0.
03020 R6=0.
03025 NM32=N3/2-1
03030 DO 3837 I=1,NM32
03040 R5=R5+RADIAL(2*I)
03050 R6=R6+RADIAL(2*I+1)
03060 3837 CONTINUE
03070 A=RADIAL(1)+RADIAL(N3+1)
03080 A=A+R6*2+4*(R5+RADIAL(N3))
03090 A=A/H/3.
03100 IF (Q4.GT.1) GO TO 3847
03110 B(Q5,K)=A
03120 GO TO 3850
03130 3847 IF (K.GT.2) GO TO 4555
03140 3850 Q1=Q1+A
03150 WRITE 3856,A,K
03160 3856 FORMAT(E14.7,I2)
03170 IF (A/Q1.GT.0.02) GO TO 3859
03180 Q2=1
03190 3859 Q2=Q2
03195 NM2=N2+1
03200 DO 4400 J=1,NM2
03210 R=RING(K)-EDG+EDG*(J-1)/N2
03220 R3=R-RING(K-1)
03230 F1=A6*LEDGE(K)*(R3/LEDGE(K)-1.)
03240 F2=A8*EXP(-(LEDGE(K)-EDG/2.-R3)/A9)**2)
03250 F=F0+F3*R*R+F1
03260 F=F+F2
03360 Y=3.7946*F**0.5/(F0+F1)
03370 IF (Y.LT.1) GO TO 4130
03380 Y=0.999999999999
03390 4130 Z=(1-SQRT(1-Y*Y))/(1+SQRT(1-Y*Y))
03400 CALL FNT1(Z,FNT,FNV)
03410 J1=1.54E-6*F*F/(F0+F1)/(FNT**2)*PREP
03420 J1=J1*EXP(-.683066*(F0+F1)**1.5*FNV/F)
03430 DO 4370 I=1,NM1
03440 Q=(I-1)*C0/N1
03450 X1=R*COS(Q)
03460 Y1=R*SIN(Q)
03470 X2=X1-X0
03480 Y2=Y1-Y0
03490 R9=SQRT(X2*X2+Y2*Y2)
03500 IF (R9.GT.R0) GO TO 4300
03510 P8=1.
03520 GO TO 4360
03530 4300 G1=R9/T0
03540 G8=8.5955*V1/4.*(G1-G0)**2
03550 IF (G8.LT.20) GO TO 4350
03560 P8=0.
03570 GO TO 4360
03580 4350 P8=EXP(-G8)*ATAN(R0/R9)/P9
03590 4360 ANGLE(I)=P8
03600 4370 CONTINUE
03610 R5=0.
03620 R6=0.
03630 DO 4385 I=1,NM12
03640 R5=R5+ANGLE(2*I)
03650 R6=R6+ANGLE(2*I+1)
03660 4385 CONTINUE
03670 A=ANGLE(1)+ANGLE(N1+1)
03680 A=A+4*(R5+ANGLE(N1))+2*R6
03690 A=A/3./N1
03700 RADIAL(J)=2*A*J1*R
03710 4400 CONTINUE

```

```

03720 H2=RING(K)
03730 H1=RING(K)-EDG
03740 N3=N2
03750 H=(H2-H1)/N3
03760 R5=0.
03770 R6=0.
03775 NM32=N3/2-1
03780 DO 4441 I=1,NM32
03790 R5=R5+RADIAL(2*I)
03800 R6=R6+RADIAL(2*I+1)
03810 4441 CONTINUE
03820 A=RADIAL(1)+RADIAL(N3+1)
03830 A=A+4*(R5+RADIAL(N3))+2*R6
03840 A=A*H/3.
03850 WRITE 4446,A
03860 4446 FORMAT(E14.7)
03870 4450 Q1=Q1+A
03880 CCC(Q5,K)=A
03890 4460 IF (A/Q1.GE.0.02) GO TO 4500
03900 4470 IF (Q2.EQ.1) GO TO 4550
03910 4500 CONTINUE
03920 4550 Q11=ALOG(Q1/F0/F0)
03930 WRITE 4551,Q1,Q11
03940 4551 FORMAT(SH SUM ,2E14.7)
03950 GO TO 2030
03960 4555 Q3=0
03970 4560 DO 4580 I=3,10
03980 Q3=Q3+B(Q5,I)+CCC(Q5,I)
03990 4580 CONTINUE
04000 4595 Q1=Q1+Q3
04005 Q11=ALOG(Q1/F0/F0)
04010 4590 WRITE 4551,Q1,Q11
04020 4600 GO TO 2030
04030 4700 STOP
04040 4800 END
04050 SUBROUTINE FNT1(X,FNT,FNV)
04060 A1=-1.3293373
04070 A2=.312530542
04080 A3=.038378
04090 A4=-.009912374
04100 A5=-.01165886
04110 B1=-.750016317
04120 B2=.092013612
04130 B3=-.004906196
04140 B4=-.020665635
04150 B5=-0.003571204
04160 C1=.443251415
04170 C2=.062606012
04180 C3=.047573837
04190 C4=.017365064
04200 D1=.249983683
04210 D2=.0920018
04220 D3=.040696975
04230 D4=.005264496
04240 AA=1+A1*X+A2*X*X+A3*X*X*X+A4*X*X*X+A5*X*X*X
04250 BB=B1*X+B2*X*X+B3*X*X*X+B4*X*X*X+B5*X*X*X
04260 BB=BB*ALOG(1/X)
04270 CC=1+C1*X+C2*X*X+C3*X*X*X+C4*X*X*X
04280 DD=D1*X+D2*X*X+D3*X*X*X+D4*X*X*X
04290 DD=DD*ALOG(1/X)
04300 FNV=(1+X)**(-1.5)*(AA+BB)
04310 FNT=(1+X)**(0.5)*(CC+DD)
04320 RETURN
04330 END
READY.

```

REFERENCES AND FOOTNOTES

1. G. A. Somorjai, *Acc. Chem. Res.* 9, 278 (1976).
2. J. R. Anderson, R. J. MacDonald and Y. Shimoyama, *J. Catal.* 20, 147 (1971).
3. R. S. Polizzotti, Ph.D. thesis, University of Illinois, Urbana, Illinois (1974).
4. S. L. Bernasek, W. J. Siekhaus and G. A. Somorjai, *Phys. Rev. Lett.* 30, 1202 (1972).
S. L. Bernasek and G. A. Somorjai, *J. Chem. Phys.* 62, 3149 (1975).
5. K. E. Lu and R. R. Rye, *Surf. Sci.* 45, 677 (1974).
6. K. Christmann and G. Ertl, *Surf. Sci.* 60, 365 (1976).
7. H. C. Yao and M. Shelef, *J. Catal.* 43, 392 (1976).
8. E. W. Müller, *Z. Phys.* 106, 541 (1937).
9. E. W. Müller, *Z. Phys.* 108, 668 (1938).
10. R. Gomer, *Field Emission and Field Ionization*, (Harvard University Press, Cambridge, Massachusetts, 1961), pp. 1-63.
11. R. H. Fowler and L. Nordheim, *Proc. R. Soc. London*, A121, 173 (1928).
12. L. Nordheim, *Proc. R. Soc. London*, A121, 626 (1928).
13. H. C. Miller, *J. Franklin Instit.* 282, 382 (1966).
A. van Oostrom, *Philips Res. Rep. Suppl.* 1, 1 (1966).
14. E. W. Müller and T. T. Tsong, *Field Ion Microscopy*, (American Elsevier Publishing Co., New York, 1969).
15. E. W. Müller, *Adv. Electron. Electron Physics.* 13, 83 (1960).
16. R. D. Young and E. W. Müller, *J. Appl. Phys.* 33, 91 (1962).
17. R. D. Young and H. E. Clark, *Phys. Rev. Lett.* 17, 351 (1966),
Appl. Phys. Lett. 9, 265 (1966).
18. T. V. Vorburger, D. Penn and E. W. Plummer, *Surf. Sci.* 48, 417 (1975).
19. R. S. Chambers, Ph.D. Thesis, University of Illinois, Urbana, Illinois (1975).

20. S. P. Sharma and G. L. Schrenk, Phys. Rev. B2, 598 (1970).
21. R. H. Good and E. W. Müller, Handb. der Phys. 21, 176 (1956).
22. G. Ehrlich and F. G. Hudda, J. Chem. Phys. 35, 1421 (1961).
23. J. R. Young, Rev. Sci. Instru. 34, 891 (1963).
24. This technique has recently also been used by T. Okano, K. Utagawa, and G. Tominaga, Jpn. J. Appl. Phys. 15, 2035 (1976).
25. G. Ehrlich and F. Hudda, Philos. Mag. 8, 1587 (1963).
26. A. E. Bell, L. W. Swanson and D. A. Reed, Surf. Sci. 17, 418 (1969).
27. A. Jason, Phys. Rev. 156, 266 (1967).
28. R. D. Young, Phys. Rev. 113, 110 (1959).
29. R. D. Young and E. W. Müller, Phys. Rev. 113, 115 (1959).
30. J. W. Gadzuk and E. W. Plummer, Rev. Mod. Phys. 45, 487 (1973).
31. D. Menzel and R. Gomer, J. Chem. Phys. 41, 3311 (1964), 41, 3329 (1964).
32. A. van Oostrom, J. Appl. Phys. 33, 2917 (1962).
33. L. D. Schmidt and R. Gomer, J. Chem. Phys. 45, 1605 (1966).
34. C. B. Duke and M. E. Alferieff, J. Chem. Phys. 46, 923 (1967).
35. G. Ehrlich, Adv. Electron. Electron Phys. 14, 255 (1963).
36. W. P. Dyke and W. W. Dolan, Adv. Electron. Electron Phys. 8, 89 (1956).
37. P. G. Shewmon, Diffusion in Solids, (McGraw-Hill Publishing Co., New York, 1958), pp. 122-125.
38. A thorough treatment on this is given by C. Herring and M. H. Nichols, Rev. Mod. Phys. 21, 185 (1949). Also, see E. Callen, Am. J. Phys. 25, 138 (1957).
39. M. Dreschsler, Z. Elektrochem. 61, 48 (1957). Also, more recently, T. T. Tsong and G. Kellogg, Phys. Rev. B12, 1343 (1975).
40. A. J. Bennett, Surf. Sci. 50, 77 (1975).

41. L. W. Swanson, R. W. Strayer and F. M. Charbonnier, *Surf. Sci.* 2, 177 (1964).
42. H. Utsugi and R. Gomer, *J. Chem. Phys.* 37, 1706 (1962).
43. The polarizability of non-metal atoms are almost 100 times smaller than those for metal atoms. See:
R. A. Alpher and D. R. White, *Phys. Fluids*, 2, 153 (1959), and
H. Liepack and M. Drechsler, *Naturwissenschaften* 43, 52 (1956).
44. The dipole moment is calculated using $\mu = qx$, where $x = 4\text{\AA}$ is assumed. See, for example, J. D. Jackson, *Classical Electrodynamics*, (John Wiley & Sons, Inc. New York, 1962) for conversion of units.
45. A. Polak and G. Ehrlich, *J. Vac. Sci. Technol.* 14, 407 (1977).
46. M. V. Smoluchowski, *Phys. Zeits.* 17, 557 (1916), 17, 585 (1916).
47. Ch. Kleint, *Surf. Sci.* 25, 394 (1971).
48. R. Gomer, *Surf. Sci.* 38, 373 (1973).
49. G. Ehrlich, *J. Chem. Phys.* 34, 29 (1961).
50. T. W. Hickmott and G. Ehrlich, *J. Phys. Chem. Solids*, 5, 47 (1958).
51. G. Ehrlich, *J. Phys. Chem.* 60, 1388 (1956).
52. L. J. Rigby, *Can. J. Phys.* 43, 532 (1965).
53. J. T. Yates, Jr. and T. E. Madey, *J. Chem. Phys.*, 43, 1055 (1965).
54. T. E. Madey and J. T. Yates, Jr., *J. Chem. Phys.*, 44, 1675 (1966).
55. T. Oguri, *J. Phys. Soc. Jpn.*, 18, 1280 (1963).
56. J. A. Becker, in *Solid State Physics*, Vol. 7, Ed. F. Seitz and D. Turnbull, (Academic Press, New York, 1958), p. 379.
57. G. Ehrlich, T. W. Hickmott and F. G. Hudda, *J. Chem. Phys.* 28, 506 (1958).
58. A. A. Holscher, *J. Chem. Phys.* 41, 579 (1964).
59. T. Oguri, *J. Phys. Soc. Jpn.* 19, 83 (1964).
60. A. van Oostrom, *J. Chem. Phys.* 47, 761 (1967).
61. T. A. Delchar and G. Ehrlich, *J. Chem. Phys.* 42, 2686 (1964).

62. J. T. Yates, Jr., R. Klein and T. E. Madey, *Surf. Sci.* 58, 469 (1976).
63. A. van Oostrom, *Philips Res. Rep. Suppl.* 1, 1 (1966).
64. B. J. Hopkins and S. Usami, in The Structure and Chemistry of Solid Surfaces, Ed. G. A. Somorjai, (John Wiley and Sons, Inc., New York, 1968), p. 67.
65. G. J. Dooley III and T. W. Haas, *J. Vac. Sci. Technol.* 7, s90 (1970).
66. P. J. Estrup and J. Anderson, *J. Chem. Phys.* 46, 567 (1967).
67. D. L. Adams and L. H. Germer, *Surf. Sci.* 26, 109 (1971).
68. T. E. Madey and J. T. Yates, Jr., *Nuovo Cimento Suppl.* 5, 483 (1967).
69. P. W. Tamm and L. D. Schmidt, *Surf. Sci.* 26, 286 (1971).
70. G. Ehrlich and F. G. Hudda, *J. Chem. Phys.* 36, 3233 (1962).
71. A. A. Holscher, *Disc. Faraday Soc.* 41, 54 (1966).
72. S. S. Brenner, in Metal Surfaces--Structure, Energetics and Kinetics, (American Society of Metals, Metals Park, Ohio, 1962), p. 305.
73. J. T. Yates, Jr. and T. E. Madey, *J. Vac. Sci. Technol.* 8, 63 (1971).
74. L. J. Rigby, *Can. J. Phys.* 43, 1020 (1965).
75. J. H. Singleton, *J. Vac. Sci. Technol.* 5, 109 (1968).
76. D. A. King, *Surf. Sci.* 9, 375 (1968).
77. B. E. Nieuwenhuys and W. M. H. Sachtler, *Surf. Sci.* 34, 317 (1973).
78. G. Ehrlich, H. Heyne and C. F. Kirk, in The Structure and Chemistry of Solid Surfaces, Ed. G. A. Somorjai, (John Wiley and Sons, Inc., New York, 1968), p. 49-1.
79. B. E. Nieuwenhuys, D. Th. Meiher and W. M. H. Sachtler, *Surf. Sci.* 40, 125 (1973).
80. K. E. Lu and R. R. Rye, *J. Vac. Sci. Technol.* 12, 334 (1975).
81. K. Christmann, G. Ertl, and T. Pignet, *Surf. Sci.* 54, 365 (1976).
82. a. W. H. Weinberg and R. P. Merrill, *Surf. Sci.* 33, 493 (1972).
b. V. H. Baldwin and J. B. Hudson, *J. Vac. Sci. Technol.* 8, 49 (1971).
c. J. N. Smith and R. L. Palmer, *J. Chem. Phys.* 56, 13 (1972).

83. B. E. Nieuwenhuys, *Surf. Sci.* 59, 430 (1976).
84. I. E. Wachs and R. J. Madix, *Surf. Sci.* 58, 590 (1976).
85. E. Ya. Zandberg and A. Ya. Tontegode, *Sov. Phys.--Solid State*, 12, 878 (1970).
86. R. W. Strayer, W. Mackie and L. W. Swanson, *Surf. Sci.* 34, 225 (1973).
87. V. J. Mimeault and R. S. Hansen, *J. Chem. Phys.* 45, 2240 (1966).
88. J. R. Arthur, Jr. and R. S. Hansen, *J. Chem. Phys.* 36, 2062 (1962).
89. J. A. Panitz, Sandia Lab. Rep. SLA-73-5798 (1974).
J. A. Panitz, in *Hydrogen Energy, Part B*, Ed. T. N. Veziroğlu, Plenum Press, New York, 1974), p. 1079.
90. E. Ya. Zandberg and A. Ya. Tontegode, *Sov. Phys. Tech. Phys.* 10, 260 (1965).
91. R. P. H. Gasser, G. Morris and A. K. Szczerupa, *Surf. Sci.* 36, 494 (1973).
92. G. J. Dooley III, and T. W. Haas, *Surf. Sci.* 19, 1 (1970).
93. B. Lang, R. W. Jeyner and G. A. Somorjai, *Surf. Sci.* 30, 440 (1972).
94. R. Klein and J. W. Little, *Surf. Sci.* 6, 193 (1967).
95. J. T. Yates, Jr. and T. E. Madey, *J. Chem. Phys.* 51, 334 (1969).
96. A. van Oostrom, in *Proceedings of the 8th International Conference on Phenomena in Ionized Gases*, Vienna, 1967. (International Atomic Energy Agency, Vienna, Austria, 1968), p. 291.
97. M. D. Scheer and J. D. McKinley, *Surf. Sci.* 5, 332 (1966).
98. R. P. H. Gasser and R. Thwaites, *Vacuum*, 17, 265 (1967).
99. G. Barnes, *Phys. Rev.* 97, 1579 (1955).
100. R. P. H. Gasser and A. K. Szczerupa, *Surf. Sci.* 49, 201 (1975).
101. Refer to Chapter IV.
102. G. J. Dooley III and T. W. Haas, *J. Chem. Phys.* 52, 993 (1970).
103. A comment on the results of Ref. 102 is given by
P. J. Estrup, *J. Chem. Phys.* 54, 1845 (1971).
104. P. J. Estrup and J. Anderson, *J. Chem. Phys.* 45, 2254 (1966).

105. H. R. Han and L. D. Schmidt, J. Phys. Chem. 75, 227 (1971).
106. P. W. Tamm and L. D. Schmidt, J. Chem. Phys. 51, 5352 (1969).
107. C. H. Huang and P. J. Estrup, Bull. Am. Phys. Soc. 19, 357 (1974).
108. P. J. Estrup, Phys. Today 28, No. 4, 33 (1975).
109. It should be noted that the LEED patterns observed by Huang and Estrup are somewhat different from those by Dooley and Haas. Huang and Estrup observed an initial (4x2) structure at < -50 C and a C(2x2) structure at < -100 C, followed by a (2x2) structure, and finally a C(1x1) structure at saturation.
110. H. Hayek, H. E. Farnworth and R. L. Park, Surf. Sci. 10, 429 (1968).
111. M. Mahnig and L. D. Schmidt, Z. Phys. Chem. (Frankfurt am Main), 80, 71 (1972).
112. E. Chrzanowski, Acta Phys. Polonica, A44, 711 (1973).
113. J. C. Riviere, Proc. Phys. Soc. 70, 676 (1957).
114. S. Berge, P. O. Gartland and B. J. Slagsvold, Surf. Sci. 43, 275 (1974).
115. U. V. Azizov, V. V. Vakhidov, V. M. Sultanov, B. N. Sheinberg and G. N. Shuppe, Sov. Phys.--Solid State, 7, 2232 (1966).
116. O. D. Protopopov, E. V. Mikheeva, B. N. Sheinberg and G. N. Shuppe, Sov. Phys.--Solid State, 8, 909 (1966).
117. L. W. Swanson, Adv. Electron. Electron Phys. 32, 193 (1974).
118. See Fig. 2.5. For more details, see Ref. 3, pp. 43-46.
119. The work function of the (110) plane may be affected indirectly, since its evaluation depends on the value of the work function for the clean average emitter.
120. L. A. Manukova, Zh. Fiz. Khim. 44, 177 (1970).
121. M. Abon and S. J. Teichner, Nuovo Cimento, Suppl. 5, 521 (1967).
122. D. O. Hayward, D. A. King, N. Taylor and F. C. Tompkins, Nuovo Cimento, Suppl. 5, 374 (1967).
123. D. O. Hayward and N. Taylor, Trans. Faraday Soc. 64, 1904 (1968).
124. R. A. Pasternak and H. U. D. Wiesendanger, J. Chem. Phys., 34, 2062 (1961).

125. No field emission patterns were given in his article.
126. T. Oguri and I. Kanomata, *J. Phys. Soc. Jpn.* 19, 1310 (1964).
127. G. Bergeret, M. Abon and S. J. Teichner, *J. Chem. Phys.* 71, 54 (1974).
128. J. M. Wilson and T. T. Bastow, *Surf. Sci.* 26, 461 (1971).
129. R. Chappell and D. O. Hayward, *J. Vac. Sci. Technol.* 9, 1052 (1972).
130. D. A. King and F. C. Tompkins, *Trans. Faraday Soc.* 64, 496 (1968).
131. The saturation coverages reported for polycrystalline molybdenum are not in good agreement. Pasternak and Wiesendanger [124] and Pryde and Parray (a) reported ratios of nitrogen to surface atoms approaching 1:1; Tardy and Teichner (b) more recently reported a ratio of $\frac{1}{2}$:1.
 (a) A. A. Parray and J. A. Pryde, *Brit. J. Appl. Phys.* 18, 329 (1967).
 (b) B. Tardy and S. J. Teichner, *J. Chem. Phys.* 70, 627 (1973).
132. These are obtained from a separate field ion microscope. (Courtesy of Dr. R. S. Chambers.)
133. D. A. Reed, private communication.
134. R. Gomer, R. Wortman and R. Lundy, *J. Chem. Phys.* 26, 1147 (1957).
135. P. W. Tamm and L. D. Schmidt, *J. Chem. Phys.* 55, 4253 (1971).
136. P. W. Tamm and L. D. Schmidt, *J. Chem. Phys.* 54, 4775 (1971).
137. See, for example, J. W. Christian, The Theory of Transformation in Metals and Alloys, (Pergamon Press Ltd., Oxford, England, 1965), pp. 440-453.
138. R. Wortman, R. Gomer and R. Lundy, *J. Chem. Phys.* 24, 161 (1956).
139. Note that a $(1-\gamma'\theta)$, rather than a $(1-\theta)$ dependence on the surface coverage is obtained from Eq. (8.12). Since γ' depends on temperature T , this looks quite different from the $(1-\theta)$ dependence of the sticking coefficient reported by Tamm and Schmidt [135]. However, a closer examination of their data reveals that the θ -dependence they found is actually $(1-\gamma\theta)$, with γ depending strongly on the surface temperature. Eq. (8.12) therefore coincides well with their results. Quantitative value, both theoretical and experimental, are difficult to obtain.

140. Due to geometrical differences, the concentration of loosely bound hydrogens at plane edges, n_p , and at cluster edges, n_c , are not the same. The stated assumption is not strictly valid. However, the concentrations in the overlayer are conceivably small, and these quantities appear only as fractions, n_c/n_{co} , and n_p/n_{po} . The difference between these is therefore second order in magnitude, and can be ignored in the first approximation. Same holds for n_t , n_t' .
141. T. W. Hickmott, J. Chem. Phys. 32, 810 (1960).
142. R. Gomer, R. Wortman and R. Lundy, J. Chem. Phys. 27, 1099 (1957).
143. B. M. W. Trapnell, Proc. R. Soc. A286, 39 (1951).
144. See, for example, P. G. Shewmon, Diffusion in Solids, (McGraw-Hills Publishing Co., New York, 1952), pp. 41-54.
145. G. Ayrault and G. Ehrlich, J. Chem. Phys. 60, 281 (1974).
146. D. W. Bassett, in Surface and Defect Properties of Solids, Vol. 2, A Specialist Periodical Report (The Chemical Society, London, 1973), pp. 34-68.
147. A. van Oostrom, J. Chem. Phys. 47, 761 (1967).
148. D. A. Reed, M.S. Thesis, University of Illinois, Urbana, Illinois, (1975).
149. See, for example, L. F. Yntema and A. L. Percy, in Rare Metal Handbook, Ed. C. A. Hampel (Reinhold Publishing Corp., New York, 1956), pp. 271-289.
150. R. S. Chambers, private communication.
151. a. A. J. Melmed, Surf. Sci. 8, 191 (1967).
b. W. Kollmar and D. Stark, Z. Phys. 178, 39 (1964).
152. a. K. M. Bowkett and D. A. Smith, Field Ion Microscopy, (American Elsevier Publishing Co., New York, 1970), p. 221.
b. M. A. Fortes and B. Ralph, Philos. Mag. 18, 787 (1968).
c. M. A. Fortes and B. Ralph, Proc. R. Soc. A307, 431 (1968).
153. W. R. Graham, F. Hutchinson, J. J. Nadakavakaren, D. A. Reed, and S. W. Schwenterly, J. Appl. Phys. 40, 3931 (1969).
154. C. Čížek, F. Pařízek, A. Orlová and J. Toušek, Czech. J. Phys. B20, 56 (1970).
155. The time required for the final stage has recently been reduced to ~ 10 min. by applying a continuous a.c. potential of 0.75 V. J. Wriggley, private communication.

156. Normal energy is only a convenient (but inaccurate) name used traditionally to refer to the quantity $p_n^2/2m$, where p_n is the momentum of the electron perpendicular to the surface. Similarly, tangential energy E_t is a convenient name for the quantity $p_t^2/2m$.
157. E. L. Murphy and R. H. Good, Jr., Phys. Rev. 102, 1464 (1956).
158. K. Besocke and H. Wagner, Surf. Sci. 53, 351 (1975).
159. This is derived from the formula relating the electric field to the potential: $F = \beta V = \alpha V/r_0$. See Fefs. 10 and 14 for details.
160. S. Nakamura, J. Elec. Microscopy (Japan), 15, 279 (1966).

VITA

Ruichen Liu was born in Peiking, China, on February 19, 1946. He attended public schools in Taiwan, China, and was graduated from Chan-kuo High School, Taipei, Taiwan, China, in June, 1964. He attended National Tsing-Hua University in Hsin-chu, Taiwan, China, and received a Bachelor of Science degree in nuclear engineering in June, 1968. He attended the graduate school of National Tsing-Hua University, majoring in nuclear engineering, from September, 1968 to June, 1969. He attended the Ohio State University in October, 1970, and received a Master of Science degree in physics in May, 1972. Since June, 1972 he has been a student in metallurgical engineering at the University of Illinois at Urbana. He served as a teaching assistant in National Tsing-Hua University from 1968 to 1969, and in the Physics Department of the Ohio State University from 1970 to 1972. Since 1972, he has been a research assistant in the Coordinated Science Laboratory, under Professor Gert Ehrlich. He is the co-author of two publications:

"Photo-Stimulated Field Emission from a Metal." Ruichen Liu, Gert Ehrlich and Richard S. Polizzotti, J. Vac. Sci. Technol. 11, 276 (1974);

"Adsorption of Nitrogen on Perfect Re(0001) Planes." Ruichen Liu and Gert Ehrlich, J. Vac. Sci. Technol. 13, 310 (1976).